Stacked Deposits of Thickened and Filtered Fluid Fine Tailings Using Geotextile Tubes to Enhance Physical Stability of Reclaimed Landforms

by

Fernando Da Silva

A thesis submitted in partial fulfillment of the requirements for the degree of

Doctor of Philosophy

in

GEOTECHNICAL ENGINEERING

Department of Civil and Environmental Engineering
University of Alberta

Abstract

Thickening tailings by adding synthetic polymer is a common practice in the mining industry. Flocculant alone in the flocculation of the oil sands' fluid fine tailings (FFT) has been used with the expectation that it would be beneficial to fine tailings particle agglomeration and dewatering. Unfortunately, significant amounts of trapped water remain in the flocculated tailings, affecting consolidation timeframes and shear strength gain, and postponing mine closure and reclamation. This research investigates a tailings management technology approach using a geotextile tube that combines filtration, dewatering, densification, and enhancing the geotechnical stability of the FFT, while effectively recycling the process water. To assure that the return water is suitable for reuse in the mine plant processes and that FFT can be dewatered and densified faster, a physicochemical treatment recipe using coagulation and flocculation was designed to assist solids/water separation and ensure fines agglomeration during pipeline transport prior to discharge into the geotextile tubes. As part of this research, a parametric analysis of the FFT dispersion and flocculation behaviors was performed to determine the causes and mechanisms that explain why significant amounts of trapped water remain when FFT is thickened with flocculation only. The parametric analysis was developed based on the fundamentals of soil behavior, supported by facts observed in the laboratory. The parametric analysis findings and recommendations are also included. The Global Industry Standard on Tailings Management (GISTM) aspires toward "zero harm to people and the environment" from tailings facilities. Aligned with the GISTM, this research describes the recipe with geotextile tubes as a feasible solution for safe management of tailings as well as enhanced physical stability of the treated FFT deposits. FFT treated with the defined recipe dewater in the geotextile tubes; the rate of dewatering is a function of the recipe,

the inline mixing process, short drainage path provided by geotextile tubes containment, internal pressure and gravity head during filling, hydraulic parameters of the geofabric material, evaporation, freeze-thaw, and the self-weight consolidation, and increased total stress by stacking the geotextile tubes to form stable deposits of thickened and filtered FFT. This research therefore has the potential to change the way mine tailings are managed by greatly reducing geotechnical risk and the complexity of closure, compared with traditional methods.

Acknowledgements

Table of Contents

List of Tables

List of Figures

List of Photographs

List of Acronyms

Acronym	Definition
ARD	Acid rock drainage
CMD	Cross machine direction
CaOH	Calcium hydroxide
CPT	Cone penetration test
CPTu	Cone penetration tests with measurement of excess pore pressure
CT	Coarse tailings
EDS	Energy Dispersive Spectrometry
ETF	External Tailings Facility
FFT	Fluid fine tailings with flocculant alone
FS	Factor of Safety
GISTM	Global Industry Standard on Tailings Management
HMW	High molecular weight
ILTT	Inline Thickened Tailings
INCA	Oxford's micro-analysis system
Km	kilometer
LSC	Large strain consolidation
IWA	IWA Publishing
m	meter
Mg/L	Milligrams per liter
m/s	meters per second
m^3	cubic meter
mm	millimeter
NPV	Net present value
PAM	Polyacrylamide
PZC	Point of zero charge
Recipe	Treated FFT with coagulation + flocculation
SAR	Sodium adsorption ratio
SEM	Scanning Electron Microscopy

Acronym	Definition
SFR	Sand-to-fines ratio
UBC	University of British Columbia
USCS	United soil classification system
VHMW	Very high molecular weight
XRD	X-ray diffraction
%	percent
°	degree
°C	degrees Celsius
<	less than
µg/L	micrograms per liter
µ/m	micrometers

List of Symbols

Symbol	Definition
AE	actual evaporation
AE/PE	The ratio of Actual AE over Potential PE evaporation
AE/PE = 0.8	The boundary between the saturated and unsaturated states
Bbar	parameter of pore pressure dissipation
CH	Clay of high plasticity
Gs	specific gravity of soils
PE	potential evaporation
ρ_d	dry density of tailings
ρ_w	density of water
Su	undrained shear strength
U_0	static porewater pressure
Wt.% solids	solids content by mass
W	saturated water content (%)
Δu	excess pore pressure

Chapter 1 Introduction

1.1   General

With continuous improvement in the beneficiation process, ore is being ground more and more finely. In many mines, more than 50% of the total tailings are finer than 75 µm, which results in large volumes of soft and wet tailings, posing challenges to the safety of mining facilities (Chang-Hong Li, 2019). The Fluid fine tailings (FFT) investigated in this research has a particle size distribution (PSD) of more than 85% fines passing 75 µm (predominantly quartz as a non-clay mineral, followed by kaolinite and illite as clay minerals), resulting in large volumes of FFT with extremely slow sedimentation due to the comprehensive effects of its physical and chemical properties; this poses challenges to the stability of the FFT deposits (Photograph 1-1). Minimizing the accumulation of soft and wet FFT deposits behind dams and ensuring that they are reclaimed progressively over the life of a project will significantly contribute to the safety of the long-term reclamation of the FFT deposits.

Photograph 1-1:   **Example of increased storage volumes of FFT deposit less capable of facilitating reclamation.**

The failure of tailings dams is often caused by the construction method and the inability of the tailings to drain down (Williams, D.J., 2021). External factors, however, also contribute to failures, these include: increased loading of the tailings dam, earthquakes, rainfall, flooding top, heavy snow and snowmelt, foundation subsidence, erosion (external and internal), slope instability, and post-closure climatic impacts. Furthermore, tailings below the phreatic surface have a slow consolidation rate, and the nearly saturated tailings reduce the dam's shear strength and effective stress(es).

Geotextile tubes that are made from woven high-strength, high-modulus synthetic fibers with distinct pore sizes that provide filtration and dewatering of the treated FFT (recipe) in a controlled manner are used in this research.

Photograph 1-2 shows the installation of the commercial size geotextile tube (100 m length x 40 m circumference), and the accelerated dewatering of the treated FFT (recipe) when discharged into the tubes.

Photograph 1-2: **Geotextile tube installation and accelerated dewatering and consolidation.**

FFT dewatered in the geotextile tube requires a physicochemical treatment that combines coagulation and flocculation, referred to herein as the "recipe" (Developed by Da Silva F. et al., 2023; 2022; 2021). The objective of the recipe is to provide solids/water separation and fines agglomeration inline, ensuring segregation does not occur prior to discharge into the geotextile tube, while the tube maximizes fines capture and accelerates dewatering and consolidation.

Figure 1-1 shows the FFT feed at 20 wt.% solids, the inline treatment with coagulation and flocculation (recipe) and the treated FFT (solids/water separation) prior to the discharge into the geotextile tubes as verified with a field trial in this research.
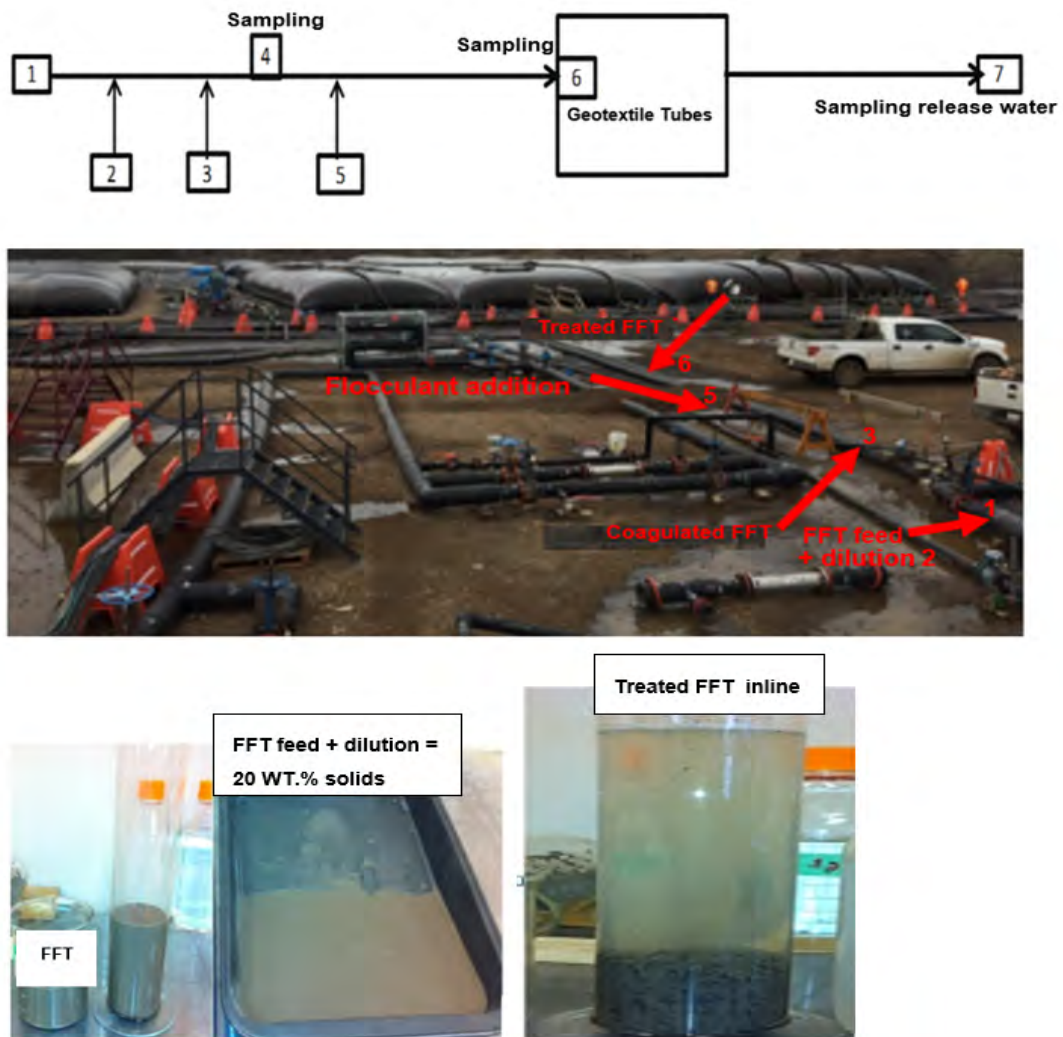
Figure 1-1: **Simplified process flow diagram of the treated FFT inline and discharged into geotextile tubes.**

The verification of the geotextile tube processing using the "recipe" (Da Silva F. et al., 2023; 2022; 2021) for FFT investigated in this research successfully demonstrates:

1) Effective fines agglomeration, enhanced dewatering, and accelerated consolidation of the FFT achieved with the coagulant alum (4.27% Al^{3+} + 8.07% Al_2O_3 and specific gravity 1.326) at concentration 0.1% and 0.65% dosage (by mass of dry solids), and flocculant (anionic PAM flocculant of medium charge density and VHMW) at concentration 0.1% and 0.1% dosage (by mass of dry solids).

2) Aluminum (Al^{3+}) loading is mainly contributed from the coagulant (alum), which is transferred to the solid phase and remains as a very small concentration in the release water. The results showed that the tailings treatment used do not generate any excess divalent or multivalent cations in the release water in the scenario of high ion-content dilution water. The mass balance and concentration analysis of the major ions in the water phases shows that most of the ions remain in the solid phases, which minimizes the negative impact of Ca^{2+} ions onto anionic PAM flocculant, inhibiting flocculation efficiency.

3) The effectiveness of the coagulation and flocculation process requires an initial slurry density of the FFT feed at 20 wt.% solids. This can be achieved by controlled dredging of the FFT and/or providing a dilution step in the process. In the former case, no initial dilution is required, and only water from the coagulation and flocculation solutions is required for the treatment.

4) If the initial slurry density of the FFT feed is higher than 20 wt.% solids, an initial dilution is required to reduce the FFT feed to 20 wt.% solids. The treatment was designed to achieve an efficient flocculation performance by maximizing agglomeration of fines to form large flocs while maximizing water release. To achieve this design criteria, the slurry density at the flocculation step should be approximately 8 wt.% solids (considering the contribution of the coagulant and flocculant solution waters) and, therefore, the initial dilution of the FFT feed should be set for this condition while maintaining the concentration and dosage of the coagulant and flocculant constant.

5) The optimal residence time for the inline mixing is 20 seconds to provide the most efficient flocculation of the FFT without shearing (no static or dynamic mixing are required). This residence time is defined by laboratory settling tests.

6) The geotextile tube acts as a filter pressure system, with most of the water recovery occurring while the tubes are being filled with the treated FFT. The filtration properties of the geotextile tubes and the short drainage path of the treated FFT contained in the tubes are key contributors in the enhanced dewatering and accelerated consolidation of the treated FFT.

7) The recipe/geotextile tube FFT management technology approach also allows for faster construction of deposits that can be stack into higher lifts without compaction, are geotechnically stable, and occupy a smaller environmental footprint compared with FFT deposits (Figure 1-2).

Figure 1-2:   Example of stacked, capped, and reclaimed geotextile tubes deposit ~3MT/year (adapted from TenCate Geosynthetic Americas deposit of dredged limestone sediments).

The stacked deposits using the recipe/geotextile tubes have the potential to offer wide-ranging benefits to the environment and society as a feasible and suitable solution for FFT management, demonstrating that reclamation is possible and post-closure long-term performance of FFT deposits is safe.

1.2   Statement of the problem, overall hypothesis, and objectives

This section describes the background of the mining process and generation of the FFT, indicates key problems remaining with the long-term performance reclamation, describes the verification of the geotextile tube process using Da Silva's recipe as a potential solution for faster reclamation of soft and wet FFT deposits, highlights the mining industry paradigms regarding the net present value (NPV) accounting, and describes the overall hypotheses and objectives of this research.

1.2.1   Background

Oil sands ore described in this research is a natural mixture of sand, water, silt (quartz) and clays (kaolinite and illite), and a type of heavy oil called bitumen. Bitumen must be removed from the oil sands ore and water mixture before being upgraded into crude oil and other petroleum products. In surface mining operations, shovels excavate the oil sands ore and trucks move it to an extraction facility where it is mixed with water to produce a pumpable slurry that can be gravity separated. As the tailings solids are approximately 72% fine sand, the coarse sand tailings (CST) settle out on deposition to form tailings dikes and beaches; much of the water and residual bitumen, and approximately half of the fines (FFT) flow into the tailings pond. CST are separated from FFT, usually by hydro-cyclone overflow. The underflow is the FFT typically thickened with flocculant, and pumped to storage facilities where process water is recovered (Figure 1-3 and Photograph 1-1).
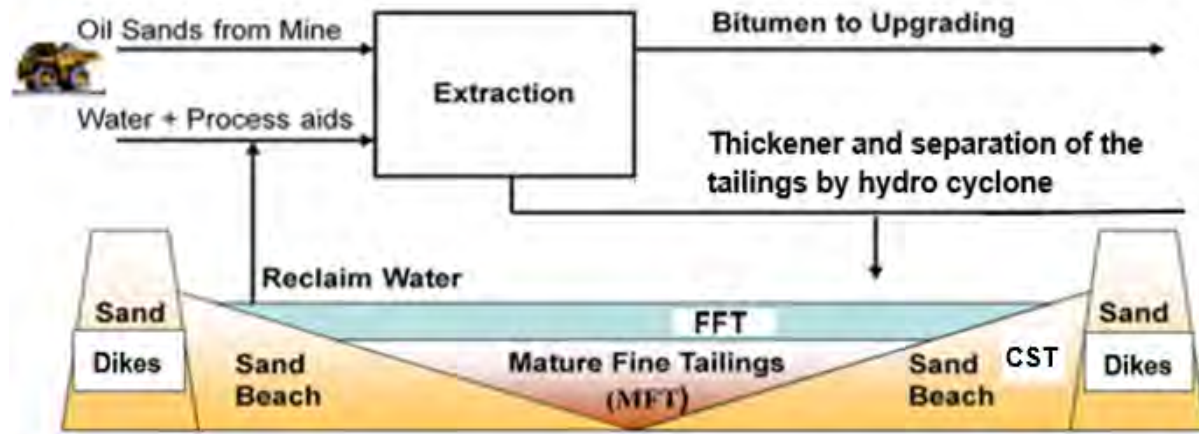
Figure 1-3: Oil sands extraction process diagram and production of coarse sand tailings (CST) and fluid fine tailings (FFT), adapted from Fair and Beier 2012. This research mainly utilizes Albian Sand's FFT.

1.2.2 Key problems with long-term reclamation performance of FFT deposits

Significant amounts of trapped water remain if FFT are thickened using flocculation only, resulting in a low rate of shear strength gain and long consolidation timeframes that pose significant challenges in converting FFT into deposits that can facilitate reclamation.

Gaps in assessing the physicochemical properties of the FFT still exist, including their dispersion and flocculation behaviors with regards to mineralogy, pore water chemistry, pH, and the mine extraction processes impacting the characteristics and mechanical properties of the FFT. This research will fill these gaps by determining the potential causes of the significant amounts of trapped water when thickening FFT with flocculation only and will provide a rationale for the recipe to increase fines agglomeration and dewatering of the FFT.

Previous studies have shown that geotextile tubes are an innovative solution in engineering projects because of their ability to modify mechanical and hydraulic properties in a controlled manner. Additionally, the geotextile tube deposits with treated FFT will act more as a filter pressure system, with most of the water recovery happening while the geotextile tubes are being filled.

1.2.3 Mining industry paradigms

Supported by NPV accounting, the mining industry (including oil sands operations) is locked into a sustainable low-cost approach, starting from low front-end costs, to achieve the most economical solution of acceptable tailings deposits, such as transporting poorly thickened tailings to a surface dam, which limits the consideration of alternatives and increases operating costs over time, leading to high back-end costs. The implementation of some existing and new approaches to technologies in tailings management that work would help to eliminate the risks posed by some conventional tailings facilities, and would place the industry in a better position of compliance with the Global Industry Standard on Tailings Management (GISTM) aspirational goal of "zero harm to people and the environment" from tailings facilities. This research suggests that the industry should be challenged to move to a more whole-of-life costing approach of tailings facilities (Williams, D.J. 2021), beginning with using the best available tailings technology that works, progressively optimizing costs, and assuring that reclamation is possible and the post-closure long-term performance of tailings deposits is safe.

1.2.4 Our understanding of the gaps

The inherent properties of FFT constituents and the mine extraction process, including pore water chemistry and pH, collectively dictate the characteristics and mechanical properties of the FFT. FFT are predominantly composed of quartz and kaolinite particles, and at pH 8, present a highly negative surface charge with a zeta potential of - 47 mV that leads to a dispersive state by the action of electrostatic repulsive forces. Significant amounts of trapped water remain when FFT is thickened with flocculation only, as shown in this schematic example, Figure 1-4.

Figure 1-4: **Schematic example of poor flocculation (particle dispersion and water retention).**

The rationale for coagulation of FFT with high-valence cations such as alum (Al^{3+}) is to lower the electrostatic repulsive forces between particles, causing charge neutralization and formation of stable micro-flocs (slow settling flocs) as shown in Figure 1-5.
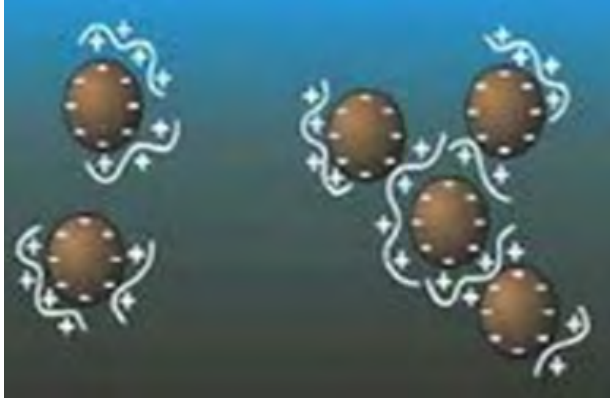
Figure 1-5:   Schematic example of quartz and kaolinite particles charge neutralization.

Efficient flocculation, fine particles agglomeration, and water separation will occur when coagulated FFT are flocculated with anionic polyacrylamide (PAM) flocculant at a relatively small concentration and dosage. A parametric analysis was performed for this research to investigate the behavioral difference between coagulated and non-coagulated FFT prior to flocculation addition to validate the flocculation efficacy as shown in Figure 1-6.
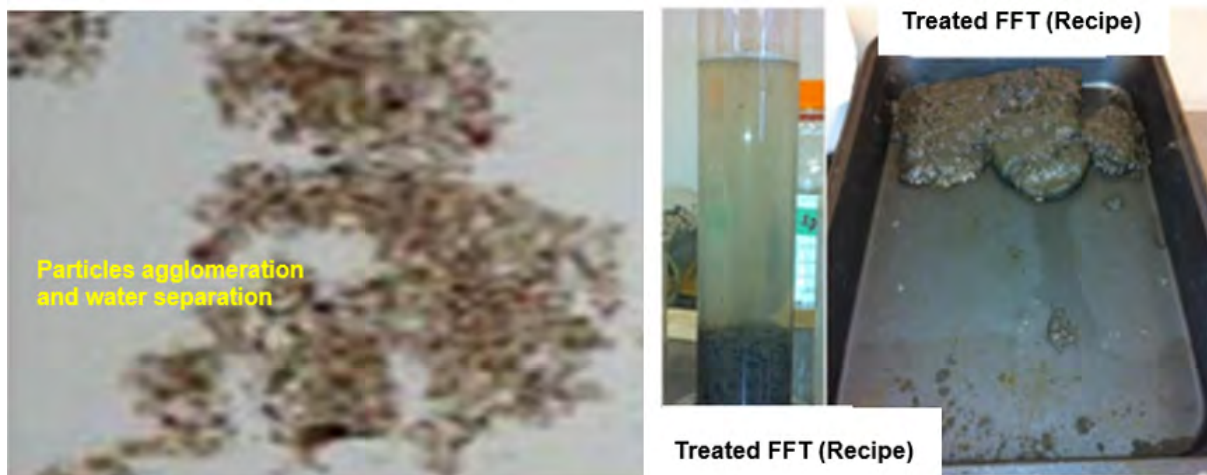
Figure 1-6:   Schematic example of efficacy flocculation of quartz and kaolinite particles using the recipe.

1.2.5   Overall hypothesis

The overall hypothesis of this research is that the FFT treated with coagulation and flocculation applied inline (recipe) will provide solids-water separation and fines agglomeration during pipeline transport prior to deposition into geotextile tubes. The treated FFT discharged into geotextile tubes will be dewatered and densified faster because the filtration properties of the geofabric material and the short drainage path provided by the geotextile tubes containment, internal pressure and gravity head during filling, evaporation, freeze-thaw, self-weight consolidation, and increased total stress by stacking the geotextile tubes to form stable deposits of thickened and filtered FFT.

1.2.6   Research objectives

The objectives of this research are to provide understanding of the a) potential causes of the significant amounts of trapped water when FFT is thickened with flocculation only; b) novel physicochemical treatment (recipe) to increase solids-water separation, fines agglomeration, and inline dewatering of the FFT prior to disposal into geotextile tubes for filtration; and c) accelerated dewatering and consolidation of the treated FFT to more rapidly form deposits stacked in higher lifts, without compaction, that are geotechnically stable for facilitating reclamation. These overall objectives will be achieved if the following supporting objectives are completed:

1) Investigate how the chemistry and pH of the process water and FFT porewater, inherent properties of the FFT constituents, and zeta potential affect the dispersion and flocculation behaviors of the FFT.

2) Investigate why thickening FFT with flocculant only is not enough to provide efficient fines agglomeration and dewatering of the FFT, and determining the gaps to be filled.

3) Develop a recipe for FFT to assist solids-water separation, fines agglomeration with maximized capture, enhanced dewatering, and accelerated consolidation.

4) Develop an inline mixing process of the FFT with coagulation and flocculation for effective flocculation prior to the discharge into the geotextile tubes.

5) Develop a solids and water mass balance of the treated FFT discharged into the geotextile tubes to understand the solids captured inside the tubes, and release water as process water either for use in the same FFT management or routed into the mining process.

6) Investigate the suitability of the recipe/geotextile tubes as a new approach to technology in tailings management for implementation in a mining operation.

1.2.7   Outline of the research

This research consists of eight chapters following a brief introduction:

- Chapter 2 – Literature review of existing publications and data related to inherent properties, soil characterization, and coagulation and flocculation behaviors of the FFT mineral components referred to in this research.

- Chapter 3 – Describes the laboratory testing including soil composition and engineering properties to evaluate the dispersion and flocculation behaviors of the FFT.

  o Identification and quantification of the FFT inherent properties such as mineralogy, zeta potential, porewater chemical analysis, PSD, and engineering properties (slurry density, specific gravity, water content, total bulk density and dry density, Atterberg limits, and void ratio). These properties are fundamental for the design of the recipe and its flocculant and coagulant dosages and concentrations.

  o Laboratory settling tests to evaluate mixing intensity, solids/water separation, and timing for settling. In addition, bleed tests were used to provide the short-term gravity drainage or passive water release of the underflow solids that were obtained from the settling tests.

  o Laboratory parametric physicochemical analysis of the FFT dispersion and flocculation behaviors to determine the cause for significant amounts of water trapped in the flocculated FFT.

  o Laboratory flume test to visually observe the discharge of the treated FFT at an end-pipe, investigate fines segregation, and obtain measurements of the undrained shear strength with time.

- o Laboratory trials using geotextile tubes to compare dewatering and consolidation behaviors of the treated FFT (recipe) to FFT with flocculant only.

- o Laboratory large strain consolidation (LSC) tests on treated FFT (recipe) with and without synthetic fibers used to evaluate improvement of the undrained shear strength.

- o Laboratory settlement testing on treated FFT using geotechnical beam centrifuge to evaluate the long-term performance behavior of the recipe compared with flocculation with flocculant only.

- o Laboratory evaporation tests conducted on water, FFT, treated FFT, and FFT centrifuge cake to investigate and compare their evaporation rates.

- Chapter 4 – Describes the field trials and processing methods used in this research.

  - o Field trial to evaluate end-pipe subaerial (above water line) discharge of the treated FFT and its segregation behavior, beach slopes, undrained shear strength, and dissipation of excess pore water pressures.

  - o Preliminary field trial to evaluate dewatering of the treated FFT into geotextile tubes. The results of this trial were used to evaluate solids and mass balance of the treated FFT (section 4.1.3).

  - o Commercial field trial on FFT inline mixing treatment (coagulation and flocculation), filling, and dewatering into the geotextile tubes.

  - o Summary of the key findings of the laboratory and field trials.

- Chapter 5 – Discussions and anticipated outcomes of this research: a brief review on the GISTM, existing and new approaches to tailings management versus industry paradigms, geotextile tubes technological suitability and new approach to tailings management, and value-adding final notes.

- Chapter 6 – Conclusions.

- Chapter 7 – Limitations and contribution to knowledge.

- Chapter 8 – Recommendations for further work.

Chapter 2 Literature Review

2.1   Introduction

The inherent properties of the oil sands constituents and the oil sands extraction process collectively dictate the characteristics and mechanical properties of the FFT. Knowledge of the FFT mineral composition and its interaction with ions, the acid-base nature of the liquid phase, and the presence of bitumen are fundamental for an overall understanding of the material engineering properties (permeability, compressibility, and shear strength). The FFT mineralogy, as part of this research, is predominantly composed of quartz particles (non-clay mineral). However, this predominance can also be kaolinite (clay mineral) and, therefore, the ratio of clay to massive minerals encountered in the FFT evaluated in this research can vary from 0.6 to 1.2. This variability depends on the location and depth from which FFT is dredged from the external tailings facility (ETF). The chemical analysis in this research focuses on the interaction between the mineral composition (i.e., FFT mineralogy) and pore water chemistry (i.e., pore solution electrolyte and ion concentration and pH), with the understanding of their significant influence on FFT dispersion/flocculation behavior. This research also includes a parametric analysis (section 3.2.7) on FFT dispersion and flocculation behaviors to investigate the causes of significant amounts of trapped water when FFT is flocculated only. This parametric analysis was developed considering the fundamentals of soil behavior and supported by observations in the laboratory.

Comprehensive reviews of different aspects of past work have appeared over time and those that are worthy of mention are listed in this chapter.

2.2   Tailings management best practice

The ongoing rate of tailings facility failures is unacceptable to both industry and society (Morgenstern et al., 2017). Mining companies, industry bodies, consulting companies, universities, and regulators have been continually improving best practice guidelines for the construction and management of tailings and mining waste facilities. There is a need for further development and implementation of new tailings management technologies and innovations, and for the application of whole-of-life costing of tailings facilities (Williams, 2021). Almost all mines

produce wet fine tailings as a by-product of the mineral extraction process. Conventionally, these tailings are stored behind dams, which are usually constructed from the tailings themselves (Vick, 1996). These structures can present a challenge for closure and reclamation and are a long-term risk and liability. To address this problem, an increasing trend in the industry is deposition of tailings in self-supporting "dry stacks," typically using pressure or vacuum filtration to rapidly dewater the tailings before stacking. Dry stacking of filtered tailings using geotextile tubes is an emerging technology that has the potential to offer several advantages over stacking filtered tailings alone, such as higher shear strength and reduced buildup of excess pore pressures during stacking, enabling the material to be stacked faster and in higher lifts without compaction, as well as reducing overall waste volumes and the deposition footprint. Geosynthetics technology is a well-established innovative solution available for geotechnical engineering projects that combines their mechanical and hydraulic properties in a controlled manner (Krystian, 2007). Geotextile tubes are made from woven high-strength, high-modulus synthetic fibers and have distinct pore sizes that can be used for filtration of the treated FFT with a proper physicochemical treatment recipe. The Honeywell Onondaga Lake Dredge and Cap project in Syracuse, New York, is an example of an adaptive management technique using geotextile tubes for sediment dewatering operations. Onondaga lake is a 4.5 km^2 lake located in the City of Syracuse, NY. The availability of salt limestone along Onondaga lake resulted in the large marshlands around the lake serving as sludge disposal from the process, leaving extensive "waste beds." The cleanup required dredging of 1.65 Mm^3 of contaminated sediments and treatment of 11.0 Mm^3 of water. Dredged sediments were pumped over 6.4 km to a processing area adjacent to the dewatering cell, where the sediments were thickened and disposed of in the geotextile tubes. Once completed, the dewatering cell was covered, capped, and vegetated (Abrams et al., 2016).

2.3   Inherent properties

The inherent properties of the FFT constituents and the mine extraction process, including pore water chemistry and pH, collectively dictate the characteristics and mechanical properties of the FFT. Mineralogy is the primary factor controlling the size, shape, and properties of soil particles. These same factors determine the possible ranges of physical and chemical properties of any given soil. A priori knowledge of what minerals are in a soil provides intuitive insight into its behavior (Mitchell, 2005). Quartz, which is a non-clay mineral, is the predominant mineral within

the fine soil particle size fraction (≤75 µm) of the FFT evaluated in this research, followed by kaolinite and illite. Quartz particles at pH > 2 present a negative surface charge (van Lierde, 1980; Hunter, 1981; Hussein et al., 1996; Gan et al., 2008). Kaolinite is the predominant clay mineral of the evaluated FFT, and it is also negatively charged at pH > 2. The behavior of kaolinite particles is dependent on the sodium adsorption ratio (SAR), electrolyte concentration, and pH (Goldberg et al., 1991). Illite soil particles have a smaller cation exchange capacity and are also pH and SAR dependent. All exchangeable cations are adsorbed on the exterior surfaces of illite and kaolinite soil particles (van Olphen, 1977). Existing literature shows that illite does not play a dominant role in determining flocculation and dispersion behaviors of kaolinite/illite mixtures (Goldberg, 1991).

2.4   Particles in water

Particles larger than 50 µm are usually visible by the naked eye. Particles between 1 to 50 µm can be viewed by light microscopes, and particle sizes below 1 µm (usual size of a wavelength of light) become difficult to identify. For particles smaller than 1 µm and ≥ 20 nm, the electron microscope provides good resolution mainly because of the shorter effective wavelength of electrons. Particles smaller than 20 nm are of similar size to dissolved macromolecules and are in the size range between particles and soluble matter. An important distinction should be made between colloidal and suspended (dispersed) material.

Particles having at least one dimension in the size range of 0.001 µm to 1 µm are known as colloids (Gregory, 2006).

- For particles smaller than 1 µm, diffusion becomes an important transport mechanism, and this feature tends to prevent particles from settling. Larger particles can settle more rapidly because diffusion is reduced; therefore, those particles tend to be removed by sedimentation over time.

- At approximately 1 µm, the importance of the surface area of particles compared with their volume begins to increase, because a large surface area provides more opportunity for the adsorption of dissolved impurities.

- For particles smaller than 1 μm, interparticle interactions are significantly impacted by external forces such as gravity and fluid drag. Colloid interactions are the key factors for aggregation and deposition of these small particles.

Regarding the interaction between dispersed particles and the dispersed medium, colloidal (dispersed) systems can be divided into two groups: lyophobic and lyophilic. In lyophobic, or 'liquid-disliking', systems, there is little to no affinity between the particles and the solvent. The stability of those systems relies on the charges of the particles. The term hydrophobic, or 'water disliking', is used specifically when water is the dispersing medium; hydrophobic, or lyophobic, systems are not very stable. Lyophilic, or 'liquid-liking', systems are more stable as there is interaction between particles and solvent; specifically, when water is the dispersing medium, the term hydrophilic ('water liking') is used. Most inorganic colloids are hydrophobic, while most organic colloids are hydrophilic (Jirgensons et al., 1962). An example of an inorganic colloid is the clay particles that cause turbidity in natural water, and an example of an organic colloid is the colloidal particles in domestic sewage (Sincero et al., 2003). Another example of a hydrophilic colloidal system is macromolecules in water, such as proteins, gums, starches, and many synthetic polymers. Most of the natural organic matter in water, such as humic substances, can be called hydrophilic colloids (Gregory, 2006).

Hydrophobic colloids are not thermodynamically stable, which can be explained by the characteristic interfacial energy between a particle and water. Smaller particles have relatively larger surface-volume ratios, therefore more interfacial energy per mass unit), whereas larger particles have lower surface-volume ratios, therefore less interfacial energy per mass unit. Upon aggregating, these smaller particles have reduced area contacting water, which reduces the interfacial energy, and they are more stable as a result. Particles in water collide with each other creating opportunities to form aggregates, but the forces of repulsion between such particles prevents the creation of aggregates because the particles are not in true contact. The most common reason is that aquatic particles nearly always have a surface charge, resulting in electrical repulsion between particles (Gregory, 2006).

2.5   Charge on particles

Many solid surfaces contain ionizable functional groups, such as –OH and –COOH. This ionizing group provides electrical charge to the particle. Particles may become charged by adsorbing ions from solution, for example, a silver bromide sol contains positively charged bromide particles (if excess of silver nitrate is present) because of the adsorption of silver ions on the surface of particles (Jirgensons et al., 1962). Charge can also be attributed to isomorphous substitution or crystal lattice defects in the internal structure of the mineral, such as the charge production of clay minerals; for example, Al^{3+} substituted by tetrahedral Si^{4+} causes deficiency of positive charge on the crystal lattice. The resulting charge is generally negative on the clay structure (Van Olphen, 1977).

2.5.1   Electrical double layer

Regardless of the origin of surface charge, a charged surface in contact with a solution of ions will result in a distribution of ions in a solution. If the surface is charged, there must be a corresponding excess of oppositely charged ions (counter-ions) in the solution near the particle to maintain electrical neutrality. The combined system of surface charge and the excess charge in the solution is known as the electrical double layer. It is initially convenient to consider a flat charged surface, such as a clay surface, in contact with an aqueous solution. The counter-ions are subject to two opposing tendencies: electrostatic attraction to the charged surface and the random effect of thermal motion. The balance between these effects is the determining factor in the distribution of charge and electric potential in solution (Gregory, 2006). The concentration of counter-ions near the particle surface is high and decreases with the increasing distance from the surface. This diffuse character of the counter-ion was recognized by Gouy (1910) and by Chapman (1913), who were the first to suggest a theoretical treatment of the counter-ion distribution.

The counter-ion atmosphere is often referred to as the diffuse or Gouy layer. The diffuse layer does not simply consist of an excess of ions of opposite charge; simultaneously, there is a deficiency of ions of the same charge (co-ion) at the neighborhood of the surface because these ions are electrostatically repelled by the particle (Van Olphen, 1977).

The Gouy and Chapman model is based on the simplified assumptions given below:

- There is an infinite, flat, impenetrable surface.

- Ions in solution are points of charge able to approach right up to the charged surface.

- The solvent (water) is a uniform medium with properties that do not depend on distance from the surface.

These approaches allow the prediction of how the electrical potential in solution varies with distance from the charged surface. For low values of surface potential, the potential in solution decreases exponentially with distance from the surface. The main challenge of the Gouy-Chapman model is the assumption of ions as point charges; ions can have significantly different sizes, particularly when hydrated, which limits the effective distance of the closest approach to a charged surface. Allowing for the finite size of ions means a region close to the surface is inaccessible to counter-ion charge. This has become known as the Stern layer, after Otto Stern, who was the first to introduce the ion size correction into double layer theory in 1924. The Stern layer involves a certain proportion of the counter-ion charge, and the remaining counter-ions are distributed within the diffuse part of the double layer, or simply the diffuse layer (Gregory, 2006).

A conceptual picture of the Stern-Gouy-Chapman model of the electrical double layer at a flat interface is shown in Figure 2-1. This shows the variation of electric potential from the surface, where its value is ψo, to a distance far into the solution, where the potential is taken as zero. Across the Stern layer, the potential falls rapidly to a value $\psi\delta$ (the Stern potential) at a distance δ from the surface; this is the boundary of the Stern layer, known as the Stern plane. Usually, δ is of the order of the radius of a hydrated ion, or approximately 0.3 nm. Although this distance is very small, the Stern layer can have a great influence on double layer properties. From the Stern plane into the solution, through the diffuse layer, the potential varies in an approximately exponential manner according to the following equation: $\psi = \psi\delta \exp(-\kappa x)$; where x is the distance from the Stern plane and κ is a parameter that depends on the concentration of salts in the suspension (or in the medium) (Gregory, 2006).
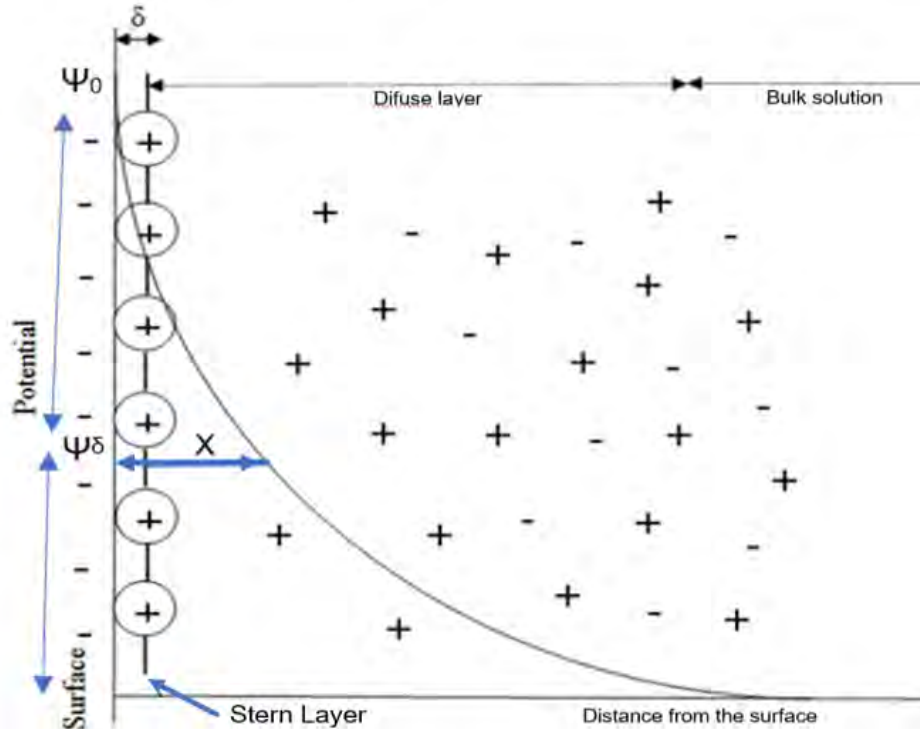
Figure 2-1:   Adapted diffuse electrical double layer from the Gouy-Chapman-Stern model.

2.5.2   Effect of electrolyte on the electrical double layer

When a flocculant electrolyte is added to the stable colloidal system, the ion distribution in the diffuse double layer, as a function of the electrolyte content of the bulk solution, demonstrates that the diffuse counter-ion atmosphere is compressed toward the surface when the bulk electrolyte concentration is increased (Figure 2-2). The degree of compression of the double layer is governed by the concentration and valence of the ions of the opposite sign from that of the surface charge, while the effect of ions of the same sign is comparatively small. At higher concentration and higher valence of the counter-ions, the double layer is more compressed.
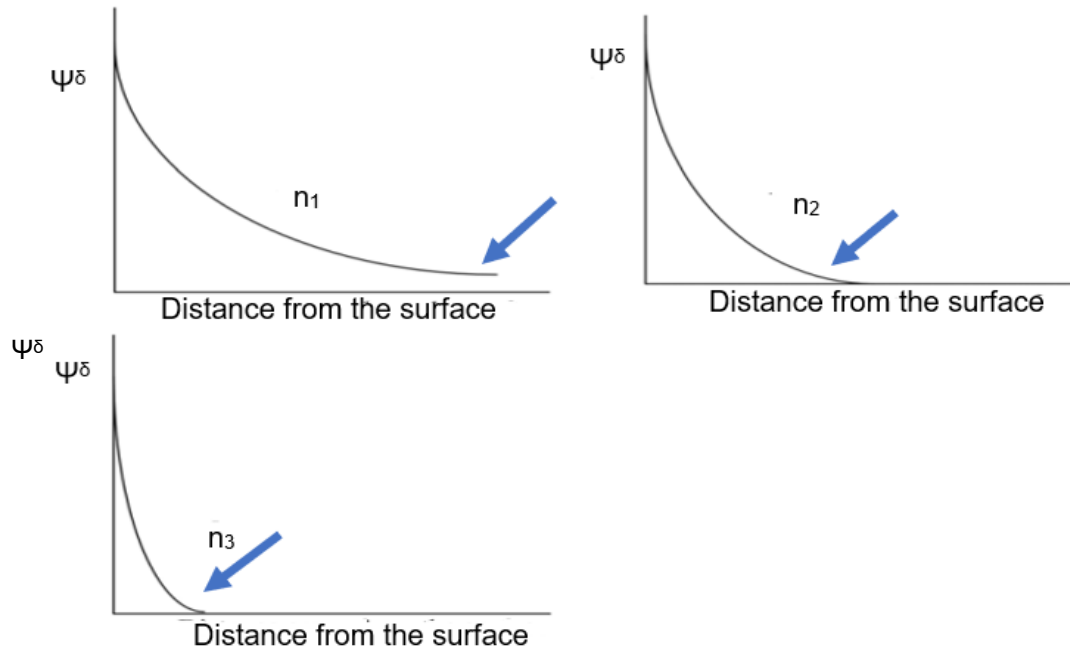
Figure 2-2: **Adapted compression of the double layer under the effect electrolyte n_1 $<n_2<n_3$. n_1, n_2, n_3 – electrolyte concentration.**

2.6 Interaction between particles

Depending on the surface properties of the particles, different types of interactions between particles happen in suspension. These interactions can result in forces of either attraction or repulsion. If attractive forces dominate, then the particles stick together and form aggregates. Particles that repel each other with dominant repulsive forces prevent the process of aggregation. The particles are stable in the latter case, whereas when aggregation forms, the resulting particles are unstable or become destabilized.

2.6.1 Repulsion

When two particles approach each other in suspension in Brownian motion, their diffuse counter-ion atmospheres begin to interfere. This interference changes the distribution of the ions in the double layer of both particles, increasing the free energy of the system. The amount of work required to bring the particles from infinite separation to a given distance can be calculated as the repulsive energy or the repulsive potential at the given distance. When the repulsive potential, VR, is plotted as a function of distance, a "potential curve" is acquired. The repulsive potential decreases exponentially with increasing particle separation. In Figure 2-3, three potential curves

for three different electrolyte concentrations of the same particles are indicated by "low," "medium," and "high," as an indicator of the electrolyte concentrations. Because the double layer starts compressing at increased electrolyte concentrations, the range of the repulsion is considerably reduced (Van Olphen, 1977).
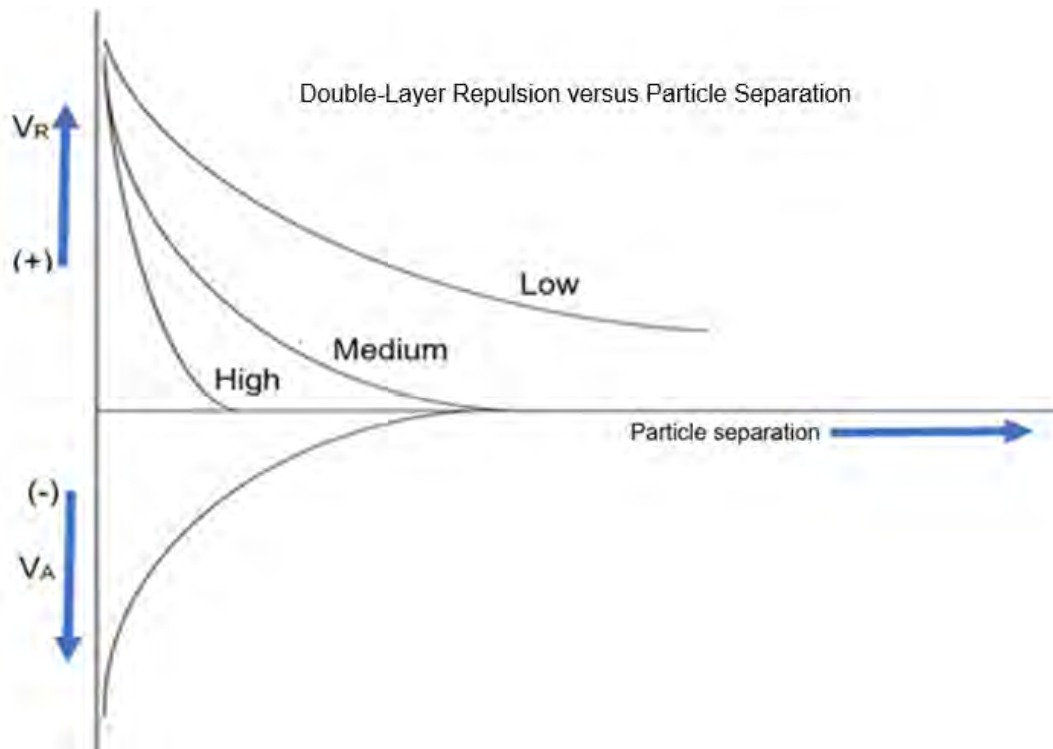
Figure 2-3: **Adapted repulsive and attractive energy as a function of particle separation (low, medium, high).**

2.6.2   The van der Waals attraction

Between all atoms and molecules, there are attractive forces of various types, which J.D. van der Waals postulated in 1873 to account for the non-ideal behavior of real gases. If the molecules are polar (i.e., with an uneven distribution of charge), then the attraction between dipoles becomes important. If only one of the interacting molecules has a permanent dipole, then this molecule can induce an opposite dipole in a nearby molecule, thus giving an attraction. Even when the atoms or molecules are nonpolar, the movement of electrons around nuclei cause fluctuating dipoles, which induce dipoles in other molecules, resulting in an attractive force. From the viewpoint of colloid stability, this is the most significant of the intermolecular interactions. It is a quantum-mechanical effect, which was first recognized by Fritz London in 1930, and the resulting

forces are sometimes known as London-van der Waals forces. Additionally, they are also known as dispersion forces because the fundamental electron oscillations involved are also responsible for the dispersion of light (Gregory, 2006).

The phenomenon of flocculation reveals the existence of interparticle attractive forces. Obviously, to compete successfully with the double layer repulsion that still exists under flocculating conditions, the attraction must be of comparable range and magnitude. The general van der Waals attractive forces appear to satisfy this requirement. Initially, it does not seem likely that the van der Waals forces would be large enough or far-reaching enough to satisfy the above-mentioned conditions, because they are small and decay rapidly with distance for a pair of atoms. However, the van der Waals attraction between atom pairs is additive; thus, the total attraction between particles containing a very large number of atoms is equal to the sum of all the attractive forces between all atoms present within both particles. The summation leads not only to a larger total force but also to a less rapid decay with increasing distance. For two atoms, the van der Waals attractive force is inversely proportional to the seventh power of the distance (or to the sixth power for the attractive energy), although for two large particles, the force is inversely proportional to the third power of the distance between the surfaces, and the attractive energy to the second power of that distance, approximately. In the lower part of Figure 2-3, the attractive energy (VA) is plotted as a function of particle separation. As mentioned before, the attraction remains practically the same when the electrolyte concentration of the medium is varied (Van Olphen, 1977).

The net potential curve of particle interaction is constructed simply by adding the attractive and repulsive potential at each particle separation, considering the attractive potential as negative and the repulsive potential as positive. Figure 2-4 (a, b, and c) shows the results of these additions for three electrolyte concentrations indicated as low, medium, and high. In constructing these three net potential curves, an additional force between the particles must be taken into consideration. This interaction is a repulsion of a very short range to which there are two possible contributions. The first of these contributions can be the "Born repulsion," which becomes effective as soon as extruding lattice points or regions come into contact, resisting the interpenetration of the crystal lattice. A second short-range repulsion is the result of specific adsorption forces between the crystal surface and the molecules of the liquid medium (such as water). Because of such adsorption forces, usually one or two monomolecular layers of water are held by the particle surface. For the

surface between the two particles to become less than the thickness of the adsorbed water layer on both particles, the absorbed water must be desorbed. The work required for this desorption appears to be short-range repulsion between the particles, which become appreciable at particle separations of the order of 1 nm or less. The short-range repulsion for the net interaction is represented by the steep rise of the potential curves at very small values for particle separations (Van Olphen, 1977).
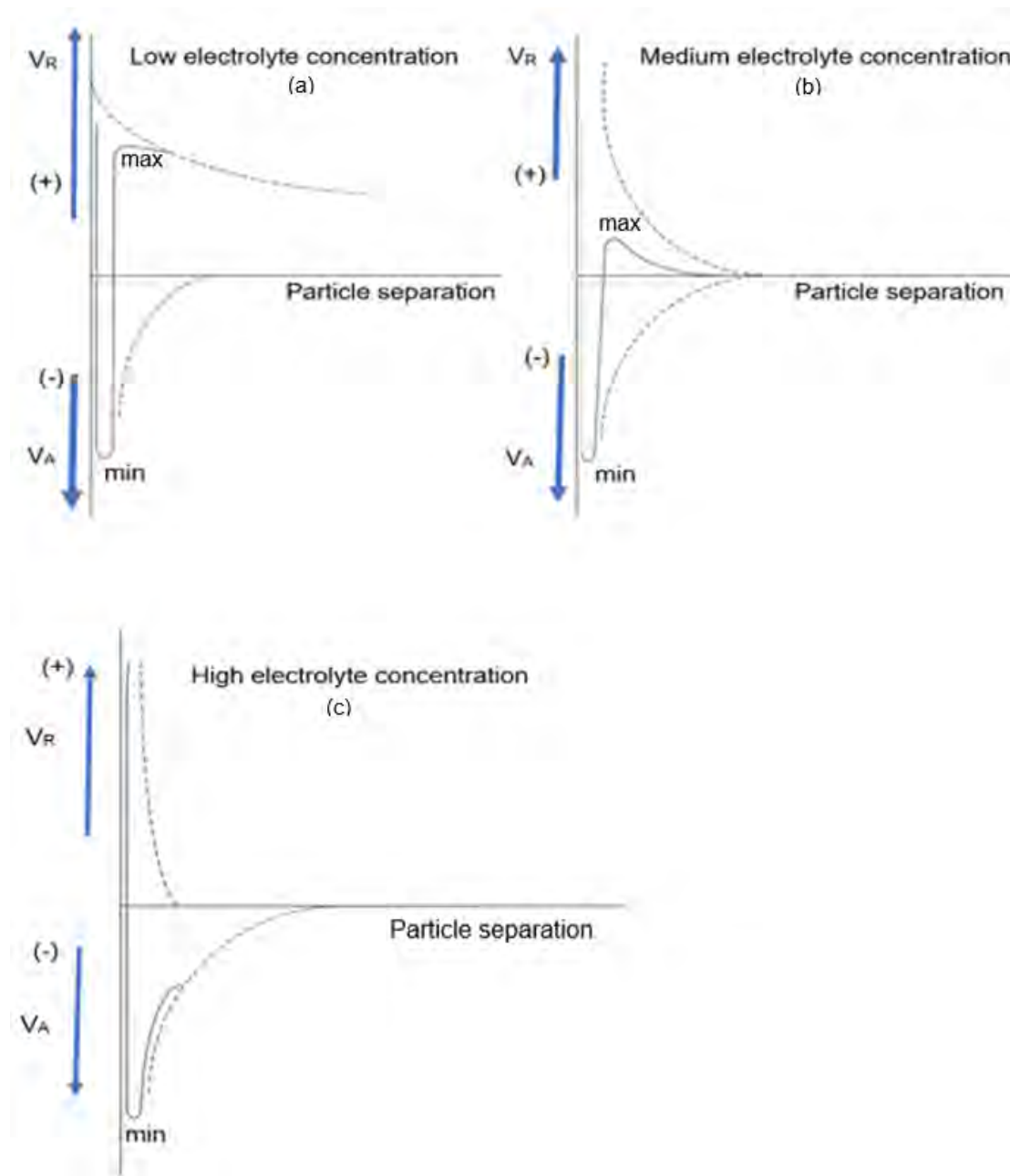
Figure 2-4: **Adapted net interaction curve as a function of particle separation (a) low, (b) medium, and (c) high.**

2.6.3 The net interaction curve and stability of a dispersed system

The net interaction curves for a low and a medium salt concentration have a minimum with predominant attraction at close approach and a maximum with predominant repulsion at greater distances. No such maximum is displayed by the curve for a high electrolyte concentration.

The interpretation of stability and flocculation in terms of the net potential curves of particle interaction is based on the following considerations:

- At a high electrolyte concentration, the potential curve shows a deep minimum only at close separation, and attraction predominates at any particle distance except at very close approach (Figure 2-4 c). If two particles approach each other in Brownian motion, they will agglomerate at the point at which they reach the position where the deep attraction minimum occurs. Particle agglomeration occurs at a maximum rate and the process is called rapid coagulation.

- If repulsion dominates part of the way during the mutual approach of the particles (curves for medium and low electrolyte concentration), the diffusion will be counteracted by the peripheral repulsive force field, and the rate of agglomeration will decrease. At medium electrolyte concentrations (Figure 2-4 b) the coagulation process is retarded by the long-range repulsion. Under these conditions, slow coagulation takes place. At very low electrolyte concentrations (Figure 2-4 a), the coagulation process is retarded to such an extent by the appreciable long-range repulsion that it may take weeks or months for coagulation to become perceptible. For all practical purposes, the system is called "stable" under these conditions.

2.6.4 Zeta potential

To this point, discussion has been about surface potential (ψo), Stern potential ($\psi \delta$), and potential at any point (ψ). There is another potential related to the electrokinetic property of the particles, called zeta potential (ξ). The zeta potential is the electric potential in the double layer at the interface between a particle that moves in an electric field and the surrounding liquid. The zeta potential is calculated from the electrophoretic mobility of the dispersed particles. Its magnitude is considered a measure of particle repulsion. Addition of the electrolyte usually causes the zeta

potential to decrease. At the flocculation value of the electrolyte (where rapid coagulation occurs), it is considered to have reached a critical value, below which the particle repulsion will no longer be strong enough to prevent coagulation. The seat of the zeta potential is the shearing plane or slipping plane between the bulk liquid and an envelope of water that moves with the particle. Zeta potential is not equal to the surface potential but is somewhat comparable, but not identical, to the Stern potential. Figure 2-5 shows a sketch of the structure and the potential profile in a double layer of a flat surface.

The efficiency and control of coagulation or flocculation steps in large-scale solid-liquid separation (either thickening or clarification) operations can be accomplished by routine measurement of zeta potentials and so-called "zeta potential control" (Riddick, 1968 as cited in Hunter, 1981). Zeta potential measurements are usually used to follow the turbidity removal of wastewater.
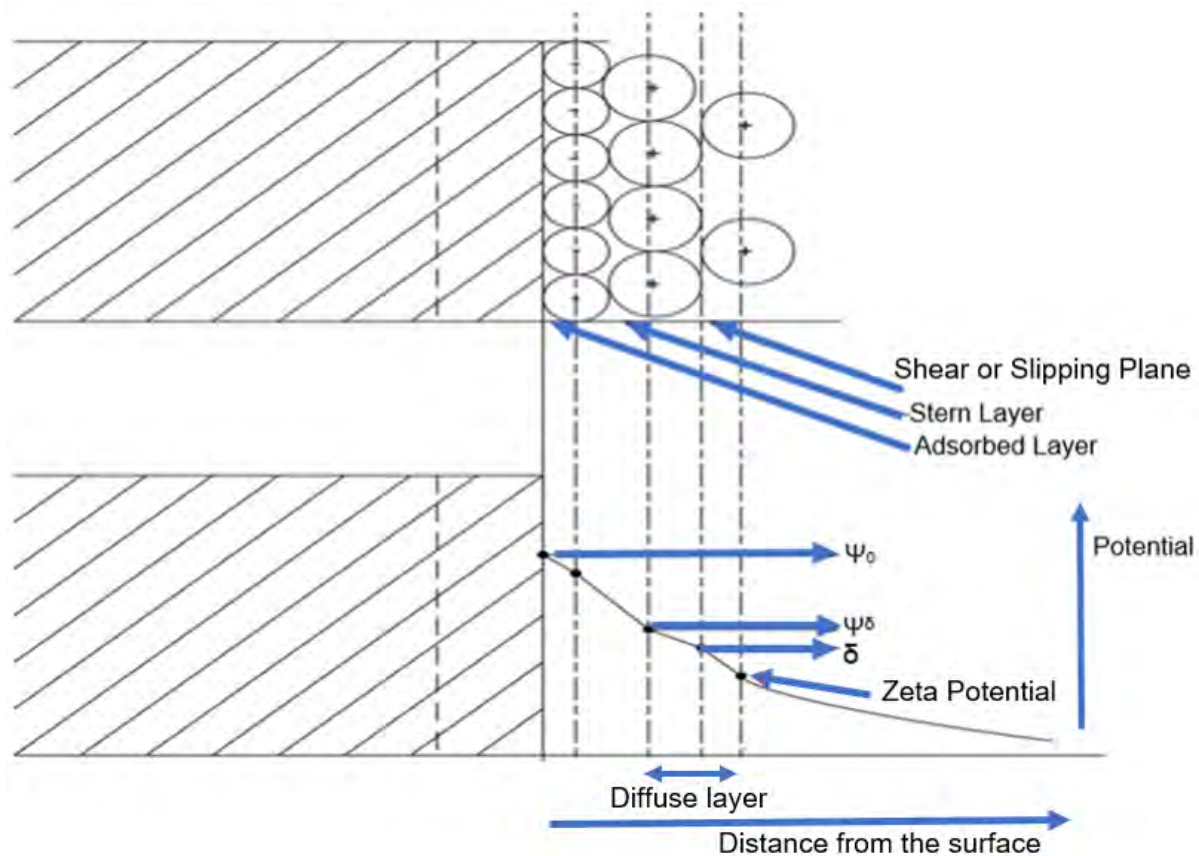
Figure 2-5: **The structure and the potential profile in a double layer of flat surface (adapted from Demirci, 1973).**

The concentration of potential-determining ions at which the zeta potential is zero is called the isoelectric point. The isoelectric point is determined by electrokinetic measurements. The surface charge is zero at the point of zero potential. The zeta potential refers to the hydrodynamic interface while the surface charge is defined for the solid-liquid interface (Butt et al., 2003).

2.6.5 Coagulation

Coagulation is an essential process in water and wastewater treatment. In the area of potable water treatment, clarification of water with coagulating agents has been practiced since ancient times, using a variety of substances—the most notable among them being crushed seeds. The Egyptians, as early as 2000 BC, used almonds smeared around a vessel to clarify river water. The early Romans were also familiar with alum, although it may not have been used for water treatment (Bratby, 2006). Nevertheless, its use as a coagulant by the Romans was mentioned in ca. 77 AD. By 1757, alum was used as a coagulant in water treatment in England, and more formally for the treatment of public water supplies in 1881 (Faust et al., 1998 as cited in Bratby, 2006). In modern water treatment processes, coagulation and flocculation are still essential steps.

Coagulation is the process of destabilizing colloids, aggregating them, and binding them together for ease of sedimentation. Coagulation is achieved by adding simple salts or by charge neutralization, resulting in a tendency in the aggregates (coagula) to be small and dense. Flocculation is limited to the cases where polymer bridging is the dominant mechanism and aggregates (flocs) tend to be larger and more open in structure. Larger structures tend to be more open and less dense. The distinction between small, compact coagula and larger, less dense flocs is an inevitable result of the stronger interparticle binding in the case of polymers, causing larger aggregates. In the area of water and wastewater treatment, coagulation refers to destabilization by dosing of appropriate additives, and flocculation refers the formation of aggregates usually by some form of fluid motion. This corresponds to the two stages shown in Figure 2-6 and could be considered chemical and physical aspects of the aggregation process (Gregory, 2006).
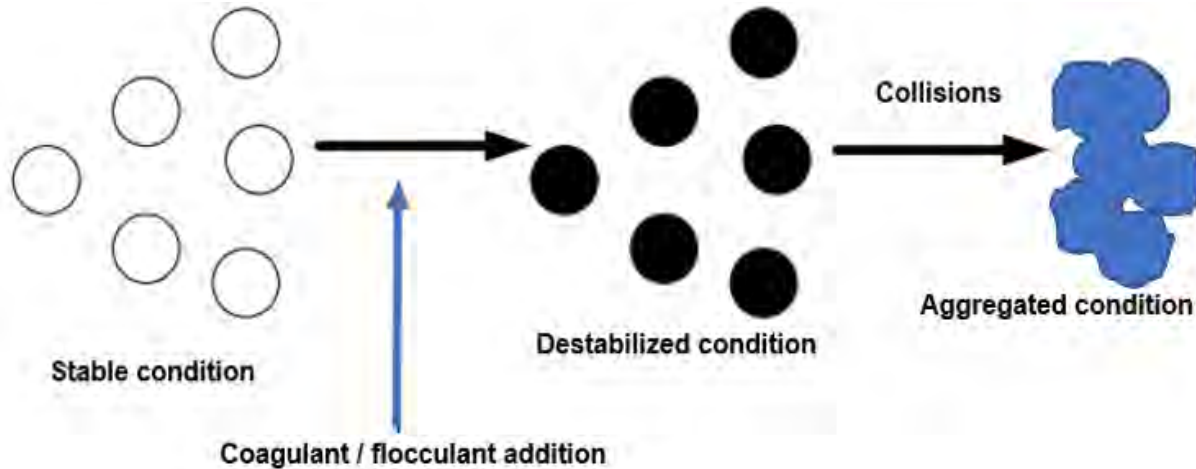
Figure 2-6:   Adapted sketch for destabilization and aggregation of particles.

The additives used to cause destabilization of colloids may be called coagulants or flocculants, depending on their mode of action. Coagulants could be inorganic salts, including those containing specifically adsorbing counter-ions, and flocculants could be long-chain polymers, which give bridging interactions. Although there are potentially many different types of destabilizing agents, the vast majority of those used in practice can be divided into two categories:

- Hydrolyzing metal coagulants.

- Polymeric flocculants (anionic and cationic).

The most widely used coagulants are based on aluminum and ferric salts. Originally their action was thought to be a result of the trivalent nature of the metals, giving Al^{3+} and Fe^{3+} ions in solution, which are expected to be very effective in destabilizing negatively charged colloids. They are effective in removing a broad range of impurities from water including colloidal particles and dissolved organic substances. Their mode of action is generally explained in terms of two distinct mechanisms:

- Charge neutralization of negatively charged colloids by cationic hydrolysis products.

- Incorporation of impurities in an amorphous hydroxide precipitate, sweep flocculation (Duan et al., 2003).

The relative importance of these mechanisms depends on factors such as pH and coagulant dosage.

Hydrolyzing coagulants have been applied routinely since the early twentieth century, and they play a vital role in the removal of many impurities from polluted waters. These impurities include inorganic particles such as clays, pathogenic microbes, and dissolved organic natural matters. Aluminum sulfate, ferric chloride and ferric sulfate are the most common additives (Duan et al., 2003).

Nearly all colloidal impurities in water are negatively charged and, therefore, may be stable due to electrostatic repulsion. Destabilization can be achieved by either adding relatively large amounts of salts, or by adding smaller quantities of cations that interact with negative colloids, thus neutralizing their charge. Highly charged cations such as Al^{3+} and Fe^{3+} should be more effective in this respect. However, over the normal range of pH values in natural waters (5 to 8), these simple cations are not found in significant concentrations because of hydrolysis, which results in a range of products (Duan et al., 2003). Figure 2-7 shows the hydrolysis of Al^{3+}.
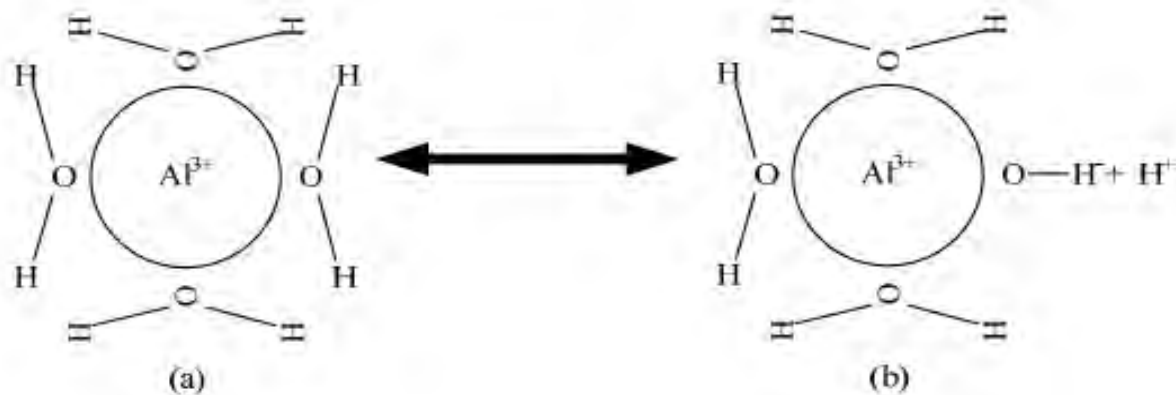
Figure 2-7: **Adapted hydrolysis of Al^{3+}. (a) Hydrated aluminum cation (only 4 of 6 water molecules shown), (b) After loss of H^+ to give $Al(OH)^{2+}$ (Gregory, 2006).**

If, for simplicity, water molecules in the hydration shell are omitted, different products of hydrolysis reactions can be given as follows:

$$Al^{3+} \rightarrow Al(OH)^{2+} \rightarrow Al(OH)_2{}^+ \rightarrow Al(OH)_3 \rightarrow Al(OH)_4{}^-$$
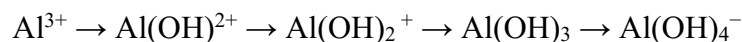
The uncharged hydroxide $Al(OH)_3$ has very low solubility in water and is likely to form a precipitate over a certain range of pH. This precipitation is important in the action of hydrolyzing metal coagulants.

All these hydrolyzed metal species can interact with different types of pollutants, achieving their removal from the medium of interest. These interaction processes are strongly related to the metal speciation, and they can be summarized into three main types:

- The metallic ionic monomeric species can neutralize the charge of the pollutants by adsorption on their surfaces (or by binding to their ionized groups).

- The metallic ionic polymeric species can bind to several particles (or molecules) of pollutant at a time.

- The pollutants can be enmeshed into growing metallic hydroxide precipitates or can be adsorbed onto their surfaces (Canizares et al., 2009).

The mechanism of coagulation of suspensions by hydrolyzing metal salts is closely related to the adsorption of dissolved hydrolysis products at low coagulant concentration, as well as the precipitation of the metal hydroxide at high concentrations. Coagulation depends on the charge of these dissolved species or the colloidal properties of the precipitate. At low concentrations, and at pH 6–7, adsorption of highly charged hydrolyzed species has a strong effect on the particle charge (Ching et al., 1994; Duan 1997 as cited in Gregory et al., 1998). At high coagulant concentration, the flocculation of colloids will depend on the aggregation of primary hydroxide precipitates that is dependent on the pH and coagulant concentration (Duan, 1997 as cited in Gregory et al., 1998).

The action of hydrolyzing coagulants is often discussed in terms of four concentration regions (Stumm et al., 1996):

- Very low coagulant dosage; particles are negatively charged and colloidally stable; no coagulation.

- Coagulant dosage is sufficient to give charge neutralization; particles are destabilized; coagulation occurs.

- Coagulant dosage is higher, giving excess adsorption, charge reversal, and re-stabilization.

- Coagulant dosage is still higher; hydroxide precipitation or "sweep flocculation".

2.6.6   Tailings basin water management

The purpose of this literature review on water management is to highlight that the implementation of existing and new approaches to tailings management could help eliminate the risks posed by conventional deposition of poorly thickened tailings behind dams, and possibly remove the risks altogether. The key features and requirements of the GISTM and the accompanying guides focus on a comprehensive range of alternatives to the conventional deposition of slurry tailings behind dams.

An important objective of effective tailings management is to protect the environment. Because the main pathway for contaminants is by water, the water balance is a very important element in any tailings management strategy. The operator of a tailings basin must always have a good understanding of the status of the pond and should be able to react quickly to unsafe situations that could adversely impact the environment (Welch et al., 1995). Problems arise when:

- There is a prolonged period of greater-than-average precipitation.

- Extreme flood events occur.

- Discharge slurry density or recirculation decrease.

- Water quality deteriorates.

- Waterways and treatment plants are undersized.

- A basin is not operated as designed.

A tailings basin is a living facility that changes with time as tailings are deposited. It is relatively easy to effectively contain the tailings solids, but the effluent must be safely passed through the system in a never-ending stream, either to the environment or recycled to the plant. The management of a tailings facility is primarily a water management problem, and it is extremely important to be able to predict the possible range in flows with a high degree of confidence.

With respect to a tailings basin, a simple definition of a wet climate is when there is a net annual accumulation of water (net inflow) that must be discharged to the environment to keep the basin in balance on an annual basis. The same principles also pertain to dry climates; however, the goals might be different. For example, in a wet climate, seasonal changes usually have a large impact on a balance, whereas in dry climates, water conservation always has a high priority, and it is important to minimize evaporation and seepage losses.

In a wet climate, where water is discharged to the environment on an annual basis, costs and environmental impacts are directly related to the quantity of water (effluent) that is treated and released. For such conditions, inflows can be minimized by:

- Keeping the watershed as small as possible to minimize the inflow from run-off.

- Providing large ponds to promote evaporation.

- Maintaining a high slurry density to minimize the inflow of process water.

- Maximizing the recirculation back to the plant to reduce the discharge to the environment and to minimize the use of fresh make-up water in the plant.

In extremely dry climates, total containment (zero discharge) is very easy to attain while evaporation and seepage loses must be minimized to encourage recirculation to the plant. In some in-between climate conditions, total containment may be possible by taking advantage of relatively higher evaporation than precipitation.

Some mine closure plans in arid climates rely on evaporation to maintain zero discharge to the environment. In other situations, permanent flooding is relied upon to inhibit the oxidation of potentially acid-generating tailings. Both situations require reliable, historical climatic data on which to make long-term predictions.

It is essential that all the parties concerned in the design, approval, and operation of a tailings facility understand that a tailings basin does not have a single, unique water balance because the input parameters can vary daily, monthly, and yearly. Average, base case conditions seldom actually occur. Precipitation and evaporation can be significant variables and often they are not well defined in remote regions because of the scarcity of historical records. Evaporation varies as the surface area of the ponds and wetted tailings changes. Seepage can only be approximately estimated unless a detailed hydrogeological investigation and analysis has been carried out. Recirculation to the plant is frequently a moving target, the discharge slurry density can vary depending on the operation of the plant and the changing plant rate. A tailings basin balance should be:

- Simple to use with data inputted in easily recognizable terms.

- Transparent and easy to understand, scrutinize, and criticize.

- Easy to vary the input parameters to model changes in operating and climate conditions.

- Able to carry out sensitivity analyses.

- Capable of being used by mine personnel and regulators as an operating (monitoring) tool during the life of tailings facility.

The water retained in the pore space of the tailings, or "water content" in the traditional soil mechanics sense, is the ratio of the weight of water over the dry weight of tailings. If the tailings are saturated, then the water content can be simply calculated as follows:

$$W = (\rho_w/\rho_d) - 1/G_s)100 \text{ or } w = (e/G_s)100$$

where: w = saturated water content (%); ρ_d = dry density of tailings; G_s = specific gravity of tailings; ρ_w = density of water (unity in the metric system); e = void ratio (vol. of voids / vol. of solids).

The dry density (or corresponding void ratio) used to calculate the saturated water content can have a significant impact on a water balance. Void ratio and density are functions of specific gravity. It is not always a simple matter to choose a realistic density. Tailings dry density depends on many factors such as specific gravity of solids particles, gradation, content of clay, gypsum and precipitates, ice inclusions in cold climates, degree of consolidation (due to self-loading), and the

distance and depth from the discharge point. Some average value must be used for design. A few general recommendations are given below:

- If the tailings are relatively coarse grained and do not contain clay minerals, then consolidation, after initial liquid/solids separation, will be relatively minor and occur quickly. In this case, most of the water squeezed out of the tailings by consolidation (due to self-loading) will end up in the pond in a relatively short period of time and, therefore, the ultimate assumed dry density can be used to calculate the water retained without introducing a significant inaccuracy in the water balance. Typical dry densities for this case might range between 1.3 and 1.4 t/m^3 for tailings with a specific gravity in the 2.7 range.

- If the tailings are finely ground and/or contain clay, gypsum, or other precipitates, then consolidation will take place more slowly and may not be completed until long after the basin has been decommissioned. In this case, a density lower than the ultimate dry density should be used for the water balance computations. This can be estimated by laboratory testing to determine the initial density and the rate at which water will be liberated by the consolidation process.

- In extremely dry climates, there can be high evaporative losses on exposed beaches that cannot be recovered. In this case, a low dry density should be used, typically in the 1.0 t/m^3 range because it does not matter to the balance whether the water is lost as evaporation or permanently kept in the pore spaces.

- In cold regions, process water that becomes entrapped as ice in the tailings mass may take years to thaw (or in permafrost regions it may never thaw). This can be modeled by increasing the saturated water content (or effectively decreasing the dry density) of the tailings. If all the discharge water, for example at a slurry density of 55% solids, is entrapped as ice, then the effective dry density could be in the 0.85 t/m^3 range.

- If a portion of a tailings mass is partially drained, then the average water content will be less than the saturated water content. The water content, in this case, must be arbitrarily reduced by estimation. This reduction is not a function of density.

2.7   Dispersion and flocculation behaviors of quartz and kaolinite particles

The analyzed FFT was pH 8 and, therefore, is predominantly composed of particles which are negatively charged and exhibit dispersive hydrophilic behavior.

Quartz particles

As mentioned above, quartz particles have negatively charged surfaces at pH > 2. This negative surface charge is enough to cause quartz particles to exist in a dispersed state by the action of the electrostatic repulsive forces (Verwey et al., 1948). These forces are affected by the ionic strength of the soil-water ionized system, which depends on the pore solution electrolyte concentration, ion types, and pH. Hydrolyzed metal ions, such as calcium and aluminum, play an important role in FFT dispersion and flocculation behaviors because they adsorb onto the particle surfaces and reduce the double layer charge to near zero. Additionally, the effect of hydrolyzed metal ions on the anionic PAM flocculant plays an important role on the flocculation of quartz particles.

Adsorption of anionic PAM flocculant on quartz surfaces is strongly dependent on pH and salinity. The definition of salinity is the saltiness or/dissolved salts content (Ca^{2+}, Al^{3+}, Mg^{2+}, K^+, Na^+, HCO_3^{3-}, Cl^-, $SO4^{2-}$) of a body of water. The percentages of ionized (COO^-) and non-ionized (COOH) functional groups of an anionic PAM flocculant are presented in Table 2-1 as a function of pH (van Lierde, 1980). The ionization of anionic PAM flocculant is complete above pH 6, and at pH 5 is already higher than 50%. At low pH, where the ionization is low, the anionic PAM flocculant chains adsorb because non-ionized groups form intramolecular hydrogen bonds. However, at high pH these links are hindered by the lack of non-ionized groups and by the presence of the various negatively charged carboxylate groups favoring chain extension.

Table 2-1:   Ionization of anionic PAM flocculant vs. pH.

pH	COO^- (%)	COOH (%)
3.5	8	92
4.0	18	82
4.5	39	61
5.0	56	44
5.5	75	25
6.0	91	9
6.5	97	3
7.0	99	1

At pH above 6.5, quartz particles present highly negative surface charges and consequently are in a dispersed state. The presence of anionic PAM flocculant does not modify this behavior because the completely ionized flocculant chains cannot be adsorbed on the negative mineral surface (Kuzkin et al, 1964; Fontana, 1961). When pH is lowered to values between 4.5 and 6.5, electrical repulsive forces between anionic PAM flocculant and quartz soil particles are reduced through the partial dissociation of the anionic PAM flocculant and the lowering of the zeta potential of quartz soil particles. Adsorption of the anionic PAM flocculant becomes possible through the hydrogen bonds between the COOH groups of the flocculant and the silanol groups of quartz, resulting in poor flocculation (Healy, 1961; Fontana, 1961; Healy et al., 1964; Slater et al., 1968). The behavior of quartz suspensions in the presence of both calcium ions and anionic PAM flocculant requires the consideration of the interactions of calcium ions on the quartz surfaces, as well as the interactions between these ions and the flocculant chains. At high pH values, anionic PAM flocculant acts as added volume of elements of high charge density, attracting counter-ions (Ferry et al., 1962). At low pH (4.5 to 6), adsorption of calcium ions onto the quartz particles is small and the zeta potential of the quartz becomes less negative when the calcium concentration increases, improving the adsorption of the anionic PAM flocculant. This adsorption occurs mainly through the hydrogen bonds at the OH sites of the quartz particles. At slightly acidic or basic pH (6.5 to 8.5) the adsorption of calcium on quartz particles can considerably reduce the zeta potential of the quartz particles, allowing the adsorption of the extended flocculant chains by carboxylate bonds (Usoni et al., 1968).

Kaolinite particles

In the presence of calcium ions, the zeta potential of kaolinite particles remains at a constant value of -15 mV at pH ≥ 4. Calcium alone has only a small effect on kaolinite coagulation (Atesok, 1988). The adsorption of anionic PAM flocculant onto the kaolinite particles is strongly dependent on the pH and salinity of the pore water. While kaolinite surfaces are negatively charged in media such as water, they exhibit positive surface charge characteristics at pH < 3 in a solution of calcium ions and at pH 9.2 in a solution of aluminum ions (Peng, et al., 1994). Kaolinite particles show large positive zeta potential values in the presence of aluminum ions (Peng, et al., 1994). In contrast, kaolinite particles maintain a near constant value (-15 mV) at pH 4 or higher in the presence of calcium ions. As pH decreases below 4, the zeta potential increases, passing a point of

zero charge (PZC) at approximately pH 3. An excess of hydrolyzed metal ions (i.e., calcium and aluminum) used to coagulate negatively charged particles of kaolinite might cause the reversal of the double layer charge and lead to a stable suspension with positive double layer charge (Matijevic et al., 1966), which could suppress the kaolinite flocculation process. Different additives have various surface reactions with kaolinite particles, which can change the zeta potential of kaolinite. As pH increases, the hydroxyl ion can react with the surfaces of kaolinite, which will make the zeta potential more negative. Sulfate and bicarbonate ions can also adsorb onto the kaolinite particles and make the zeta potential more negative (Masliyah et al., 2011). The edge surface of kaolinite particles carries a net negative charge arising from the dissociated edge silanols. This negative charge density on the edge surfaces may explain the strong dependence on the pH and presence of cations for anionic PAM flocculant adsorption on kaolinite particles. Flocculation of kaolinite suspensions with anionic PAM flocculant are affected by of the flocculant's molecular weight and ionic charge. In addition, adsorption of anionic PAM flocculant on kaolinite particles is strongly dependent on pH and salinity (Pefferkorn, 1987). The suggested adsorption mechanism of anionic PAM flocculant on kaolinite particles is by hydrogen bonding. However, it is possible for anionic PAM flocculant to be attracted to the positively charged sites of kaolinite particles by electrostatic attraction. This electrostatic attraction may easily be overcome by the repulsive effect of the overall negatively charged kaolinite particles (Peng et al., 1994). The flocculation process of kaolinite particles can deteriorate as calcium concentration increases, similar to the previously described behavior of quartz particles. In addition, precipitation of calcium hydroxyl onto the kaolinite particles covers up the active functional groups of the anionic PAM flocculant, which prevents the formation of hydrogen bonding between kaolinite particles and anionic PAM flocculant.

2.8 Existing research on oil sands mature fine tailings flocculation behavior using flocculant only

Management and reclamation of large inventories of legacy and mature fine tailings (MFT) represent a continuing and significant challenge to surface mine operators in the Alberta Oil Sands because of the complex chemical and physical behavior of these tailings. Suncor's tailings recovery operations (TRO$_{TM}$) and Shell Canada's atmospheric fines drying use anionic polymers to flocculate MFT to remove fine tailings solids from aqueous suspension. Addition of

anionic PAM polymer to MFT results in the creation of a complex synthetic material: polymer-amended MFT (PAMFT).

Existing research investigating the fundamental properties and characteristics governing PAMFT dewatering will lead to a better understand of how these factors contribute to overall material behavior, including strength development and consolidation. This existing work confirms that the addition of anionic PAM polymer does little to change the zeta potential of the input raw MFT, because the resulting material is colloidally stable. The work also indicates how residual bitumen and fabric act independently and in combination to reduce the permeability of PAMFT and enable retention of water within the material's fabric, especially when it is stored in lifts that exceed the depth at which the combination of evaporative drying and underdrainage are effective.

This existing research indicates that the PAMFT fabric includes abundant micropores with tortuous flow paths and little connectivity between pores. The size and configuration of the pores effectively traps water within the PAMFT fabric. Residual bitumen may also block pore throats or form a hydrophobic barrier that limits the effectiveness of evaporation for material deposited below a depth of 15 cm in thick lift deposits. Residual bitumen may also prevent diffusion of trapped water upward through deposited material and contributes to the plasticity and compressibility exhibited by PAMFT when it is deposited in lifts thicker than 20 cm (Boxill, 2016).

Chapter 3 Key Laboratory Testing

3.1   Introduction

This chapter presents the key laboratory testing, findings, and processing methods used to accomplish the objectives of this research, as established in Chapter 1 (section 1.2.6), focusing on the physicochemical treatment recipe for the FFT that provides solids-water separation, dewatering, and fines agglomeration inline and the rationale for choosing geotextile tubes as a filtration process to accelerate dewatering and consolidation of the treated FFT to form stable reclaimed landforms.

3.2   Laboratory testing

Laboratory testing was performed to evaluate soil composition and engineering properties.

3.2.1   Mineralogy

The identification and quantification of FFT mineralogy is considered critical for the successful manipulation of clay and non-clay mineral behavior along with the pore water chemistry and pH. Bulk X-ray diffraction analysis (XRD), elemental analysis by X-ray energy dispersive spectrometry (EDS), and scanning electron microscopy (SEM) were performed to characterize the mineralogy of the analyzed FFT. Quantitative elemental analysis was performed by an Oxford INCA micro-analysis system attached to a JEOL JSM-6610 SEM. Mineralogy is the primary factor controlling the size, shape, and properties of soil particles, and these same factors determine the possible ranges of physical and chemical properties of any given soil. Prior knowledge of what minerals are in a soil provides insight into its behavior (Mitchell, 2005).

FFT is predominantly non-clay minerals (55.5% quartz <75 μm) and clay minerals (23.2% kaolinite and 11.6% illite <2 μm). Other mineral amounts such as microcline (highest), clinochlore, siderite, pyrite (lowest), anatase, rutile, albite, dolomite, and calcite add up to approximately 9.7% in total.

Quartz, which is a non-clay mineral, is the predominant mineral within the fine particle size fraction of the FFT used in this research. At pH > 2, quartz particles possess a negative charge, show dispersive behavior, and are more hydrophilic (van Lierde, 1980; Hunter, 1981; Hussain et al., 1996, and Gan et al., 2008). Kaolinite is a clay mineral with negatively charged surfaces at pH > 2 (Goldberg et al., 1991). The behavior of kaolinite particles is dependent on the SAR, electrolyte concentration, and pH. Illite is non-swelling in nature, has a lower cation exchange capacity than kaolinite, and is also pH and SAR dependent.

The key results of XRD, SEM, and elemental analysis are presented below, showing situations of the predominance of non-clay minerals (quartz) as well as situations with the predominance of clay minerals such as kaolinite. Three representative samples were selected for mineralogical analysis such as: Treated FFT at 20 wt.% solids (predominance quartz); Treated FFT at 15 wt.% solids (predominance quartz); and FFT with flocculant only (FFT) at 39 wt.% solids (predominance kaolinite).

The treated FFT at 20 wt.% solids (predominance quartz) – Quantitative elemental analysis was performed on treated FFT samples by an Oxford INCA micro-analysis system attached to a JEOL JSM-6610 SEM. The INCA system is designed to obtain standardless quantitative elemental analysis from rough samples by SEM. The INCA system has enhanced light element capabilities, and it is able to identify beryllium (Be) and quantify boron (B) and carbon (C). Figure 3-1 (lower left) shows the scanning electron photomicrograph of treated FFT at 20 wt.% solids (predominantly quartz); it consists of aggregates of angular, subangular, and subrounded clay- to medium-silt–sized particles. The upper left panel of Figure 3-1 illustrates the bulk sample. Oxygen (O) and silicon (Si) dominate the elemental spectrograph, respectively forming approximately 56.3% and 24.2% of the sample. Aluminum (Al) is common, forming approximately 11.3% of the sample. Carbon (C) is moderately abundant, forming approximately 2.6% of the sample. Trace to minor amounts of sodium (Na), magnesium (Mg), sulfur (S), chlorine (Cl), potassium (K), calcium (Ca), titanium (Ti), and iron (Fe) are present.

Figure 3-1: Treated FFT at 20 wt.% solids (predominantly quartz) quantitative elemental distribution.

The treated FFT at 20 wt.% solids (predominance quartz) generated a good quality diffractogram indicating the sample is mainly composed of crystalline compounds. XRD analysis shows the crystalline components of the sample mainly consist of approximately 96% silicates (quartz [SiO_2], kaolinite [$Al_2Si_2O_5(OH)_4$], illite [$(K,H_3O)Al_2Si_3AlO_{10}(OH)_2$], microcline [$KAlSi_3O_8$], albite [$NaAlSi_3O_8$], and clinochlore [$(Mg,Fe,Al)_6(Si,Al)_4O_{10}(OH)_2$]). Iron carbonate scale (siderite [$FeCO_2$]), calcium magnesium carbonate scale (dolomite [$CaMg(CO_3)_2$], calcite and magnesian [$(Ca,Mg)CO_3$]), and titanium oxide (anatase [TiO_2] and rutile [TiO_2]) each form approximately 1% of the sample. Minor volumes of calcium carbonate scale (calcite [$CaCO_2$]) and iron sulfide scale or corrosion products (pyrite [FeS_2]) occur in minor amounts.

Elemental analysis of the treated FFT at 20 wt.% solids (predominance quartz) also suggests the presence of non-crystalline carbon-, oxygen-, and aluminum-bearing compounds. Trace volumes of chlorine-bearing compounds were detected during elemental analysis.

Comparison of EDS and XRD results of the treated FFT at 20 wt.% solids (predominance quartz)– In many cases, the EDS weight percent calculation for some of the elements was different from the XRD weight percent calculation. EDS analysis identifies and quantifies elements present in both crystalline and non-crystalline components. XRD analysis only detects elements in crystalline compounds because only crystalline components of the sample diffract X-rays. XRD weight percent calculation, therefore, can only include those elements present in the crystalline compounds. It must be emphasized that each element identified by XRD analysis should also be detected by EDS; however, the reverse is not necessarily true. Note: hydrogen (H) cannot be detected in the EDS analysis.

Tables 3-1 and 3-2, and Figures 3-1 to 3-3 summarize the following comments regarding the comparison of EDS and XRD results. The treated FFT at 20 wt.% solids (predominance quartz) showed a moderate to good correlation between the XRD and EDS results. A moderate difference with respect to silicon was found in the sample.

- Silicon was measured at 24.18% in the elemental analysis, while XRD analysis detected 34.80% silicon.

Minor differences with respect to carbon, oxygen, and aluminum were noted in the sample:

- In the elemental analysis, carbon formed 2.61% of the sample, while 0.32% carbon was detected in XRD analysis.

- EDS analysis detected 56.25% oxygen, while XRD analysis detected 52.36% oxygen.

- In the elemental analysis, aluminum forms 11.25% of the sample, while 7.75% aluminum was detected in XRD analysis.

The treated FFT at 20 wt.% solids (predominance quartz) EDS results for carbon, oxygen, and aluminum are greater than the XRD results, indicating the presence of non-crystalline carbon-, oxygen-, and aluminum-bearing compounds. The XRD result for silicon is greater than the EDS result, indicating this element occurs in well-crystalline compounds.

The X-ray beam scans an area of approximately 250 mm^2; however, the electron beam in the EDS that generates the elemental analysis scans a much smaller area of approximately 6 mm^2. Despite attempts to obtain the elemental analysis from the most representative area of the sample,

the irregular distribution of the materials in the sample might have skewed the EDS results in some instances.

Apparent differences in the elemental weight percent calculation of the above-mentioned elements are a function of:

1) The presence of non-crystalline components in the sample.

2) The difference in the area analyzed by each method.

Table 3-1: **Comparison of elemental composition by EDS and XRD analysis of the treated FFT at 20 wt.% solids (predominance quartz).**

Sample 1	H	C	O	Na	Mg	Al	Si	S	Cl	K	Ca	Ti	Fe
EDS analysis	-	2.61	56.25	0.18	0.61	11.25	24.18	0.36	0.04	1.93	0.30	0.40	1.88
XRD analysis	0.50	0.32	52.36	0.11	0.33	7.75	34.80	0.11	-	1.54	0.52	0.84	0.83
Hydrogen (H); Carbon (C); Oxygen (O); Sodium (Na); Magnesium (Mg); Aluminum (Al); Silicon (Si); Sulfur (S); Chlorine (Cl); Potassium (K); Calcium (Ca); Titanium (Ti); Iron (Fe);													

Table 3-2: **EDS and XRD results of the treated FFT at 20 wt.% solids (predominance quartz).**

ELEMENTS:	DOMINATE: O, Si COMMON: Al	MODERATE: C MINOR-TRACE: Na, Mg, S, Cl, K, Ca, Ti, Fe
COMPOUNDS:		
Formula	*Name*	*Percentage*
SiO_2	Quartz	55.5%
$Al_2Si_2O_5(OH)_4$	Kaolinite	23.2%
$(K,H_3O)Al_2Si_3AlO_{10}(OH)_2$	Illite	11.6%
$KAlSi_3O_8$	Microcline	3.2%
$NaAlSi_3O_8$	Albite	1.3%
$(Mg,Fe,Al)_6(Si,Al)_4O_{10}(OH)_2$	Clinochlore	0.8%
$FeCO_3$	Siderite	1.0%
$CaMg(CO_3)_2$	Dolomite	0.9%
$(Ca,Mg)CO_3$	Calcite, magnesian	0.5%
TiO_2	Anatase	0.7%
TiO_2	Rutile	0.7%
$CaCO_3$	Calcite	0.4%
FeS_2	Pyrite	0.2%

The treated FFT at 20 wt.% solids (predominance quartz) generated a good quality diffractogram, indicating it is composed mainly of crystalline compounds. XRD analysis shows the crystalline components of the sample mainly consisted of silicates (approximately 96%). Iron carbonate scale, calcium magnesium carbonate scale, and titanium oxide each form approximately 1% of the sample. Calcium carbonate scale and iron sulfide scale or corrosion products occur in minor amounts. Elemental analysis also suggests the presence of non-crystalline carbon-, oxygen-, and aluminum-bearing compounds. Trace volumes of chlorine-bearing compounds were detected during elemental analysis.
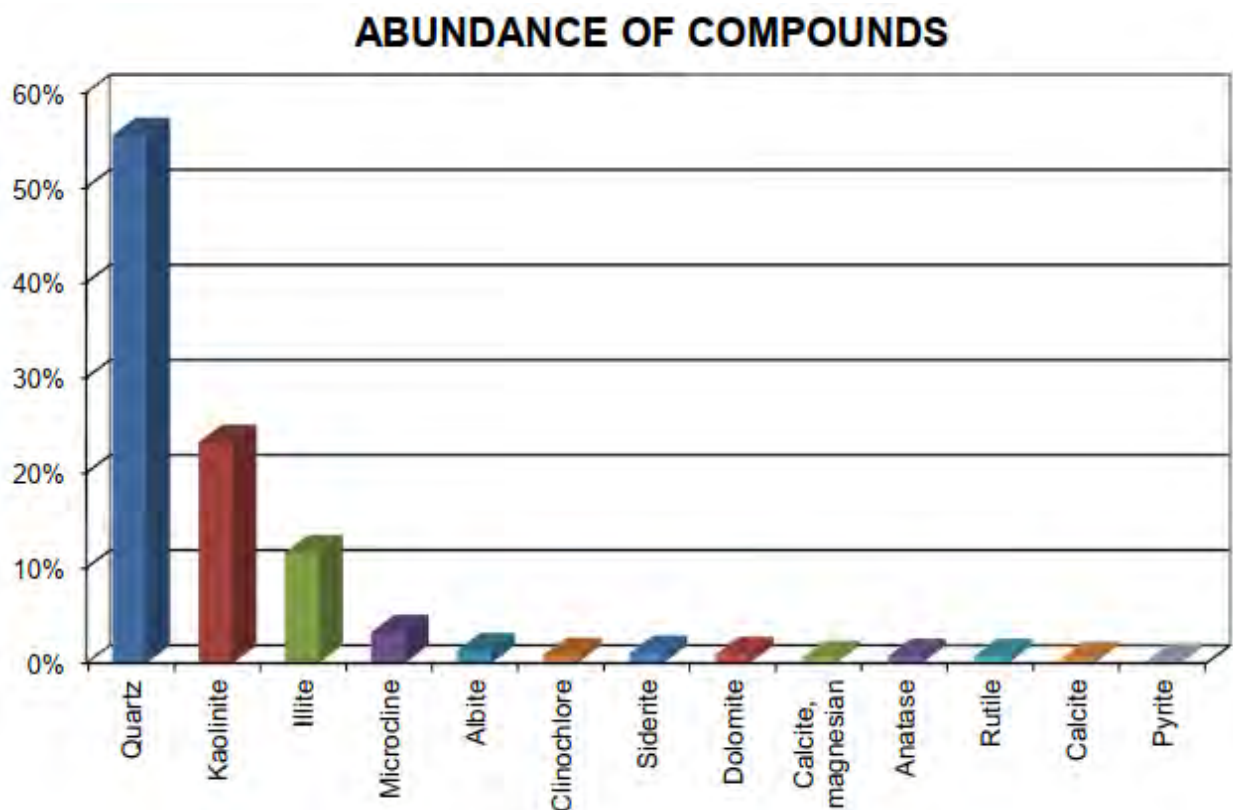
Figure 3-2: **Abundance of compounds of the treated FFT at 20 wt.% solids (predominance quartz).**
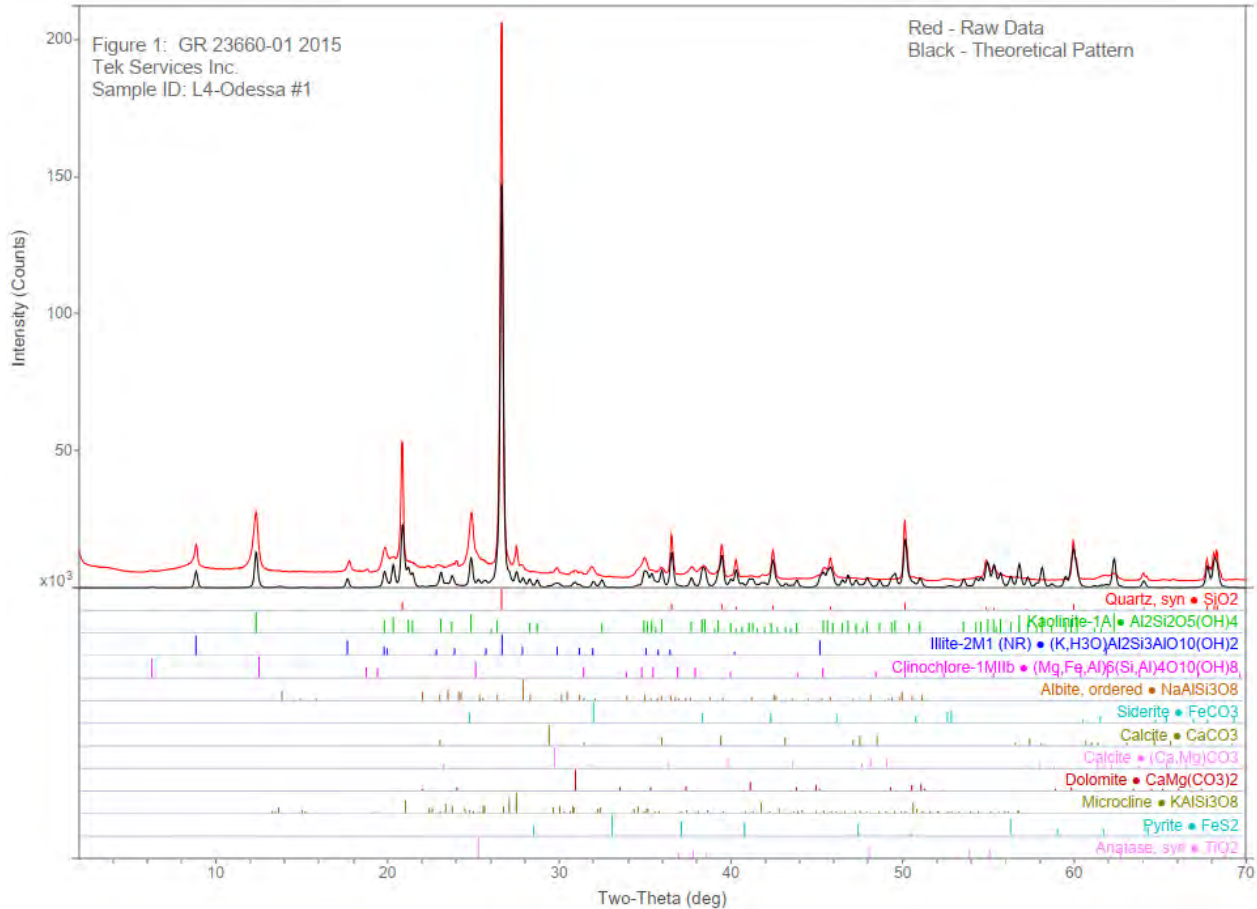
Figure 3-3: Elemental spectrograph of the treated FFT at 20 wt.% solids (predominance quartz).

The treated FFT at 15 wt.% solids (predominance quartz) – This sample generated a good quality diffractogram indicating the sample is mainly composed of crystalline compounds. XRD analysis shows the crystalline components of the sample consist of approximately 85% silicates (quartz [SiO_2], kaolinite [$Al_2Si_2O_5(OH)_4$], illite [$(K,H_3O)Al_2Si_3AlO_{10}(OH)_2$], microcline [$KAlSi_3O_8$], and albite [$NaAlSi_3O_8$]), 4% iron carbonate scale (siderite [$FeCO_3$]), 4% iron sulfide scale or corrosion products (greigite [Fe_3S_4] and pyrite [FeS_2]), 2% titanium oxide (anatase [TiO_2] and rutile [TiO_2]), 2% salt (halite [$NaCl$]), 1% copper oxide corrosion products (tenorite [CuO]), 1% calcium magnesium carbonate scale (dolomite [$CaMg(CO_3)_2$]), and 1% calcium carbonate scale (calcite [$CaCO_3$]).
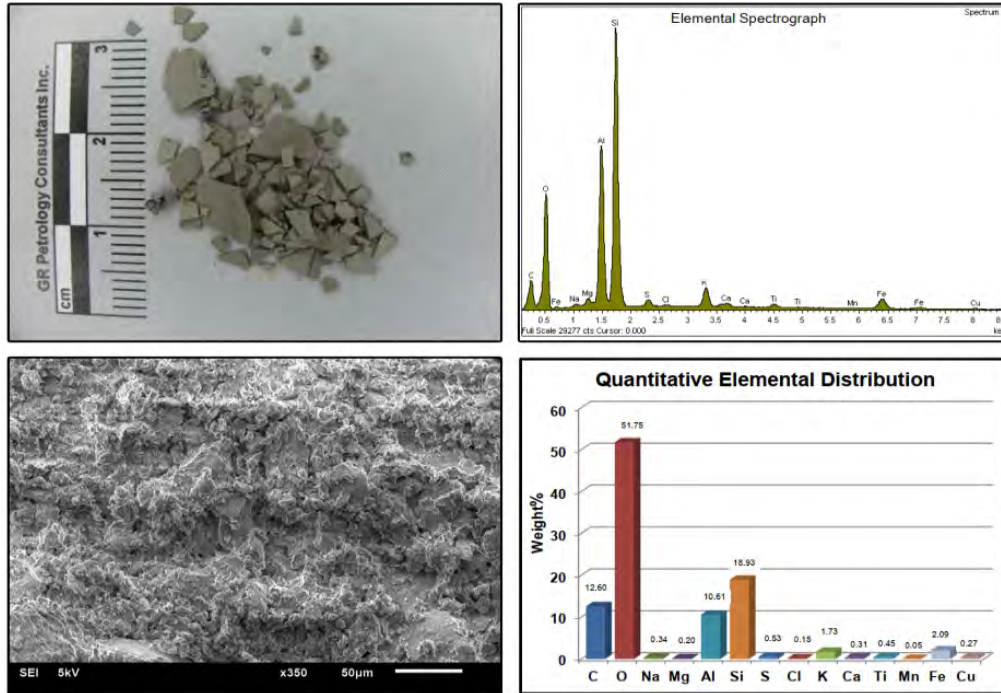
Figure 3-4: **Treated FFT at 15 wt.% solids (predominance quartz) quantitative elemental distribution.**

Elemental analysis of the treated FFT at 15 wt.% solids (predominance quartz) also suggests the presence of non-crystalline carbon- and oxygen-bearing compounds. Trace volumes of manganese-bearing compounds were detected during elemental analysis.

Tables 3-3 and 3-4, and Figures 3-4 to 3-6 summarize the following comments regarding the comparison of EDS and XRD results of the treated FFT at 15 wt.% solids (predominance quartz). The sample showed a good correlation between the XRD and EDS results. Moderate differences with respect to carbon and silicon were found in the sample.

- Carbon was measured at 12.60% in the elemental analysis, while XRD analysis detected 0.59% carbon.

- In the elemental analysis, silicon forms 18.93% of the sample, whereas XRD analysis calculated silicon to be 28.95%.

Minor differences with respect to oxygen and iron were found in the sample.

- EDS analysis detected 51.75% oxygen, while 49.12% oxygen was detected in XRD analysis.

- Iron represents 2.09% in the EDS analysis, while XRD analysis detected 4.19% iron. The EDS results for carbon and oxygen are greater than the XRD results, indicating the presence of non-crystalline carbon- and oxygen-bearing compounds. The XRD results for silicon and iron are greater than the EDS results, indicating these elements occur in well-crystalline compounds.

Table 3-3: **Comparison of elemental composition by EDS and XRD analysis of the treated FFT at 15 wt.% solids (predominance quartz).**

Sample 2	H	C	O	Na	Mg	Al	Si	S	Cl	K	Ca	Ti	Mn	Fe	Cu
EDS analysis	-	12.60	51.75	0.34	0.20	10.61	18.93	0.53	0.15	1.73	0.31	0.45	0.05	2.09	0.27
XRD analysis	0.60	0.59	49.12	0.74	0.11	8.64	28.95	1.99	0.97	1.19	0.45	1.50	-	4.19	0.96
Hydrogen (H); Carbon (C); Oxygen (O); Sodium (Na); Magnesium (Mg); Aluminum (Al); Silicon (Si); Sulfur (S); Chlorine (Cl); Potassium (K); Calcium (Ca); Titanium (Ti); Manganese (Mn); Iron (Fe); Copper (Cu)															

Table 3-4: **EDS and XRD results of the treated FFT at 15 wt.% solids (predominance quartz).**

ELEMENTS:	DOMINATE: O COMMON: C, Al, Si	MODERATE: Fe MINOR-TRACE: Na, Mg, S, Cl, K, Ca, Ti, Mn, Cu
COMPOUNDS:		
Formula	*Name*	*Percentage*
SiO_2	Quartz	41.2%
$Al_2Si_2O_5(OH)_4$	Kaolinite	30.8%
$(K,H_3O)Al_2Si_3AlO_{10}(OH)_2$	Illite	9.6%
$KAlSi_3O_8$	Microcline	2.1%
$NaAlSi_3O_8$	Albite	1.3%
$FeCO_3$	Siderite	3.9%
Fe_3S_4	Greigite	3.1%
FeS_2	Pyrite	1.2%
TiO_2	Anatase	1.7%
TiO_2	Rutile	0.8%
$NaCl$	Halite	1.6%
CuO	Tenorite	1.2%
$CaMg(CO_3)_2$	Dolomite	0.8%
$CaCO_3$	Calcite	0.7%
		100.0%
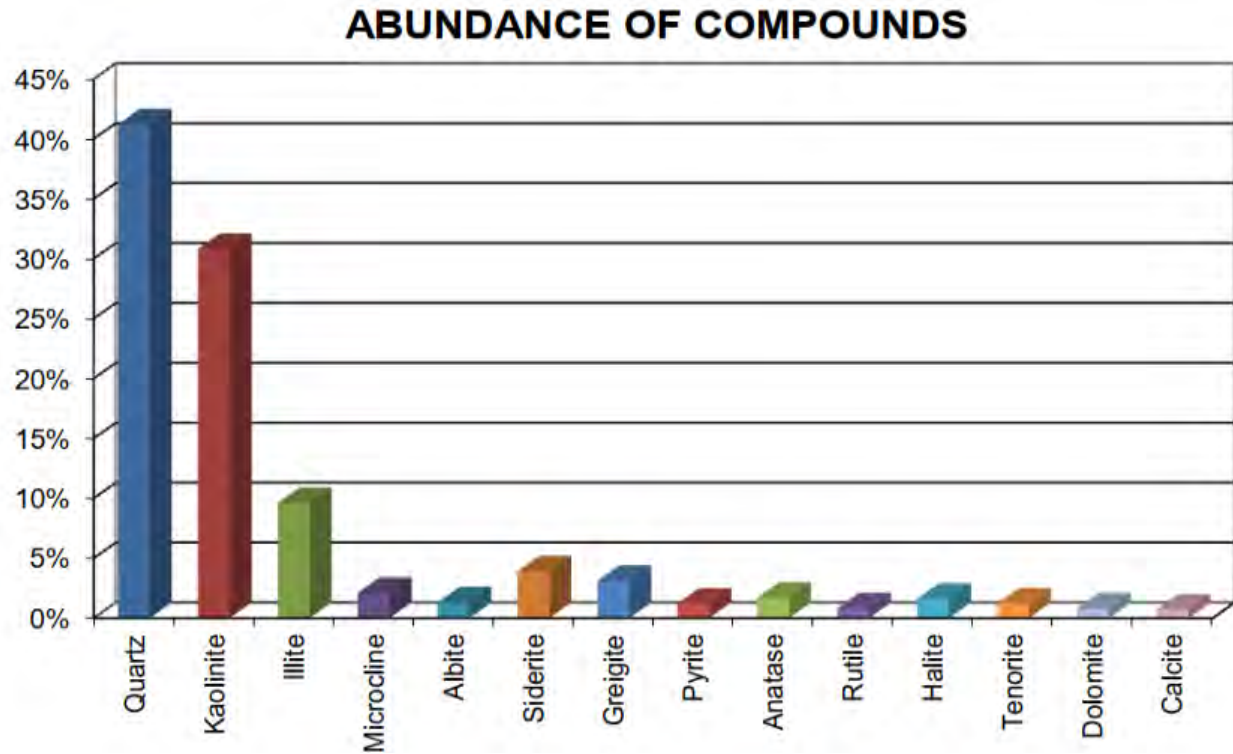
Figure 3-5:   EDS and XRD results of the treated FFT at 15 wt.% solids (predominance quartz).
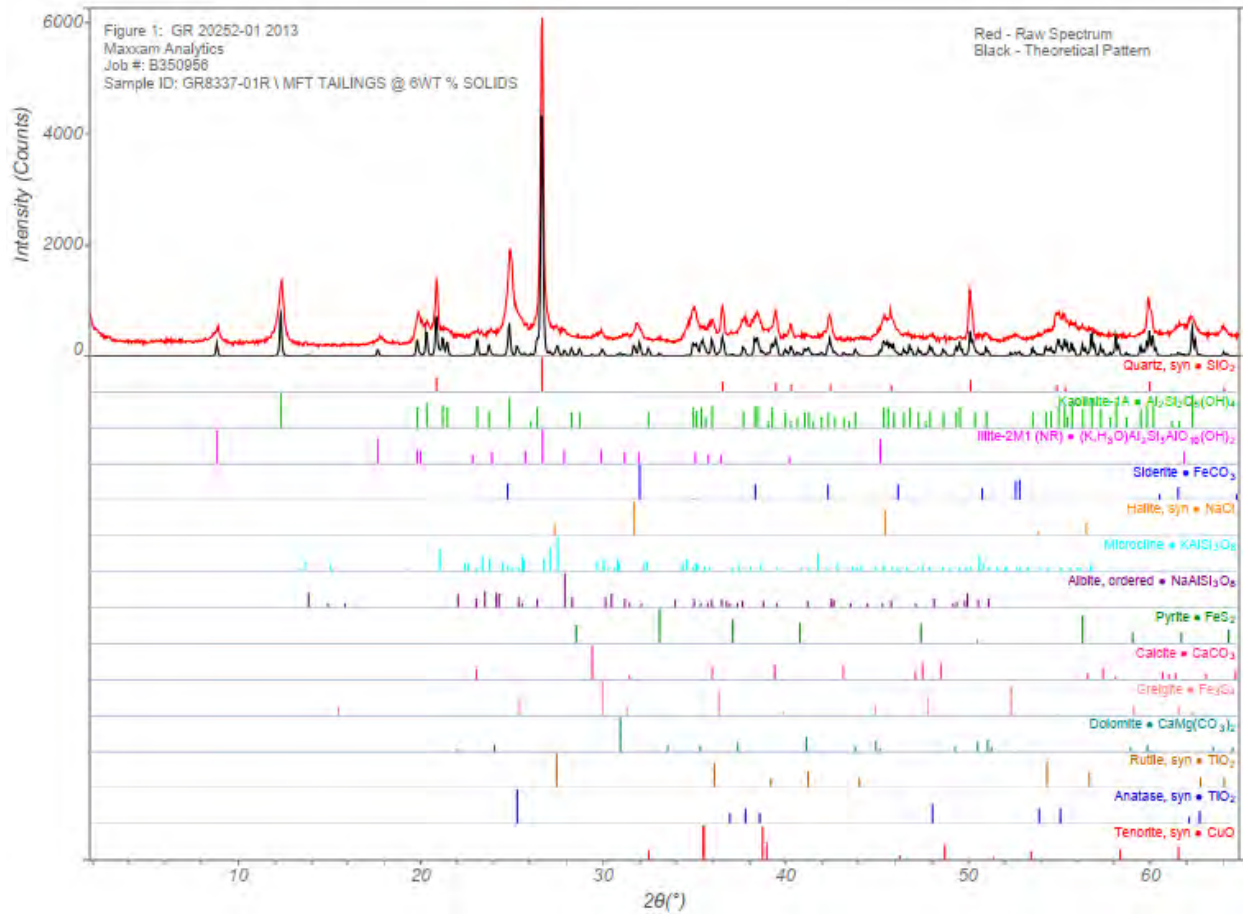
Figure 3-6: **Elemental spectrograph of the treated FFT at 15 wt.% solids (predominance quartz).**

The FFT at 39 wt.% solids (predominance kaolinite) – This sample generated a good quality diffractogram indicating the sample is mainly composed of crystalline compounds. The scanning electron photomicrograph on Figure 3-7 (lower left) shows FFT at 39 wt.% solids (predominance kaolinite) consists of aggregates of angular, subangular, and subrounded clay- to silt-sized particles. The upper left photograph of Figure 3-7 illustrates the bulk sample. Oxygen (O) and silicon (Si) dominate the elemental spectrograph, respectively forming approximately 54.9% and 23.1% of the sample. Carbon (C), aluminum (Al), and iron (Fe) are moderately abundant, respectively forming approximately 7.0%, 9.4%, and 2.0% of the sample. Trace to minor amounts of sodium (Na), magnesium (Mg), phosphorus (P), sulfur (S), chlorine (Cl), potassium (K), calcium (Ca), titanium (Ti), manganese (Mn) and copper (Cu) are present.
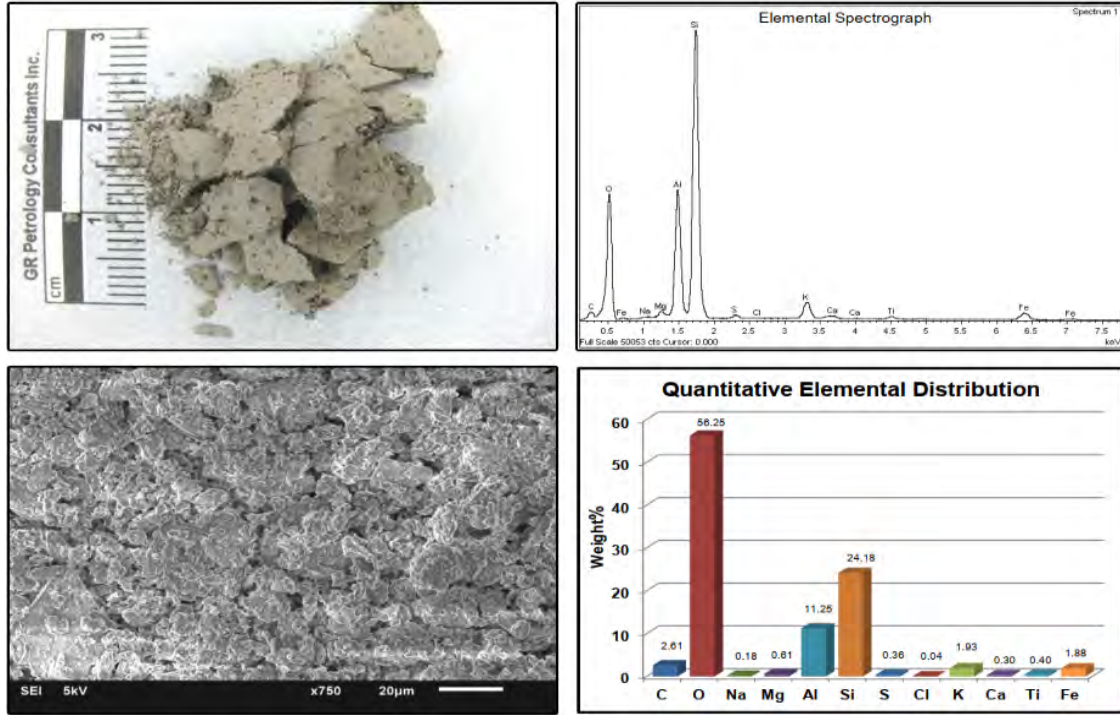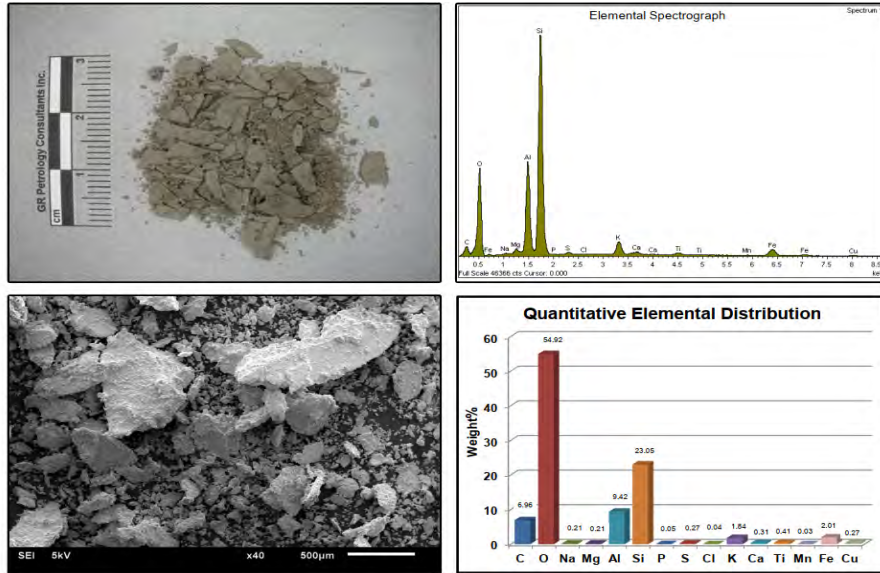
Figure 3-7: **FFT at 39 wt.% solids (predominance kaolinite)quantitative elemental distribution.**

XRD analysis of the FFT at 39 wt.% solids (predominance kaolinite) shows the crystalline components of the sample consist of approximately 99% silicates (kaolinite [$Al_2Si_2O_5(OH)_4$], quartz [SiO_2], illite [$(K,H_3O)Al_2Si_3AlO_{10}(OH)_2$], microcline [$KAlSi_3O_8$], and albite [$NaAlSi_3O_8$]) with minor amounts of iron carbonate scale (siderite [$FeCO_3$]) and titanium oxide (rutile [TiO_2]). Elemental analysis also suggests the presence of non-crystalline carbon-bearing compounds. Trace volumes of magnesium-, phosphorus-, chlorine-, sulfur-, calcium-, manganese-, and copper-bearing compounds were detected during elemental analysis.

Tables 3-5 and 3-6, and Figures 3-7 to 3-9 summarize the following comments regarding the comparison of EDS and XRD results of the FFT at 39 wt.% solids (predominance kaolinite). The FFT at 39 wt.% solids (predominance kaolinite) showed a good correlation between the XRD and EDS results; minor differences with respect to carbon, aluminum, and silicon.

- Carbon was measured at 6.96% in the elemental analysis, while XRD analysis detected 0.08% carbon.

- In the elemental analysis, aluminum forms 9.42% of the sample, whereas XRD analysis calculated aluminum to be 12.02%.

- Silicon represents 23.05% in the EDS analysis, while XRD analysis calculated silicon to be 31.67%.

The EDS results for carbon and oxygen are greater than the XRD results, indicating the presence of non-crystalline carbon- and oxygen-bearing compounds. The XRD results for silicon and iron are greater than the EDS results indicating these elements occur in well-crystalline compounds.

Table 3-5: Comparison of elemental composition by EDS and XRD analysis on FFT at 39 wt.% solids (predominance kaolinite).

Sample 3	H	C	O	Na	Mg	Al	Si	S	Cl	K	Ca	Ti	Mn	Fe	Cu
EDS analysis	-	6.96	54.92	0.21	0.21	9.42	23.05	0.27	0.04	1.84	0.31	0.41	0.03	2.01	0.27
XRD Analysis	0.87	0.08	54.17	0.06	-	12.02	31.67	-	-	0.61	-	0.12	-	0.39	-
Hydrogen (H); Carbon (C);Oxygen (O); Sodium (Na); Magnesium (Mg); Aluminum (Al); Silicon (Si); Sulfur (S); Chlorine (Cl); Potassium (K); Calcium (Ca); Titanium (Ti); Manganese (Mn); Iron (Fe); Copper (Cu)															

Table 3-6: EDS and XRD results of the FFT at 39 wt.% (predominance kaolinite).

ELEMENTS:	DOMINATE: O, Si COMMON:	MODERATE: C, Al, Fe MINOR-TRACE: Na, Mg, S, Cl, K, Ca, Ti, Mn, Cu
COMPOUNDS:		
Formula	*Name*	*Percentage*
$Al_2Si_2O_5(OH)_4$	Kaolinite	52.3%
SiO_2	Quartz	40.1%
$(K,H_3O)Al_2Si_3AlO_{10}(OH)_2$	Illite	4.6%
$KAlSi_3O_8$	Microcline	1.3%
$NaAlSi_3O_8$	Albite	0.7%
$FeCO_3$	Siderite	0.8%
TiO_2	Rutile	0.2%
		100.0%
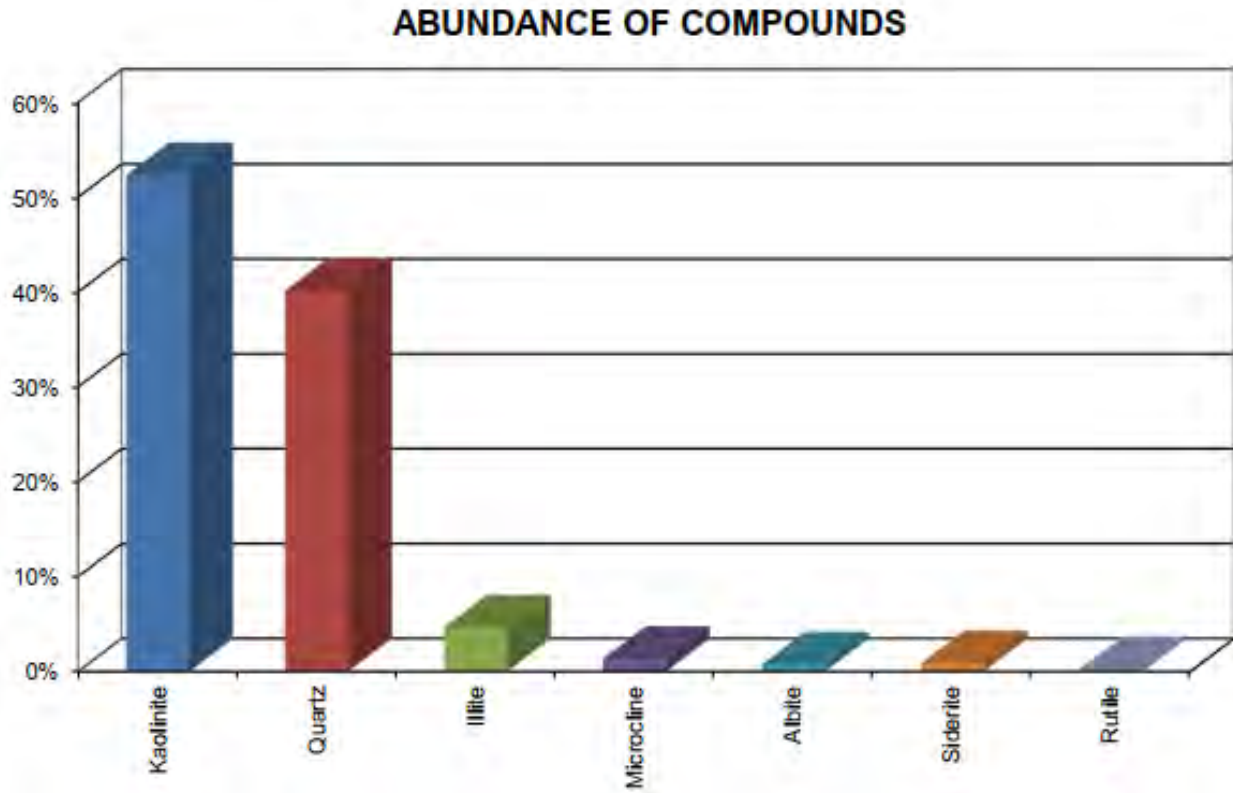
Figure 3-8:   FFT at 39 wt.% solids (predominance kaolinite) EDS and XRD results.
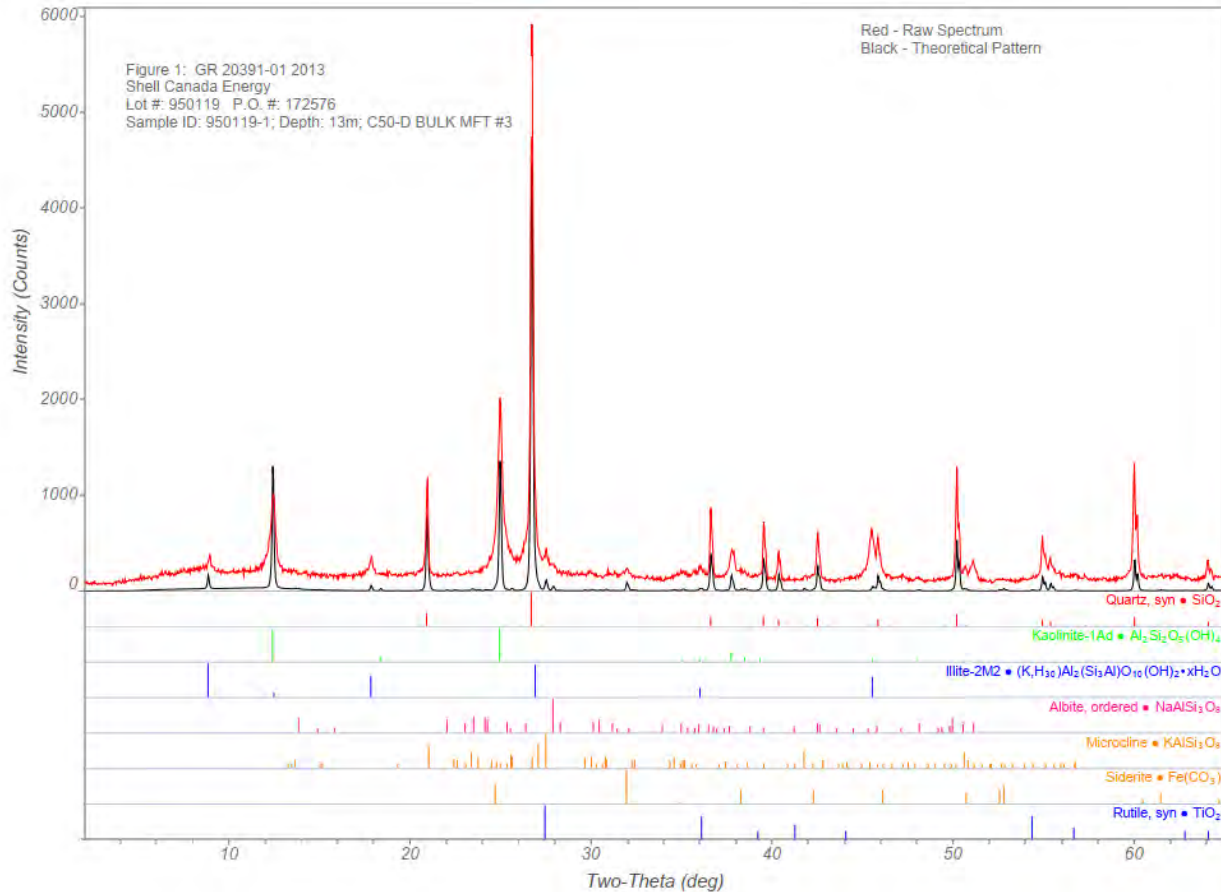
Figure 3-9: **Elemental spectrograph of the FFT at 39 wt.% solids (predominance kaolinite).**

3.2.2 Zeta potential

All particles in suspension exhibit a zeta potential, or surface charge. The measurement and knowledge of the zeta potential is critical for optimizing processes, predicting particle stability and interactions, and as a simple method of quality control. Zeta particle potential measurements are dependent upon the nature of both the particle and the characteristics of the suspension; generally, the size and concentration of particles are key parameters in determining which technique or instrument is applicable.

In solution, the presence of a net charge on a particle affects the distribution of ions surrounding it, resulting in an increased concentration of counter-ions. The region over which this influence extends is called the electrical double layer. Conventionally, this layer is thought of as existing as two separate regions: an inner region of strongly bound ions known as the "Stern layer"

and an outer layer of loosely associated ions called the "diffuse layer." This concept is sketched in Figure 2-5 representing the ion distribution around a charged particle. As the particle moves through a solution, due to gravity or an applied voltage, the ions move with it. At some distance from the particle there exists a "boundary," beyond which ions do not move with the particle. This is known as the surface of hydrodynamic shear, or the slipping plane, and exists somewhere within the diffuse layer. The potential that exists at the slipping plane is defined as the zeta potential.

The zeta potential is crucial in determining the stability of a colloidal suspension. When all particles have a large negative or large positive charge, they will repel each other, and the suspension will be stable. If the zeta potential is low, the tendency for flocculation is higher. Another important consideration when discussing zeta potential is pH; in fact, quoting a zeta potential without considering pH is nearly meaningless. For suspensions of most materials, a plot of zeta potential versus pH exhibits an isoelectric point, which is the pH where the net charge on the particles is zero. At this point, the suspension is highly unstable and flocculation is most likely to occur, as shown in Figure 3-10 (left) and (right). There are different techniques (methods or instruments) to measure zeta potential. The key is to choose the most appropriate method for the mineralogy of the sample.
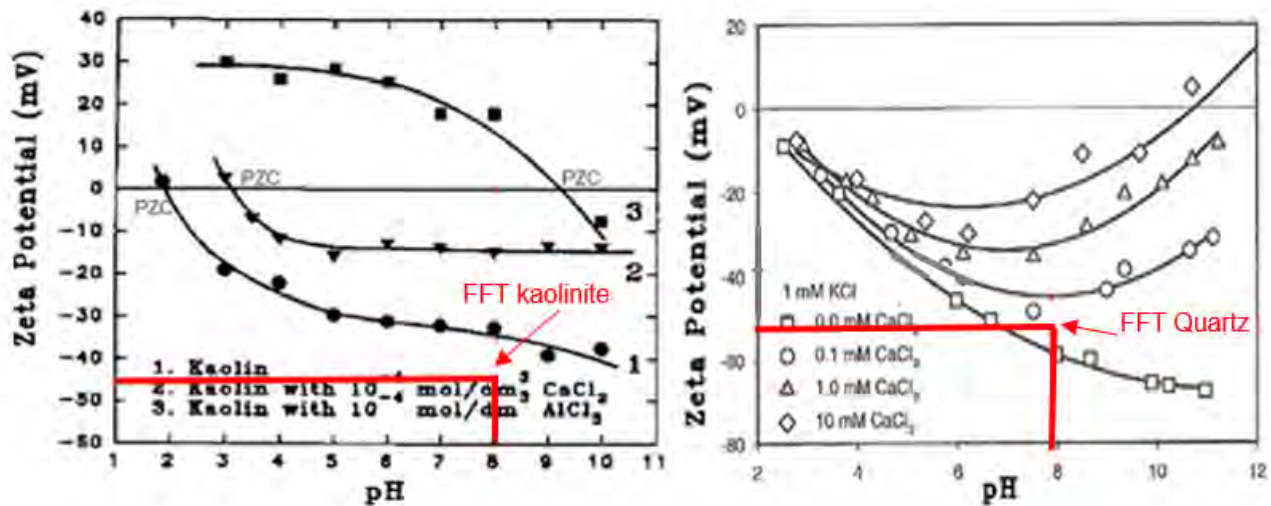
Figure 3-10: **Zeta potential of kaolinite (left) adapted from Peng and Di (1994) and zeta potential of quartz (right) adapted from Masliyah, J.H (2011), both showing particle behavior with increased cations.**

The FFT mineralogy as part of this research is predominantly composed of quartz particles (non-clay mineral), as shown by Samples 1 and 2.his predominance, however, can also be kaolinite (clay mineral) as shown by Sample 3; therefore, the ratio of clay to massive minerals encountered in the FFT can vary from approximately 0.6 to 1.2. This variation depends on the location where FFT are dredged from the ETF.

Quartz particles at pH > 2 have a negative surface charge that increases as the pH increases (Gan et al., 2008). Quartz particles at pH 8 present a highly negative surface charge that is enough to result in a dispersive state through the action of electrostatic repulsive forces. These forces are affected by the ionic strength of the soil-water-ionized system, which depends on the pore solution electrolyte concentration and ion types.

In the presence of high-valence cations, such as aluminum, the repulsive forces of quartz particles are reduced, resulting in coagulation of the particles. The mechanism of coagulation effectively lowers the electrostatic repulsive forces between particles, causing charge neutralization and allowing the particles to come closer together and form stable micro-flocs (slow-settling flocs). Charge neutralization is equivalent to compressing the diffuse double ionic layer energy barrier (i.e., reducing the double ionic layer charge to near zero).

Kaolinite is the predominant clay mineral within the fine particle size fraction of the FFT. The behavior of kaolinite mineral particles is dependent on the SAR, electrolyte concentration, and pH (Goldberg et al., 1991). Kaolinite has negatively charged surfaces at pH > 2. Kaolinite exhibits a large positive value of zeta potential in the presence of aluminum (Al^{3+}). The zeta potential decreases from + 30 mV to - 7 mV as the pH increases from 3 to 10, with a PZC at pH 9 (Figure 3-10).

Illite is non-swelling in nature, has a lower cation exchange capacity than kaolinite, and is also pH and SAR dependent. All exchangeable cations are adsorbed on the exterior surfaces of illite and kaolinite particles (van Olphen, 1977). Existing data show that illite does not play a dominant role in determining flocculation and dispersion behaviors of kaolinite/illite mixtures (Goldberg, 1991).

Therefore, the chosen instrument to measure FFT zeta potential must have the ability to measure zeta potential in slurries of greater than 10 wt.% solids (up to 60 wt.% solids depending on the sample). The zeta-probe must be also able to measure zeta potential in concentrated solutions of particles in the size range 1 nm to 10 μm (clays and silts/or fine quartz) and up to 75 μm (silts/or fine quartz).

The zeta potential tests for this research were performed at University of British Columbia (UBC) using a zeta-probe called a "Zeta Meter."

Tests were performed on representative aliquots of 3 samples at natural pH, as indicated in Table 3-7. The representative samples were centrifuged to obtain a clear supernatant. The original sample concentrations of ions and dissolved materials were retained to avoid changing the sample original conditions. A small drop of each representative sample was placed in the clear centrifuged supernatant, and then placed in the Zeta Meter sample cell for testing. Particles were tracked in each sample to get an average for the zeta potential. The pH was also measured for each slurry. There was not much variation in pH for the samples, which ranged from pH 7.5 to 8. The zeta potential results are shown in Table 3-7.

Table 3-7:   Zeta potential results FFT at 39 wt.% solids and treated FFT at 20 wt.% solids.

Sample	Zeta potential (mV)	pH	Notes
FFT at 39 wt.% solids (predominance kaolinite)	- 47	8	FFT (flocculant alone)
Treated FFT at 20 wt.% solids (predominance quartz)	- 14	7.50	Treated FFT (coagulation + flocculation)

3.2.3   Water chemical analysis

The chemical analyses performed in this research focused on the interaction between the mineral composition (i.e., FFT mineralogy) and pore water chemistry (i.e., pore solution electrolytes, ion concentrations, and pH) with the aim of understanding their significant influence on FFT dispersion and flocculation behaviors. Routine chemical analyses were necessary for characterization of the ion concentrations and pH of the FFT pore water, plant process water, and release water from the treated FFT that can be used as recycle water (section 4.1.3). In addition to pH, the key component of the FFT pore water chemistry is the calcium content due to its significant impact on the flocculation behavior of the FFT. The FFT pore water contains 18 ppm calcium ions

and process reclaim water usually contains 19 ppm calcium ions. The FFT has a measured zeta potential of ‑ 47 mV at pore water pH 8 (Table 3-7).

3.2.4   Particle size distribution (PSD)

Particle size distribution (PSD) was obtained with the sieve and dirt-hydrometer method (including residual bitumen). Quartz particles passing a 75 µm sieve that are pH dependent can significantly influence FFT mechanical and physical properties. At pH > 2, quartz particles possess a negative charge, show dispersive behavior, are more hydrophilic, and therefore behave like clay minerals. The PSD of the treated FFT obtained from a commercial field trial of stacked geotextile tubes, referred to in this research, shows that the fines content finer than 75 µm varied from 87% to 100%, and that the clay content finer than 2 µm varied from 31.6% to 50.5%. The sand-to-fines ratio (SFR) varied from 0.02 to 0.16. Although kaolinite particle sizes could exist in the range of 0.2 µm to 11 µm and quartz particles also could exist in the range of 0.1 µm to 2 µm (Mitchell, 2005), the assumption was the amount of non-clay minerals in the treated FFT could vary between 40% and to 55%, approximately.

In the oil sands industry however, the sand-silt boundary is defined as being at 45 µm. The PSDs of the oil sands typical FFT and the FFT of this research are shown in Figure 3-11.
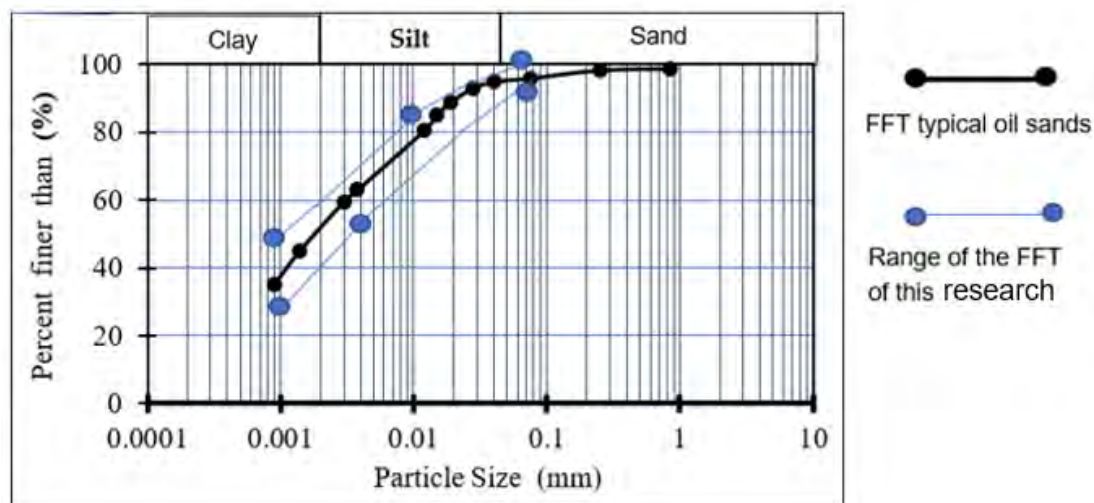
Figure 3-11:   Plots of oil sands typical FFT PSD and range of the FFT PSD of this research.

3.2.5   Engineering properties

Maintaining the initial slurry density of the FFT at 20 wt.% solids was part of the methodology to control variations of the feed densities while maintaining unaltered coagulant and flocculant dosages. The FFT feed at 20 wt.% solids has been demonstrated to enhance mixing and energy dissipation, and to maximize flocculant adsorption at relatively low dosages. The measured average properties of the FFT of this research were solids specific gravity, 2.50; water content (geotechnical), 360.0%; solids content, 20 wt.% solids; total bulk density, 1.15 t/m^3; dry density, 0.25 t/m^3; and void ratio of 9. These initial properties are fundamental for the design of the recipe, including flocculant and coagulant dosages and concentrations and release water volumes. The results obtained immediately after the geotextile tubes were completed (filled up to the specified max height by the manufacturer), were solids specific gravity, 2.48; water content, 86.9%; solids content, 53.6 wt.% solids; total bulk density, 1.47 t/m^3; dry density, 0.79 t/m^3; and void ratio, 2.16. The laboratory and field test results indicated that the treated FFT was dewatered in the geotextile tubes during filling, providing significant enhanced fines capture as indicated by its dry density and void ratio. USCS classification was CH, liquid limit was 76.8%, plastic limit was 29.0%, and the liquid index was 47.8%.

A rigorous control of the FFT slurry density intake was part of the inline mixing process to provide the required amount of water (reclaim process water) for adjustment of the initial slurry density to 20 wt.% solids if it was higher than 20 wt.% solids.

3.2.6   Settling and bleed testing

Coagulation was applied prior to flocculation to neutralize the electrical charges of particles and reduce or even eliminate repulsion between them. Coagulation was carried out using an inorganic coagulant of high-valence cations such as Alum (4.27% Al^{3+} + 8.07% Al_2O_3 at specific gravity 1.326) concentration 0.1% and dosage 0.65%. The coagulant solution was prepared by weighing a calculated amount of the coagulant (in powder form) in a tared container before it was added to a beaker of reclaim process water. The coagulant solution was then mixed on a stir plate until the chemical dissolved completely (approximately 5 to 10 minutes). The coagulant solution remained stable and could be used for treatment of the FFT more than 5 days after preparation.

Flocculation was carried out using an anionic PAM flocculant of medium charge density and very high molecular weight (VHMW) at concentration 0.1% and dosage 0.1% was used to bridge the micro-flocs that were formed by coagulation to obtain an effective flocculation. The flocculant solution was prepared by weighing a calculated amount of the flocculant (in powder form) in a tared container before it was added to a beaker of reclaim process water. The flocculant solution was allowed to mix on a stir plate for approximately 15 minutes. The flocculant solution remained stable and could be used for treatment of the FFT more than 3 days after preparation.

For each test, the amount of FFT was determined by placing it in a beaker and recording the weight. The required amount of dilution water (process water) was then added to reduce the solids content to 20 wt.% solids. The diluted slurry was mixed with a bench-top mixer for 10 minutes before the coagulant solution was added and allowed to mix for an additional 10 minutes. The flocculant solution was then added by syringe or by pouring from a beaker, depending on the amount, to the mixing slurry. The mixing intensity was carefully selected to avoid shearing or breaking of the micro-flocs to allow for the visible formation of large flocs. Once the required time of 0 to 60 seconds for flocculation occurred, a positive test result was achieved when the solid and water portions of the slurry were physically separated. The separation of solids and water was clearly visible in a graduated cylinder by the presence of a clear water column (overflow) above agglomerated solids (underflow). A 10-minute bench-top settling test was performed to evaluate the effectiveness of the coagulant and flocculant additives in settling the FFT suspension. If the FFT suspension settled out to form a clear water column within 10 minutes after starting the test and a distinct deposit of solids was observed at the bottom of the cylinder, the test result was deemed "positive", and the deposit thickness was measured. If the slurry suspension did not settle out within this time, the test result was deemed "negative". In the event of a positive result, the settled solids were separated from the water column and transferred to a pan for a bleed test. In the event of a negative result, the sample was discarded. There was no requirement to perform long-term settling tests because of the very high settling rates, complete removal of suspended solids, significant underflow formation (fines-agglomeration), and solids volume reduction obtained by the treatment recipe to dewater FFT.

As shown in Photograph 3.1, a bleed test was performed to evaluate the short-term gravity drainage or passive water release of the underflow solids that were obtained from positive settling tests. In the event of a positive settling test result, the column of clear water was removed by decanting and the underflow solids were transferred to a 2-L capacity pan (sample pan). The

sample pan was set on a 20° inclined surface and oriented such that there was adequate space to allow for the accumulation of bleed water at the lower end of the pan. The sample pan was left uncovered at the ambient room temperature of the testing laboratory (approximately 20 °C). The sample pan was inspected twice per day, and any accumulated bleed water was removed. The underflow solids deposited in the pan was subsampled at four specific time intervals of 0, 24, 48, and 72 hours after the start of the bleed test, to allow for each subsample to be tested for moisture content by mass.
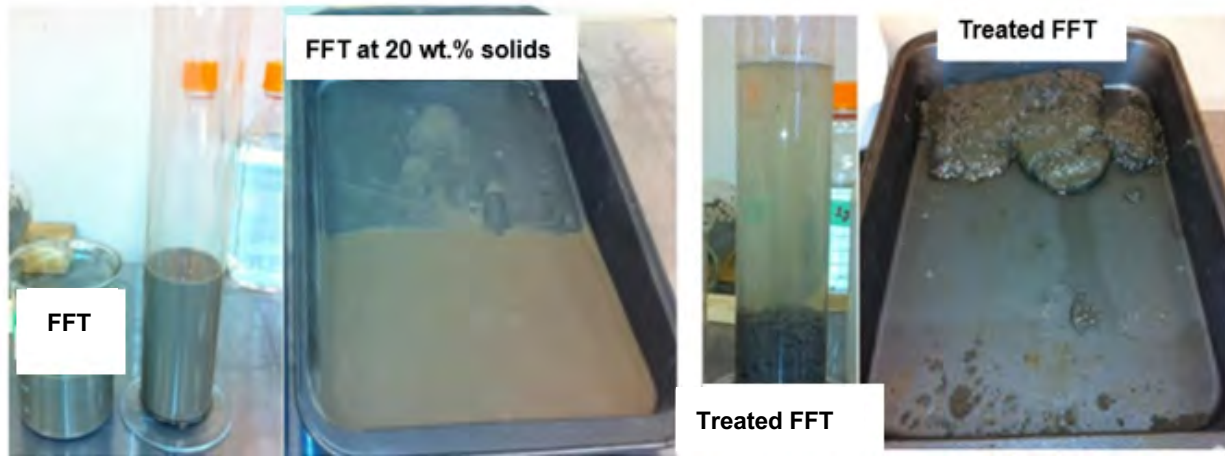
Photograph 3-1:   **FFT and treated FFT settling and bleed tests.**

3.2.7   Laboratory parametric physicochemical analysis of FFT dispersion and flocculation behaviors

This research includes a parametric physicochemical analysis of FFT dispersion and flocculation behaviors to determine the causes for significant amounts of trapped water in the flocculated FFT with flocculant only.

This parametric analysis was developed considering the fundamentals of soil behavior, supported by the observations in the laboratory. A pure kaolinite powder (≤2 micron obtained from Sigma-Aldrich Canada) and pure quartz flour (≤75 micron obtained from Heemskirk Canada) were mixed with reclaim process water (at different Ca^{2+} ions concentrations) to be used as soil slurry for laboratory observations focused on the dispersion and flocculation behaviors of kaolinite and quartz suspensions as a function of pH, hydrolyzed salts (calcium and aluminum), and anionic PAM flocculant.

Quartz is a non-clay mineral and the predominant mineral within the fine particle size fraction of the FFT evaluated in this research. At pH > 2, quartz particles present a negative surface charge that increases as the pH increases (Gan et al., 2008; Hussain et al., 1996 and Hunter, 1981). The reason for this behavior is that the particle surface reacts with water, forming silicic acid which in turn dissociates, forming a silicic anion at the surface and a hydrogen ion that diffuses into the solution. This chain of events negatively charges the solid surface, as the diffusing H^+ carries away a positive charge and leaves the negative charge behind. This negative surface charge is sufficient to lead quartz particles to a dispersive state by action of electrostatic repulsive forces (Verwey et al., 1948). These forces are affected by the ionic strength of the soil-water-ionized system, which depends on the pore solution electrolyte concentration, ion types, and pH.

Figure 3.12 and Photograph 3.2 show the dispersion behavior of quartz particles versus pH.
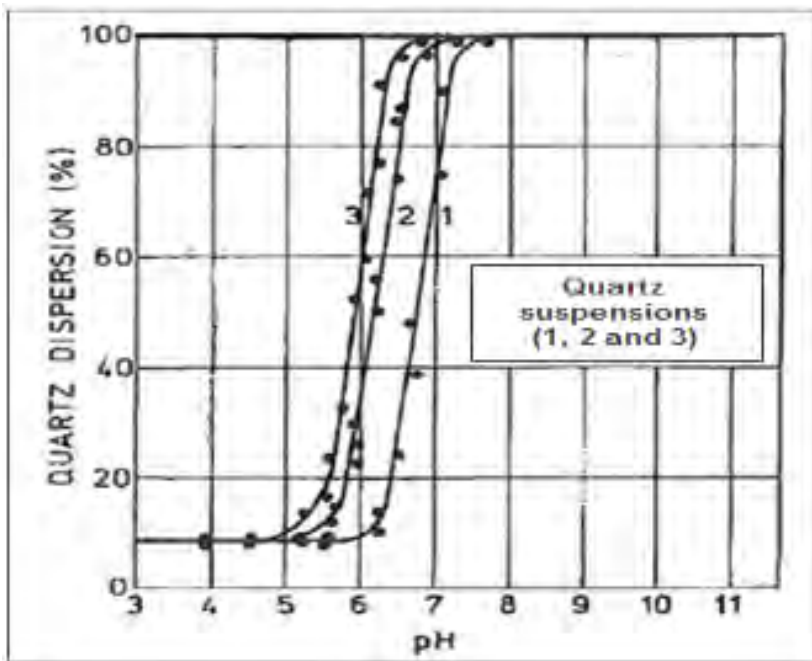
Figure 3-12:   Dispersion of quartz particles vs. pH – Adapted from A. van Lierde (1980).
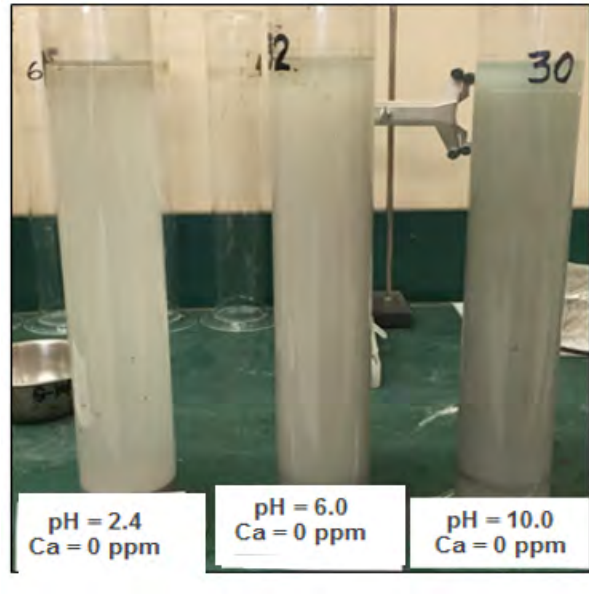
Photograph 3-2: **Quartz particles vs. pH – Laboratory observation of this research.**

Hydrolyzed metal ions, such as calcium and aluminum, play an important role in FFT dispersion and flocculation behaviors because they adsorb onto particle surfaces and reduce the double layer charge to near zero, as shown in Figure 3-10 (Zeta potential of quartz and kaolinite particles versus pH).

Furthermore, the effect of hydrolyzed metal ions on the interaction behavior of anionic PAM flocculant plays an important role on the flocculation of quartz particles, as shown in Photograph 3-3 (A and B).

(A) (B)
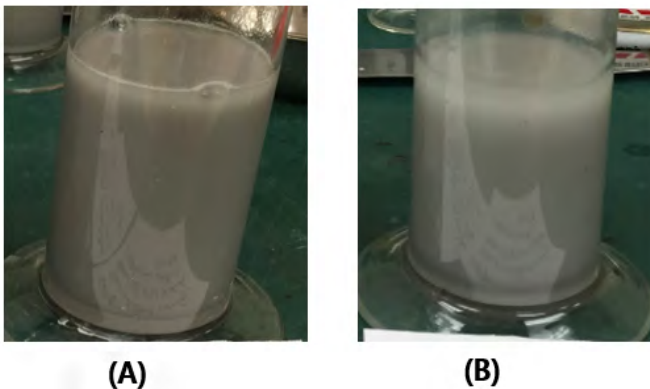
Photograph 3-3: **Quartz suspensions at pH 8: (A) with 40 ppm Ca^{2+}, and (B) with 72 ppm Ca^{2+}, both with anionic PAM flocculant only.**

Adsorption of anionic PAM flocculant on quartz surfaces is strongly dependent on pH and salinity. Salinity is the saltiness or dissolved salts content (calcium, aluminum, magnesium, potassium, sodium, bicarbonates, chlorides, and sulfates) of a body of water. The percentages of ionized (COO⁻) and non-ionized (COOH) functional groups of anionic PAM flocculant are presented on Table 2-1 as a function of pH (A. Van Lierde, 1980). Table 2-1 shows that ionization of PAM is complete above pH 6, and at pH 5 is already higher than 50%. At low pH, where the ionization is low, flocculant chains adsorb because non-ionized groups form intramolecular hydrogen bonds. At high pH, however, such links are hindered by the lack of non-ionized groups and by the presence of the various negatively charged carboxylate groups, favoring chain extension.

At pH above 6.5 to 7, quartz particles present a highly negative surface charge and are consequently in a dispersed state. The presence of anionic PAM flocculant does not modify this behavior because the completely ionized flocculant chains cannot be adsorbed onto the negative particle surface (Kuzkin et al., 1964; Fontana, 1961). When pH is lowered to values between 4.5 and 6.5, electrical repulsive forces between the anionic PAM flocculant and quartz particles are reduced by the partial dissociation of the anionic PAM flocculant and to the lowering of the zeta potential of quartz particles. Adsorption of the flocculant becomes possible through the hydrogen bonds between the COOH groups of the anionic PAM flocculant and the silanol groups of quartz particles, resulting in poor flocculation (Healy, 1961; Fontana 1961; Slater et al., 1968). Understanding the behavior of quartz suspensions in the presence of both calcium ions and anionic PAM flocculant requires the consideration of the interactions of calcium ions onto quartz surface as well as the interactions between these ions and the anionic PAM flocculant chains. At high pH values, the anionic flocculant acts as an element of high charge density, attracting counter-ions (Ferry et al., 1962). At low pH (4.5 to 6), the adsorption of calcium ions onto quartz surfaces is small, and the zeta potential of the quartz particles becomes less negative as the calcium concentration increases, improving the adsorption of the anionic PAM flocculant. This adsorption mainly occurs due to the hydrogen bonds at the OH sites of the quartz surfaces. At slightly acidic (6.5) to basic pH (8.5), the adsorption of calcium onto quartz surfaces can considerably reduce the zeta potential of quartz particles, allowing the adsorption of the extended anionic flocculant chains by carboxylate bonds (Usoni et al., 1968). It was observed in this research that at pH 8, quartz particles showed poor flocculation performance in the presence of calcium at concentrations of 40 and 72 ppm and anionic PAM flocculant. Photograph 3-3 (A and B) show stable suspensions

of quartz particles. This observation confirms that as Ca^{2+} ions are predominant with a very low concentration of $CaOH^+$, those positively charged divalent ions influence the behavior of the anionic PAM flocculant. Calcium ions can be adsorbed onto the COO^- functional groups of the anionic PAM flocculant to form $(-COO)_2$ Ca. $CaOH^+$ may also be adsorbed onto $-COO^-$ functional groups to form $(-COO)Ca(OH)$. As the concentration of calcium increases, more Ca^{2+} ions are available to adsorb onto the anionic PAM flocculant; however, when in excess, these Ca^{2+} ions are partially attracted as counter-ions in the double layer of the adsorbed anionic flocculant chains, causing steric stabilization at the particle surface. Steric stabilization results from covering the particles with the anionic flocculant, preventing the particles from getting close to the range of attractive forces and thereby allowing quartz particles to be dispersed. It was also observed in this research that the impact of excess calcium at pH 8 on the flocculation of quartz can be reversed with the addition of metal salts of a higher valence than calcium, such as aluminum ions. A proper concentration and dosage of aluminum ions provided efficient flocculation of quartz particles, as shown in Photograph 3-4. Quartz suspensions at pH 8 with 40 and 72 ppm calcium concentrations showed efficient flocculation when coagulated with ~100 mg/L aluminum ions at 0.65% dosage, prior to flocculation with 30% charge density HMW anionic PAM at a concentration of 0.1% and dosage 0.1%. While kaolinite surfaces are negatively charged in media such as water, they exhibit positive surface charge characteristics at pH < 3 in the solution of calcium ions, and at pH 9.2 in the solution of aluminum ions, as shown in Figure 3-13 (Peng et al., 1994). Kaolinite has a large positive zeta potential in the presence of aluminum ions (Peng et al., 1994). In contrast, kaolinite maintains a close to constant zeta potential value (-15 mV) at pH ≥ 4 in the presence of calcium ions. As pH decreases below 4, kaolinite zeta potential increases when passing by the PZC at approximately pH 3. Figure 3-13 shows kaolinite zeta potential versus pH in solutions of water, calcium ions and aluminum ions.
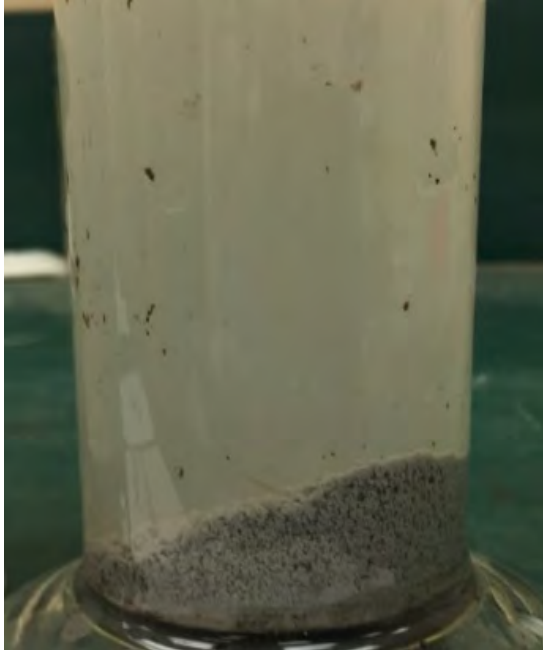
Photograph 3-4: Coagulated + flocculated quartz suspension with alum and anionic PAM flocculant, respectively.
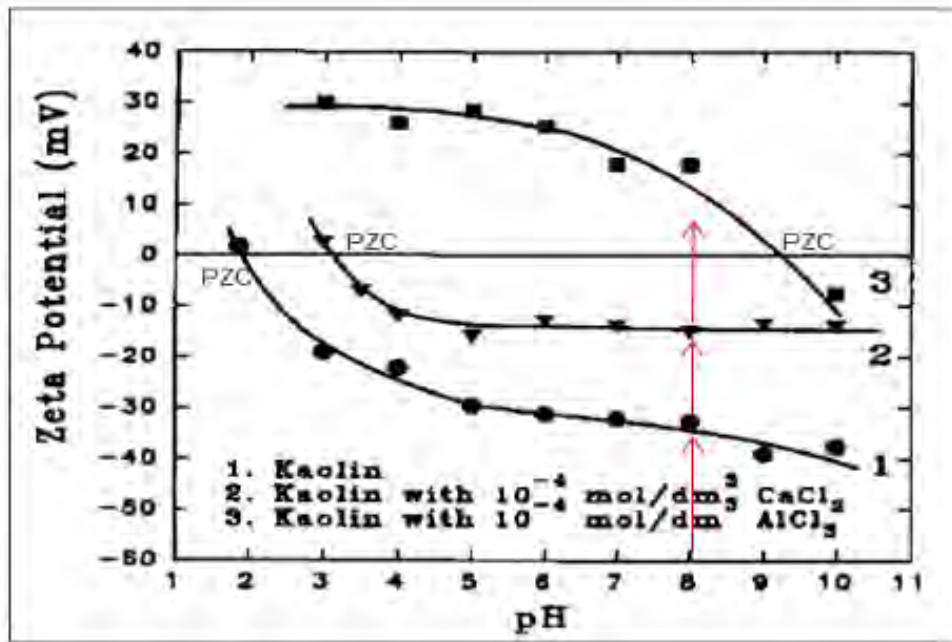
Figure 3-13: Zeta potential of kaolinite particles vs. pH – adapted from Peng and Di (1994).

An excess of hydrolyzed metal ions (i.e., calcium and aluminum) used to coagulate negatively charged particles of kaolinite might cause the reversal of the double layer charge and lead to a stable suspension with a positive double layer charge (Matijevic et al., 1966), which could suppress the kaolinite flocculation process. This behavior has been observed by this research when comparing the images in Photograph 3-5 (A and B).
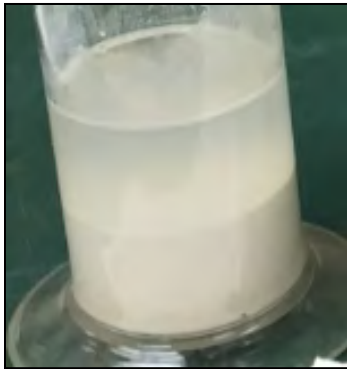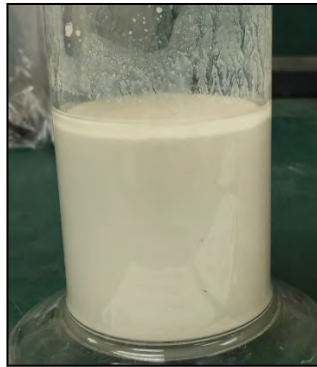
(A)   (B)

Photograph 3-5:   **Kaolinite suspensions at pH 8, and anionic PAM flocculant: (A) flocculation with 40 ppm Ca^{2+}, (B) suppressed flocculation with 72 ppm Ca^{2+}.**

Different additives have various surface reactions with kaolinite, which can change the zeta potential of kaolinite. When increasing pH, the hydroxyl ion can react with the surface of kaolinite, which will make the zeta potential more negative.

Sulfate and bicarbonate ions can adsorb onto the kaolinite surface and make the zeta potential more negative. Flocculation of kaolinite suspensions with anionic PAM flocculant are affected by flocculant molecular weight and ionic charge. In addition, adsorption of anionic PAM flocculant onto kaolinite particles is strongly dependent on pH and salinity (Pefferkorn, 1987).

The edge surface of kaolinite carries a net negative charge arising from the dissociated edge silanols. The suggested adsorption mechanism of anionic PAM flocculant onto kaolinite particles is by hydrogen bonding. However, it is possible for anionic PAM flocculant to be attracted to the positively charged sites of kaolinite by electrostatic attraction. This electrostatic attraction may be easily overcome by the repulsive effect due to the overall negatively charged kaolinite particles (Peng et al., 1994).

This research also shows that the impact on the flocculation of kaolinite, caused by an excess of calcium at pH 8, can be reversed by the addition of metal salts of a higher valence than calcium, such as aluminum ions. A proper concentration and dosage of aluminum ions provided an efficient flocculation of kaolinite particles, as shown in Photograph 3-6.
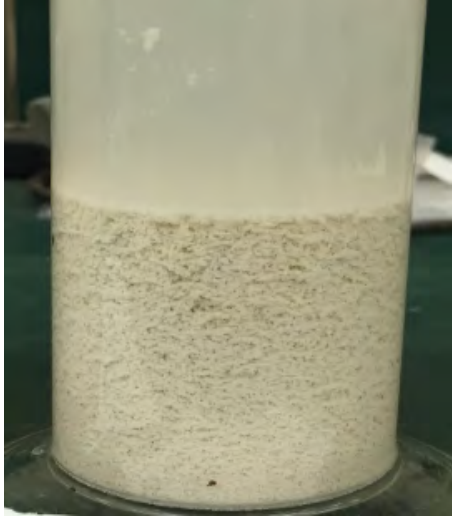
Photograph 3-6: **Kaolinite suspension with 72 ppm Ca^{2+} + coagulated with alum (Al^{3+}) and flocculated with anionic PAM flocculant.**

Photograph 3-7 shows a quartz and kaolinite mixture by weight (wt.%), using 55 wt.% and 45 wt.% particles respectively. The mixture was prepared at 15 wt.% solids, water pH of 8.45, and Ca^{2+} ion concentration of 72 ppm.

Photograph 3-7: **Mixture of quartz particles (55 wt.%) + kaolinite particles (45 wt.%) + 72 ppm Ca^{2+} ions to form a suspension at 15 wt.% solids.**

Photograph 3-8 shows the dispersion and flocculation behaviors of the quartz and kaolinite mixture of Photograph 3-7. The mixture was coagulated with a concentration of 0.1% aluminum ions at a 0.65% dosage (by mass of dry solids), prior to flocculation with medium charge density HMW anionic PAM flocculant at a concentration of 0.1% and dosage of 0.1% (by mass of dry solids). An efficient flocculation (Photograph 3-8 A) was obtained using coagulant prior to flocculant addition to the mixture (Photograph 3-7). It was observed that using anionic PAM flocculant only resulted in poor flocculation (Figure 3-8 B).

(A)   (B)
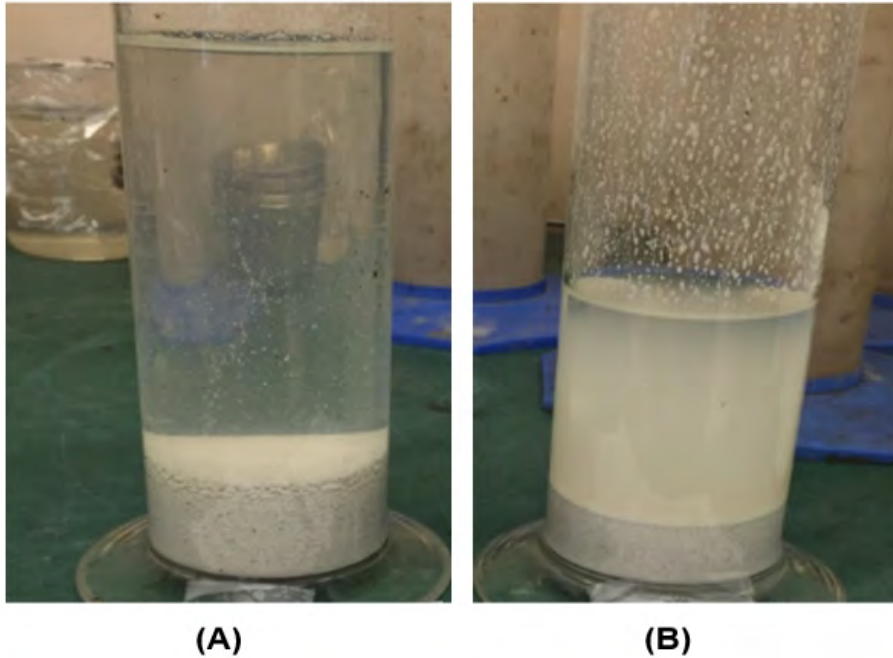
Photograph 3-8:   **Mixture quartz and kaolinite: (A) coagulated + flocculated;**
                        (B) flocculated only.

In summary, the individual examination of the dispersion and flocculation behaviors performed on quartz and kaolinite particles have shown that both particles have similar issues regarding the adsorption of anionic PAM flocculant due to pH, and that the presence of hydrolyzed metal ions (i.e., calcium and aluminum) could cause adverse effects on the flocculation of quartz and kaolinite particles. It has been verified that an excess of Ca^{2+} ions at pH $\geq$ 8 causes poor flocculation of the mixture quartz and kaolinite with flocculant only. In addition, this examination has shown the effectiveness of using aluminum ions as a coagulation aid in remediating the issues caused by the excess of Ca^{2+} ions on the flocculation of the quartz and kaolinite mixture at pH $\geq$ 8.

Photograph 3-9 shows the actual treated FFT at initial slurry density 20 wt.% solids, coagulated with 0.1% aluminum ions concentration at a 0.65% dosage (by mass of dry solids), prior to flocculation with medium charge density HMW anionic PAM flocculant at concentration of 0.1% and dosage of 0.1% (by mass of dry solids).

Photograph 3-9:   Coagulated + flocculated FFT.

Settling and bleed tests were performed after the flocculant solution was added to the coagulated FFT. A positive test was achieved when the solids and water portions of the slurry were physically separated. The separation of solids and water was clearly observed by the presence of a clear water column (overflow) above agglomerated solids (underflow). The time for solids and water separation was 14 seconds.

Figures 3-14 and 3-15 show that the FFT has a zeta potential of ‑ 47 mV (approximately) at pore water pH 8. The treated FFT has a zeta potential of ‑ 14 mV (approximately) at pore water pH 7. The treated FFT pore water has Ca^{2+} ions from the process water used for dilution and from the coagulant and flocculant solutions.
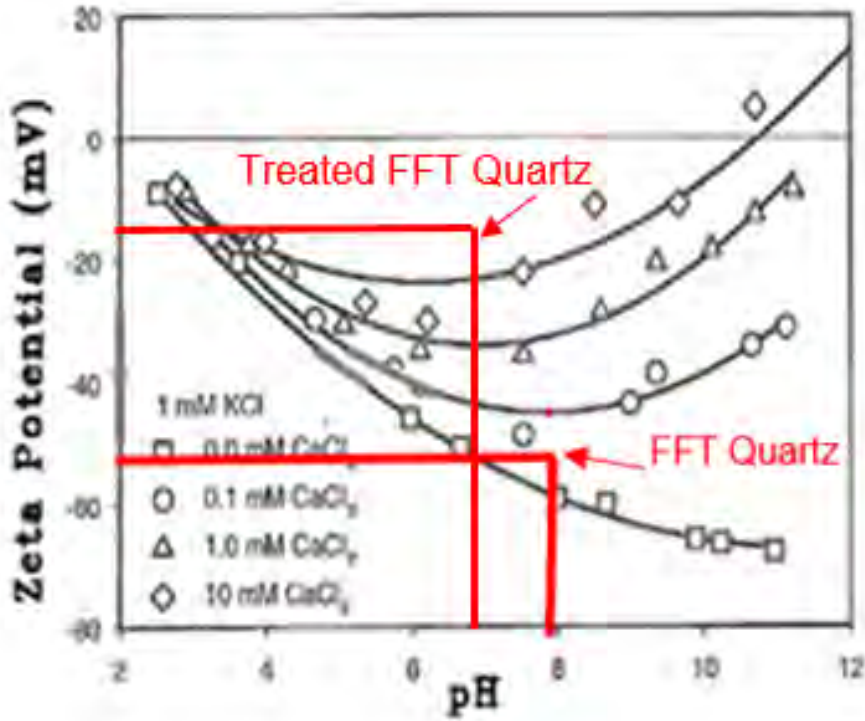
Figure 3-14: FFT and treated FFT vs. Ca^{2+} and pH – adapted from Masliyah (2004).
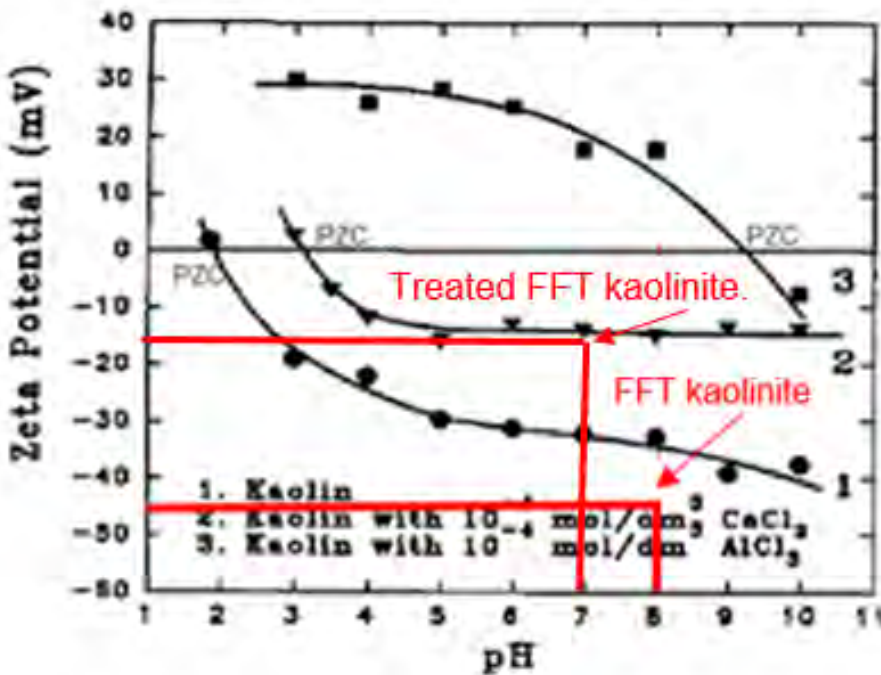
Figure 3-15: FFT and treated FFT vs. Ca^{2+}, Al^{3+}, and pH – adapted from Peng and Di (1994).

3.2.8   Flume test

A laboratory flume test was performed to visually observe the discharge of the treated FFT at an end pipe to investigate fines segregation and obtain measurements of the in-situ shear strength with time. Photograph 3-10 (C) shows the treated FFT discharged in the flume and Figure 3-16 shows the gain in undrained shear strength and solids content as a function of time.
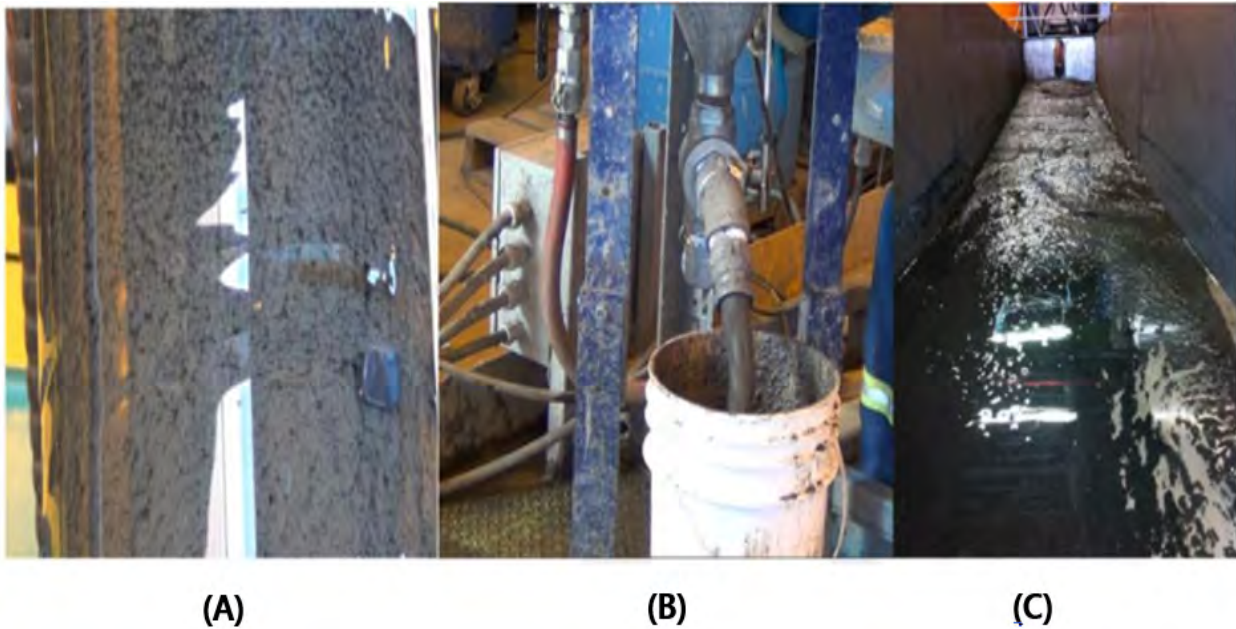
Photograph 3-10:   Lab treated FFT: (A) thickener, (B) thickener discharge, and (C) flume testing showing beach above water.

The treated FFT discharged in the flume achieved an undrained shear strength of 5 kPa between Day 16 and 37 and an undrained shear strength of 10 kPa between Day 37 and 45. The flume test results showed that more than 95% of the fines were captured on the formed beach.
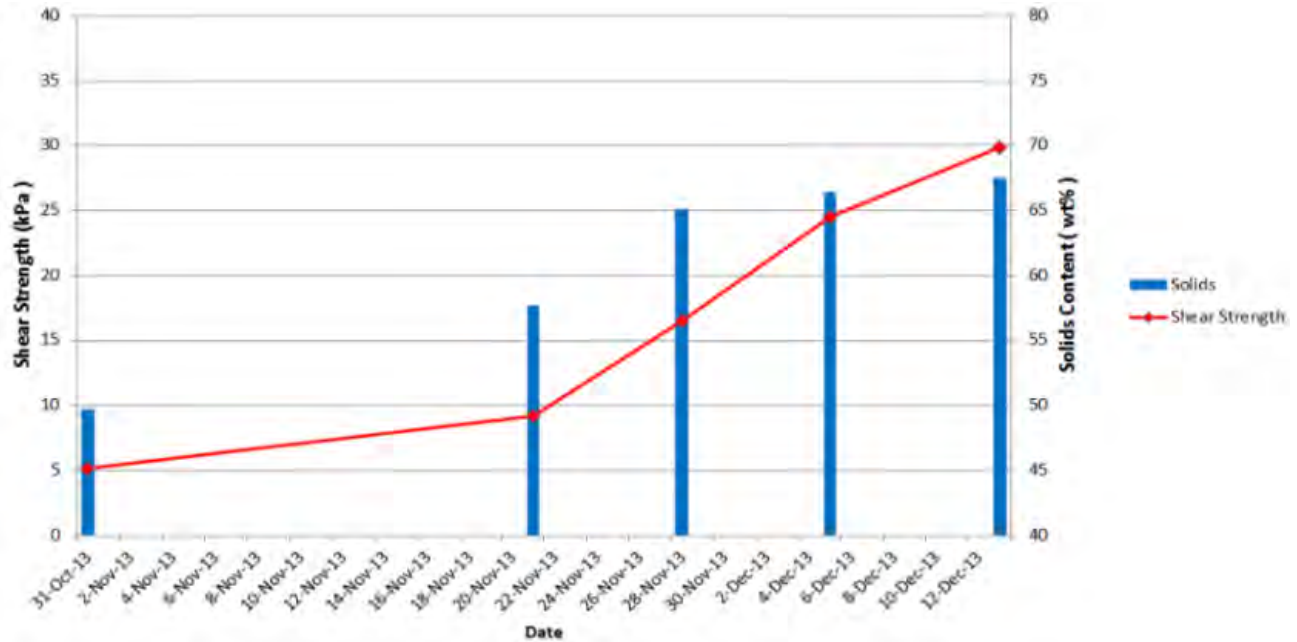
Figure 3-16: **Lab flume test on the discharged treated FFT (time vs. shear strength).**

3.2.9 Trials to evaluate FFT and treated FFT at 20 wt.% solids discharge into geotextile tubes

Photograph 3-11 shows the treated FFT inline underflow to be discharged into the geotextile tube, Photograph 3-12.

(A)   **(B)**
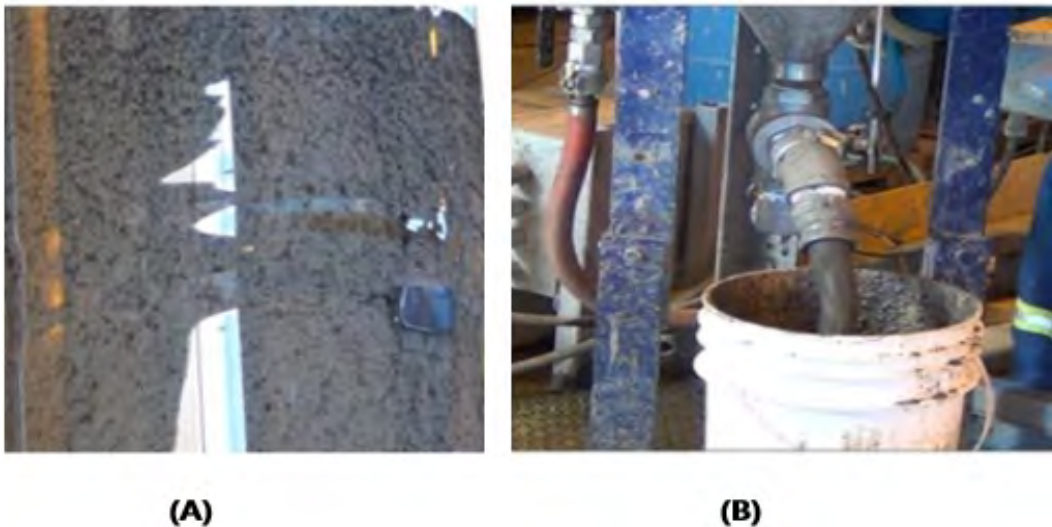
Photograph 3-11: **(A) Thickener (FFT coagulation + flocculation in a mixing tank), and (B) thickener underflow (treated FFT) to be discharged into a geotextile tube.**
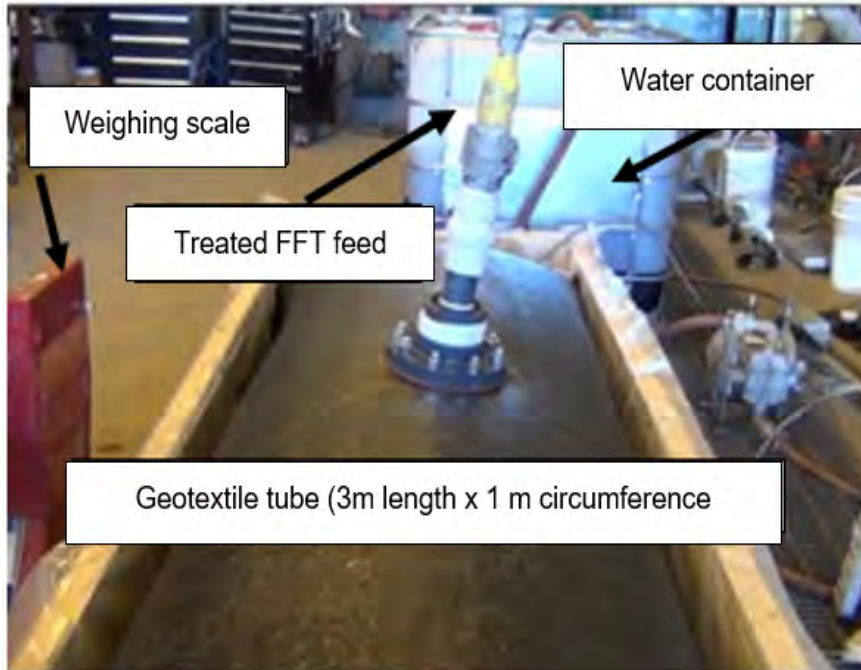
Photograph 3-12: **Geotextile tube test set up: inlet port (treated FFT from the thickener line), scale, and collection of released water into a container.**

A successful geotextile tube testing using treated FFT was opened for sampling and geotechnical testing 10 days after the geotextile tube was filled (Photograph 3-13 A). The treated FFT shear strength in the geotextile tube after a 10-day period was measured to be approximately 8 kPa and the solids content 55 wt.% solids, as shown in the Photograph 3-13 B.
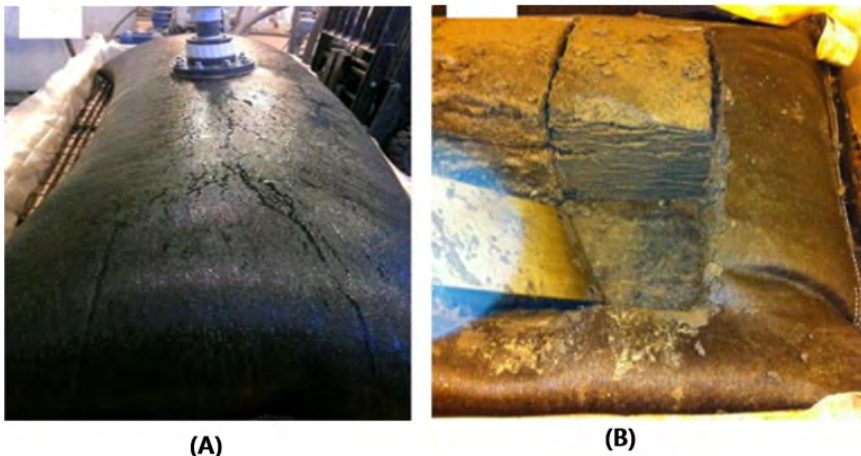
Photograph 3-13: **(A) Successful completion of filling the geotextile tube, and (B) opening the tube for sampling and testing on material behavior after a 10-day period.**

A geotextile tube test failed when FFT with flocculant only at 8 wt.% solids was discharged into the tube, which clogged the geofabric openings and released no water; therefore, the tube behaved as a waterbed-like mattress (Photograph 3-14). This tube was opened several months after filling for sampling and testing, as shown in Photographs 3-15 A and B.

Photograph 3-14: **FFT with flocculant only at 8 wt.% solids discharged into a geotextile tube. No water was released, and the tube behaved as a waterbed-like mattress during several months after filling.**

Photograph 3-15: **A and B show fines clogging the geofabric openings, impeding water release.**

In summary, an effective physicochemical treatment must be used to successfully filter/dewater the treated FFT into the geotextile tubes. The discharge of FFT with flocculant only into the tubes will clog the fabric openings, impeding the release of water and resulting in an unsuccessful use of the geotextile tubes as a filtration and dewatering process technology. The treated FFT discharged into the geotextile tube can achieve 6 kPa undrained shear strength after a 10-day period. Laboratory test results showed that the treated FFT provides 99% fines capture.

The hydraulic conductivity test results from the treated FFT thickener underflow samples indicated that a significant amount of initial water release was provided by the physicochemical recipe. Hydraulic conductivities changed from 2.56×10^{-3} to 5.87×10^{-5} cm/s at the discharge, and from 5.87×10^{-5} to 3.20×10^{-7} cm/s after 16 days. Geotextile bags are commercially available and are widely used by the mining industry. This laboratory scale trial provided adequate results for dewatering of FFT using the recipe/geotextile tubes technology.

3.2.10   Large strain consolidation (LSC) tests

LSC tests with shear strength and hydraulic conductivity measurements were performed on samples of the treated FFT at 20 wt. solids with the recipe from the thickener underflow discharge in Photograph 3-10 (B). The tests were conducted to determine the relationship between void ratio and vertical effective stress (compressibility), the relationship between void ratio and hydraulic conductivity (permeability), and the relationship between void ratio and undrained shear strength. The LSC tests were conducted to investigate the performance of the recipe when discharged at an end pipe. The LSC test, performed at the University of Alberta, is a multi-step loading test. The test apparatus and procedures have been slightly modified to allow vane shear tests to be performed at different void ratios (Scott et al., 2008). The consolidation cell is 140 mm inside diameter and can accommodate samples up to 200 mm high. The wall friction is minimized by choosing the appropriate initial height of the sample so the sample at high stresses (≥ 10 kPa) has a diameter to height ratio of approximately 2.5 to 3. In addition, the height of the sample should be kept as high as possible to minimize errors in measuring the thickness of the sample.

Each sample was tested at effective stress ranges from approximately 0.5 kPa to 2239.4 kPa. LSC tests were performed on two samples: shear strength was measured in one sample and compressibility and permeability were measured in the other sample. The reason for a second sample was to avoid any sample disturbance caused by the vane shear strength tests that could affect the compressibility and permeability measurements. Both samples were tested at the same time under the same loading conditions. The hydraulic conductivity was measured at the end of consolidation for each loading step. The upward gradient in the test was kept as small as possible so the seepage force did not exceed the applied stress. The shear strength was measured using a laboratory vane apparatus at the end of the consolidation and prior to applying the subsequent load. Results of the LSC tests are presented in Figures 3-17 to 3-19 and in Table 3.8.
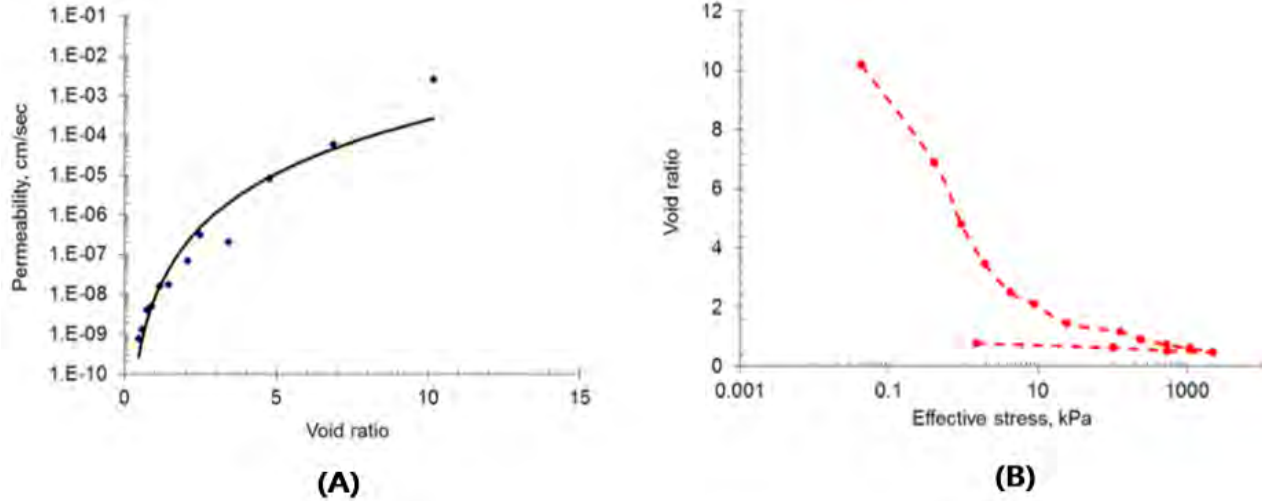
Figure 3-17: **(A) Treated FFT permeability – Cell 1, and (B) treated FFT compressibility – Cell 1.**

Table 3-8: **LSC test results of the treated FFT with coagulation applied prior to flocculation.**

Load	Effective stress (kPa)		Height (mm)		Solid content (wt.% solids)		Void ratio		Hydraulic conductivity (cm/sec)		Shear strength (kPa)	
	Cell 1	Cell 2	Cell 1	Cell 2	Cell 1	Cell 2	Cell 1	Cell 2	Cell 1	Cell 2	Cell 1	Cell 2
Self-weight	0.043	0.056	65.0	68.0	19.7	24.1	10.190	7.872	2.56×10^{-3}	1.46×10^{-2}	-	0.2
2	0.41	0.47	45.8	46.7	26.6	32.90	6.890	5.095	5.87×10^{-5}	5.45×10^{-5}	-	0.5
3	0.94	1.05	33.7	33.4	34.28	42.70	4.790	3.355	8.07×10^{-6}	1.50×10^{-6}	-	1.2
4	1.96	1.97	26.6	24.9	41.09	53.69	3.450	2.245	2.11×10^{-7}	2.48×10^{-7}	-	2.1
5	4.33	4.35	20.3	22.2	50.07	56.91	2.490	1.893	3.20×10^{-7}	1.54×10^{-7}	-	3.0
6	9.15	8.51	18.0	19.6	54.40	61.62	2.100	1.557	8.77×10^{-8}	7.03×10^{-8}	-	5.0
7	24.3	24.3	14.3	16.4	63.18	68.70	1.457	1.139	1.76×10^{-8}	2.37×10^{-8}	-	9.0
8	129.8	115.6	12.6	15.5	68.23	70.99	1.164	1.022	1.60×10^{-8}	1.75×10^{-8}	-	12.0
9	243.8	243.9	11.1	14.7	73.40	73.27	0.906	0.912	4.98×10^{-9}	6.74×10^{-9}	-	17.5
10	528.9	528.9	10.1	13.8	77.22	75.82	0.737	0.797	4.01×10^{-9}	3.97×10^{-9}	-	25.0
11	1099.1	1099.1	9.3	12.8	80.65	78.99	0.600	0.665	1.29×10^{-9}	2.43×10^{-9}	-	37.5
12	2239.4	2239.4	8.5	12.1	84.16	81.25	0.471	0.577	7.6×10^{-10}	1.5×10^{-9}	-	58.0
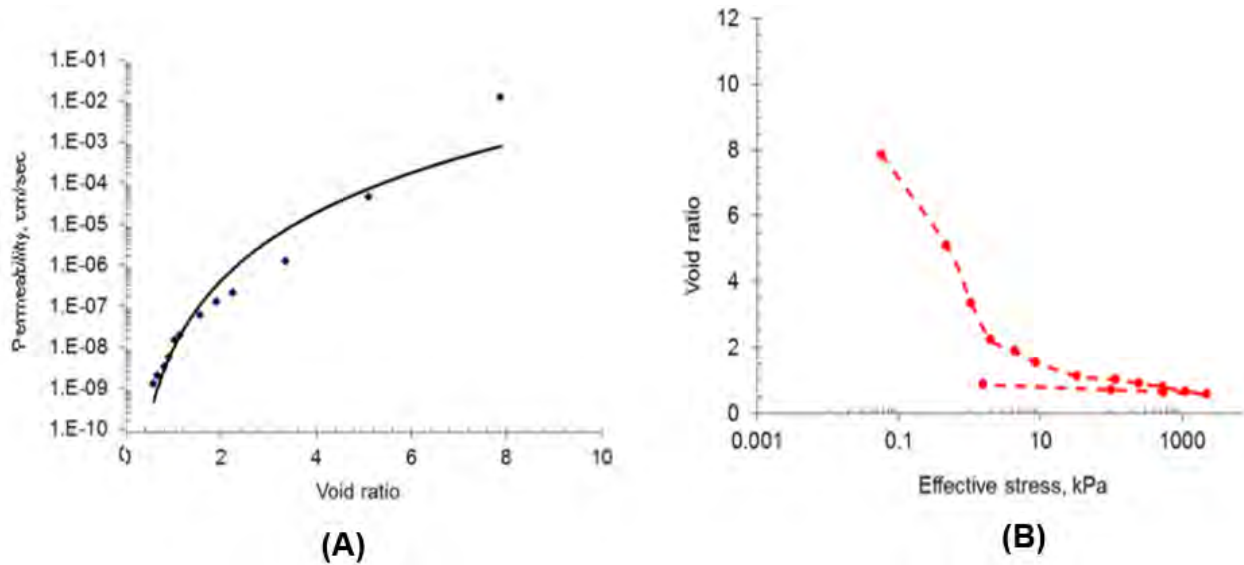
Figure 3-18: **(A) Treated FFT permeability – Cell 2, and (B) treated FFT compressibility – Cell 2.**
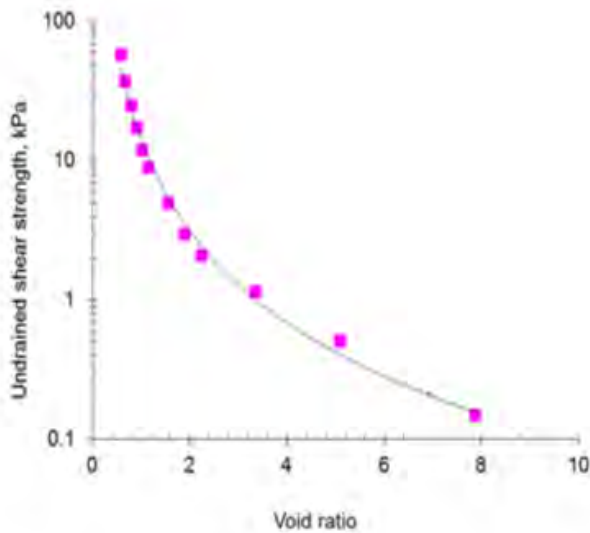
Figure 3-19: **Treated FFT shear strength – Cell 2.**

The hydraulic conductivity test results from treated FFT laboratory thickener underflow samples (Photograph 3-10B) indicated that a significant amount of initial water release was provided by the recipe. Hydraulic conductivities changed from 2.56×10^{-3} cm/s to 5.87×10^{-5} cm/s at the discharge, and from 5.87×10^{-5} cm/s to 3.20×10^{-7} cm/s after 16 days.

Thickening tailings by adding synthetic polymers is a common practice used by most mining operators; this process relies on the flocculants' beneficial effects of agglomerating fine tailings particles. However, significant amounts of trapped water remain in the flocculated tailings affecting consolidation timeframes, postponing shear strength gain, and causing long consolidation timeframes that pose significant challenges in the conversion of the FFT into deposits capable of facilitating reclamation.

The following Photographs 3-16 to 3-20 show images of LSC test results to exemplify why flocculant only is not enough to provide efficient dewatering of FFT, and how coagulant addition improves excess pore pressure dissipation and consequently consolidation of the FFT.
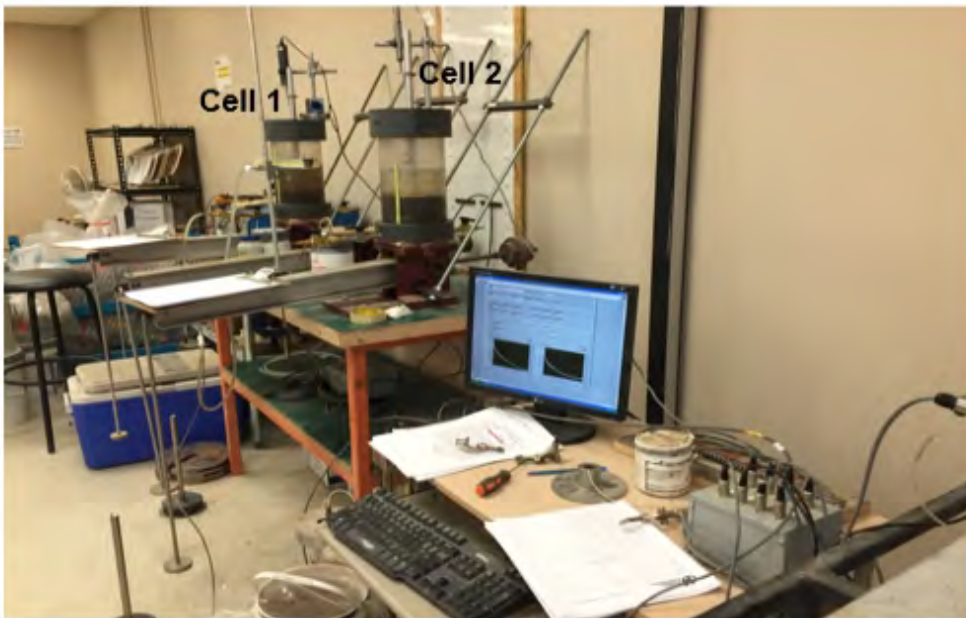
Photograph 3-16:   **Large strain consolidation Test 1 Cell 1 (with flocculation only) and Test 2 Cell 2 (with coagulation and flocculation).**
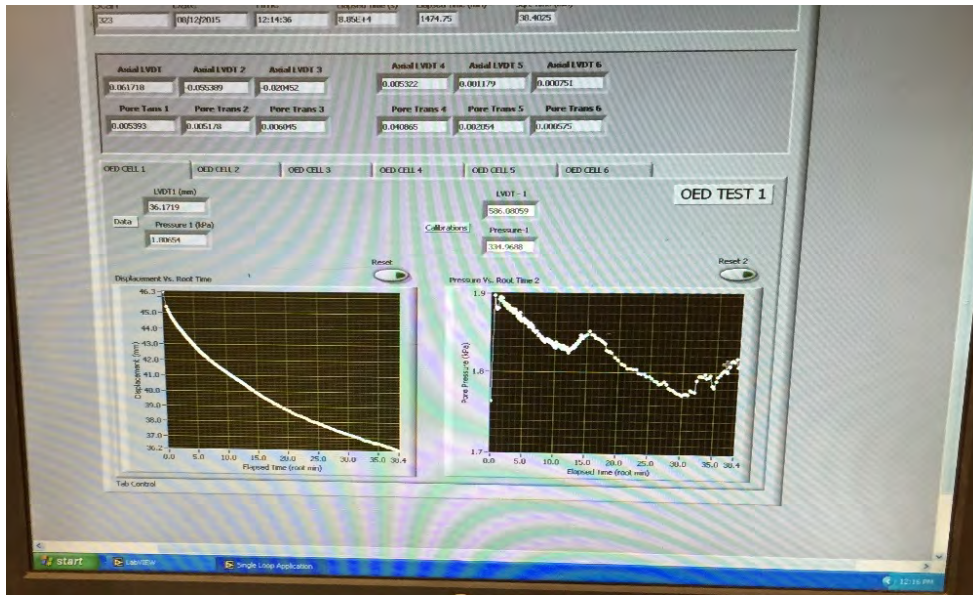
Photograph 3-17:   Large strain consolidation Test 1 Cell 1 displacement (left screen) and pore pressure dissipation (right screen) illustrate the results with flocculant only.
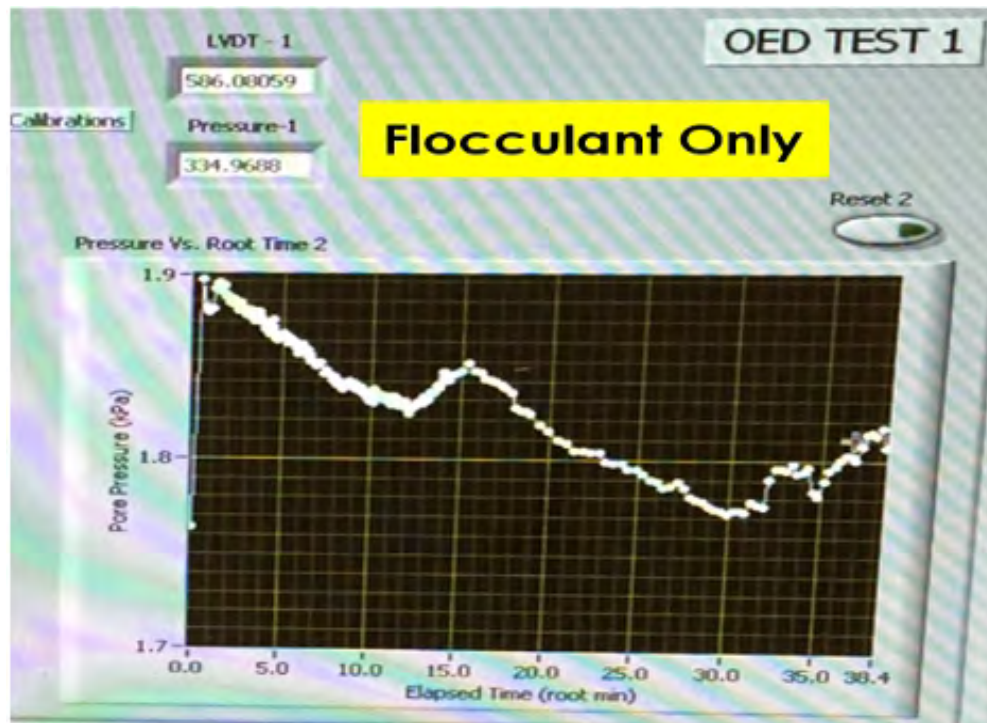
Photograph 3-18:   LSC Test 1 Cell 1 illustrates the results of the pore pressure dissipation.
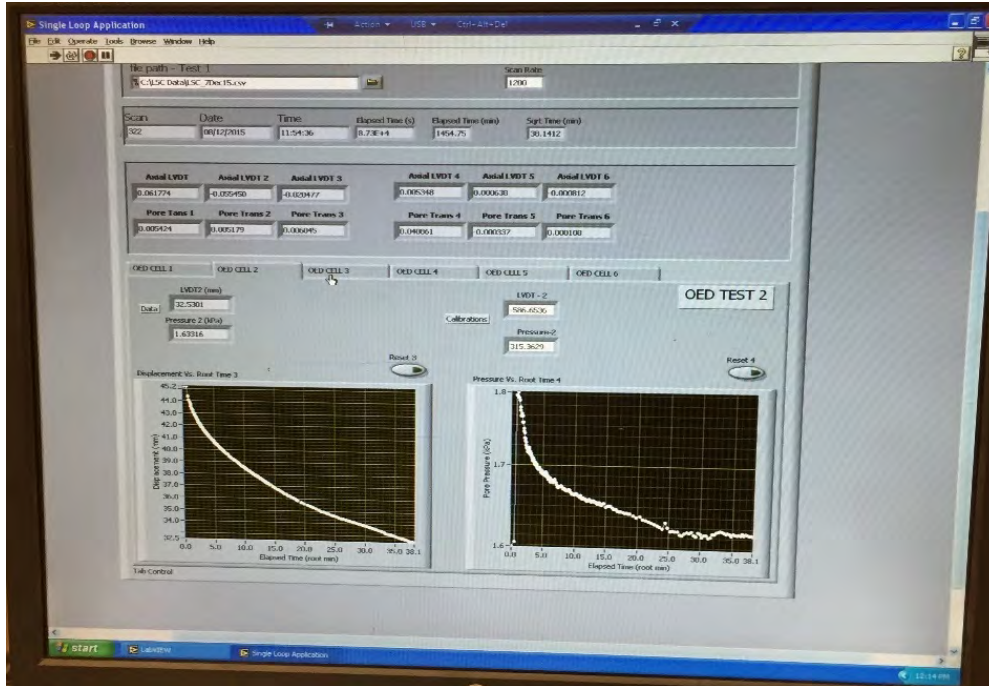
Photograph 3-19: **LSC Test 2 Cell 2 displacement and pore pressure dissipation illustrate the results with coagulation applied prior to flocculation.**
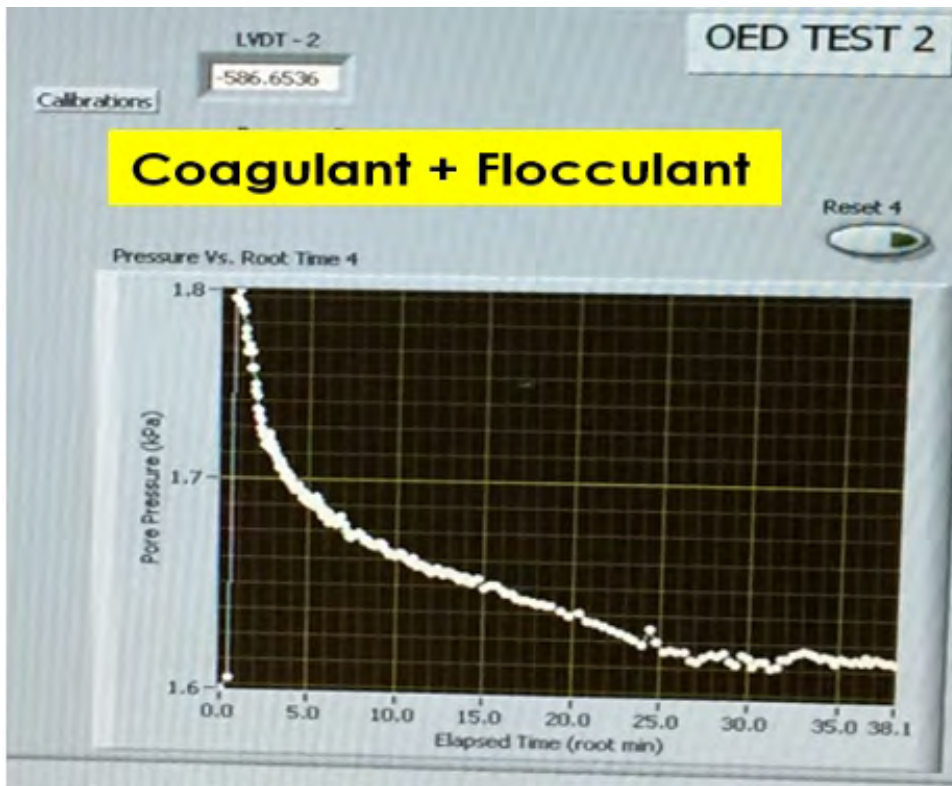
Photograph 3-20: **LSC Test 2 Cell 2 illustrates the results of the pore pressure dissipation.**

3.2.11   Large strain consolidation tests on treated FFT using synthetic fibers

LSC tests with measurements of shear strength and hydraulic conductivity were also performed on geo-composite samples using synthetic fibers to investigate the increased shear strength behavior of the treated FFT. This is an experimental study, and its supporting data indicate that the geo-composite recipe successfully assists FFT solids/water separation by decreasing the time of dewatering, providing rapid consolidation, and increasing undrained shear strength with time. The process also responds quite well to a relative rapid loading to form deposits of enhanced physical stability compared with conventional wet soft tailings deposits. These LSC tests were used to simulate the discharge of the geo-composite recipe in open pit deep deposits.

The LSC test was performed at the University of Alberta. Each sample was tested under an effective stress range from approximately 0.5 kPa to 640 kPa to cover the stress range that the geo-composite recipe might experience in the field (i.e., open pit deep deposits). LSC tests were performed on two samples: one to measure the shear strength and another to measure compressibility and permeability. The geo-composite recipe proposed in this study uses coagulation and flocculation with the reinforcement of the shear strength provided by the synthetic fibers. The use of synthetic fibers for improving soil engineering mechanical properties has been addressed by other authors, as referenced in this research. Photograph 3-21 shows a settling test performed on the geo-composite recipe. The initial slurry density of the FFT was 20 wt.% solids, the FFT was coagulated with 0.1% aluminum ions concentration at 0.65% dosage (by mass of dry solids) prior to flocculation with 30% charge HMW anionic PAM polymer at concentration of 0.1% and dosage 0.1% (by mass of dry solids). Nylon fibers with 8-mm length at 0.7% concentration (by mass of dry solids) were mixed throughout the flocculant solution prior to addition to the coagulated FFT.

Photograph 3-21: **Settling test performed on the geo-composite recipe (treated FFT with fibers).**

Table 3-9 shows the results of the LSC tests on treated FFT without fibers, and Figures 3-20 to 3-22 show their respective graphics.

Table 3-9: **LSC/ e / k / S_u test results from treated FFT without fibers.**

Effective Stress (kPa)	Void Ratio (e)	Solids Content (%)	k (m/s)	Shear Strength S_u (kPa)
0.1	6.89	27	3.91×10^{-7}	0.13
0.7	5.00	34	Not measured	0.30
1.0	4.20	38	Not measured	Not measured
1.91	3.23	44	4.25×10^{-8}	0.70
3.87	2.27	53	9.68×10^{-9}	Not measured
6.32	1.87	58	3.93×10^{-9}	1.87
10.0	1.16	69	1.90×10^{-9}	2.86
19.21	1.01	72	2.11×10^{-10}	4.93
38.42	0.87	75	1.76×10^{-10}	6.70
76.84	0.68	79	8.02×10^{-11}	9.70
153.7	0.53	83	7.80×10^{-11}	15.16
307.3	0.41	86	2.19×10^{-11}	21.47
640.3	0.31	89	7.50×10^{-12}	36.71
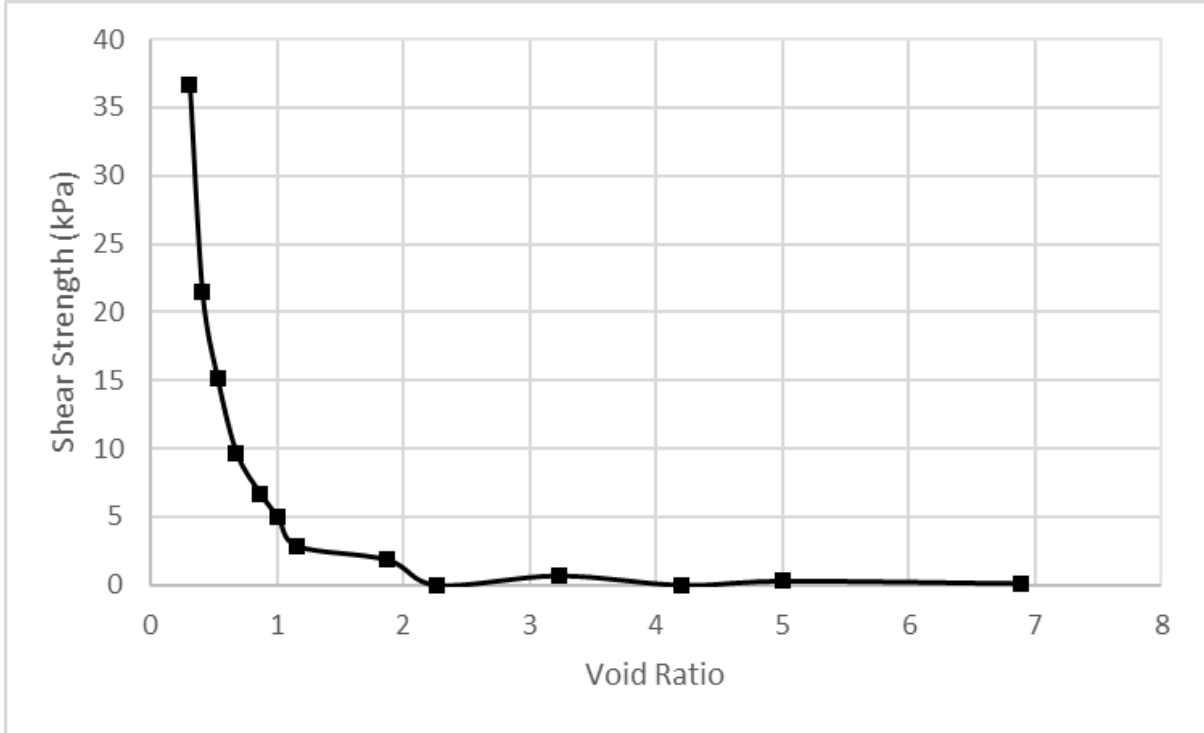
Figure 3-20: **Undrained shear strength (Su) vs. void ratio – treated FFT without fibers.**
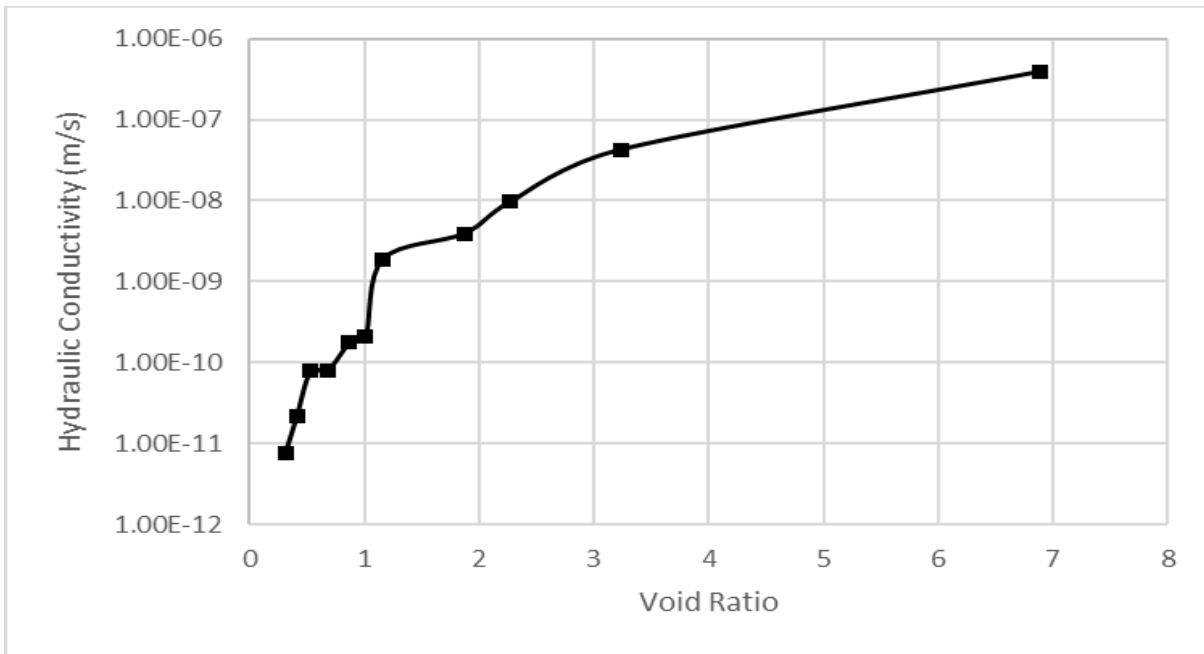
Figure 3-21: **Hydraulic conductivity (k) vs. void ratio – treated FFT without fibers.**
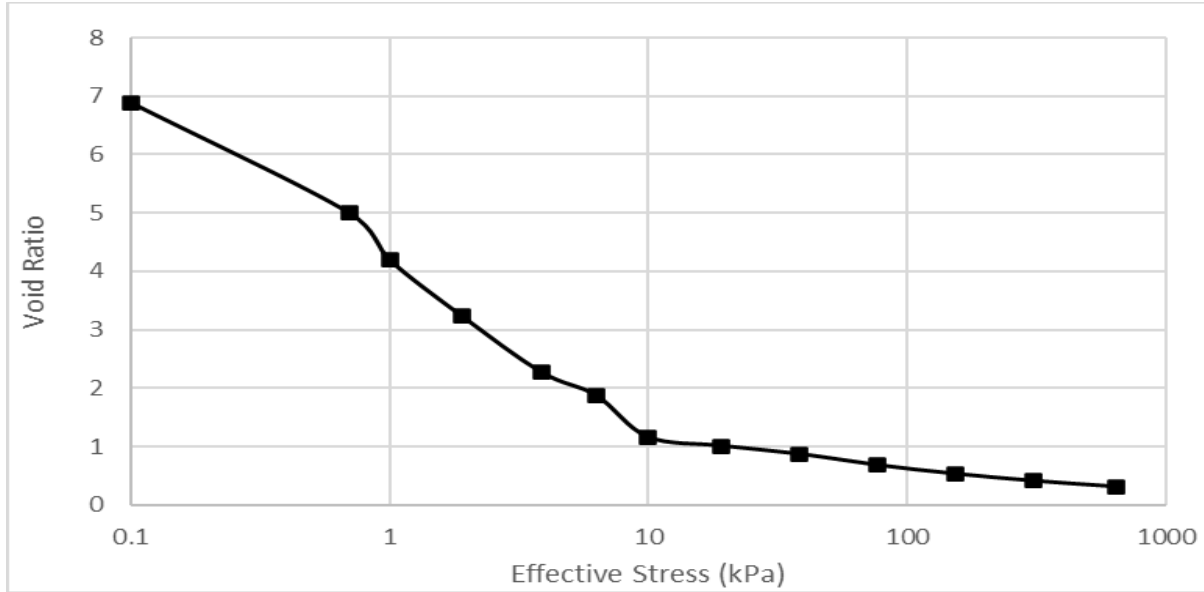
Figure 3-22: Void ratio vs. effective stress – treated FFT without fibers.

Table 3-10 shows the results of the LSC tests on treated FFT with fibers, and Figures 3-23 to 3-26 show their respective graphics. In addition, Figure 3-27 shows the undrained shear strength versus depth for the treated FFT with and without fibers. Furthermore, Figures 3-28 and 3-29 show the excess pore pressure dissipation and settlement results with fibers, respectively.

Table 3-10: LSC/ e / k / S_u test results from the treated FFT with fibers.

Effective Stress (kPa)	Void Ratio (e)	Solids Content (%)	k (m/s)	Shear Strength S_u (kPa)
0.5	3.00	46	3.26E-07	Not measured
1.47	2.00	56	4.40E-08	Not measured
1.79	1.88	58	2.58E-08	Not measured
2.76	1.64	61	1.94E-08	0.31
4.25	1.51	63	6.63E-09	Not measured
6.21	1.34	66	2.34E-09	1.70
8.66	1.17	69	9.27E-10	2.00
13.26	1.07	71	5.27E-10	9.80
24.29	0.97	73	3.40E-10	14.40
40.39	0.88	75	1.10E-10	34.00
100.0	0.78	77	8.20E-11	76.90
200.0	0.68	79	2.06E-11	116.00
400.0	0.60	81	8.49E-12	180.00
640.0	0.46	85	-	260.00
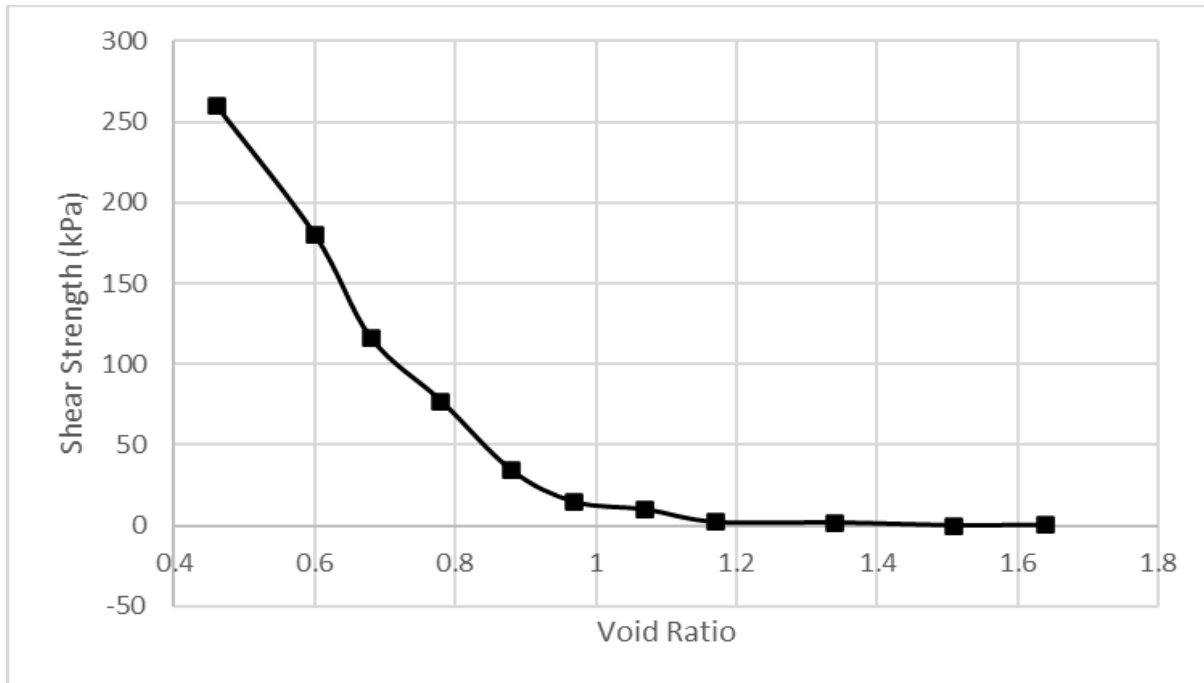
Figure 3-23: Undrained shear strength (Su) vs. void ratio – treated FFT with fibers.
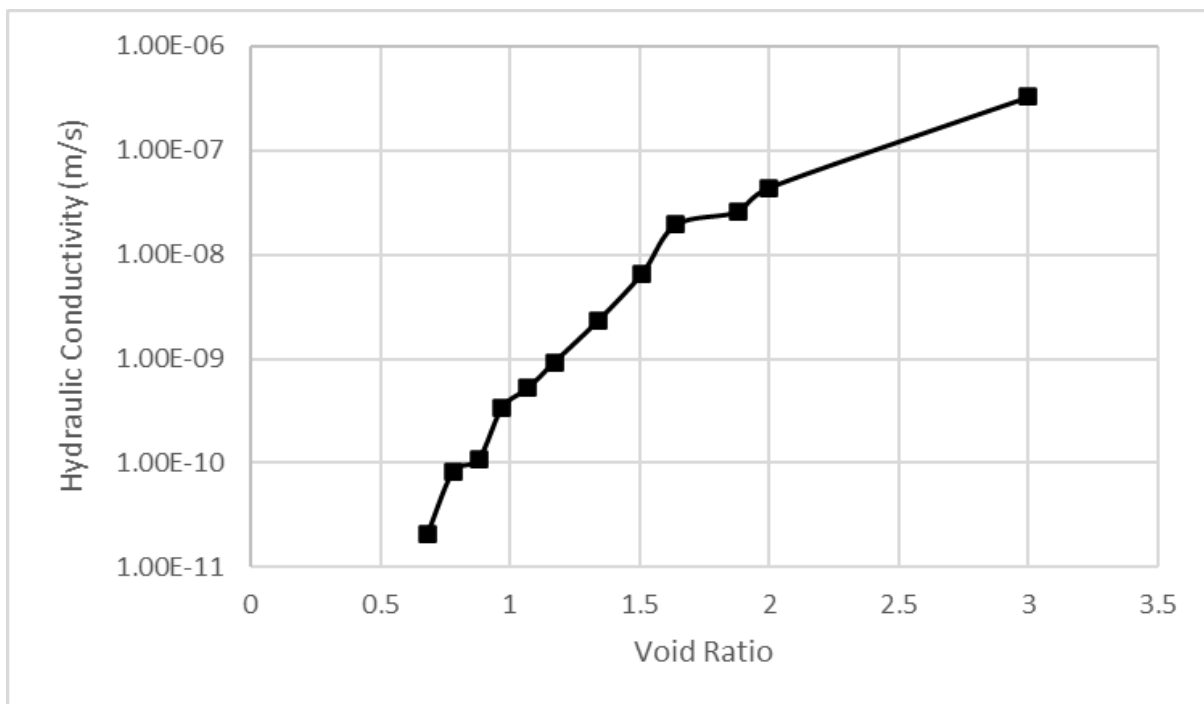
Figure 3-24: Hydraulic conductivity (k) vs. void ratio – treated FFT with fibers.
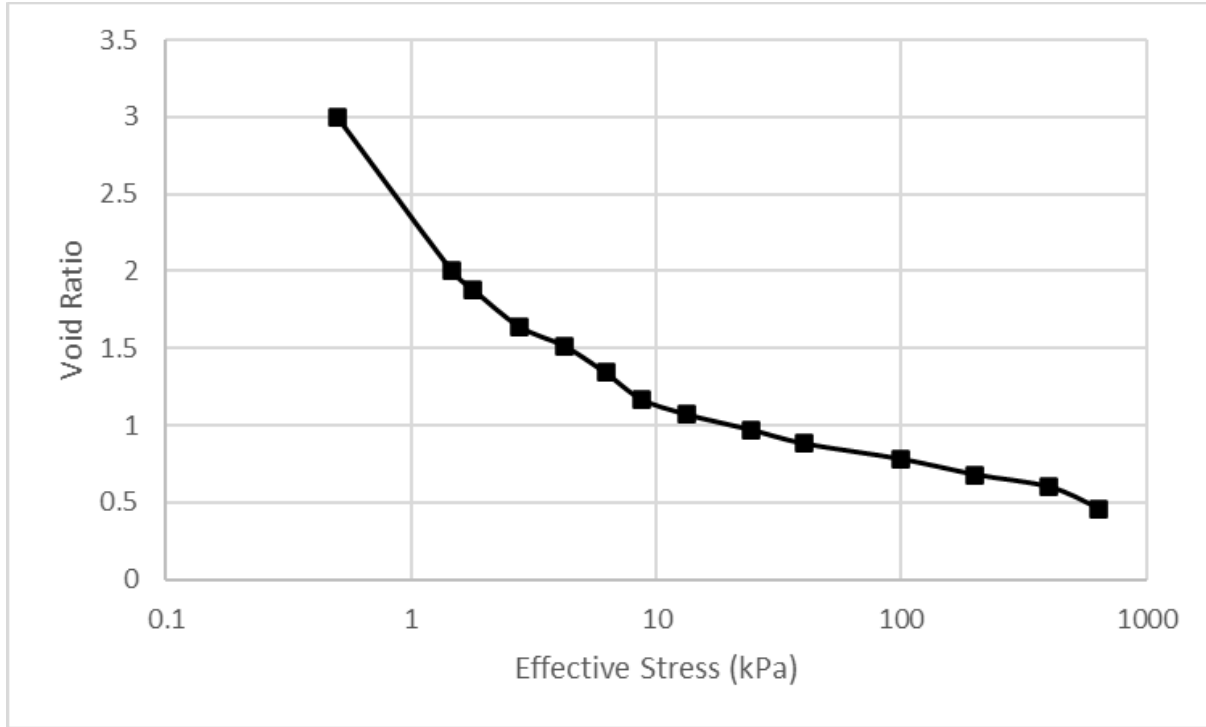
Figure 3-25: **Void ratio vs. effective stress – treated FFT with fibers.**
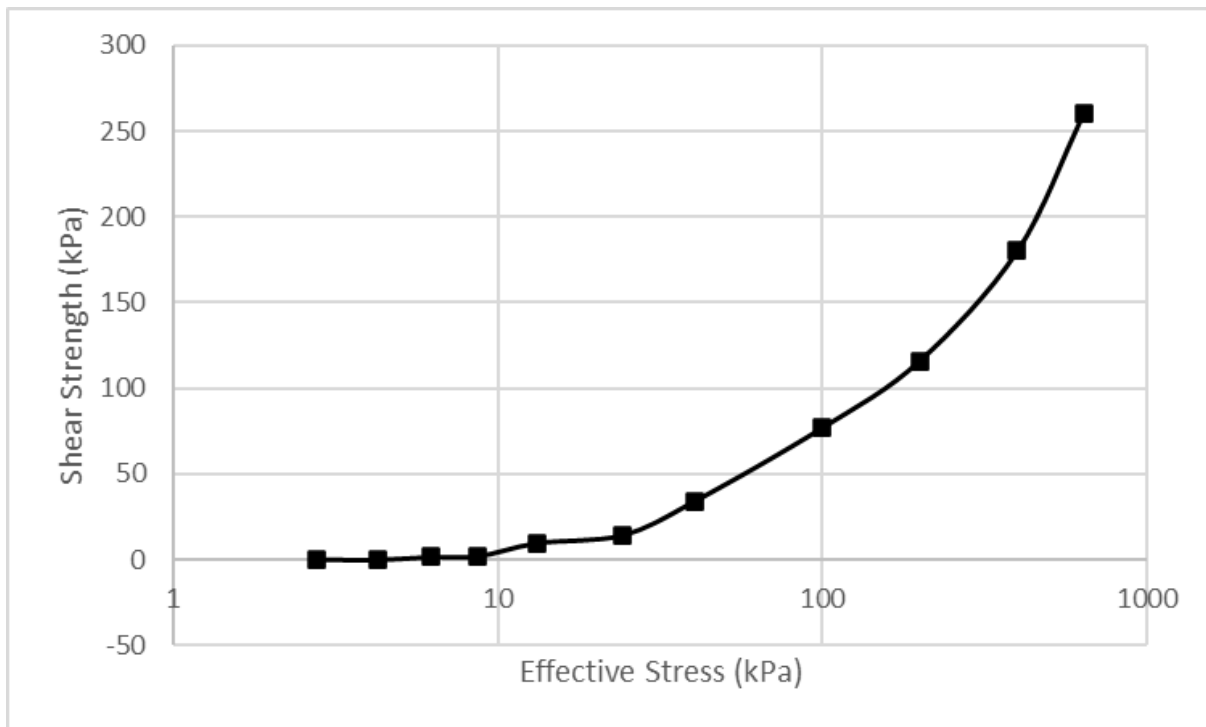
Figure 3-26: **Undrained shear strength (Su) vs. effective stress – treated FFT with fibers.**
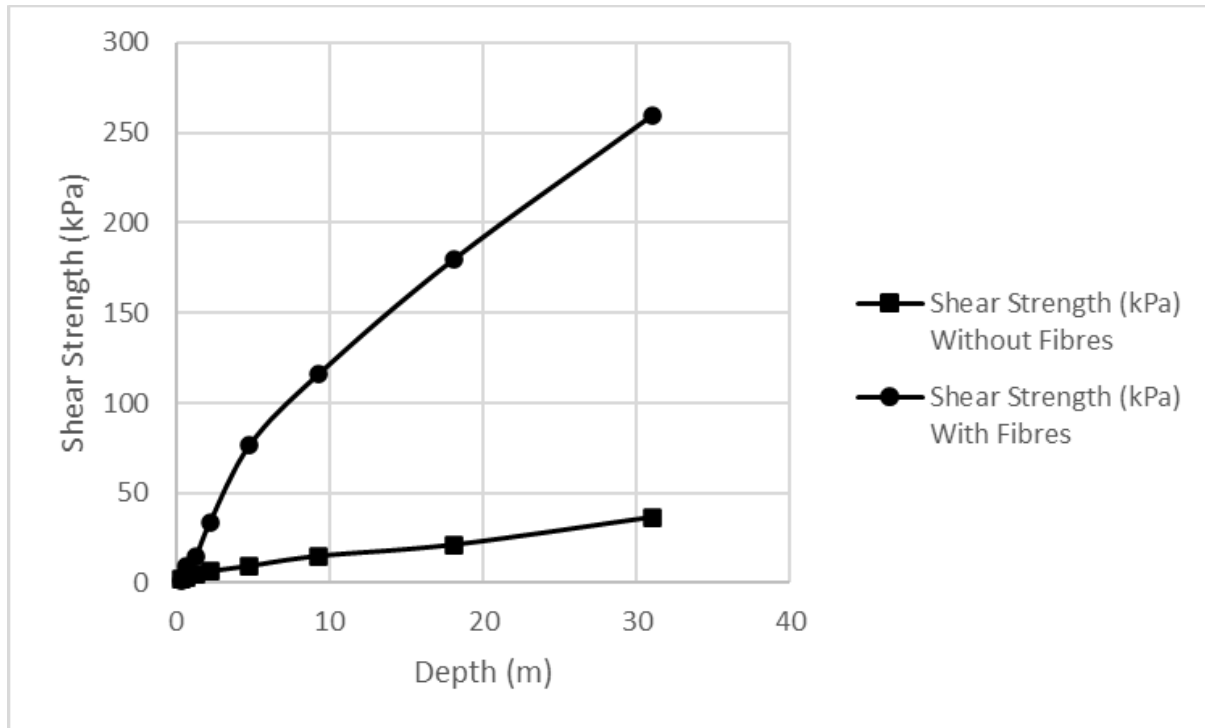
Figure 3-27: **Undrained shear strength (Su) vs. depth – treated FFT with and without fibers.**
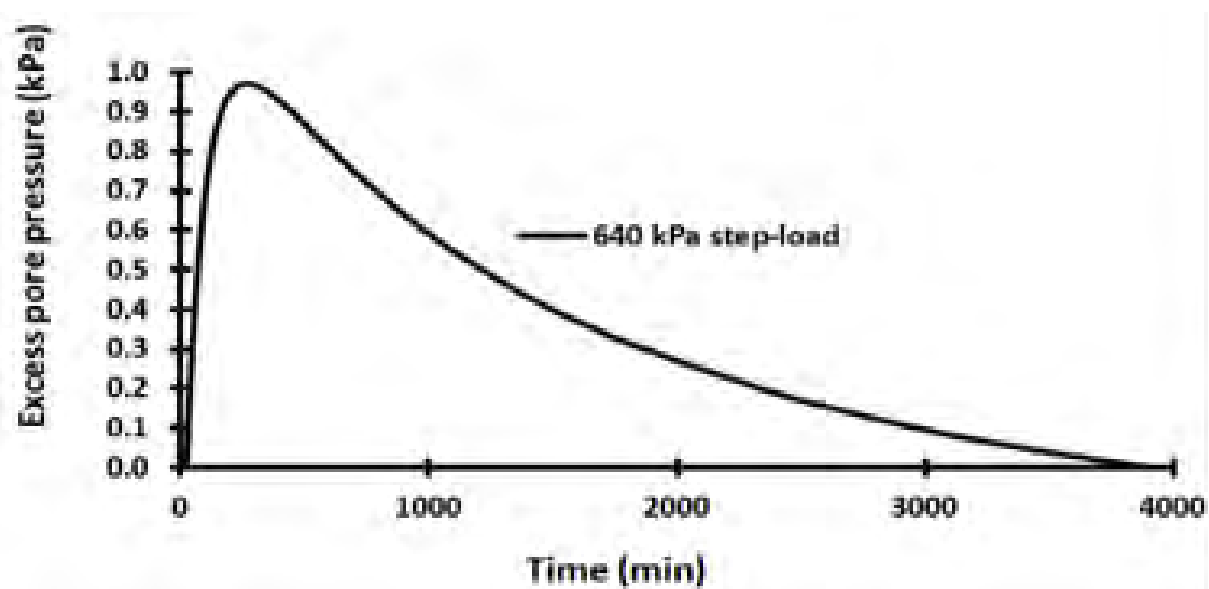
Figure 3-28: **Excess pore pressure dissipation vs. time – treated FFT with fibers.**
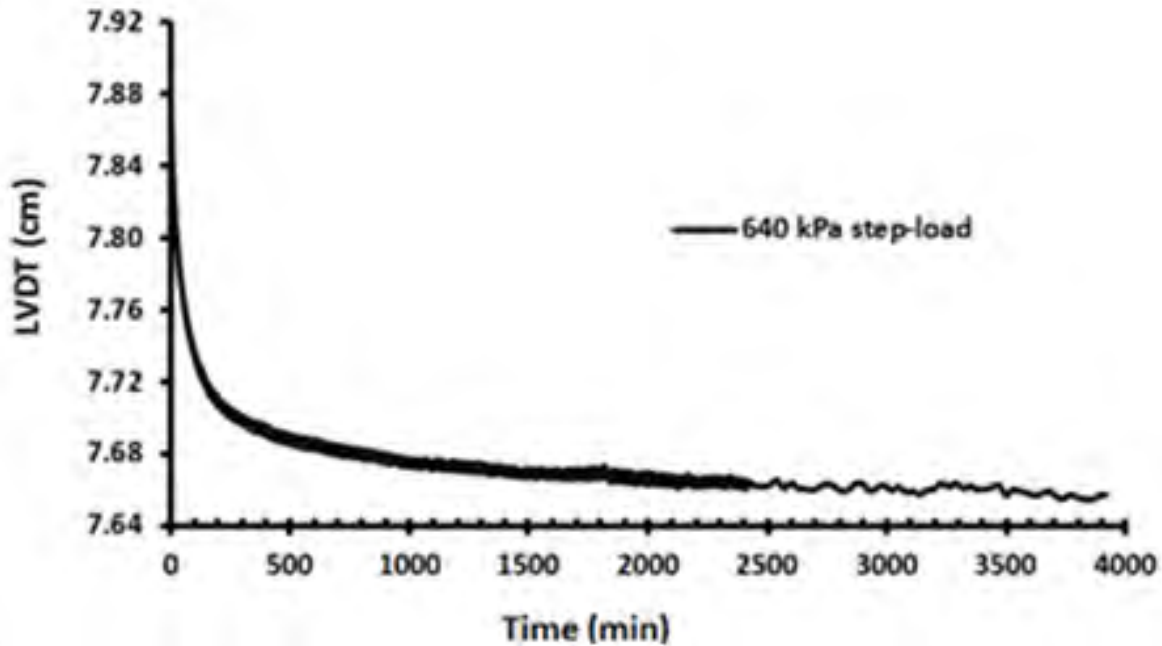
Figure 3-29: Time vs. settlement – treated FFT with fibers.

In summary, the fundamentals of the FFT dispersion-flocculation behavior and the enhanced undrained shear strength of the FFT deep deposits using synthetic fibers as a geo-composite recipe have been investigated and presented in this research. The supporting data indicate that the geo-composite recipe successfully assists FFT solids/water separation in decreasing the time of dewatering, providing rapid consolidation, and increasing undrained shear strength with depth compared with the same treatment without fibers.

3.2.12   Settlement of the treated FFT (recipe) using geotechnical beam centrifuge testing

Geotechnical materials behave differently at different stress levels; vertical stress is a key point. Due to the high *g*-forces generated during centrifuge spinning, a similar stress profile as in the prototype could be created even in a scaled model, through which the material in the centrifuge model could have the same behavior as that in the prototype. The scaling law should be employed to determine the appropriate model configurations to simulate a certain prototype and analyze the data collected during the test. Photographs 3-22 to 3-24, and Figures 3-30 to 3-35 present the results of the beam centrifuge tests.
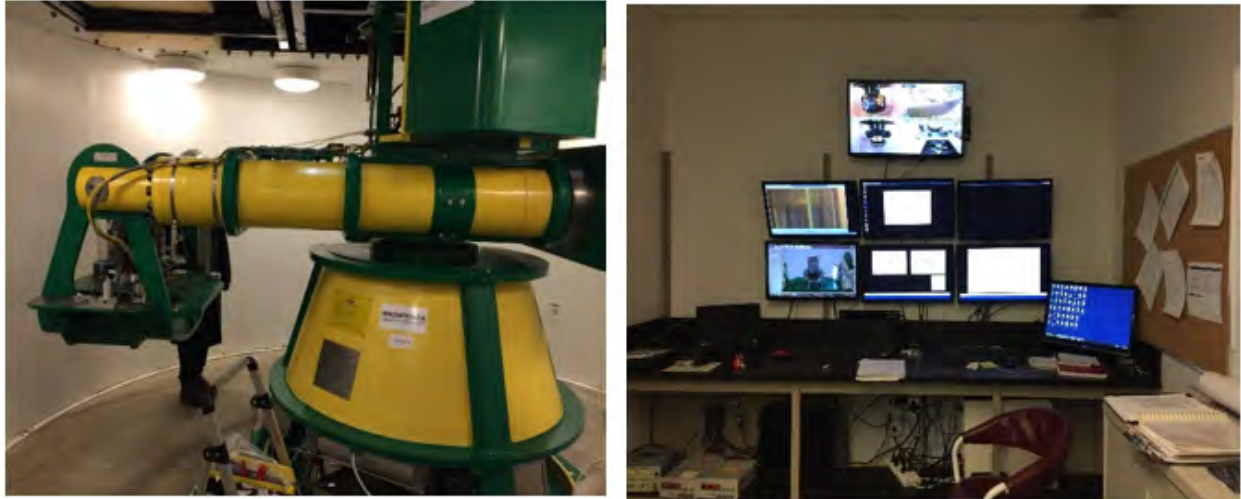
Photograph 3-22:   Geotechnical beam centrifuge apparatus and control room.

Photograph 3-23:   End of the test sample (left) and sampling from the testing cell (right).

Photograph 3-24:   End of the test sample (left) and sampling from the testing cell (right).
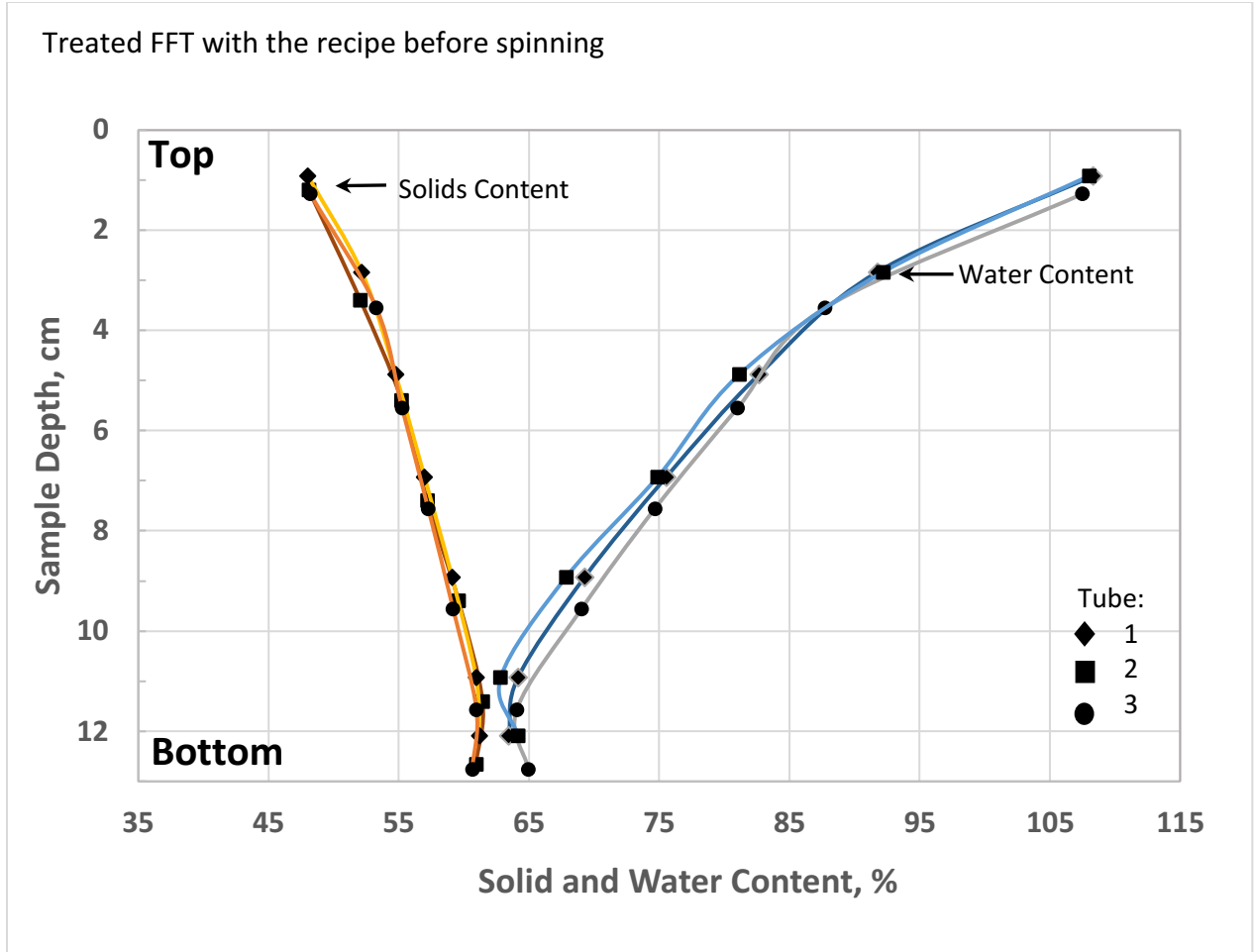
Figure 3-30: **Treated FFT with the recipe before spinning; average solids content = 56% and average water content 78.7% top to bottom.**
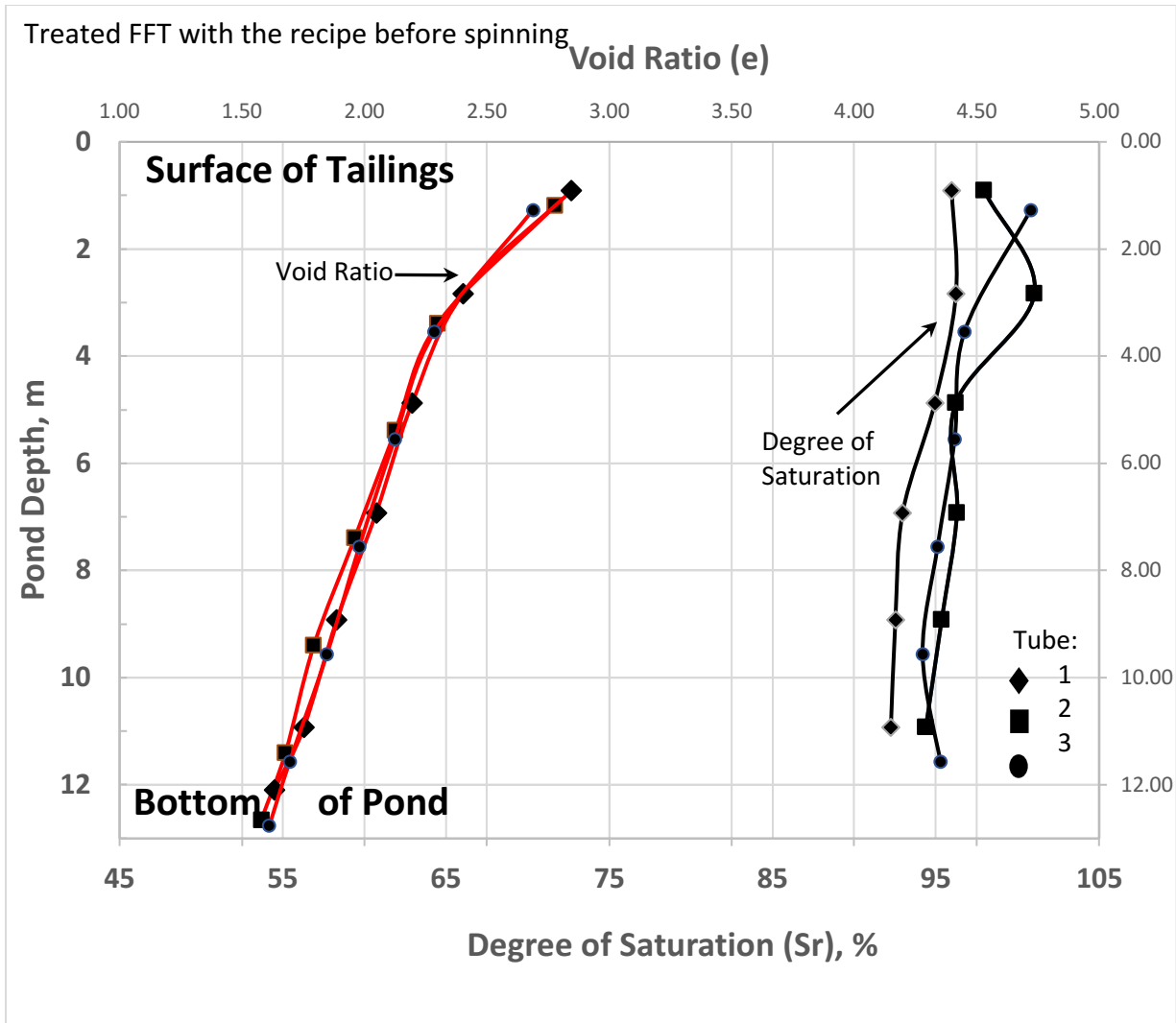
Figure 3-31: Treated FFT with the recipe before spinning; average void ratio = 2.06; degree of saturation = 100%; solids content 56%; wet density = 1.50 t/m³; and dry density = 0.83 t/m³.
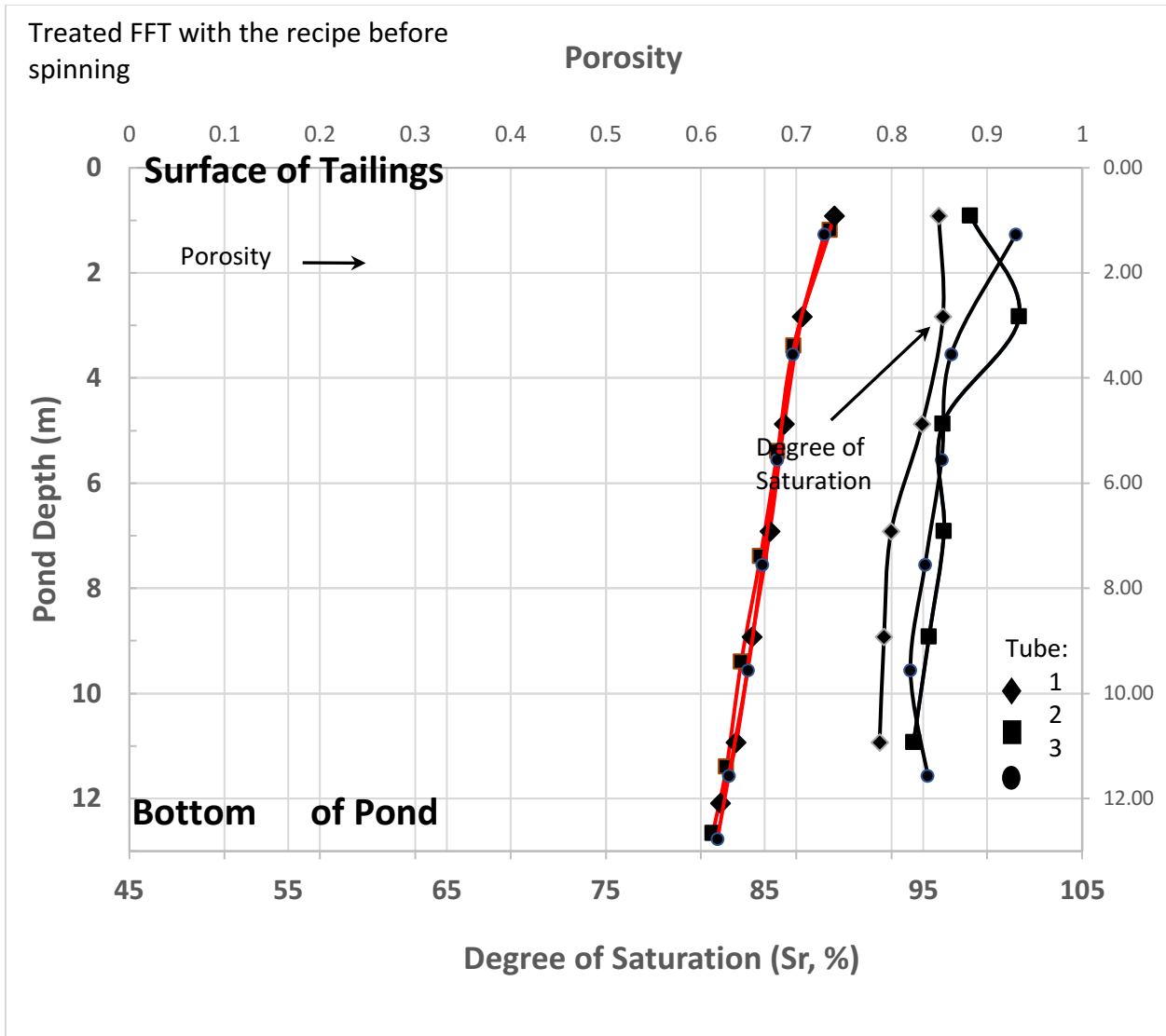
Figure 3-32:   Treated FFT with the recipe before spinning; average porosity = 0.63
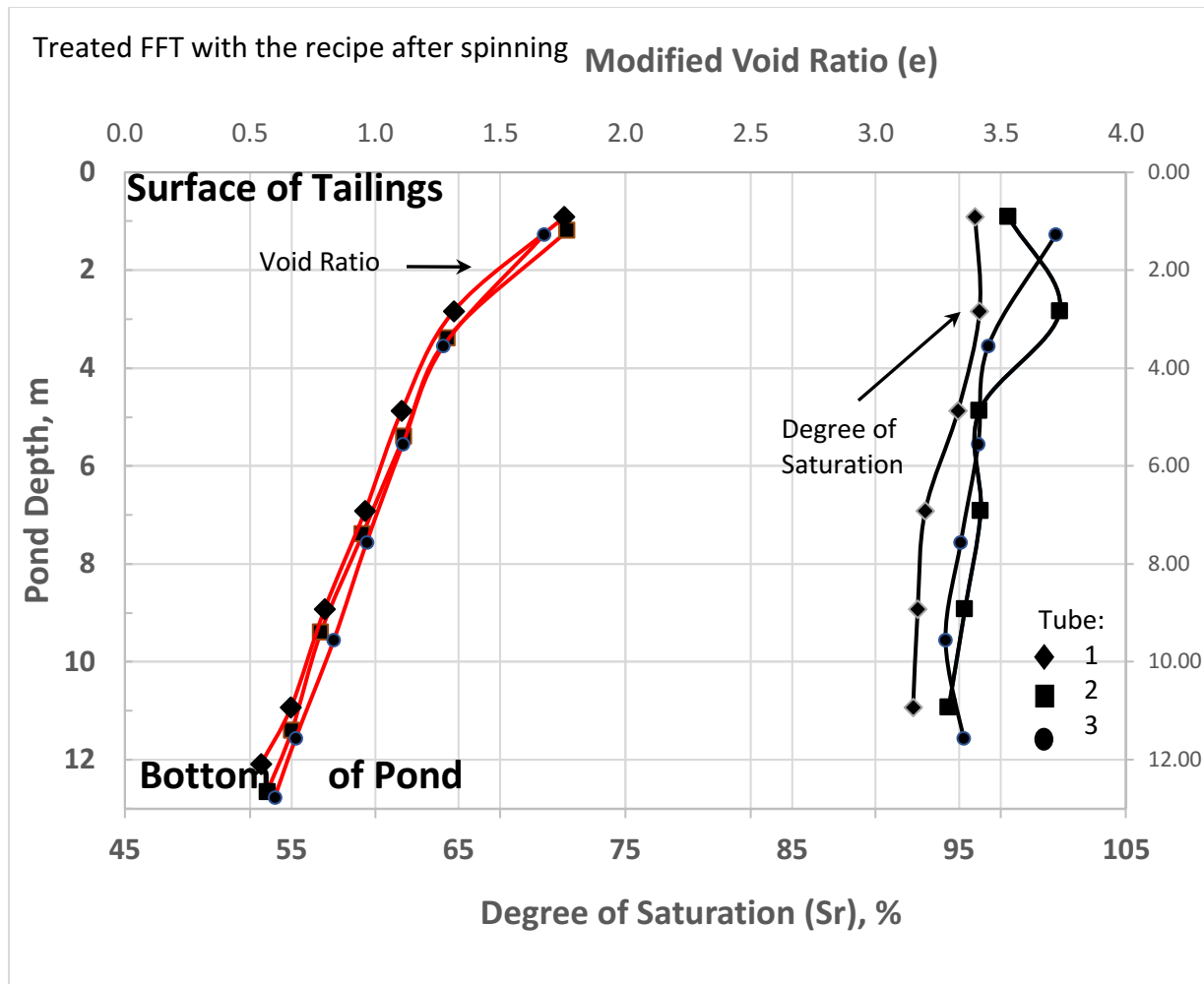
Figure 3-33: **Treated FFT with the recipe after spinning; average modified void ratio € = 1.02; degree of saturation = 100%; solids content = 71.4% wet density = 1.75 t/m³; and dry density = 1.25 t/m³.**

In summary, upon reviewing the laboratory geotechnical beam centrifuge test results, volume change could be a criterion for acceptance of ready-to-reclaim FFT within 10 years of the end of mine-life. Porosity, of course, is the volume of water divided by the total volume. Previous experience has shown that FFT must have a minimum shear strength of 10 kPa to allow the surface to be reclaimed. Field trials as part of this research have indicated that a shear strength of 10 kPa is reached at a porosity of 0.5, which is equivalent to 70 wt.% solids. Figure 3-39 shows that porosity 0.5 is reached at depth of 6 m of the treated FFT deposit. Atmospheric drying and/or freeze/thaw effects will be needed to decrease the surface porosity to an acceptable value that will allow reclamation.
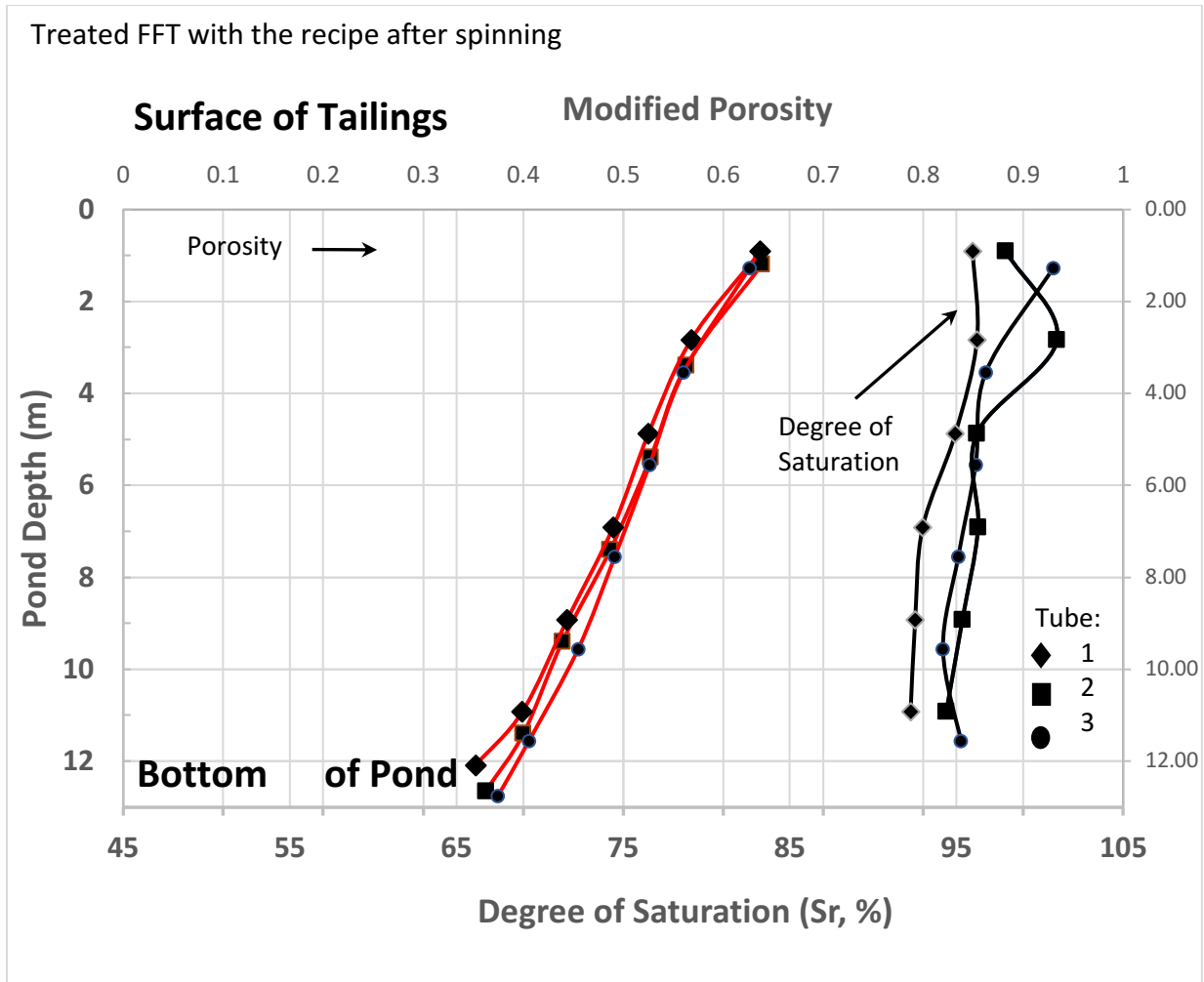
Figure 3-34: **Treated FFT with the recipe after spinning; average modified porosity = 0.49**

Results of Figure 3-35 indicate that the coagulated-flocculated FFT sample settles more, and faster, and consequently dissipates the excess pore pressure faster than the centrifuge cake obtained with flocculant only.
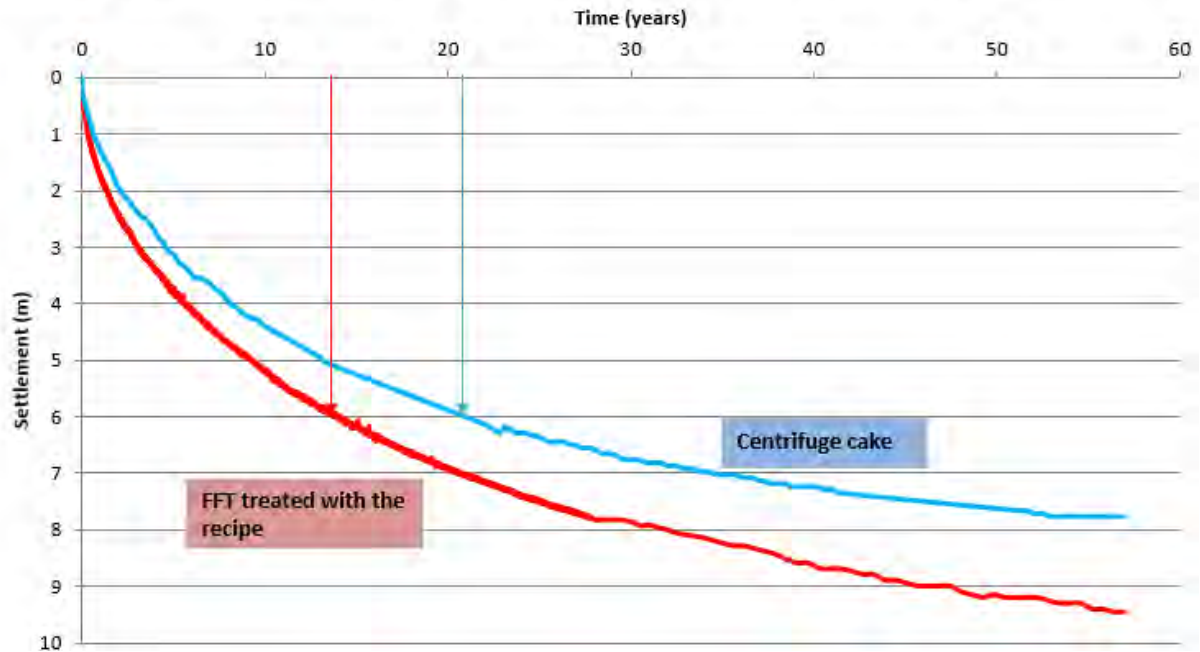
Figure 3-35: **Results from beam centrifuge testing comparing self-weight consolidation behaviors between treated FFT with the recipe and a centrifuged cake with flocculant only.**

3.2.13   Laboratory evaporation tests

Evaporation tests were conducted on FFT with flocculation only, treated FFT (recipe), and centrifuge cake with flocculation only to investigate and compare their evaporation rates. Test results shown in Figure 3-36 indicated that at the early portions of the plots, the actual rate of evaporation of the recipe is close to the potential rate of evaporation of water and is higher than the actual evaporation of the FFT and centrifuge cake with flocculant only.
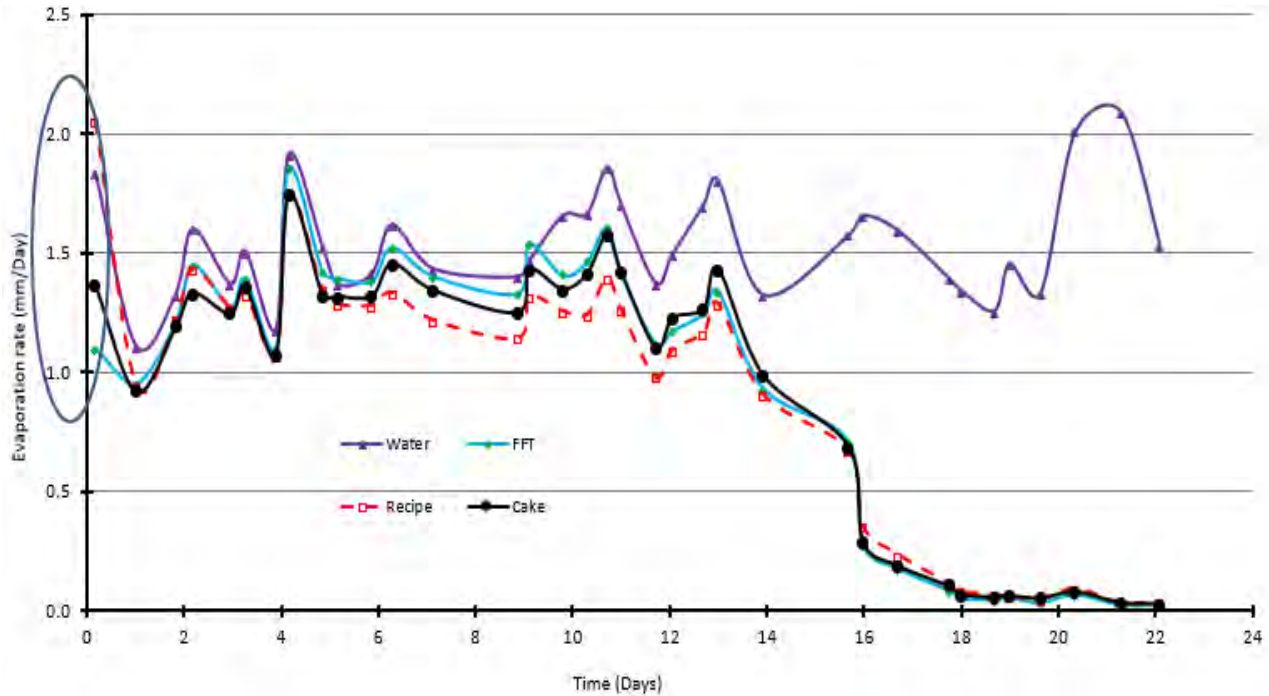
Figure 3-36: **Rate of potential evaporation (water), and actual evaporation of samples vs. time.**

As shown in Figure 3-37, through the ratio of the actual evaporation (AE) and potential evaporation (PE), the FFT and centrifuge cake with flocculant only dewater much slower (i.e., AE/PE ≤ 1) than the recipe. However, the recipe evaporates at a potential rate ≥ 1 (i.e., AE/PE ≥ 1) when the sample is saturated in the early stage of the drying process, which is attributed to the fact that the recipe has an open soil structure. The results also suggest that the recipe entraps residual bitumen that becomes part of the treated FFT open soil structure. In contrast, the residual bitumen films on the surfaces of the FFT and centrifuge cake with flocculant only start to break down as drying continues, and the AE/PE ratios continue to gradually increase to 0.96 and remain constant until Day 10. Eventually, the AE/PE ratios start to decrease to a value of 0.8 on Day 12. During this time the AE/PE ratio of the recipe continues to decline gradually and reaches a value of 0.8 on Day 10.

The AE/PE ratio of 0.8 is the boundary between the saturated and unsaturated states of the samples. As drying proceeded in the unsaturated region (i.e., AE/PE <0.8) all the AE/PE ratios started to decline rapidly to reach their lowest values (residual) of close to zero (all the surfaces of the samples become desiccated).

In summary, the recipe loses water much faster and reaches the boundary region (i.e., AE/PE = 0.8) earlier than the FFT and the centrifuge cake with flocculant only.
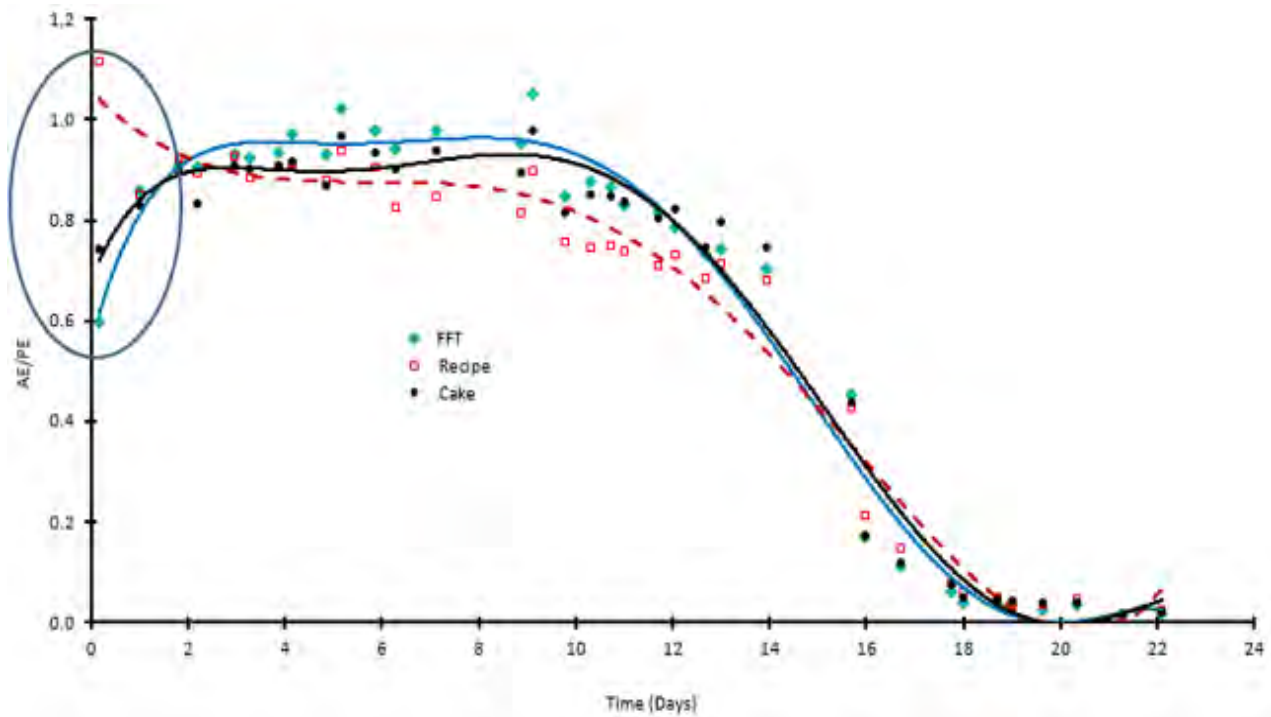
Figure 3-37:   AE/PE ratios for FFT, recipe, and cake vs. time.

Once the recipe is discharged into the geotextile tubes, the filtration properties of the geofabric and the short drainage path of the containment are the key contributors to the enhanced dewatering and accelerated consolidation. Evaporation and freeze-thaw have also been identified as contributors for dewatering with time.

Chapter 4 Field Trials

4.1   Field trials

This chapter presents the field trials, findings, and processing methods used to answer the questions posed in Chapter 1 (section 1.2.6), focusing on the physicochemical recipe and the rationale for choosing geotextile tubes as a filtration process to accelerate dewatering and consolidation of the treated FFT to form stable reclaimed landforms. In addition, this chapter includes a field trial on treated tailings with the recipe for end-of-pipe subaerial discharge, and the solids and mass balance results of the treated FFT discharged into geotextile tubes during the preliminary field trial.

4.1.1   End-of-pipe subaerial (above pond water line) discharge of treated tailings

Photographs 4-1 to 4-7 show the treated tailings with the recipe for a subaerial end-of-pipe deposition field trial, including sampling and in situ field testing. The subaerial deposit demonstrated the formation of a homogeneous, non-segregating, high shear strength and a relatively steep beach slope compared to the existing beach (Figure 4-1 and Photograph 4-6). The end-of-pipe subaerial field trial was performed for gold mine tailings with mineralogy of predominantly quartz at pH 8.

Mineralogical analyses (XRD) of the tailings used in this study indicate approximately 92% felsic minerals having a high quartz content (57.0%), 18.0% feldspars, 13.0% illite-mica muscovite, 7.0% kaolinite, and approximately 8% mafic minerals. PSD analysis showed 41.5% clay-sized particles, 58% silt-sized particles, and 0.5% sand-sized particles. Specific gravity was 2.76, average liquid 43%, plastic limits 22.5%, and plasticity index 20.5%. Porewater pH was 8.
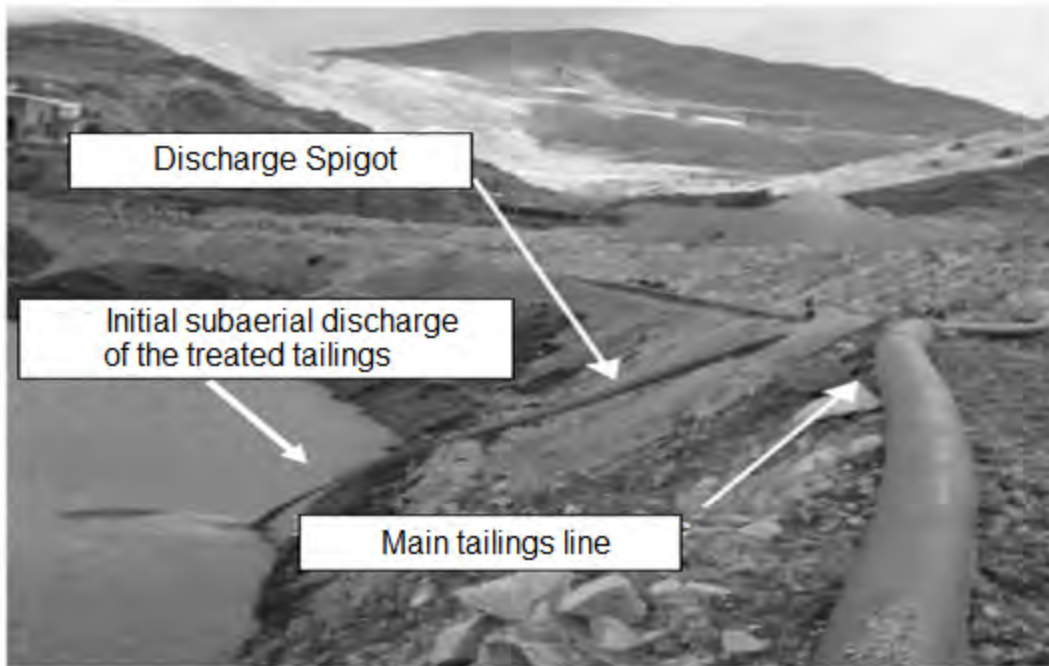
Photograph 4-1: **Field trial set up for the treated tailings (inline coagulation + flocculation) subaerial discharge.**
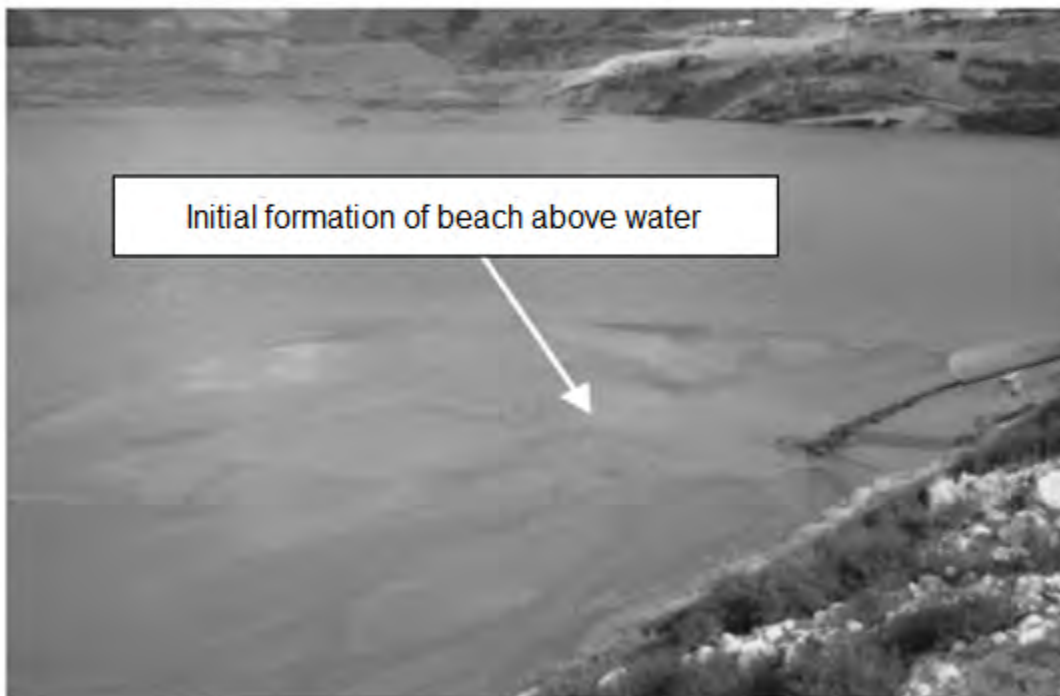
Photograph 4-2: **Initial formation of beach above water.**

Continuous subaerial discharge on the tailings trial beach
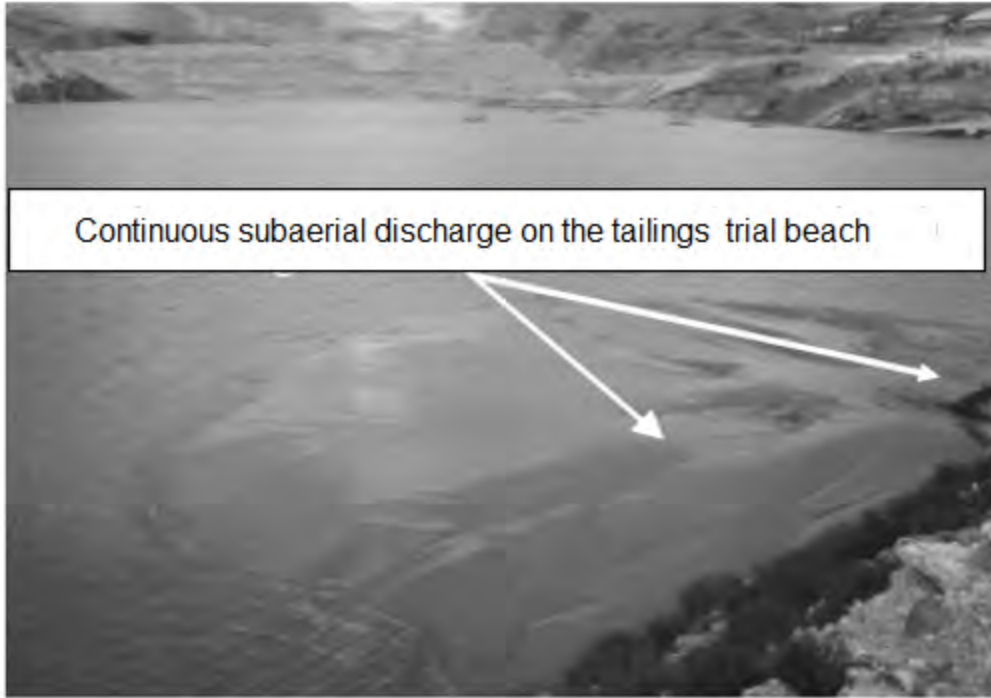
Photograph 4-3: **Continuous formation of beach above water upon discharge of the treated tailings.**

Monitoring of the treated tailings in line performance

Photograph 4-4: **Sampling at the treated tailings at the discharge point.**
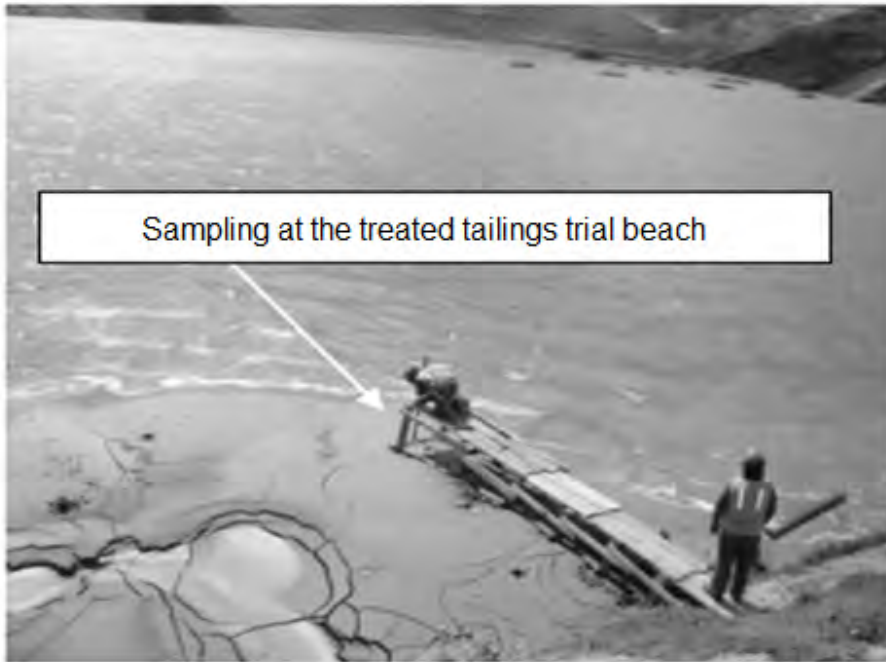
Photograph 4-5:   Sampling at the treated tailings trial beach above water.

Cone penetration tests with pore water pressure measurement (CPTu) were performed to compare the shear strength of the existing tailings beach (flocculation only) with the treated tailings trial beach (recipe). Figure 4-1 shows the CPTu locations on the tailings existing beach and the treated tailings trial beach.
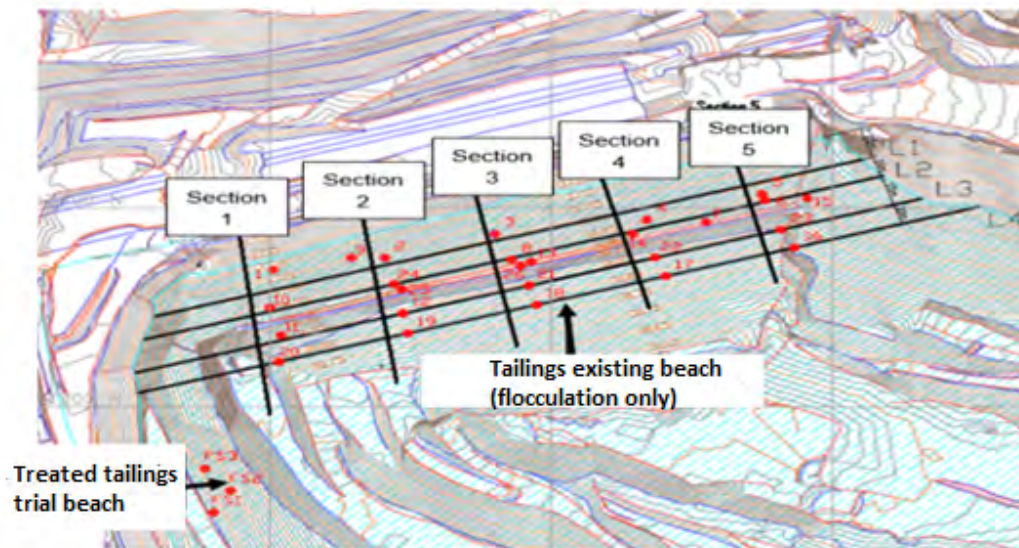
Figure 4-1:   Plan view of the CPTu tests on tailings existing beach (flocculation only) and treated tailings trial beach.

The existing FFT beach had been deposited over several years, while the treated tailings trial beach was deposited over approximately 45 days prior to the CPTu tests. The trial beach achieved far higher shear strengths, as shown in Figure 4-2.
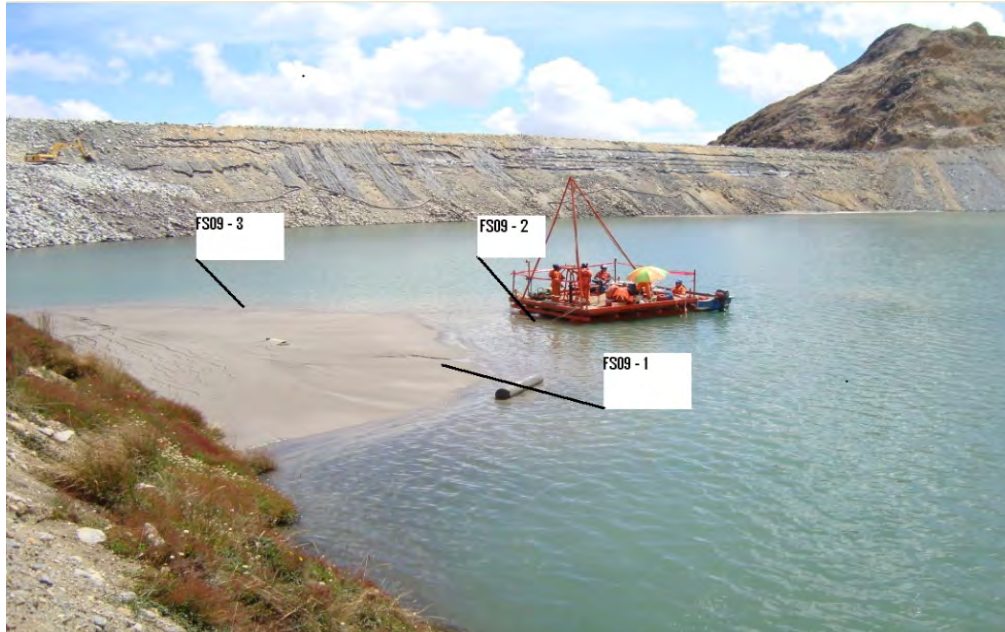
Photograph 4-6:   Performing CPTu tests from the barge at the trial beach.
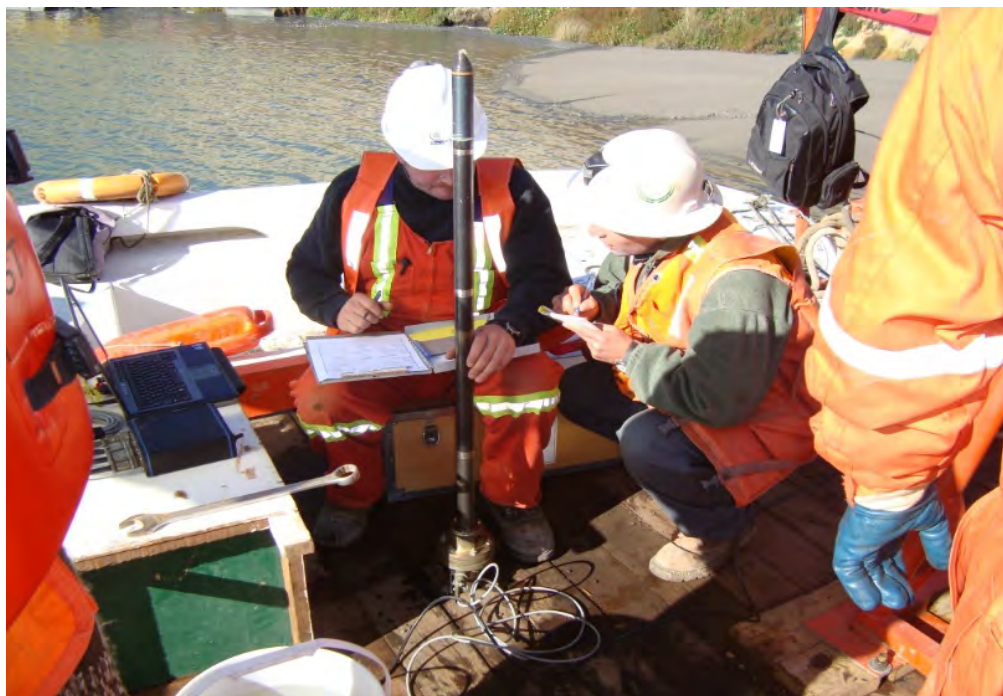
Photograph 4-7:   Obtaining CPTu data from the barge.
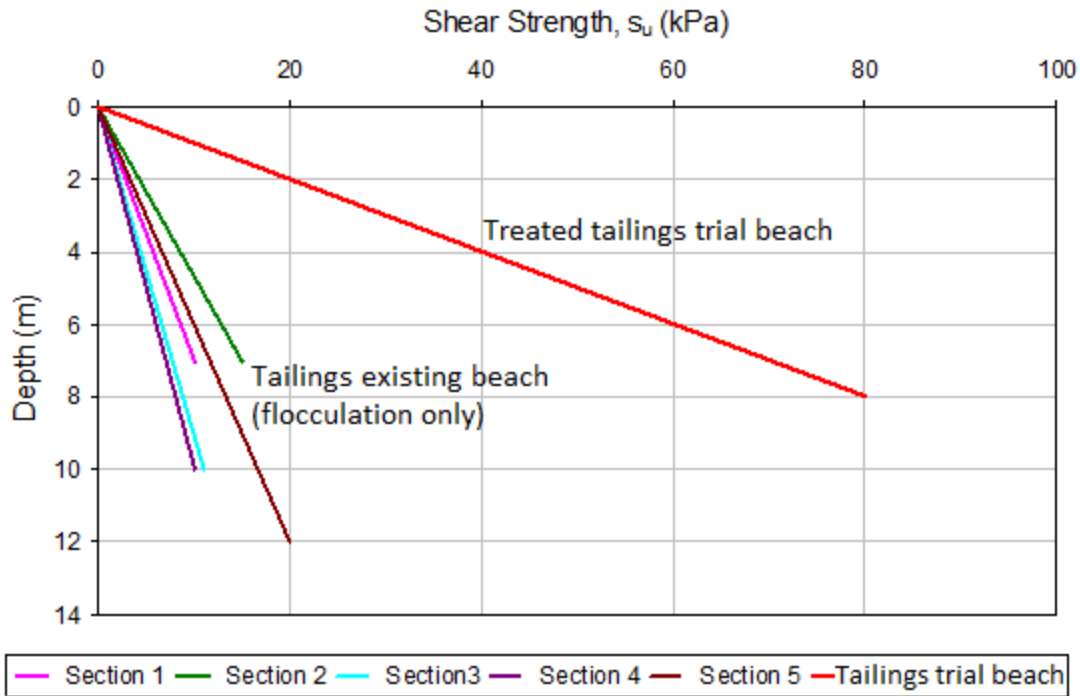
Figure 4-2: Shear strength results of the tailings existing beach (flocculant only) and treated tailings trial beach vs. depth (sections Figure 4-1).

Figure 4-3 shows the excess porewater pressure vs. depth (m) plots of the existing FFT (flocculation only) deposit and treated FFT (coagulant + flocculant) field trial.
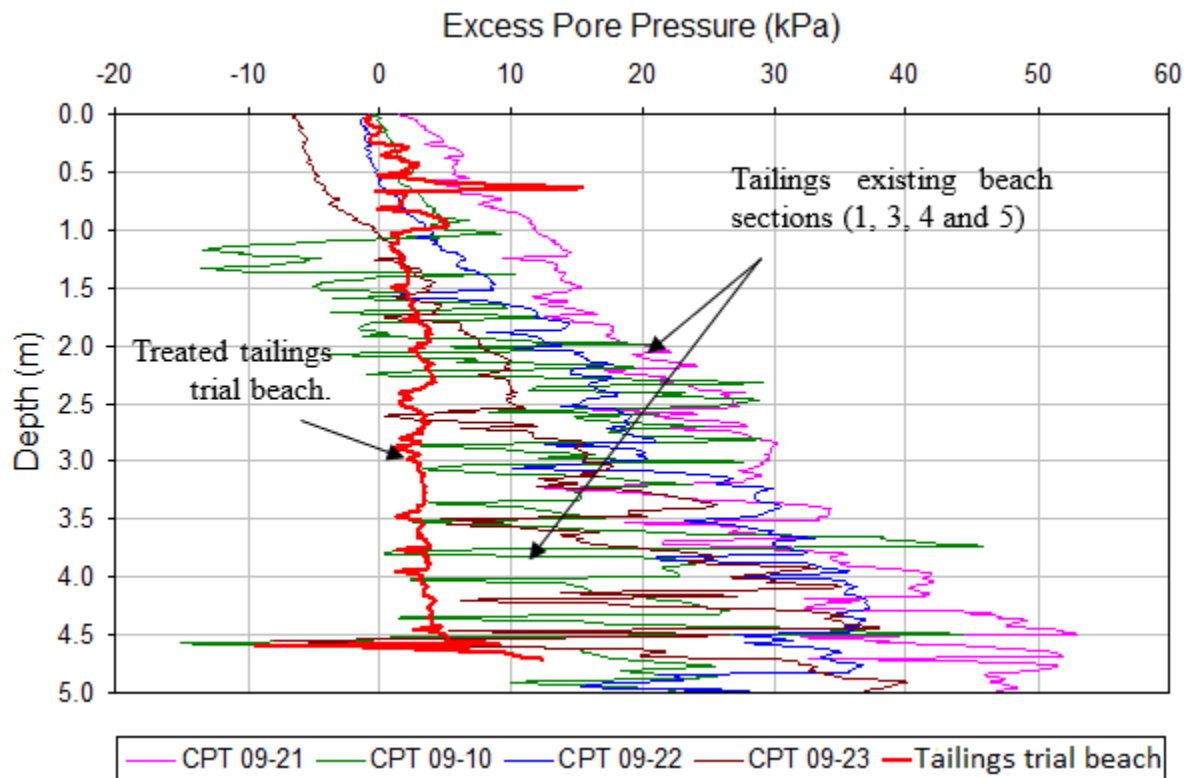
Figure 4-3: **CPTu test results of the excess pressure obtained from the existing tailings beach (flocculant only) and treated tailings trial beach (coagulant + flocculant) vs. depth (sections Figure 4-1).**

In summary, the CPTu results for the undrained shear strength and excess porewater pressure for both the existing tailings beach (flocculation only) and treated tailings trial beach (coagulation + flocculation) show that much faster dissipation of excess pore pressures and faster consolidation were obtained from the treated tailings trial beach (coagulation + flocculation). In addition, the field trial on the treated tailings trial beach confirmed the efficacy of the physicochemical recipe, which resulted in a steeper, homogeneous, non-segregating deposit of improved dewatering and consolidation and a higher shear strength deposit compared with the existing tailings beach (flocculation only).

4.1.2 Preliminary field trial to evaluate dewatering of the treated FFT into the geotextile tubes

A preliminary field trial using two geotextile tubes of 18.3 m circumference and 30 m length placed in an elongated shape side by side were filled (completed) on November 3, 2014, with inline treated FFT (coagulated and flocculated) to assess dewatering, filtration, and fines capture performance including solid and water mass balance, along with the changes in the chemistry of treated FFT release water. FFT used for the field trial consisted of approximately 70 wt.% water, which was the major constituent. The process water supplied for the trial had high concentrations of dissolved divalent cations such as 86 ppm of Ca^{2+} and 26 ppm of Mg^{2+}, 700 ppm of dissolved solids, and pH 7.88. The process water was used in all steps of the trial to treat FFT, including dilution and coagulant and flocculant solutions preparation. The treatment was designed to provide FFT fines agglomeration and water separation inline prior to the discharge into the geotextile tubes. Chemicals used in coagulation and flocculation may be reactive with the solid surface where different anions and cations are released from the solid minerals in the FFT.

The photograph 4-8 shows a preliminary field trial to evaluate dewatering of the treated FFT discharged into geotextile tubes, monitoring of the geotechnical engineering properties, and solid and water mass balance (section 4.1.3).

Photograph 4-8: Field trial to evaluate dewatering of the treated FFT discharged into geotextile tubes, including solids and water mass balance (section 4.1.3).

FFT feed at 28 wt.% solids was diluted, coagulated, and flocculated in different stages to achieve an effective chemical treatment. In the first stage, the FFT was diluted to 20 wt.% solids using process water. In the second stage, the dilution occurs by inline addition of the coagulant solution, and in the third stage, the dilution occurs by inline addition of the flocculant solution; at this stage the treated FFT achieved 8 wt.% solids inside the pipeline prior to the discharge into geotextile tubes. Collectively, FFT was diluted 4.5 times during the entire process. The quick release of water during the first five hours after deposition of the treated FFT in the tubes was in fact release of dilution waters added during the process. During this time, the solids content buildup in the tubes was 27 wt.% solids, which is comparable to the solids content of the FFT feed.

The solids content in the tubes increased to 50 wt.% solids over 7 days with measurements taken at the center of the tubes. Undrained shear strength in the tubes at the same location was measured to be 5 kPa, with original FFT undrained shear strength considered zero. Data were collected from six piezometers with built-in thermistors, installed in three different longitudinal orientations (crest, middle, and beach) with sensor tips located close to the cross-sectional center of the tubes, as shown in Figure 4-4.
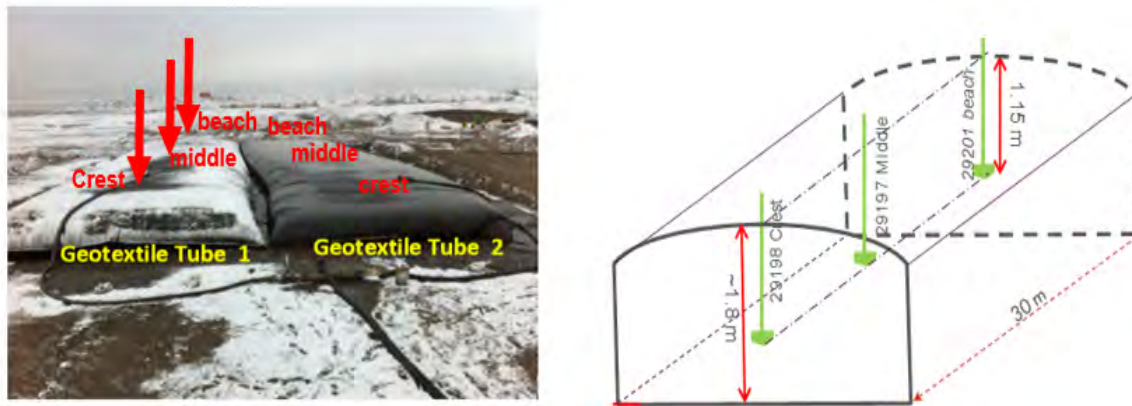
Figure 4-4:   Location of the piezometers and thermistors in geotextile tube 1.

Figures 4-5 and 4-6 show piezometric monitoring data obtained from November 3, 2014, (when the tubes were completed) to December 7, 2014. This preliminary field trial validated that the treated FFT with the recipe dewaters in the geotextile tube and the rate of dewatering is a function of the recipe; the inline mixing process; short drainage path provided by the geotextile tube containment; internal pressure and gravity head during the filling; hydraulic parameters of the geofabric material; self-weight consolidation; evaporation and freeze-thaw.
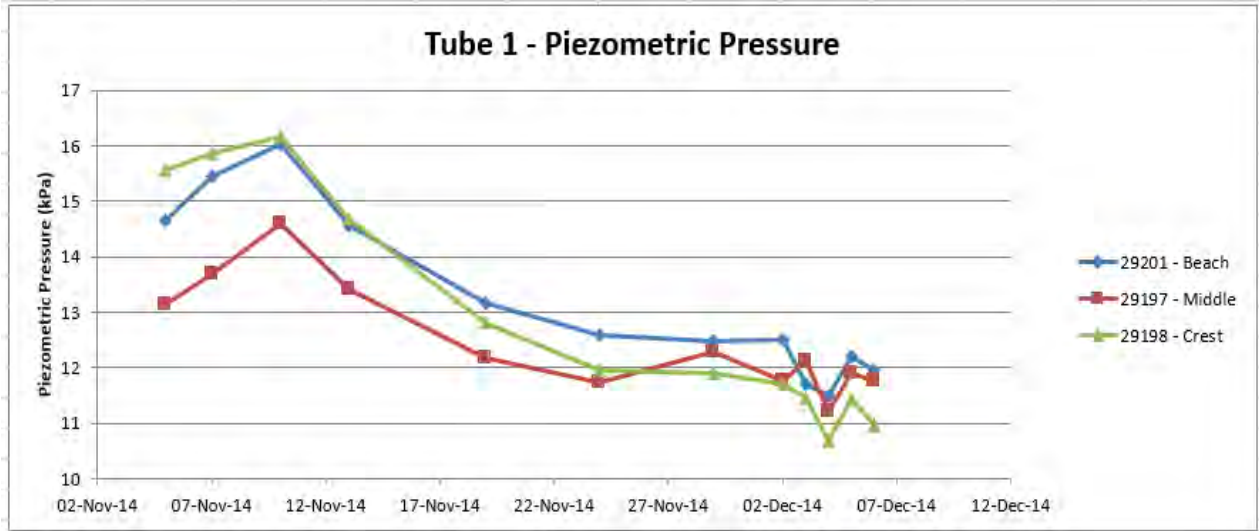
Figure 4-5: **Piezometric monitoring data collected from geotextile tube 1.**
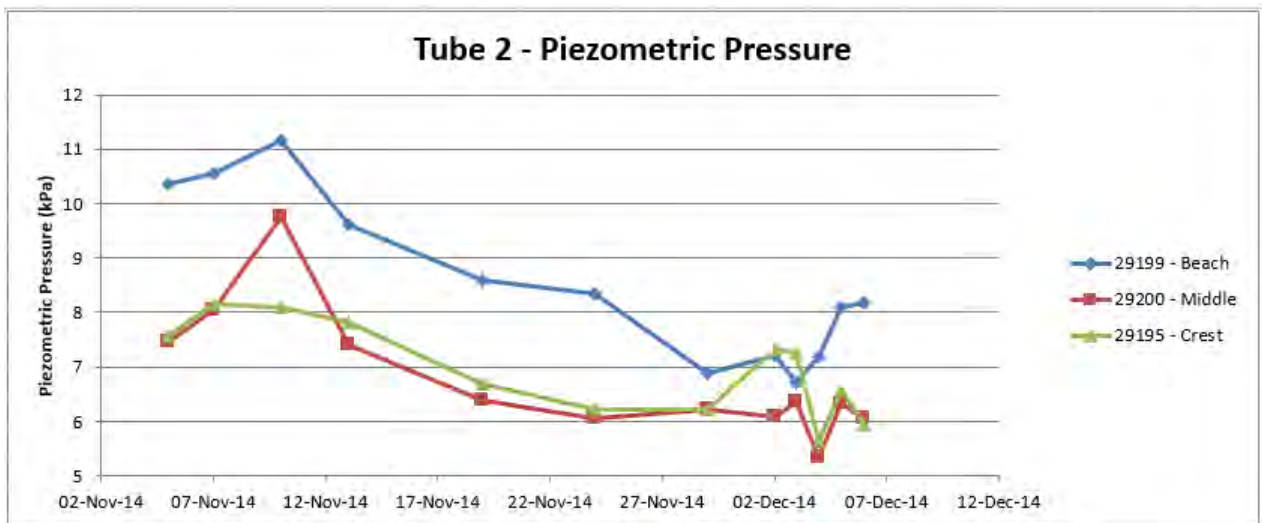
Figure 4-6: **Piezometric monitoring data collected from geotextile tube 2.**

Figures 4-7 and 4-8 show the in-situ shear strength (vane shear tests) measured during the period shown in the figures. The last in-situ shear strength results were obtained on December 10, 2014. The temperature measurements indicate that tubes were frozen at the perimeter, while the tube's center temperatures were still varying from +2 to +5 °C.
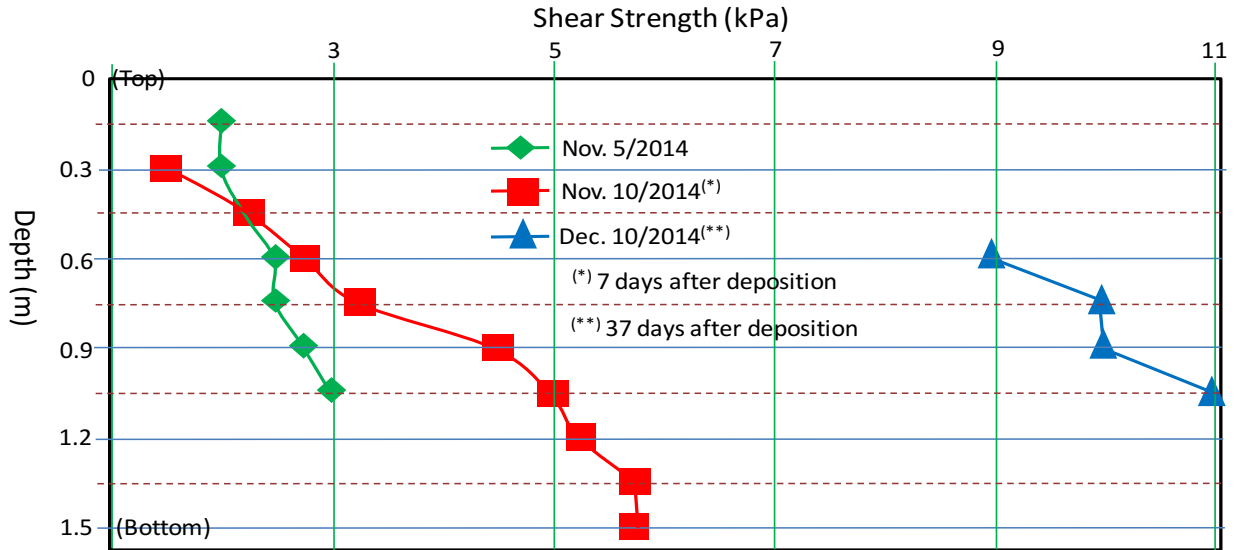
Figure 4-7: Undrained shear strength (kPa) monitoring data collected from geotextile tube 1.
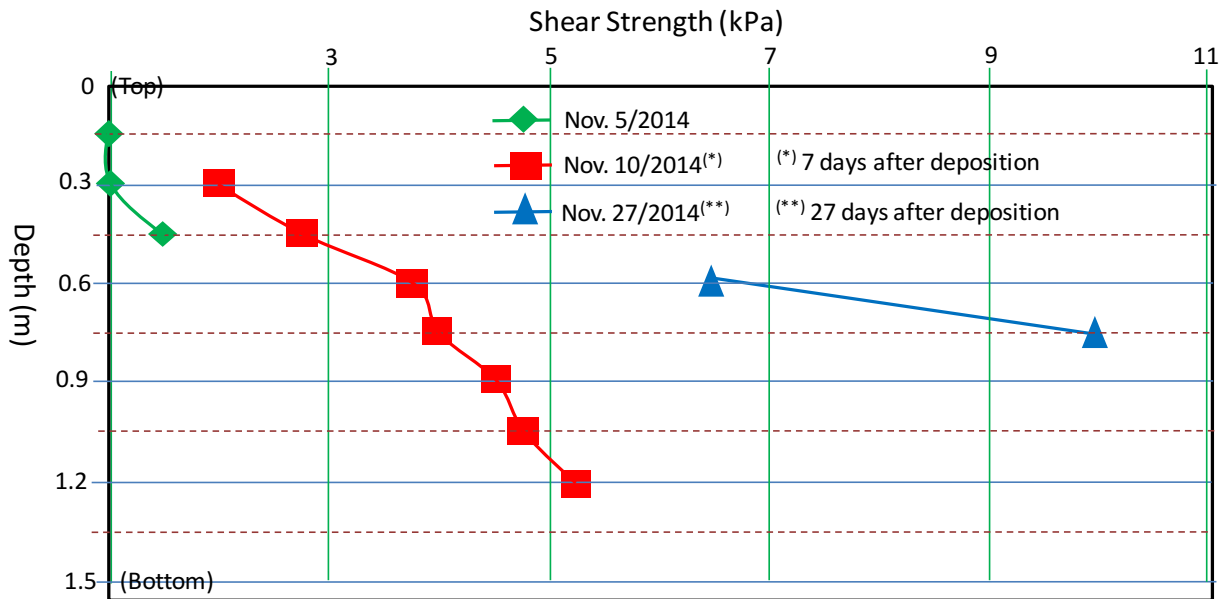
Figure 4-8: Undrained shear strength (kPa) monitoring data collected from geotextile tube 2.

After 30 days of deposition of the treated FFT in the tubes (December 3, 2014) the solids content and shear strength at the center of the bags were measured as 55 wt.% solids and 10 kPa, respectively. No further gain in solids content and shear strength was seen because of the physical limitation to dewatering due to the frozen peripheral soil/pore water.

Real-time measurements of temperature and piezometric changes were taken by a data logger monitoring system. Figures 4-10 and 4-11 show the continuing monitoring of dewatering, solids content, and strength gain during the spring and summer of 2015; this completed the dewatering evaluation and interpretation of the solids content and undrained shear strength gain.

Photograph 4-9 and Figure 4-9 show the dewatering and consolidation of the treated FFT in the geotextile tubes considering a completed seasonal cycle (Nov. 3, 2014 to Oct. 29, 2015), showing the geotextile tubes possibly complete dewatered at the end of the seasonal cycle.

Photograph 4-9: **Evaluating consolidation, dewatering solid contents and shear strength gain with time.**
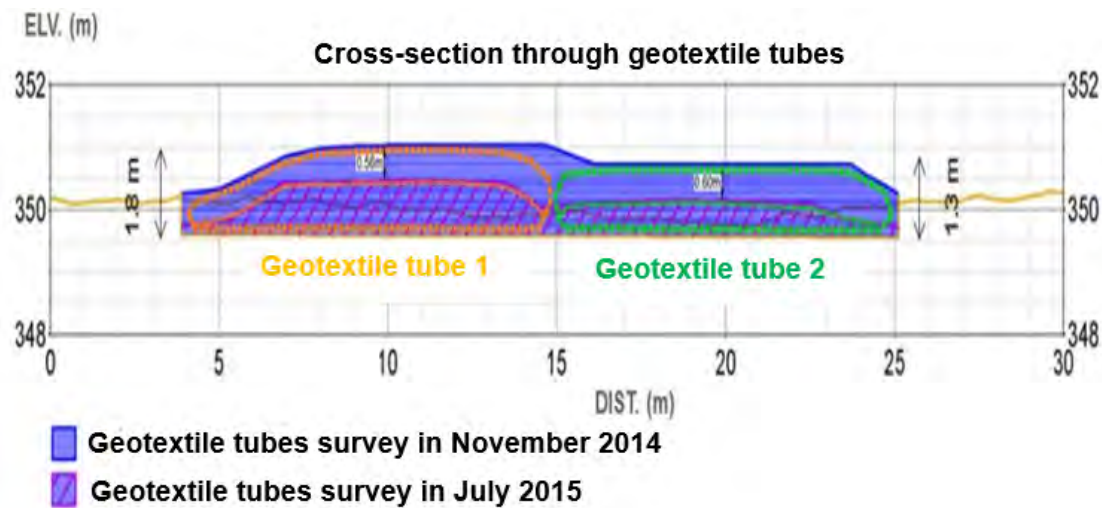
Figure 4-9: **Cross section through the geotextile tubes 1 and 2.**
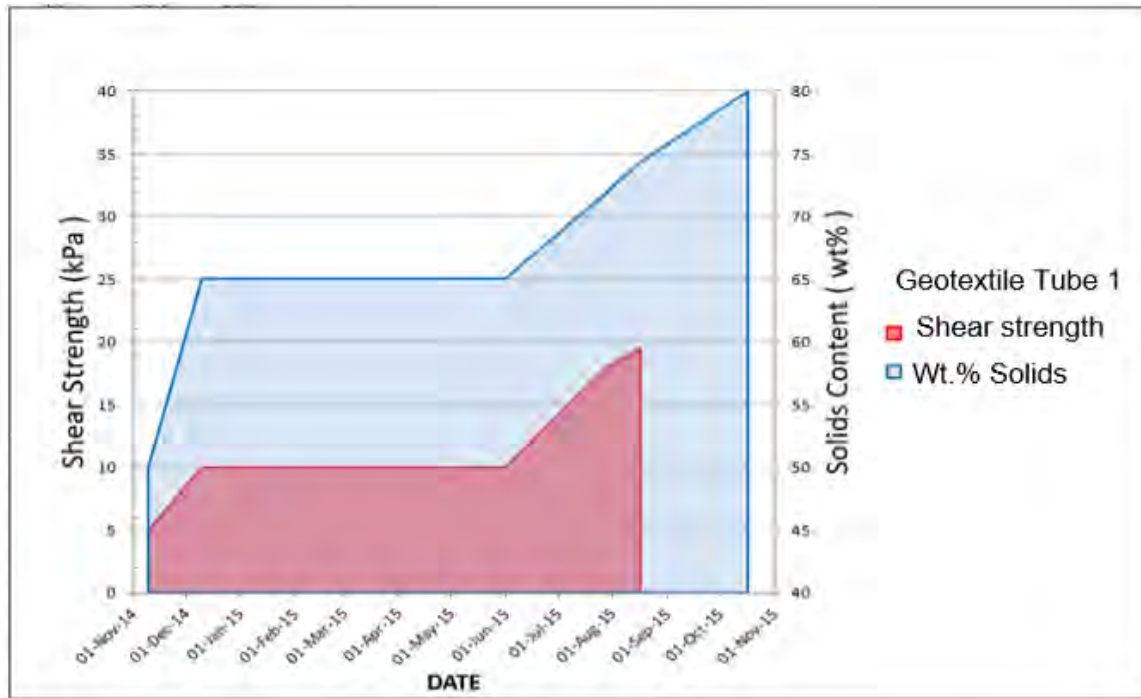
Figure 4-10: Undrained shear strength (kPa) and solids content (wt.%) monitoring data collected from geotextile tube 1 (Nov. 14, 2014 to Nov. 15, 2015).
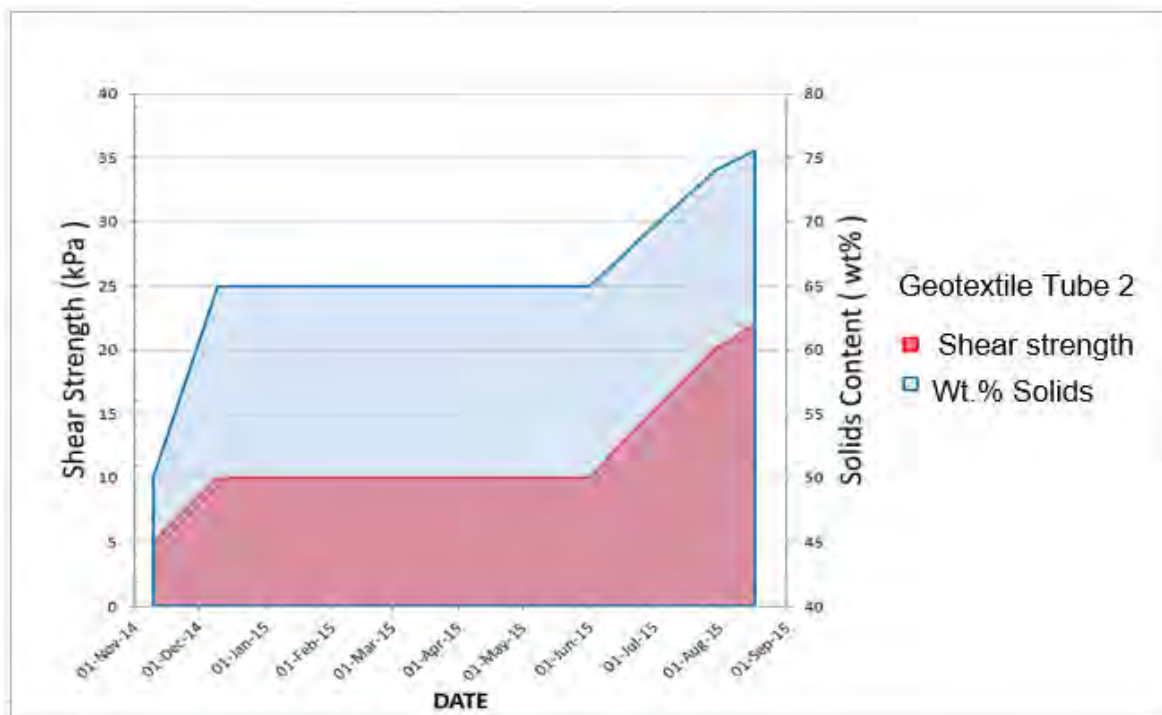
Figure 4-11: Undrained shear strength (kPa) and solids content (wt.%) monitoring data collected from geotextile tube 2 (Nov. 14, 2014 to Nov. 15, 2015).

4.1.3 Solids and water mass balance for dewatering the treated FFT using geotextile tubes

The solids retained inside the tubes are considered captured solids, and the release water is considered process water; this water is used either for the same FFT management or may be routed into the mining process. In this specific trial, the process water was used as dilution water for the FFT and for preparation of coagulant and flocculant solutions. To conduct the trial, 61 batches of FFT were trucked by a vacuum truck to the test site. The percent solids in each FFT batch were measured with an average solids content of 28 wt.% solids. The specific gravity of the solids was 2.5. The following steps were performed before pouring the treated FFT into the tubes.

1) FFT was pumped inline for upstream processing (a constant volume supplied by vacuum trucks and discharged in a mixing tank for dilution and subsequent coagulation of the FFT).

2) FFT was diluted with the mining process water to achieve 20 wt.% solids, which was the initial slurry density suitable for coagulation and flocculation as described in the following steps.

3) Alum [4.27% Al^{3+} + 8.07% Al_2O_3 and specific gravity 1.326] solution was used inline as a coagulant at a fixed concentration of 0.1% (27 kg of alum/27 m^3 process water) and a dose of 6470 g/t of dry solids.

4) Downstream of step (3), Flopam A 3338 as an anionic flocculant solution was injected inline to flocculate the coagulated solids. Flopam A 3338 was added at a fixed concentration of 0.1% (4 kg of A 3338/4 m^3 process water) and dose of 1050 g/t of dry solids.

5) Following step (4), the treated FFT was poured into the geotextile tubes. Each tube was filled to maximum volumetric holding capacity (as per manufacturer safety requirement, the maximum allowable height was 1.83 m) of the selected size of the tube used in the trial.

While the tube was being filled to its maximum allowed holding capacity, dewatering of the treated FFT occurred. The solids were retained inside the tube and water was filtered out of the tube. During this process, all streams were sampled for solid/water and chemical composition of the aqueous phase to understand some of the process unknowns.

The objective of the treatment used in the geotextile tubes trial was not to treat the supplied process water. Instead, the treatment was designed to provide fines agglomeration and water separation while avoiding generation of any excess of divalent or multivalent cations in the recovered water. Figure 4-12 shows the simplified process flow diagram for the entire process used in the mass balance approach. This process flow diagram was verified with the field trial.
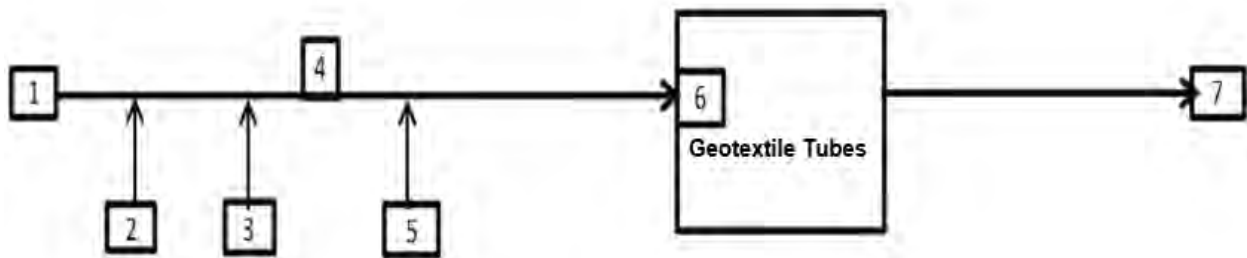
Figure 4-12:   Simplified process flow diagram of the treated FFT inline and discharged into geotextile tubes.

Definition of the streams and sampling points are:

Stream #1: FFT stream.

Stream #2: Process water used as a dilution water to dilute FFT to 20 wt.% solids in the stream for effective coagulation and flocculation.

Stream #3: Coagulant addition stream using alum at a concentration of 0.1% by weight as coagulation, added inline to the diluted stream.

Node #4: This is a sampling point where samples were taken periodically to measure the wt.% solids and to analyze chemistry of the aqueous phase.

Stream #5: Polymer addition stream where flocculant (Anionic Flopam A 3338 at concentration of 0.1% by weight) was injected inline to flocculate the coagulated solids coming from upstream of the process.

Node #6: Sampling point where samples were collected to measure the wt.% solids in the slurry and to perform chemical analyses on the aqueous phase to understand the chemistry of the free water.

Stream #7: Release water stream from the tubes. Samples were collected and analyzed for major cations and anions to understand the chemistry of the release water.

Between Node #6 and Stream #7, solid core samples were retrieved from the tubes and analyzed for wt.% solids, pore water chemistry, and in situ shear strength of the deposits. All the streams before joining the upstream slurry were analyzed for solids/water contents and water chemistry (major analysis). The volume of each stream used for each batch was measured. A typical batch of the deposition consisted of 12 m^3 of FFT (Stream #1), 5 m^3 of dilution water (Stream #2), 27 m^3 of coagulant solution (Stream #3), and 4.4 m^3 of polymer solution (Stream #5). Table 4-1 shows the solid/water contents used in the mass balance conducted for this research.

Table 4-1:   Volume of each stream used in the field trial.

Stream/ Node #	Stream/ Node description	Slurry volume (m^3)	wt.% Solids
1	FFT	12.0	28.0
2	Dilution water (process water)	5.0	0.00
3	Coagulant stream (Alum solution)	27.0	0.00
4	Coagulated FFT sample (Node 4)	44.0	8.70
5	Polymer solution stream	4.0	0.00
6	Flocculated FFT stream (Node 6)	48.0	8.00

Solid and water mass balance calculations – In this field trial, the easily measured parameter was to record the volume of each stream used to fill the tube and take grab samples at predefined points (Nodes #4 and #6, inside the bag, and for each stream added inline) for additional measurements. The first basic step in a mass balance is to calculate the volume of solids and fluids in the slurry following the process flow diagram from Figure 4-12, and then convert these into mass using the specific gravity of the solids and liquid in the streams.

- Solid mass fraction conversion.

Stream #1 (FFT stream) was analyzed for wt.% solids, slurry bulk density, and solids specific gravity. The rest of the streams were measured for wt.% solids and water during the trial period. The average values of the measured parameters for FFT stream were:

- Slurry bulk density = 1.2 tonnes/m^3.
- FFT solids fraction = 28 wt.% solids.
- Specific gravity of solids in FFT = 2.5.

As mentioned earlier, to conduct a mass balance on the water and solids contents in the slurry in each stream, the first approach is to convert all the solids in the streams to a volumetric basis so that the volume of water (refer to as fluid phase volume) in the slurry can be accurately calculated. The following correlation was used:

$$\emptyset_{sl,v} = \cfrac{1}{1 + SG_s \left(\cfrac{1}{\emptyset_{sl,m}} - 1\right)} \ldots \ldots (1)$$

where:

$\emptyset_{s,l,v}$ = solids fractions of the slurry on a volumetric basis

$\emptyset_{sl,m}$ = solids fractions of the slurry on a mass basis = 28 wt.% solids (for Stream #1)

SGs = Specific gravity of solids = 2.5 (for solids in Stream #1)

From the correlation (1) the solid fractions of the slurry on volumetric basis was 13.5%. This means 28 wt.% solids represents 13.5% of the slurry volume in the FFT. Therefore, in 12 m^3 of FFT, the solids volume based on the above correlation will be (13.5% × 12 m^3) = 1.62 m^3. Other input streams do not have solids; therefore, their volumetric representation will remain unchanged. Specific gravity of other streams (fluid phase) is considered as that of water. The mass of any phase (solid or fluid/water) in a stream is the product of specific gravity and volume of that phase. Percent mass representation of any phase (solid or fluid/water) in any stream is fraction of a phase in the total stream mass multiplied by 100.

Inline Flocculation Mass Balance on Solids – Table 4-2 represents a complete mass balance for solids when FFT was added inline and then discharged into the tubes after treatment with different reagents. Once the flocculated FFT is release into the tubes, the mass in the tubes will change with time through the release of the water; because of this change, a separate mass balance is presented in the following section.

Errors in the field-measured data can be back-checked with the calculated mass balance as shown in Table 4-2; for example, the sum of all the masses from Streams #1, #2, and #3 must be equal to the mass of the sample collected at Node #4, which is a sampling point in the trial. If this is not true, then there are errors in the field analyses or in the calculations. The error between Nodes #3 and #4 as shown in Table 4-2 is simply subtracting the subtotal from Node #1 to #3 from #4. If the result is zero for the mass of solids, this means the field measurements are correct. The mass balance results in Table 4-2 do not have any errors with respect to the field measurement at Nodes #4 and #6.

Table 4-2:   Solid and water mass balance (inline).

Stream/ Node #	Stream/ node description	Volume (m^3)			Specific gravity		Mass (T)		wt.% Solid	wt.% Fluid
		Slurry	Fluid	Solid	Solids	Fluid	Solids	Fluid		
1	FFT	12.0	10.38	1.62	2.5	1.0	4.04	10.38	28.0	72.0
2	Proc. Water (dilution)	5.0	5.00	0.00		1.0	0.00	5.00	20.8	79.2
3	Alum solution	27.0	27.00	0.00		1.0	0.00	27.00	8.7	91.3
Subtotal	(Node 1+2+3)	44.0	42.38	1.62			4.04	42.38	8.7	91.3
4	Coagulated FFT	44.0	42.38	1.62	2.5	1.0	4.04	42.38	8.7	91.3
Error	Nodes 3 & 4	0.0	0.00	0.00			0.00	0.00	0.00	0.00
5	Polymer sol	4.0	4.0	0.00		1.0	0.00	4.00	8.0	92.0
Subtotal	Node 5+4	48.0	46.38	1.62			4.04	46.38	8.0	92.0
6	Flocculated FFT	48.0	46.38	1.62	2.5	1.0	4.04	46.38	8.0	92.0
	Errors in M/Balance (Node 4+5 = 6)						0.00	0.00	0.00	0.00

By carefully reviewing the mass balance, it can be concluded that at the start of this process, the solids fraction of the FFT slurry stream (#1) was 28 wt.% solids, which was diluted down to 8 wt.% solids at the stage of flocculation addition. This changes the volume of the fluid from 10.38 m^3 to 46.38 m^3, representing 4.5 times additional water that needs to be handled at the front- and back-end of the process, in addition to the water in the FFT. Figure 4-13 shows the cumulative

water added during the process with respect to unit water volume in FFT Stream #1. Stream #2, dilution of FFT with additional water, is only required if the FFT solids content is higher than 20 wt.% solids. Streams #3 and #5 are waters from the coagulant and flocculant solutions. Nodes #4 and #6 are only measurement (monitoring) points. Because the proposed treatment in this research will be utilizing existing tailings lines, it is necessary to evaluate if there will be any issues with infrastructure shortage. Therefore, we cannot draw any conclusions at this time regarding sizing of the water management systems.
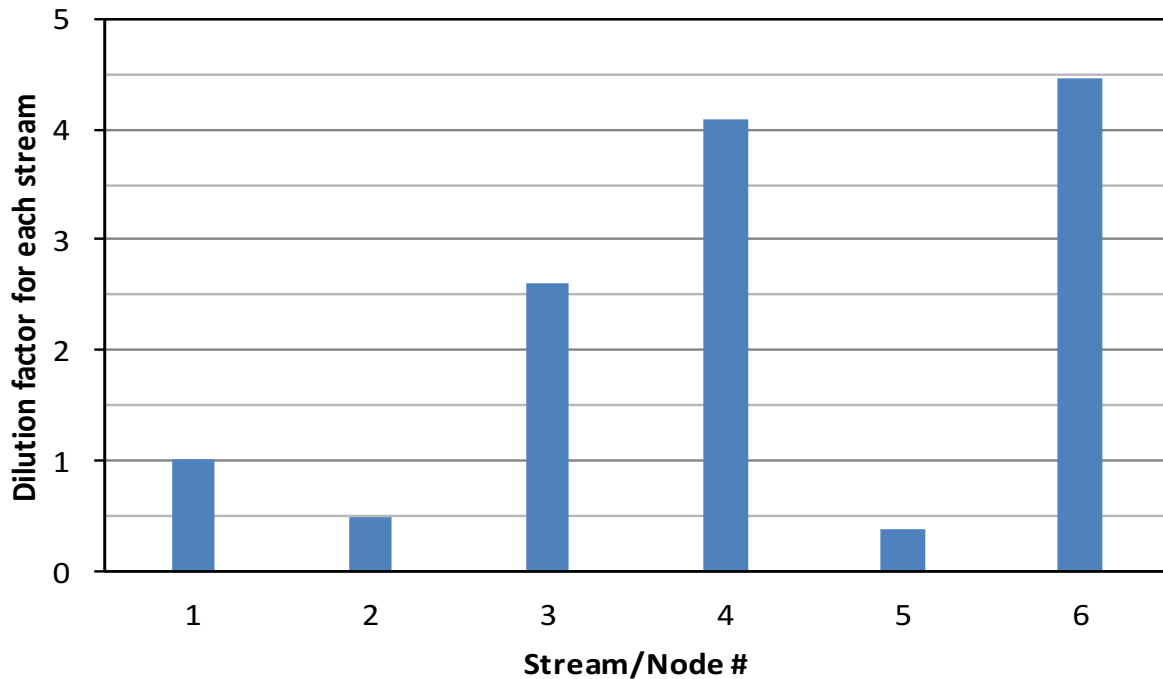
Figure 4-13:   Relative water volume after every stream addition to the process.

Balance after deposition in the geotextile tubes – Once the treated FFT was poured into the geotextile tube, instantaneous dewatering was observed. However, it will be extremely difficult, although not impossible, to measure the exact volume of water released by collecting in a sump and avoiding seepage losses. In this trial, the volume of the water released from the geotextile tubes was not measured. During the pour, the water split into two parts: the volume of water retained inside the tube and water released from the geotextile tube. This split of water reported in Table 4-3 is an indirect measurement (back-calculated).

In the trial program, core samples were collected from the geotextile tubes for solids and water analysis. Pore water chemistry was also analyzed from the core samples. Grab samples were collected from the release water and analyzed for chemistry. Four key data points were selected to evaluate the dewatering and solids consolidation into the geotextile tubes. The mass of release water was calculated using the difference between the starting mass of water and the residual from the core sample. Since the density of water is unity, the mass for water reported can be interpreted as volume (m^3) of water. Table 4-3 shows the solid/water mass balance of the core samples collected from the geotextile tube at different time intervals.

Table 4-3:   Solid and water mass balance on the core samples from the geotextile tube.

Stream/ Node #	Stream Node description	Mass (T)				% Mass in tubes		Cum. Wt.% water release	Drying time (days)
		Solid	Water (tubes)	Cum. Water release	Total	Solid	Water		
6	Flocculated tube	4.04	46.38	0.00	50.42	8.0	92.0	0.00	0.0
Inside	5 h after tube is filled (1st batch)	4.04	10.9	35.50	50.42	27.0	73.0	76.45	0.2
	7 days after tube is filled (1st batch)	4.04	4.0	42.30	50.42	50.0	50.0	91.29	7.0
	30 days after tube is filled (1st batch)	4.04	3.3	43.10	50.42	55.0	45.0	92.87	30.0

Calculations in Table 4-3 reveal the majority of dewatering from the tubes occurs during the first five hours after deposition, which may be attributed to the release of the dilution waters added to the original FFT feedstock. The concentration of the solids by mass after the first five hours of deposition is approximately 27 wt.% solids, which is close to that of the original FFT used in the trial. Next, core samples were collected from the tube after 7 and 30 days, which had

50 wt.% and 55 wt.% solids, respectively. Comparing the results from the end-of-pipe and after five hours with the 7-day samples shows that there is a significant initial increase in dewatering from 8 wt.% to 50 wt.% solids. Figure 4-14 shows a summary of the dewatering of the flocculated FFT poured into the geotextile tubes as a function of time.
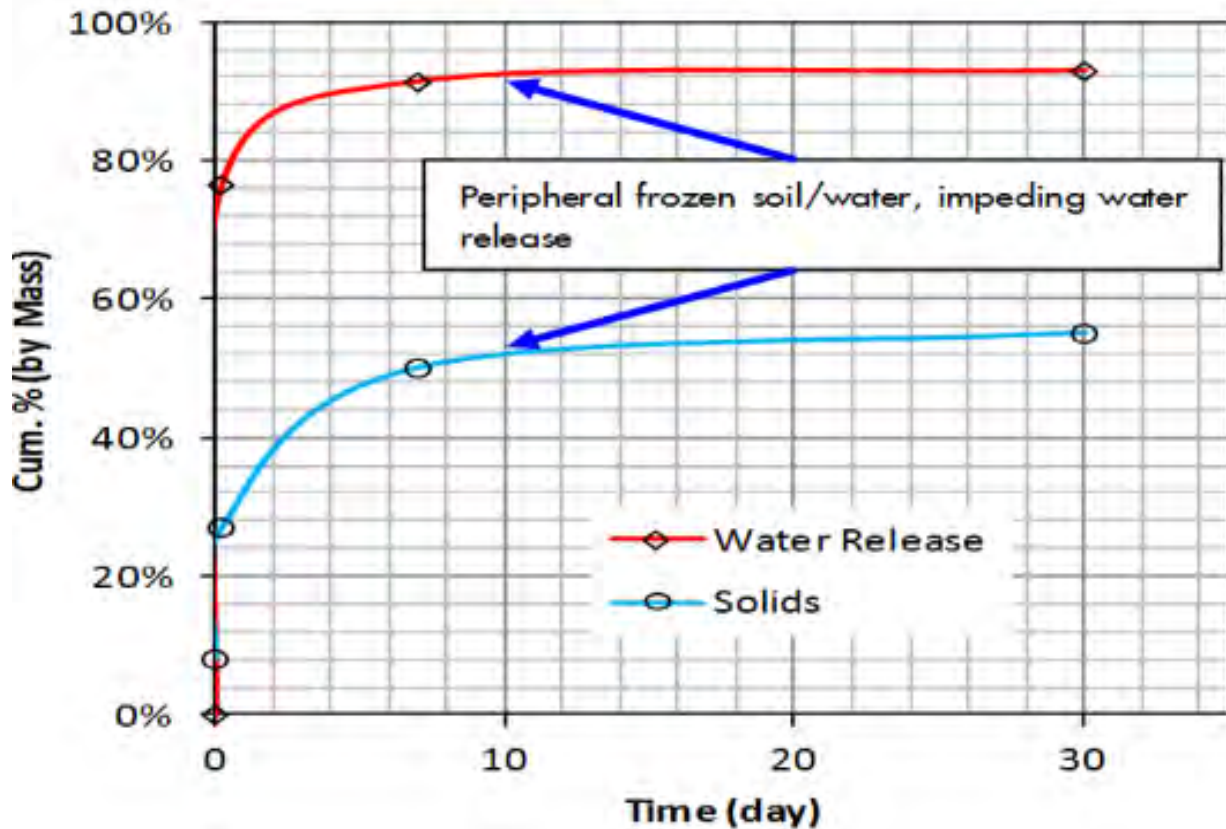
Figure 4-14: **Variation in wt.% solids and moisture contents within 30 days after deposition (Nov. 3, 2014 = time zero).**

After 30 days, the sample does not show a change in dewatering kinetics because of the physical limitation to dewatering caused by the peripheral frozen soil/pore water that impedes water release. Photograph 4-10 shows the test site weather condition after collecting the Day 7 samples. Figures 4-15 and 4-16 show the temperature measurements inside and outside (ambient temperature) the tubes from November 3 (the day when the tubes were completed) to December 5 (30 days after the bags were filled completely with treated FFT). Additional water release will likely occur during the "thaw" cycle of the freeze-thaw process during the spring season as freeze/thaw is a well-known dewatering process for shallow fine tailings deposits.

Photograph 4-10: Geotextile tubes trial after collecting the seven-day core sample (photograph taken on Dec. 5, 2014.)
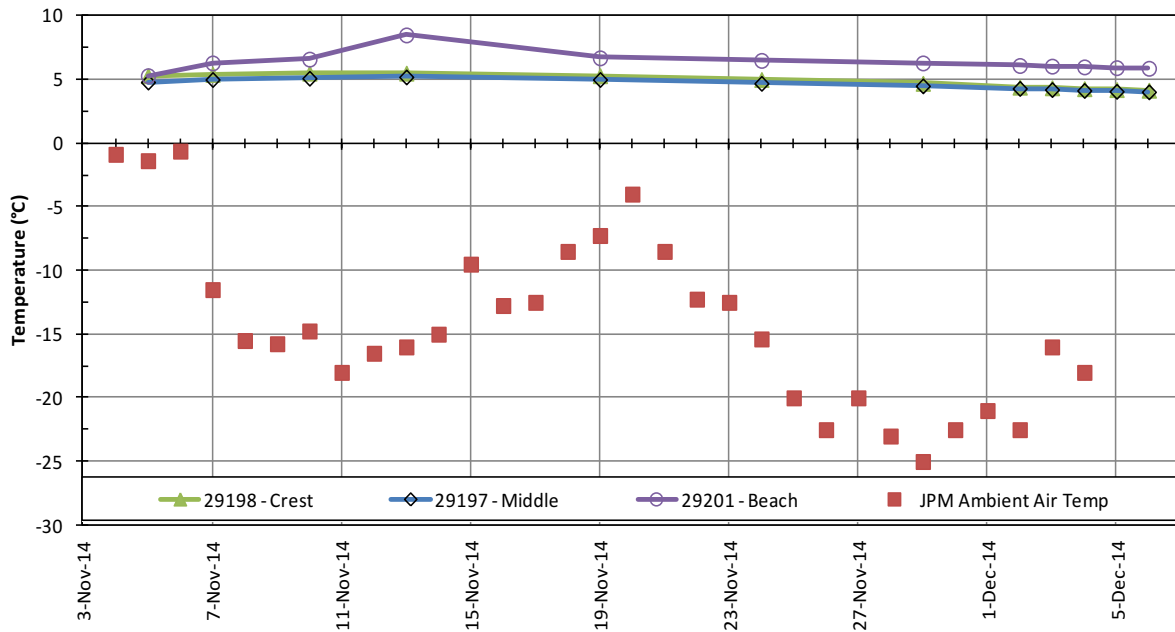
Figure 4-15: Internal and ambient temperature measurements in geotextile tube 1.
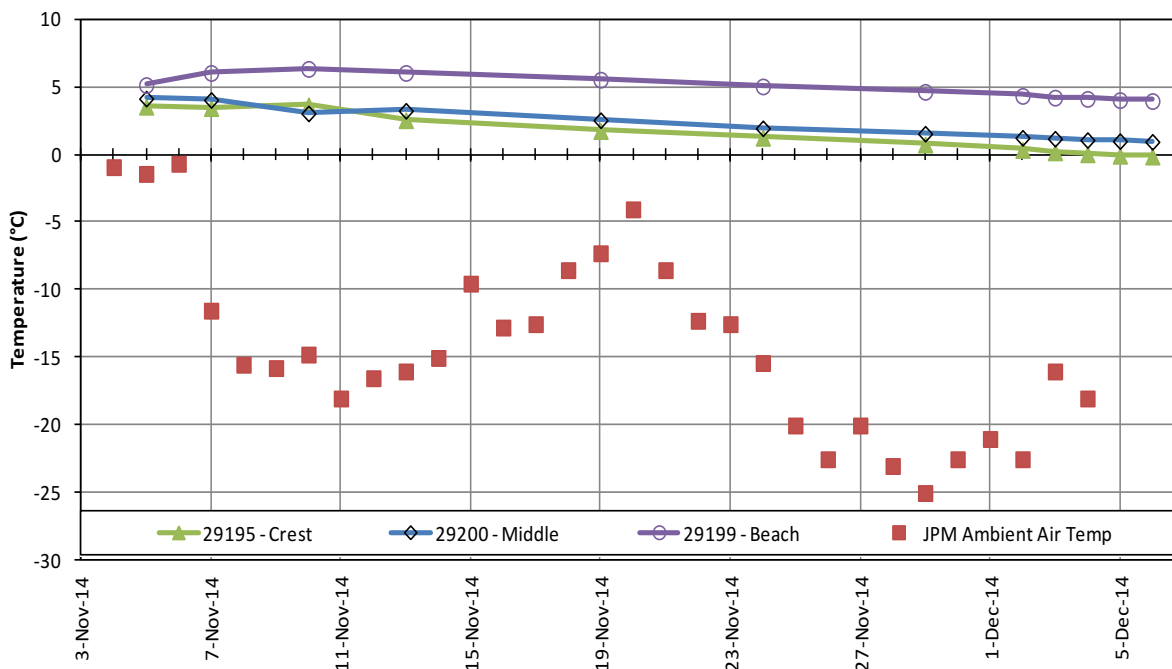
Figure 4-16:   Internal and ambient temperature measurements in geotextile tube 2.

Chemistry Mass Balance Calculations – The chemical analyses of the mixed inline streams and the release water from the geotextile tubes show changes in the chemistry throughout the treatment process. Process water contained high concentrations of dissolved divalent cations (mainly Ca^{2+} ions), was used to investigate their impacts on the flocculation of quartz and kaolinite at pH ≥ 8. The mass balance and concentration analyses of the major ions in the water phases show that majority of the ions remained in the solid phases after deposition. The concentration of Ca^{2+} in the release water was the same as in the process water used for the field trial. The major source of Al^{3+} in the process is from alum (coagulant stream), which has a concentration of 0.015 mg/L in the release water. Based on the process flow diagram shown in Figure 4-12, all the process streams and samples collected at Nodes #4 and #6 were analyzed for major anions and cations to understand the chemistry of the release water. Table 4-4 shows the concentration of individual process streams, Node #4, and Node #6.

To calculate the mass balance of the anions and cations, the fluid phase volumes from Table 4-2 for the Streams #1, #2, #3, #5 and Nodes #4 and #6 were used. Table 4-5 shows the results of the mass balance conducted on the process flow diagram shown in Figure 4-12.

Table 4-4:   Concentration of major anions and cations in the process streams.

Stream/ Node #	Stream node description	Concentration of major ions (mg/L)							
		HCO$_3$ $^{2-}$	SO$_4$ $^{2-}$	Cl$^-$	Ca^{2+}	Mg^{2+}	Na$^+$	K$^+$	Al^{3+}
1	FFT	420	190	150	47	22	260	22	0.12
2	Proc. water (dilution)	440	180	59	86	26	110	16	0.0091
3	Alum solution	40	550	72	92	28	160	10	110
Subtotal	(Node 1+2+3)								
4	Coagulated FFT	310	430	74	97	35	170	59	0.012
	Release/ retained (Node 1+2+3+4)								
5	Polymer sol	540	190	180	43	13	140	51	0.037
Subtotal	Subtotal (Node 4+5)								
6	Flocculated FFT	330	460	110	99	36	220	19	0.011
7	Release/Retained water of anions/cations (Node 4+5-6)								
	Tube Run-off water	290	470	99	86	31	180	15	0.015

The streams masses were compared on an individual basis to see the impact of the input streams on the product stream. Carefully reviewing the results in Table 4-5, the cumulative mass for Streams #1, #2, and #3 should be equal to the mass at Node #4, which is calculated from the chemical analysis results of Node #4 (sampling point) collected during the deposition of material in the process. If there is a difference in the masses, this suggests some sort of chemical reaction.

Table 4-5:   Mass of major anions and cations in the process streams.

Stream/ Node #	Stream / node description	Fluid volume	Mass of major ions (kg)								Unit load
		(m^3)	HCO$_3$ $^{2-}$	SO$_4$ $^{2-}$	Cl$^-$	Ca^{2+}	Mg^{2+}	Na$^+$	K$^+$	Al^{3+}	kg/m^3
1	FFT	10.38	4.36	1.97	1.56	0.49	0.23	2.70	0.23	0.00	1.11
2	Proc. water (dilution)	5.00	2.20	0.90	0.30	0.43	0.13	0.55	0.08	0.00	0.92
3	Alum solution	27.00	1.08	14.85	1.94	2.48	0.76	4.32	0.27	2.97	1.06
	Subtotal (Node 1+2+3)	42.38	7.64	17.72	3.80	3.40	1.11	7.57	0.58	2.97	1.06
4	Coagulated FFT	42.38	13.14	18.23	3.14	4.11	1.48	7.21	2.50	0.01	1.18
	Release/Retained (Stream 1+2+3 - Node 4)	0.00	-5.5	-0.5	0.7	-0.7	-0.4	0.4	-1.9	3.0	-0.12
5	Polymer solution	4.00	2.2	0.8	0.7	0.2	0.1	0.6	0.0	0.0	1.11
	Subtotal (Node 4+5)	46.38	15.3	19.0	3.9	4.3	1.5	7.8	2.5	0.0	1.17
6	Flocculated FFT	46.38	15.3	21.3	5.1	4.6	1.7	10.2	0.9	0.0	1.27
	Release/Retained (Node 4+5-6)	0.00	0.01	2.35	1.25	0.31	0.13	2.44	-1.6	0.0	-0.10
7	Tube Run-off water	45.00	12.6	21.2	4.5	3.9	1.4	8.1	0.7	0.0	1.16
Chemistry difference between 6 and 7			2.7	0.2	0.6	0.7	0.3	2.1	0.2	0.0	0.11

When the mass of Node #4 is subtracted from the sum of Streams #1, #2 and #3 and results in a negative number, this indicates that the mass has increased in the liquid phase by means of some reaction(s) in the slurry. Conversely, a positive result means those cations or anions have been transferred from the liquid phase onto the solids, which is commonly referred to as cation exchange reactions taking place at the soil particle surfaces.

Comparing the coagulated FFT (Node #4) with the collective mass of the input streams (#1 to #3), it can be concluded from the sign conventions for HCO_3^-, SO_4^{2-}, Ca^{2+}, Mg^{2+}, and K^+ that they are released into the fluid (aqueous) phase of the slurry where Cl^-, Na^+ and Al^{3+} are retained into the solid phase. This change in chemical composition suggests that cation exchange reactions are happening on the solid surfaces.

Similarly, comparing the chemistry of the flocculated stream (Node #6) with the sub-total from the upstream sites (Node #4 + Stream #5) a major shift in the overall chemistry is seen. In the flocculated FFT, only K^+ is released into the fluid (aqueous) phase while other major cations and anions are retained in the solid phase. The difference in the ion mass of flocculated FFT (Node #6) and the release water (Stream #7) indicates that all the cations and anions have positive values. This means the cations and anions are retained in the solid phase.

Comparing all the streams individually for mass loading of cations and anions, the most complicated is the coagulant stream (Stream #3). The unit loading of anions and cations masses for all streams is approximately 1 kg/m³, suggesting that all the stock solutions (coagulant Stream #3 and polymer Stream #5) were prepared in similar type of water (the water used from Stream # 2).

Generally, the concentration of anions and cations show encouraging results for the release water chemistry.

The concentration of calcium (Ca^{2+}) in the release water is the same as the process water used for the tests. In addition, Al^{3+} has a negligible concentration of 0.015 mg/L in the release water. Therefore, there is no indication of any excess divalent or multivalent cations in the release water. Comparing the volumes of fluid added into the process from different streams, the volume of the alum solution stream #3 is three times that of the raw FFT stream #1 plus the dilution stream (#2) volume. See Figure 4-13 to understand the rationale behind the change in unit volume of water

from the alum solution stream (#3). This suggests that this stream alone is a major contributor to the change in the downstream process chemistry.

The geotextile tube run-off or release water stream #7 was sampled at different intervals of time. The same concentrations of ions in the release water were reported each time the sample was collected. The concentrations of the anions and cations are presented in Table 4-4 (Stream #7). The 45 m^3 run-off volume shown in Table 4-5 from the geotextile tube is considered an approximation for complete drying when all water is released. Table 4-6 shows the mass of major cations and anions in the release water from the geotextile tubes.

Table 4-6:   Mass of major anions and cations in the released water from the geotextile tubes.

Stream/ Node #	Stream / node description	Fluid volume	Mass of major ions (kg)									Unit load
		(m^3)	HCO$_3$ $^{2-}$	SO$_4$ $^{2-}$	Cl$^-$	Ca^{2+}	Mg^{2+}	Na$^+$	K$^+$	Al^{3+}	kg/m^3
6	Flocculated FFT	46.4	15.3	21.3	5.1	4.6	1.7	10.2	0.9	0.0	1.27
7 (release water)	5 h after geotextile tube is filled at the 1st batch	35.5	9.9	16.7	3.5	3.0	1.1	6.4	0.5	0.0	1.16
	7 days after geotextile tube is filled at the 1st batch	6.9	1.9	3.2	0.7	0.6	0.2	1.2	0.1	0.0	1.16
	30 days after geotextile tube is filled at the 1st batch	0.7	0.2	0.1	0.0	0.0	0.0	0.0	0.0	0.0	0.43

As mentioned above, the concentration of the major ions remains the same, but the mass loading varies depending on the volume of water released, and subsequently the unit mass loading is also reduced. In a nonreactive environment (solid surface), the sum of the individual species masses should be equal to the corresponding species in the flocculated FFT Stream #6, and the unit loading should continue decreasing. If this is not true, then the solid surface is reactive and cations are released during the dewatering process, causing the ion concentrations and overall mass to change.

In summary, the following can be drawn from the above discussions:

a) The effectiveness of the coagulation and flocculation process requires an initial slurry density of the FFT at 20 wt.% solids. This can be achieved by controlled dredging of the FFT and/or providing a dilution step in the process. In the former case, no initial dilution is required, and only water from the coagulation and flocculation solutions is required for the treatment.

b) If the initial slurry density of the FFT is higher than 20 wt.% solids, an initial dilution is required to reduce this FFT stream to 20 wt.% solids. The treatment was designed to achieve efficient flocculation performance by maximizing agglomeration of fines to form large flocs while maximizing water release. To achieve this design criteria, the slurry density at the flocculation step should be approximately 8 wt.% solids and, therefore, the initial dilution of the FFT should be set for this condition while maintaining the concentration and dosage of the coagulant and flocculant constant.

c) The initial change in the fraction of solids from 8 wt.% (end-of-pipe) to 27 wt.% solids (average) in the geotextile tube 5 hours after filling shows the effective coagulation and flocculation process; this released water is the dilution water (including coagulant and flocculant solutions) used in the process.

d) The quick release of water during the first 5 hours of deposition (discharge) of the treated FFT in the geotextile tube is part of the design criteria mentioned above for effective coagulation/flocculation. The slurry density at the initial deposition in the geotextile tube should be approximately 27 wt.% solids and, therefore, the initial dilution of the raw FFT should be also set for that condition while maintaining the concentration and dosage of the coagulant and flocculant constant.

e) The unit change in the volume of water is 4 times greater in the coagulated stream and 4.5 times in the flocculated FFT stream than the unit volume of water in the original FFT (average 28 wt.% solids). Those unit changes represent the volumes of initial dilution from 28 wt.% to 20 wt.% solids plus the coagulation and flocculation solution volumes, as per their fixed concentrations and dosages required for the treatment.

f) Comparing the results at end-of-pipe and after five hours with the data after 7 days, there is a significant initial increase in dewatering from 8 wt.% to 50 wt.% solids.

g) After 30 days of deposition, temperature measurements indicated that the tubes were frozen at their perimeter. However, at the center of the tubes, temperatures were still above freezing (+2 to +5 °C), the undrained shear strength remained at 10 kPa, and solids content was 55 wt.% solids, confirming the limitation of dewatering and strength gain due to the peripheral frozen condition of the tubes, impeding water release.

h) The last in-situ shear strength measurements were obtained on December 10, 2014, because of the difficulty of drilling through the frozen tube perimeter to reach their center.

i) Real-time measurements of temperature and piezometric changes were taken by a data logger monitoring system installed in three sections of each tube.

j) The unit loading of ions from different process streams shows that similar water was used in the chemical preparations and is responsible for changing the chemistry downstream.

k) The process water used for the trial has a high divalent cation concentration (86 ppm Ca^{2+}). The concentration of Ca^{2+} in the release water is the same as the process water used for the tests. Al^{3+} loading is mainly contributed from the coagulant (alum) stream, which is transferred to the solid phase and remains in very low concentration in the release water. The results showed that the tailings treatments used do not generate any excess divalent or multivalent cations in the release water in the scenario of high ion-content dilution water.

l) The mass of the ions in various streams shows ion transfer from aqueous to solid phases and vice versa and are not discouraging. The mass balance and concentration analysis of the major ions in the water phases shows most of the ions remain in the solid phases after deposition.

m) As a result, this research through the solid and water mass balance analysis has identified that the negative impact of excess of calcium ions on flocculation of the FFT can be minimized/or even eliminated by aluminum ions (higher valence cations) at pH≥8.

4.1.4 Commercial field trial on FFT inline mixing, filling, and dewatering into the geotextile tubes

Dilution was applied inline to the FFT prior to the addition of coagulant. Once the FFT was diluted and coagulated, the flocculant was added for solids/water separation and fines agglomeration during pipeline transporting. The key factors for efficient flocculation in the pipeline are the recipe, residence time of the mixing process (20 seconds), and the flow rate in the pipeline, which defined the location of the flocculant injection (Photograph 4-11) to minimize shearing during pipeline transporting prior to discharge into the geotextile tubes. Samples of the FFT feed and the treated FFT inline were collected for visual quality control (floc sizes and solid/water separation) and laboratory testing (Photograph 4-12).

Photograph 4-11:   Geotextile tubes field trial inline mixing process layout, and location of the flocculant injection/addition.

Photograph 4-12: **Geotextile tubes field trial sampling location of the treated FFT prior to the discharge in the tubes.**

Filling and rate of dewatering in the geotextile tubes – The treated FFT dewaters in the geotextile tubes, and the rate of dewatering is a function of the recipe, the inline mixing process, the short drainage path of the geotextile tubes containment, the internal pressure and gravity head during filling, hydraulic parameters of the geofabric material, evaporation, freeze-thaw, self-weight consolidation, and increased total stress by stacking the geotextile tubes.

Photograph 4-13 shows the effective filtration and dewatering of the geotextile tubes with stacking (loading).

Photograph 4-13: Geotextile tubes field trial filling and dewatering.

Geotextile tubes mechanical, filtration, and physical properties – Tables 4-7, 4-8, and 4-9 show the commercial-size geotextile tubes (GT500) mechanical, filtration, and physical properties referred to in this research.

Table 4-7: Geotextile tubes GT500 mechanical properties.

Mechanical properties	Test method	Unit	Minimum average roll value	
			MD*	CD*
Width tensile strength/ultimate	ASTM D4595	kN/m	78.8	109.4
Width tensile elongation	ASTM D4595	%	20 max.	20 max.
Factory seam strength	ASTM D4884	kN/m	70	
CBR puncture strength	ASTM D6241	N	8,900	
Apparent opening size (AOS)	ASTM D4751	mm (U.S. Sieve)	0.43 (40)	
UV resistance (retained after 5,000 hrs)	ASTM D4355	%	80	

(*) MD = Machine direction (material off the roll); CD = material across the roll

Table 4-8: Geotextile tubes GT500 filtration properties of the engineered woven yarn

Filtration properties	Test method	Unit	Typical average
Pore size distribution (O_{50})	ASTM D6767	Micron	80
Pore size distribution (O_{95})	ASTM D6767	Micron	195

Table 4-9:   Geotextile tubes GT500 physical properties

Physical properties	Test method	Unit	Typical average
Mass/unit area	ASTM D5261	g/m^2	585
Thickness	ASTM D5199	mm	1.8

Geotextile tubes GT500 parameters – Tensile strength of the geofabric is the key reinforcing parameter of the geotextile tubes deposit to allow for stacking at low undrained shear strength. The stacked tensile strength is 220 kN/m (Photograph 4-14). This parameter is based on lab analysis cross machine direction (CMD) provided by the manufacturer. The ultimate strength of the geotextile tube is represented by T (ult.) = T (work) × (FS id × FS ss × FS cd × FS bd × FS creep) where: T (work) = 220 kN; FS id (installation damage) = 1.3; FS ss (seam strength) = 2; FS cd (chemical degradation) = 1.0; FS bd (biological degradation) = 1.0; and FS creep = 1.0.

In the context of geotextile tubes, the maximum tensile force in the geofabric will be mobilized during the filling (pumping of the treated FFT into the geotextile tube). After pumping, as the slurry solidifies, this force relaxes. Therefore, small FS creep can be assigned to the geotextile tube such as FS = 1.06. A verification of the FS for circumferential direction can be expressed by: FS = T (work tensile strength) ÷ (T ult.) and therefore, Factor of Safety (FS) = 220 ÷ [24.93 (1.3 × 2.0 × 1.0 × 1.0 × 1.06)] = 3.2.
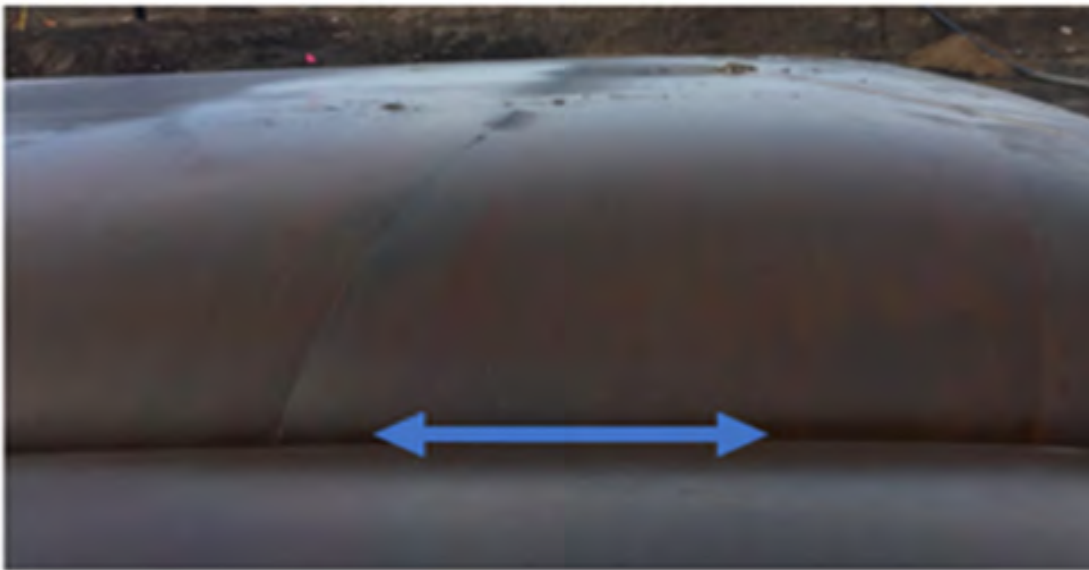
Photograph 4-14:   Geotextile tubes field trial stacked 2 layers, tensile strength 220 kN/m.

Tables 4-10 shows the parameters of the selected geotextile tube for the commercial field trial investigated by this research. Filling the geotextile tubes is controlled by the specific strength and hydraulic parameters of the geofabric (seams and intake ports) that limit the intake pressure and the filling maximum height of the geotextile tubes (2.9 m).

Table 4-10: Geotextile tubes GT500 parameters.

Input		Output
Geotextile tube length	100.0 m	Max. length = 100 m
Geotextile tube height	2.9 m	Max. circumferential tensile force = 24.93 (kN/m)
Geotextile tube circumference	44.0 m	Max. average axial tensile force = 23.00 (kN/m)
Density of the fill material	1.2 t/m^3	Geotextile tube base contact width = 20.66 m
Seam type	Circumferential	Cross section area = 55.21 m^2
Fill port type	Rigid mech.	Volume/length = 55.21 m^3/m
Fabric type	GT 500	(%) max. fill capacity = 36%
		Pressure at the base = 34.256 kPa
		Circumferential direction FS = 3.2
		Axial direction FS = 3.0
		Fill port rupture FS = 3.2

Photograph 4-15 shows a geotextile tube of commercial-size: 100 m length and 44 m circumference being filled to its maximum height.

Photograph 4-15:   Geotextile field trial with commercial tubes with size of 100 m length and circumference of 44 m.

Investigating stacking, undrained shear strength, and consolidation behaviors – Shelby tube samples were collected for geotechnical laboratory testing to determine index properties and shear strength from triaxial testing, including consolidation. In-situ and laboratory "vane shear" tests were performed to monitor shear strength gain with time. Real-time geotechnical monitoring instrumentation (piezometers and thermistors) were installed to monitor

consolidation and dewatering. Field trials under a loading condition, such as stacking two layers of commercial-sized geotextile tubes as shown in the Photograph 4-16, were performed to evaluate and monitor the undrained shear strength and pore pressure behaviors during one completed seasonal cycle (spring, summer, fall, and winter).

Photograph 4-16:   Geotextile field trial completion of stacked 2 layers.

The summarized results from the undrained shear strength and pore pressure dissipation parameters are shown in Tables 4-11 and 4-12 and indicate that the treated FFT remains contractive inside the geotextile tubes, generating and dissipating excess pore pressures.

Table 4-11: Pore pressure dissipation of geotextile tubes field trial stacked in two layers.

Parameter	Geotextile tube (initial condition)	After 1 year	Seasonal cycle completed
Static pore pressure U_0 (kPa)	19.62	10.79	
Excess pore pressure Δu (kPa)	9.86	2.35	
Bbar	0.50	0.22	Pore pressure dissipation

Table 4-12 shows that the undrained shear strength of the FFT increases with time, responding quite well to the rapid loading of two layers of geotextile tubes. The second layer was stacked immediately following the completion of the first layer (still at 2 kPa undrained shear strength).

Table 4-12: Undrained shear strength of geotextile tubes field trial stacked in two layers.

Parameter	Geotextile tube filling completed	After 1 year	Comments
Peak	2.0 kPa	15.0 kPa	Field and laboratory monitoring data
Remolded	0.3 kPa	2.8 kPa	

Forecasted physical stability – The tensile strength with low elongation provided by the geofabric is a key reinforcing parameter of the geotextile tube deposit to allow stacking at low undrained shear strength (2 kPa), usually achieved when the filling of the geotextile tube is completed to the height recommended by the manufacturer. Consider using geotextile tubes of commercial-size 100 m length × 44 m circumference, with a total volume capacity of 5521 m^3. Based on field trial results, during the first year of installation, the treated FFT within the tubes will achieve 85 wt.% solids and a dry density of 1.75 t/m^3; therefore, the total dry solids captured per tube will be approximately 9662 t. Assuming the installation of 400 commercial tubes to form two layers per year, the total capture of dry solids per year would be approximately 3.86 Mt. Stacking 20 layers of tubes to form a ~ 30 m high deposit, occupying an area of approximately 700 m × 700 m at an average slope 2(H):1(V) and similar drainage conditions, based on the results of this research, approximately 38.6 Mt dry solids during 10 years of operation could be captured. Assuming the lower to mid zones of the deposit would already have sufficient time to dissipate the majority of the excess pore pressure is reasonable; therefore, the effect of the slow rate of loading (construction of the deposit) from the upper layers would allow time for drainage of the layers below and, therefore, would have effectively no increase in pore pressure in those zones of the deposit. In this case, under our loading and drainage conditions, it is possible to have drained and undrained responses during shear. Depending on the operation criteria, life-of-mine planning, available real estate, and tailings management plan, the geotextile tube technology described in this research could allow a progressive reclamation of 3.86 Mt/year, which would look like Photographs 4-17 and 4-18 of the example deposit shown below.

Photograph 4-17: **Example of stacked geotextile tubes deposit including capping (adapted from TenCate Geosynthetic Americas).**

Photograph 4-18: **Example of stacked geotextile tubes capped and reclaimed (adapted from TenCate Geosynthetic Americas).**

Summary of the key findings of this research (Chapters 3 and 4):

- **Dispersion and flocculation behavior of the FFT.**

The analyzed FFT was at pH 8 and predominantly composed of fine soil particles of quartz and kaolinite, which are negatively charged and exhibit dispersive and hydrophilic behaviors. A parametric analysis of quartz and kaolinite particle dispersion and flocculation behaviors was performed to determine the potential causes of the significant amounts of trapped water in the flocculated FFT. The parametric analysis was performed using quartz flour and pure kaolinite materials. Alum, an inorganic coagulant, was used as a coagulant aid to increase the ability of quartz and kaolinite soil particles to settle and release water after flocculant addition. Anionic PAM flocculant of medium charge density (30%) and high molecular weight (HMW) was used to flocculate the coagulated FFT. The effect of the calcium and aluminum concentrations and the pore water pH on the flocculation of the FFT using anionic PAM flocculant was investigated. In summary, it was observed that:

a) The increased calcium cations concentration (i.e., >31 ppm) and pH (i.e., ≥ 8) can cause adverse effects on the adsorption of anionic PAM flocculant on quartz and kaolinite particles.

b) The poor flocculation of quartz and kaolinite observed at pH ≥ 8 was likely due to the adsorption of calcium ions onto anionic PAM flocculant, causing steric stabilization at the particle surfaces and inhibiting the formation of hydrogen bonding by covering up the active functional groups of the particles.

c) Efficient fines agglomeration and dewatering of quartz and kaolinite particles was achieved with coagulation of the particles by alum (Al^{3+} ions) prior to anionic PAM flocculant addition.

- **Physicochemical treatment of the FFT (recipe).**

Laboratory test and field trial results indicated:

a) To control variation of the feed densities, achieve enhanced mixing and maximized flocculant adsorption at relatively low dosages and concentrations of flocculant and coagulant, dilution is required to maintain the initial slurry density of the FFT at 20 wt.% solids to optimize flocculation if the initial slurry density is higher than 20%.

b) The recipe is most effectively applied inline to promote solids agglomeration and water separation during pipeline transport.

c) Inline mixing of the coagulated FFT with flocculant solution does not require static or dynamic mixing. The optimal residence time is 20 seconds to provide the most efficient flocculation, fines agglomeration (large floc formation), and solid/water separation.

d) In the presence of high-valence cations, such as Al^{3+}, the repulsive forces of quartz and kaolinite minerals are reduced, resulting in the coagulation of the particles.

e) Efficient fines agglomeration and dewatering of quartz and kaolinite soil particles were achieved with coagulation of the particles by Al^{3+} ions prior to anionic PAM flocculant addition. The FFT treated with Al^{3+} and anionic PAM flocculant had a measured zeta potential of -14 mV at pore water pH 7. The FFT before treatment had a measured zeta potential of -47 mV at pore water pH 8.

- **Solid and water mass balance for dewatering FFT using geotextile tubes.**

At the beginning of November 2014, a preliminary field trial using an inline coagulation and flocculation treatment was applied to treat FFT prior to discharge into two geotextile tubes of 18.3 m circumference and 30 m length to assess dewatering, filtration, and fines capture. The trial also included a solid and water mass balance along with the changes in the chemistry of the release water as described below:

a) FFT consisted of approximately 70 wt.% water, which was the major constituent. The supplied water for the trial was mine process water, consisting of high concentrations of dissolved divalent cations such as 86 ppm of Ca^{2+} at pH 8. This process water was used in all steps of the trial to treat FFT, including dilution and coagulant and flocculant solution preparation. The objective of the treatment of the FFT was to provide fines agglomeration and water separation, efficient filtration and dewatering in the geotextile tubes to accelerate consolidation and enhance shear strength of the treated FFT.

b) The FFT was diluted from 28 wt.% solids down to 8 wt.% solids in different stages to achieve an effective chemical treatment. In the first stage, the FFT was diluted to 20 wt.% solids using process water. In the second stage, the dilution occurred through inline addition of the coagulant solution, and in the third stage, the dilution occurred through inline addition of the flocculant solution; at the final stage the treatment achieved 8 wt.% solids inside the pipeline and prior to discharge into the tubes. Collectively, FFT was diluted 4.5 times during the entire process.

c) The quick release of water during the first five hours after treated FFT deposition into the tubes was the release of the dilution water added during the process. During this period, the solids content increased in the tubes to 27 wt.%, which was comparable to the solids content of the FFT feed.

d) Dewatering in the geotextile tubes increased the solids content from 8 wt.% to 50 wt.% after 7 days. Undrained shear strength at the same location was 5 kPa.

e) After 30 days (December 2014) of deposition of the treated FFT into the geotextile tubes, the solids content and shear strength at the center of the tubes were 55 wt.% and 10 kPa, respectively. No further gain in solids content and shear strength was seen because of the physical limitations to dewatering caused by the frozen condition of the peripheral soil/pore water. The temperature measurements indicated that the tubes were frozen at their perimeter while the center was still at +2 to +5 °C.

f) Real-time measurements of temperature and piezometric changes were collected by a data logger monitoring system. Continuous monitoring of dewatering, solids content, and strength gain extended until spring and summer 2015 to complete the dewatering evaluation, wt.% solid contents, and shear strength gain interpretation. The results indicated solids content in the range of 75 to 85 wt.% solids and shear strength in the range of 35 to 40 kPa.

g) Chemical analysis of mixed inline streams and the release water from the geotextile tubes showed changes in the chemistry throughout the treatment process. Process water consisting of high concentrations of dissolved divalent cations such as Ca^{2+} (86 ppm) and pH 8 was used as dilution water for the FFT feed, and as the water for preparing the coagulant and flocculant solutions. The mass balance and concentration analyses of the major ions in the water phases show that majority of the ions remained in the solid phases after deposition. The concentration of Ca^{2+} in the release water was the same as in the process water used for the field trial. The major source of Al^{3+} in the process is from alum (coagulant stream), which has a concentration of 0.015 mg/L in the release water. Therefore, the analysis shows that the coagulation with alum eliminated any possibility of impact on the flocculation of quartz and kaolinite particles caused by the excess of calcium ions at pH≥8.

- **Stacking of the geotextile tubes deposit at low undrained shear strength.**

Laboratory test and field trial results indicated:

a) Once the treated FFT are discharged into the geotextile tubes, the filtration properties of the geofabric and the short drainage path of the containment are the key contributors for enhanced dewatering and accelerated consolidation. Evaporation and freeze-thaw

were also identified as contributors to dewatering over time. Test results indicated that: the actual rate of evaporation of the treated FFT is close to the potential rate of evaporation of water and is higher than the actual evaporation of the FFT. The treated FFT evaporates at a potential rate (i.e., AE/PE $\geq$1) when the sample is saturated in the early stage of the drying process. The treated FFT loses water much faster and reaches the boundary region between the saturated and unsaturated states (i.e., AE/PE = 0.8) earlier than the FFT.

b) The commercial geotextile tubes used in this research have a stacked tensile strength of 220 kN/m. Tensile strength of the geofabric is the key reinforcing parameter of the geotextile tubes deposit to allow for stacking at low undrained shear strength. Field trials indicated that the undrained shear strength of the treated FFT increases with time and responds quite well to the rapid loading of two layers of geotextile tubes. The second layer can be stacked immediately following the completion of the first layer, still at 2 kPa undrained shear strength.

c) Monitoring the undrained shear strength and pore pressure behaviors during one completed seasonal cycle (spring, summer, fall, and winter) indicated that the treated FFT inside the geotextile tubes more rapidly dissipates excess porewater pressure.

d) Geotextile tube deposits with treated FFT seem to act similarly to a filter pressure system, with most of the water recovery happening while the geotextile tubes are being filled. Fines capture ranges between 97% and 99% (51% silts and 47% clays). The treated FFT inside the geotextile tubes has shown a considerable gain in shear strength over a one-year period, reaching over 15 kPa as an average shear strength of the deposit.

Chapter 5 Discussion and Anticipated Outcomes

5.1   Brief review on GISTM

The GISTM aspires toward "zero harm to people and the environment" from tailings facilities. It elevates accountability to the highest organizational levels, with new requirements for independent oversight. It expects global transparency and disclosure to improve stakeholder understanding. It sets the design basis of "'Extreme' Consequence Classification external loading criteria or the current Classification, with upgrade to 'Extreme' maintained throughout the tailings facility lifecycle," including at closure. Many active tailings facilities are not classified as having an "Extreme" consequence classification and may need to be re-classified and/or upgraded to meet "Extreme." At post-closure, the site settings (climatic, topographic, and seismic) of the mine will dominate the long-term performance of tailings facilities. The post-closure classification is "Extreme" because tailings facilities must remain safe, stable, and non-polluting in perpetuity. This criterion is in line with current tailings dam guidelines. The extreme consequence return interval is 1 in 10,000 years, which is presumed to be equivalent to "in perpetuity." The purpose of the GISTM is to provide "a framework for safe tailings facility management, while affording operators flexibility as to how best to achieve this goal; in other words, to be self-regulating. The design, construction, operation, monitoring, and closure of tailings facilities are required to be robust enough to minimize the risk of harm to the people and environment (**Williams, D.J., 2021**).

5.2   New approaches to tailings management vs. industry paradigms

As briefly discussed in the section 1.2.3 of this research (mining industry paradigms), there are still several barriers to the implementation of innovative tailings management, starting from the way that tailings management is costed, supported by NPV accounting. The mining industry is locked into a sustainable low-cost approach starting from low front-end costs to achieve the most economical solution of an acceptable tailings deposit, such transporting tailings as a slurry to

a surface dam, which limits alternatives to be considered and increases operating costs over time and leads to high back-end costs. The implementation of existing and new approaches to technologies in tailings management could help to eliminate the risks posed by some conventional tailings facilities, and to place the industry in a better position of compliance with the GISTM aspirational goal of "zero harm to the people and the environment" from tailings facilities. Therefore, the industry should be challenged to move to a more whole-of-life approach (**Williams, 2021**) by starting to use the best available tailings technology that works, then progressively optimizing costs, assuring that reclamation is possible and post-closure long-term performance of the tailings deposits is safe.

5.3   Technology suitability

The use of geotextile tubes with the "recipe" will be part of a potentially comprehensive range of alternatives to the conventional deposition of slurry tailings behind dams. The implementation of stacked deposits of thickened and filtered FFT using geotextile tubes to enhance physical stability of reclaimed landforms could help to minimize the risks posed by conventional tailings facilities, possibly removing the risks altogether. The success of tailings disposal in the geotextile tubes requires a physicochemical treatment of the FFT by combining coagulation and flocculation, called the "recipe." The recipe allows solids/water separation and fines agglomeration in the pipeline prior to discharge of the treated FFT into the geotextile tubes. This approach allows for geotechnically stable thick layer deposits (stacked up to 40 m high) and early closure and reclamation.

Dewatering in the geotextile tubes is a function of:

- Inline recipe addition to a FFT feed, flow rate, and residence time mixing process.

- Short drainage path of the geotextile tubes containment.

- Internal pressure and gravity head during filling.

- Filtration properties of the geofabric.

- Evaporation.

- Freeze-thaw.

- Self-weight consolidation and stacking (loading).

The photographs below show examples of stacked filtered tailings, paste tailings, conventional tailings deposit and geotextile tubes technology, as referred in this research.
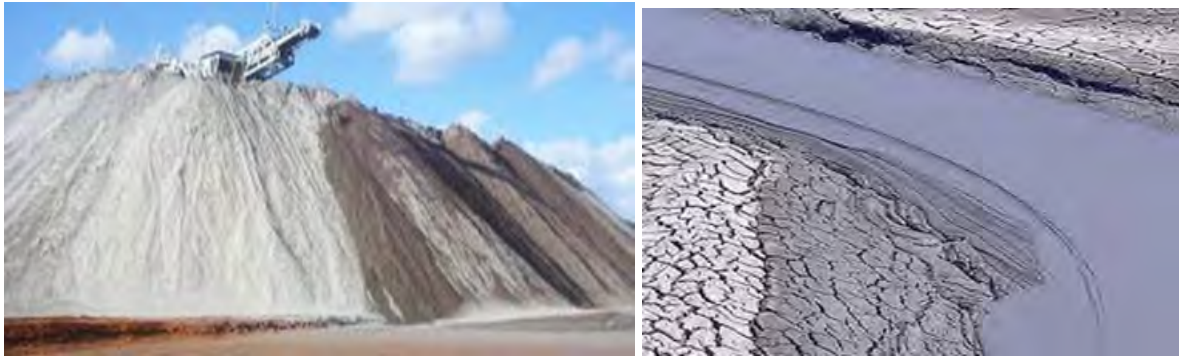
Photograph 5-1:   Example of filtered tailings (left) and paste tailings (right).

Photograph 5-2:   Example of conventional tailings deposit flow liquefaction failure (Fundao – Brazil).

Photograph 5-3: Example of a large-scale application of geotextile tubes.

Comparison of alternative tailings disposal parameters:

Table 5-1 shows methods of tailings disposal and a comparison of their disposal parameters.

Table 5-1: Comparison of alternative tailings disposal parameters.

Methods of tailings disposal	Incoming (wt.% solids)	Outcoming (wt.% solids)	Typical Yield stress (Pa)	Typical Angle deposition (%)	Typical water recovery (%)
Conventional	25-45	30-55	10-100	0.5-2.0	50-60
Thickened	30-45	50-70	10-300	1.0-3.0	60-70
Paste	60-65	70-85	100-1,000	3.0-10.0	80-90
Filtered	60-65	>70	>1,000	NA	>90
Geotextile Tubes	**20-30**	**50-85**	**>1,000**	**NA**	**>90**

Note: Despite the perceived advantages, there are number of factors that determine whether an alternative technology is suitable.

Factors influencing suitability:

1) **Energy supply** – Required energy to remove water from the slurry: filtered and thickened tailings and paste methods will likely require more energy to transport than a conventional slurry and geotextile tubes.

2) **Climate** – Successful implementation of filtered and thickened tailings disposal methods is often seen in dry climates (desiccation aid). Treated FFT disposal in geotextile tubes can be successfully implemented in a variety of climates.

3) **Production rates** – Filtered and paste technologies are unproven for high production rates (>100 kt/day). Thickened methods provide moderate production (30–50 kt/day); conventional disposal remains the only proven technology at mines with high production rates. Geotextile tubes can be comparable to moderated production, occupying a smaller footprint.

4) **Economics** – Data show that alternative tailings technology methods are more expensive than conventional disposal.

5) **Operational** – Maintaining uniform deposition slopes is a challenge for paste and thickened methods because of fluctuations in ore characteristics, tailings gradations, and percent solids. No constraints have been identified for operationality of geotextile tubes because of fluctuations in ore characteristics and tailings initial slurry densities and gradation.

6) **Topography** – Thickened and paste tailings require flat topographies and embankment support. Filtered tailings can be implemented in a variety of terrains provided stability, operational, and closure requirements are taken into consideration. Geotextile tubes can be implemented in a variety of terrains and could be used as a buttress for filtered tailings in co-disposal deposits.

7) **Seismicity** – Mitigation measures to address concerns about physical stability of alternative tailings disposal may contradict many of the perceived benefits. Geotextile tube containment provides ideal conditions of drainage and shear strength reinforcement to minimize liquefaction issues.

8) **Water** – The conservation and reuse of water are the main drivers for implementation of the alternative methods of tailings disposal. Tailings treatment should be about creating reclaimable water which reduces freshwater intake. Filtered and geotextile tube methods save significant amounts of water and allow reuse (recycling) to the mine operation process, with paste providing fewer advantages. Limited water supply is an important driver for mining operations.

Drivers for implementation of filtered tailings & geotextile tubes:

1) **Space conservation:** Filtered tailings and geotextile tubes are stockpiled at a higher dry solid content (dry t/m^3) and much smaller footprint than conventional tailings disposal. No transportation of solids or compaction are required for geotextile tubes deposits.

2) **Reduced environmental risks**: Less water in the tailings and lower containment structures are favorable attributes for permitting because more water is recovered from the thickener/or geotextile tubes and less freshwater make-up is required.

3) **Improved compliance**: Environmental regulations have become more stringent, influencing mining companies' decisions toward filtered tailings dry stack disposal, which includes geotextile tubes deposits.

4) **Better handling in cold conditions:** Cold conditions can make water handling difficult, making filtered tailings and geotextile tubes disposal technologies attractive.

5) **Physical stability:** Compared with filtered tailings, geotextile tube deposits provide the advantage of geotechnically stable thick layers stacked up to 40 m high without compaction and allow early closure and reclamation. In addition, the treated tailings are contained in the geotextile tubes, eliminating erosion and risks of liquefaction.

6) **Chemical stability:** As filtered tailings and geotextile tubes are unsaturated stacks and susceptible to oxidation, if the tailings are acid generating the oxidation process can result in acid drainage. In the case of geotextile tubes, depending on the design of the physicochemical treatment recipe, acid drainage could be prevented. To assess the chemical stability of the stacked geotextile tubes, it will be necessary to determine the acid-producing minerals (primary and secondary) and acid-neutralizing minerals that may be present, along with the metal-leaching potential to predict future geochemical behavior. The primary mineralogical composition has a strong influence on the oxidation processes and, therefore, understanding mineralogical and geochemical interactions is essential to understand the parameters controlling acid mine drainage formation and to develop effective prevention measures.

5.4   Treated FFT with the recipe combined with geotextile tubes as a new approach to tailings management

The implementation of the Da Silva's recipe/geotextile tube processing as a new solution for the accumulation of large volumes of soft and wet tailings deposits, assuring that reclamation is possible and post-closure long-term performance of tailings deposits is safe, involve optimizing dewatering and fines capture by thickening and filtration and addressing key design considerations for Da Silva's physicochemical recipe. This includes:

1) Investigation of the inherent properties of the FFT constituents and their extraction process, including water chemistry and pH, to understand their impacts on the mechanical and physical properties of the FFT.

2) Evaluate the dispersion and flocculation behaviors of the FFT particles to define dosages and concentration of coagulant and flocculant, and to define the inline mixing process to minimize shearing of the treated FFT during transporting prior to discharge into the geotextile tubes.

3) Optimizing dilution of the FFT initial slurry density for enhanced mixing and energy dissipation to achieve efficient flocculation at relatively low dosages and concentrations of coagulant and flocculant.

4) Performing laboratory settling tests to define the residence time of flocculation.

5) Performing laboratory bleed testing, as described in this research, to evaluate the short-term gravity drainage or passive water release of the discharged underflow solids that are obtained from the laboratory settling tests of the treated FFT. The bleed test will provide a visual observation of the size of flocs and particle agglomeration outside the cylinder, as well as an indication of the increased solids content as a function of the recipe, including evaporation over time.

6) Selecting an inline mixing process based on residence time and FFT flow rates in the pipeline to define the point of flocculant injection prior to the discharge of the treated FFT in the geotextile tubes. The residence time of the recipe is 20 seconds to provide for the most efficient flocculation, fines agglomeration (large floc formation), and solid/water separation. Data from this research have indicated that inline mixing of the coagulated FFT with flocculant solution does not require static or dynamic mixing.

7) Validating that the treated FFT dewaters in the geotextile tubes and the rate of dewatering is a function of the recipe, the inline mixing process, the short drainage path, and filtration media provided by the tubes, geofabric hydraulic properties, increased total stress due to loading, evaporation, and freeze-thaw over time.

The enhanced physical stability of the geotextile tubes deposit has been validated by a commercial field trial and laboratory test results presented in this research.

1) The commercial geotextile tubes have a stacked tensile strength of 220 kN/m. Tensile strength of the geofabric is the key reinforcing parameter of the geotextile tubes deposit to allow for stacking at a low undrained shear strength, such as 2 kPa.

2) It is possible to install 400 commercial-size (40 m circumference × 100 m length) tubes to form two layers per year (see example Photograph 5-3), as a construction rate, which would provide a total capture of 3.86 Mt of dry solids per year. If 20 layers of tubes are stacked to form a ~ 30 m high deposit, occupying an area of approximately 700 m × 700 m, at an average slope 2(H):1(V) and at similar drainage conditions as per the results of this research, a total of 38.6 Mt dry solids could be captured in 10 years of operation. Therefore, the effect of the slow rate of construction of the deposit (loading) from the upper layers would allow time for drainage of the layers below and the excess pore pressure in those zones of the deposit would be highly dissipated. In this case, under our loading and drainage conditions, it is possible to have drained and undrained responses during shear.

5.5 Value-adding final notes

Every mine is unique with respect to setting, material properties, water supply, mineral process employed, environmental obligations, and energy cost. Therefore, it is difficult to prescribe a universal method of tailings disposal, because each case must be evaluated on its own merits. Therefore:

1) It is encouraging that methods to create more reclaimable water for reuse in the processes close to the mine are advancing rapidly and contributing to less freshwater make-up requirements.

2) Early assessments of tailings properties with regards to sedimentation, rheology, geotechnics, geochemistry, and field conditions of the projected impoundment area are key to evaluating the potential for implementing alternative tailings methods.

3) Basic data comparisons of capital and operational expenditures between the different alternatives should be identified at a prefeasibility or feasibility level of engineering to assist in early decision-making regarding tailings disposal.

4) In many cases, filtering can result in improved density and tailings storage efficacy, so when space is at a premium, filtering the tailings prior to disposal has potential. The operating costs are considerable, but some of these costs may be offset by creating reclaimable water, reducing space, improving dam stability, and minimizing environmental risks.

5) Selection of the alternative tailing's deposition technique will be done on a case-by-case basis, considering the specific conditions and requirements at a mine site.

Chapter 6 Conclusions

The primary objective of this research was to provide an understanding of the potential causes of the significant amounts of trapped water remaining when thickening FFT with flocculation only, resulting in a low rate of shear strength gain and long consolidation timeframes that pose significant challenges in the conversion of FFT into deposits capable of facilitating reclamation.

To this end, this parametric analysis has identified that poor flocculation of the FFT (quartz and kaolinite) in the range of pH 8 is likely due to the adsorption of excess of Ca^{2+} ions onto the anionic PAM polymer, causing steric stabilization at the particle surfaces and inhibiting the formation of hydrogen bonding by covering up the functional activity groups of the particles. As a result, this research has also identified that the negative impact of excess of calcium ions on flocculation of the FFT can be minimized/or even eliminated by aluminum ions (higher valence cations) as evidenced through simple but essential laboratory tests that investigated the inherent properties of the FFT constituents, porewater chemistry and pH, dispersion and flocculation behaviors, and zeta potential, including solid and water mass balance analysis.

As described in the solid and water mass balance analysis of this research, the unit loading of ions from different process streams confirms that a similar type of water (process water) was used in the chemical preparations (coagulant and flocculant solutions) and is responsible for changing the chemistry downstream. The process water used for a preliminary geotextile tube field trial with the recipe intentionally had high divalent cations concentration (86 ppm Ca^{2+}). The concentration of Ca^{2+} in the release water was the same as the process water used for the tests. Al^{3+} loading was mainly contributed from the coagulant (alum) stream, which was transferred to the solid phase and remained as a very small concentration in the release water. The results showed that the recipe provided effective flocculation of the FFT in the scenario of high Ca^{2+} content dilution water, confirming the benefits of coagulation with alum (Al^{3+}).

Another key finding of this research was identified by the evaporation tests confirming that the treated FFT with the recipe (coagulation + flocculation) loses water faster and reaches the boundary between the saturated and unsaturated state (i.e., AE/PE = 0.8) earlier than FFT and centrifuged FFT with flocculation only. The recipe entraps the residual bitumen in the FFT and forms an open soil structure, as confirmed by fines capture, quality of the release water, and hydraulic conductivity of the treated FFT. In contrast, the residual bitumen films on the surface of the FFT with flocculation only start to break down as drying continues, and the AE/PE ratios continue to gradually increase to reach a value of 0.96 and remain constant until Day 10. Eventually, the AE/PE ratios decrease to reach a value of 0.8 on Day 12. During this time, the AE/PE ratio of the recipe continues to decline gradually and reaches a value of 0.8 on Day 10. This is an indication that the recipe also reduces and/or minimizes the potential impacts on the flocculation of the FFT caused by the residual bitumen.

Furthermore, when reviewing the laboratory geotechnical beam centrifuge test results, we suggest that volume change could be a criterion for acceptance of FFT ready to reclaim within 10 years of the end of mine life. Porosity is the volume of water divided by the total volume. Previous experience has shown that FFT must have a minimum shear strength of 10 kPa to allow for the surface to be reclaimed. Field trials as part of this research have indicated that a shear strength of 10 kPa is reached at a porosity of 0.5, which is equivalent to 70 wt.% solids. The laboratory beam centrifuge test results from this research show that the porosity of 0.5 is reached at depth of 6 m in deposits formed by the treated FFT discharged as an open-end method. Therefore, atmospheric drying and/or freeze/thaw effects will be needed to decrease the surface porosity to an acceptable value that will allow reclamation. The results of this research also indicate that the treated FFT sample settles more and faster, and consequently dissipates the excess pore pressure faster than for the centrifuge cake and FFT with flocculant only.

Laboratory testing was performed to evaluate soil composition and engineering properties such as mineralogy, zeta potential, PSD, slurry density, specific gravity, water content, total bulk density, dry density, void ratio, undrained shear strength, and pore pressure dissipation. This research demonstrates that establishing and understanding of critical linkages between the fundamental properties governing dewatering enabled better conceptualization and understanding of the observed coagulation and flocculation behaviors and performance of the treated FFT.

Identification and quantification of the FFT mineralogy is considered "critical" for the successful manipulation of clay and non-clay mineral behavior along with the porewater chemistry and pH. FFT is composed of non-clay minerals (55.5% quartz <75 μm size) and clay minerals (23.2% kaolinite and 11.6% illite <2 μm size). Other mineral amounts such as microcline (highest), clinochlore, siderite, pyrite (lowest), anatase, rutile, albite, dolomite, and calcite add up to approximately 9.7% in total. The FFT mineralogy as part of this research is predominantly composed of quartz particles (non-clay mineral). However, some localized variations in the FFT feed originated in the ETF were observed, where the predominance of quartz was replaced by predominance of kaolinite; this caused the ratio of clay to massive minerals encountered in the FFT used in this research to vary from approximately 0.6 to 1.2.

The author of this research has also participated and collaborated on a filter press commercial trial at an oil sands operation as JV partner. The recipe used in this research, with a variation using high dosage of coagulant, was selected for use in a commercial filter press field trial. The residence time of pressing was between 20 and 30 minutes per batch, and the discharged solids content of the filter press cake on the conveyor belt was consistent at approximately 70 wt.% solids. In addition, as shown in this research, the recipe was successfully applied in subaerial discharge for gold mine tailings, showing its application in a variety of tailings management processes.

The starting point tests, analyses, and results mentioned above enabled a clear understanding of the problem and provided key input material properties and valuable information to achieve the overall objective of this research.

This research also aimed to satisfy the six specific objectives presented in Chapter 1. These objectives and their specific conclusions are summarized in Table 6.1.

Table 6-1:   Summarized research conclusions.

ID No.	Research Objective	Conclusions
1	Investigate how the chemistry of the process water and pH and FFT porewater chemistry, inherent properties of the FFT constituents, and zeta potential affect the dispersion and flocculation behaviors of the FFT.	Quartz and kaolinite dispersion/flocculation behaviors are impacted by pH and porewater salinity (hydrolyzed salts: Ca, Al, Mg, K, bicarbonates, chlorides, and sulfates). The analyzed FFT is at pH 8 and predominantly composed of fine quartz and kaolinite soil particles with highly negative surface charge of zeta potential −47 mV exhibiting dispersive and hydrophilic behaviors by action of electrostatic repulsive forces. Increased porewater Ca^{2+} concentration >31 ppm and pH ≥ 8 is likely the cause of the significant amount of trapped water remaining if FFT are flocculated with anionic flocculant only (poor flocculation). FFT is predominantly non-clay mineral (<75 μm fine quartz) followed by clay minerals (kaolinite and illite). Typical PSD is 97% finer than 75 μm and 37% finer than 2 μm, consistent with the mineralogy results. Solids content 28 wt.% solids, bulk density 1.15 t/m^3, and specific gravity 2.5.
2	Investigate why thickening FFT with flocculant only is not enough to provide an efficient fines agglomeration and dewatering of the FFT, and what are the gaps to be filled.	Laboratory parametric analysis on the dispersion and flocculation behaviors of the FFT, as well as evaporation tests and geotechnical beam centrifuge testing comparing FFT with flocculant only to FFT with the recipe, have indicated that coagulation prior to flocculation addition is the missing step. Efficient fines agglomeration and dewatering of the FFT (quartz and kaolinite particles) were achieved with coagulation of the particles by aluminum ions prior to anionic PAM polymer flocculant addition.
3	Develop a recipe for FFT to assist solids-water separation, fines agglomeration with maximized capture, enhanced dewatering, and accelerated consolidation.	Effective fines agglomeration, enhanced dewatering, and accelerated consolidation of the FFT were achieved at relatively low dosages and concentrations of coagulant (alum Al^{3+}) and flocculant (anionic PAM flocculant). The treated FFT with the recipe had a measured zeta potential of - 14 mV and porewater pH 7. Flocculation with flocculant only has shown zeta potential of -40 mV (more dispersive/hydrophilic behavior) at the same pH.
4	Develop an inline mixing process of the FFT with coagulation and flocculation for effective flocculation prior to the discharge into the geotextile tubes.	The effectiveness of the coagulation and flocculation process requires an initial slurry density of the FFT feed at 20 wt.% solids. This can be achieved by controlled dredging of the FFT and/or providing a dilution step in the process. In the former case, no initial dilution is required, only waters from the

ID No.	Research Objective	Conclusions
		coagulation and flocculation solutions are required for the treatment.
		If the initial slurry density of the FFT feed is higher than 20 wt.% solids, an initial dilution is required to bring down FFT feed to 20 wt.% solids. The treatment was designed to achieve an effective flocculation performance by maximizing agglomeration of fines to form big flocs while maximizing water release. To achieve this design criteria, the slurry density at the flocculation step should be approximately 8 wt.% solids (considering the contribution of the coagulant and flocculant solution's water) and, therefore, the initial dilution of the FFT feed should be set for this condition while maintaining the concentration and dosage of the coagulant and flocculant constant.
		The FFT solids/water separation and fines agglomeration is achieved by inline coagulation and flocculation addition prior to the discharge into the geotextile tubes. The optimal residence time for the inline mixing is 20 seconds to provide the most efficient flocculation of the FFT without shearing (no static or dynamic mixing are required). This residence time is defined by laboratory settling tests.
		Filling the geotextile tubes is controlled by the specific strength and hydraulic parameters of the geofabric (seams and intake ports) that limit the intake pressure and the filling height of the geotextile tubes.
		Field data indicated that, during filling, dewatering is a function of the recipe and inline mixing process, short drainage of the geotextile tube containment, internal pressure and gravity head during filling, hydraulic parameters of the geofabric material, evaporation, freeze-thaw, self-weight consolidation, and increased total stress by stacking (loading).
		Once the treated FFT are discharged in the geotextile tubes, the filtration properties of the geofabric and the short drainage path of the containment are the key contributors to the enhanced dewatering and accelerated consolidation. Evaporation and freeze-thaw are also identified as contributors to dewatering with time.
		The geotextile tube deposits with treated FFT act more as a filter pressure system, with most water recovery happening while the bags are filled. Fines capture ranges between 97% and 99% (60% silts and 37% clays, approximately). The material inside the

ID No.	Research Objective	Conclusions
		geotextile tubes shows a considerable gain in strength over 30 days after the filling of the tube is completed, reaching over 10 kPa undrained shear strength.
		Tensile strength with low elongation provided by the geofabric is a key reinforcing parameter of the stacked geotextile tubes deposit, allowing for stacking at low undrained shear strength (2 kPa), usually achieved when the filling of the geotextile tube is completed at the recommended filling maximum height by the manufacturer.
		Geotechnical instrumentation and field and laboratory test results have indicated that the treated FFT inside the tubes continue to dissipate excess pore pressure (consolidate), and undrained shear strength increases with time to form a stable deposit of thickened and filtered FFT.
5	Develop solids and water mass balance of the treated FFT discharged into the geotextile tubes to understand the solids/ions captured inside the tubes and the release water as process water either for use in the same FFT management or routed into the mining process.	The initial change in the fraction of solids from 8 wt.% (end-of-pipe) to 27 wt.% solids (average) in the tube 5 hours after pouring shows an effective coagulation and flocculation process, and this released water is the dilution water (including coagulant and flocculant solutions) used in the process.
		The unit change in the volume of water is 4 times greater in the coagulated FFT stream and 4.5 times in the flocculated FFT stream compared with the unit volume of water in the original FFT feed at 28 wt.% solids (average). Those units represent the volumes of initial dilution of FFT feed to 20 wt.% solids plus the coagulation and flocculation solution volumes, as per their fixed concentrations and dosages required for the treatment.
		Comparing the results of end-of-pipe and after five hours with the 7-day samples, there is a significant initial increase in dewatering from 8 wt.% solids to 50 wt.% solids.
		After 30 days of deposition, temperature measurements indicated that the tubes were frozen at their perimeter. However, at the center of the tubes, temperatures were still above freezing (+2 to +5 °C), the undrained shear strength remained at 10 kPa, and solids content was 55 wt.% solids, confirming the limitation of dewatering and strength gain due to the peripheral frozen condition of the tubes, impeding water release.

ID No.	Research Objective	Conclusions
		The unit loading of ions from different process streams shows a similar type of water (process water) used in the chemicals preparation and is responsible for changing the chemistry downstream.
		The process water used for the trial has high divalent cation concentration (86 ppm Ca^{2+}). The concentration of Ca^{2+} in the release water was the same as the process water used for the tests. Al^{3+} loading was mainly contributed from the coagulant (alum) stream, which was transferred to the solid phase and remained at a very low concentration in the release water. The results show that the FFT treatment used does not generate any excess divalent or multivalent cations in the release water in the scenario of high ion-content dilution water.
		The mass of the ions in various streams shows ion transfer from aqueous to solid phases and vice versa, and are not discouraging. The mass balance and concentration analysis of the major ions in the water phases show that the majority of the ions remain in the solid phases after deposition.
		Comparing the volumes of fluid added into the process from different streams, the volume of the alum solution stream is three times that of FFT feed plus the dilution stream volume. This suggests that this stream alone is a major contribution to the change in the downstream process chemistry.
		Tube run-off or release water was sampled at different intervals of time. The same concentration of ions in the release water was reported each time the sample was collected. The run-off volume obtained was considered as an approximation for complete drying when all the water will be released.
		The recipe (coagulation and flocculation) developed by this research could be suitable for any other mining tailings management, but will need a trial to prove the benefits.
6	Investigate the suitability of the recipe/geotextile tubes as new approach to tailings management technology to be implemented in mining operations.	**Factors influencing suitability:** **Energy supply** – Required energy to remove water from the slurry: filtered and thickened tailings and paste methods will likely require more energy to transport than a conventional slurry and geotextile tubes. **Climate –** Successful implementation of filtered and thickened tailings disposal methods are often seen in

ID No.	Research Objective	Conclusions
		dry climates (desiccation aid). Treated FFT disposal in geotextile tubes can be successfully implemented in a variety of climates.
		Production rates – Filtered and paste technologies are unproven for high production rates (>100 kt/day). Thickened methods provide moderate production (30–50 kt/day), and conventional disposal remains the only proven technology at mines with high production rates. Geotextile tubes can be comparable to a moderated production, occupying a smaller footprint.
		Economics – Data show alternative tailings technology methods to be more expensive than conventional disposal.
		Operational – Maintaining uniform deposition slopes is a challenge for paste and thickened methods because of fluctuations in ore characteristics, tailings gradations, and percent solids. No constraints have been identified for operationality of geotextile tubes because of fluctuations in ore characteristics and/or tailings initial slurry densities and gradation.
		Topography – Thickened and paste require flat topographies and embankment support. Filtered tailings can be implemented in a variety of terrains provided stability, operational, and closure requirements are taken into consideration. Geotextile tubes can be implemented in a variety of terrains and could be used as a buttress for filtered tailings in co-disposal deposits.
		Seismicity – Mitigation measures to address concerns about physical stability of alternative tailings disposal may contradict many of the perceived benefits. Geotextile tube containment provides ideal conditions of drainage and shear strength reinforcement to minimize liquefaction issues.
		Water – The conservation and reuse of water are the main drivers for implementation of alternative methods of tailings disposal. Filtered tailings and geotextile tube methods save significant amounts of water and allow for reuse (recycling) to the mine operation processes, with paste providing fewer advantages. Limited water supply is an important driver for mining operations.
		Drivers for implementation – Comparing filtered tailings and geotextile tubes:
		Space conservation: Filtered tailings and geotextile tubes are stockpiled at a higher dry solid content (dry

ID No.	Research Objective	Conclusions
		t/m^3) and much smaller footprint than conventional tailings disposal. In addition, no transportation of solids or compaction are required for geotextile tubes deposits.
		Reduced environmental risks: Less water in the tailings and lower containment structures are favorable attributes for permitting because more water is recovered from the thickener/or geotextile tubes and less freshwater make-up is required. **Improved compliance**: Environmental regulations have become more stringent, influencing mining companies' decisions toward dry stack tailings disposal, which includes geotextile tube deposits. **Better handling in cold conditions**: Cold conditions can make water handling difficult and filtered and geotextile tube disposal technologies attractive. **Physical stability**: Filtered tailings and geotextile tube deposits allow for geotechnically stable thick layer deposits (stacked up to 40 m high) without compaction, allowing for early closure and reclamation. **Chemical stability**: Because filtered tailings and geotextile tubes are unsaturated stacks and susceptible to oxidation, if the tailings are acid generating the oxidation process can result in acid drainage. In the case of geotextile tubes, depending on the design of the physicochemical treatment recipe, acid drainage could be prevented. To assess the chemical stability of the stacked geotextile tubes, it will be necessary to determine the acid-producing minerals (primary and secondary) and acid-neutralizing minerals that may be present, along with the metal-leaching potential to predict future geochemical behavior. The primary mineralogical composition has a strong influence on the oxidation processes; therefore, the mineralogical and geochemical interactions are essential aspects to understand as the parameters controlling acid mine drainage formation and to develop effective prevention measures. In addition, geotextile tubes can be filled and dumped in water from bottom-split barges, creating subaqueous deposits that contribute to minimize acid drainage.

Chapter 7 Limitations and Contributions to Knowledge

7.1 Limitations

The Global Industry Standard on Tailings Management (GISTM) aspires toward "zero harm to people and the environment" from tailings facilities. Aligned with the GISTM, this research considers the Da Silva's recipe/geotextile tube processing approach as a feasible alternative to filtration technology processes to provide safe tailings facility management and enhanced physical stability of the FFT deposits.

As confirmed by this research, the increased Ca^{2+} and pH cause adverse effects on the adsorption of anionic PAM polymer on quartz and kaolinite particles, causing steric stabilization at the particle surfaces and inhibiting the formation of hydrogen bonds. Poor flocculation of quartz and kaolinite observed in this research between pH 8 and 8.45 at a Ca^{2+} porewater concentration >31 ppm are likely the cause of the significant amount of trapped water remaining in the FFT flocculated with anionic flocculant only. Further work is required to investigate the adsorption of Ca^{2+}, Al^{3+}, and anionic PAM on quartz and kaolinite particles in the range of Ca^{2+} concentrations and pH mentioned above, focusing on hydrogen bonding and steric stabilization at the particle surface.

The recipe evaporates at a potential rate ≥ 1 (i.e., AE/PE ≥ 1) when the sample is saturated in the early stage of the drying process, which is possibly attributed to the fact that the recipe has an open soil structure. In addition, the evaporation results suggest that the recipe entraps residual bitumen in the tailings and it becomes part of that open soil structure, as indicated by the continued decrease in the AE/PE ratio to reach a value of 0.8, which is two days earlier than the flocculated tailings with flocculant only. Further work would be required to confirm the entrapment of bitumen in the open structure of the treated FFT (coagulated and flocculated quartz and kaolinite particles).

This research recognizes that geotextile tubes are unsaturated stacks and are susceptible to oxidation. If the tailings are acid generating, the oxidation process can result in acid drainage, and depending on the design of the physicochemical treatment recipe, acid drainage could be prevented. However, the research findings are limited, and should expand more into investigating chemical stability. Further work would be required to determine the acid-producing minerals (primary and secondary) and acid-neutralizing minerals that may be present, along with the metal-leaching potential to predict future geochemical behavior. The primary mineralogical composition has a strong influence on the oxidation processes and, therefore, understanding the mineralogical and geochemical interactions is essential to understand the parameters controlling acid mine drainage formation and to develop effective prevention measures that could be part of the tailings treatment recipe.

7.2 Contribution to knowledge

Stacked deposits of thickened and filtered FFT using geotextile tubes have the potential to change the way that mine waste is managed, greatly reducing geotechnical risk and the complexity of closure compared with traditional methods. To this end, this research demonstrates that geotextile tubes combined with a novel physicochemical recipe is a feasible alternative approach for filtration and fines capture, accelerated dewatering and consolidation, and reinforcing the shear strength of the FFT facilitating reclamation and post-closure long-term safety performance.

The verification of the geotextile tube processing using Da Silva's recipe for FFT successfully demonstrates:

1) Effective fines agglomeration, enhanced dewatering, and accelerated consolidation of the FFT achieved with the coagulant alum (4.27% Al^{3+} + 8.07% Al_2O_3 and specific gravity 1.326) at concentration 0.1% and 0.65% dosage (by mass of dry solids), and flocculant (anionic PAM flocculant of medium charge density and VHMW) at concentration 0.1% and 0.1% dosage (by mass of dry solids).

2) Aluminum (Al^{3+}) loading is mainly contributed from the coagulant (alum), which is transferred to the solid phase and remains as a very small concentration in the release water. The results showed that the tailings treatment used do not generate any excess

divalent or multivalent cations in the release water in the scenario of high ion-content dilution water. The mass balance and concentration analysis of the major ions in the water phases shows that most of the ions remain in the solid phases, which minimizes the negative impact of Ca^{2+} ions onto anionic PAM flocculant, inhibiting flocculation efficiency.

3) The effectiveness of the coagulation and flocculation process requires an initial slurry density of the FFT feed at 20 wt.% solids. This can be achieved by controlled dredging of the FFT and/or providing a dilution step in the process. In the former case, no initial dilution is required, and only water from the coagulation and flocculation solutions is required for the treatment.

4) If the initial slurry density of the FFT feed is higher than 20 wt.% solids, an initial dilution is required to reduce the FFT feed to 20 wt.% solids. The treatment was designed to achieve an efficient flocculation performance by maximizing agglomeration of fines to form large flocs while maximizing water release. To achieve this design criteria, the slurry density at the flocculation step should be approximately 8 wt.% solids (considering the contribution of the coagulant and flocculant solution waters) and, therefore, the initial dilution of the FFT feed should be set for this condition while maintaining the concentration and dosage of the coagulant and flocculant constant.

5) The FFT solids/water separation and fines agglomeration is achieved by inline coagulation and flocculation addition prior to the discharge into the geotextile tubes. The optimal residence time for the inline mixing is 20 seconds to provide the most efficient flocculation of the FFT without shearing (no static or dynamic mixing are required). This residence time is defined by laboratory settling tests.

6) The geotextile tube acts as a filter pressure system, with most of the water recovery occurring while the tubes are being filled with the treated FFT. The filtration properties of the geotextile tubes and the short drainage path of the treated FFT contained in the tubes are key contributors in the enhanced dewatering and accelerated consolidation of the treated FFT.

7) The recipe/geotextile tube FFT management technology approach also allows for faster construction of deposits that can be stack into higher lifts without compaction, are geotechnically stable, and occupy a smaller environmental footprint compared with FFT deposits.

Identification of key factors impacting dewatering of the FFT with flocculation only enabled the selection of essential laboratory and field tests on geotextile tubes processing combined with the Da Silva's physicochemical recipe as an alternative for FFT dewatering and filtration methods.

Key insights from this research allowed the development of characterization tools not consistently considered in the industry, such as parametric analysis on FFT dispersion and flocculation behaviors, evaporation tests, beam centrifuge testing, and solids and water mass balance for dewatering analysis to investigate the solids, water, and ions behaviors inside the geotextile tube.

This research shows that these tests can be applied to the screening and evaluation of a wide range of tailings amendment strategies and provide a consistent basis for comparing the ability of various tailings amendments to achieve the desired performance criteria by combining a physicochemical recipe with the geotextile tube mechanical and hydraulic properties in a controlled manner.

Through a parametric analysis on the dispersion and flocculation behaviors of FFT, this research has identified that the poor flocculation of the FFT (quartz and kaolinite) in the range of pH 8 is likely due to the adsorption of excess of Ca^{2+} ions onto anionic PAM polymer, causing steric stabilization at the particle surfaces and inhibiting the formation of hydrogen bonding by covering up the functional activity groups of the particles. As a result, this research has also identified that the negative impact on flocculation of the FFT caused by excess of calcium ions can be minimized, or even eliminated, by aluminum ions (higher valence cations), as evidenced through simple but essential laboratory tests that investigated the inherent properties of the FFT constituents, porewater chemistry and pH, settling, and zeta potential.

Assessment of the dispersion and flocculation behaviors of the FFT through parametric analysis focused on understanding the behavior of quartz and kaolinite materials separately and combined at different conditions of pore water chemistry and pH to investigate FFT flocculation with flocculant only and with the amended recipe (coagulation and flocculation).

The evaporation tests confirmed that the treated FFT with the recipe (coagulation + flocculation) loses water faster and reaches the boundary between the saturated and unsaturated state (i.e., AE/PE = 0.8) earlier than FFT and centrifuged FFT with flocculation only. In addition, the evaporation tests suggest that the recipe entraps the residual bitumen in the tailings to become part of the treated FFT open structure, as demonstrated by fines capture, quality of the release water, and hydraulic conductivity. In contrast, the residual bitumen films on the surfaces of the FFT with flocculation only start to break down as drying continues, and the AE/PE ratios continue to gradually increase to reach a value of 0.96 and remain constant until Day 10. Eventually, the AE/PE ratios start to decrease to reach a value of 0.8 on Day 12. During this time, the AE/PE ratio of the recipe continues to decline gradually and reaches a value of 0.8 on Day 10. This is an indication that the recipe also reduces and/or minimizes the potential impacts on the flocculation of the FFT caused by the residual bitumen.

Laboratory geotechnical beam centrifuge test results obtained by this research while investigating the treated FFT (recipe), FFT and a centrifuge cake using flocculant only indicate that the recipe sample settles more and faster and consequently dissipates the excess pore pressure more rapidly than the FFT and centrifuge cake obtained with flocculant only, confirming the benefits of the recipe (coagulation + flocculation). Apart from the use of geotextile tubes, based on these research results, we suggest that the volume change could be a criterion for acceptance of FFT (recipe) ready to reclaim within 10 years of the end of mine-life. Porosity, of course, is the volume of water divided by the total volume. Previous experience has shown that FFT must have a minimum shear strength of 10 kPa to allow for the surface to be reclaimed. Field trials as part of this research have indicated that a shear strength of 10 kPa is reached at a porosity of 0.5, which is equivalent to 70 wt.% solids. Test results from this research on FFT (recipe) show that the porosity 0.5 is reached at depth of 6 m of a deposit with the recipe. Therefore, atmospheric drying

and/or freeze/thaw effects, or any other engineered solution, would be needed to decrease the surface porosity to an acceptable value that will allow reclamation.

By using a comprehensive approach to solids and water mass balance characterization, it has been identified that solids, water, and ion transfer in streams of the inline mixing process, before discharge into the geotextile tubes, which can be confirmed while ensuring the quality and volumes of the release water to achieve a chemically and geotechnically stable treated and filtered FFT deposit that does not pose a threat to the environment.

A business case exercise was developed for operational application of geotextile tubes based on the commercial field trial results performed during this research at an oil sands operation site. This business case considered an optimized plan for: (1) 44 years deposition; (2) one dedicated area (no relocations); (3) 3,063,510 m^2 utilized area; (4) 32,258 geotextile tubes; (5) 116 Mt (dry) capture; (6) total geotextile tubes costs (7.8 CAD $/dT); (7) total labor costs (1.5 CAD $/dT); (8) total chemicals (3.2 CAD $/dT); (9) total miscellaneous costs (2.9 CAD $/dT); Capex (4.0 CAD $/dT); Opex (6 + 7 + 8 + 9 = 15.4 CAD $/dT). The total Capex + Opex = 19 CAD $/dT. This should be evaluated case-by-case for different oil sands operation sites.

In general, at oil sands operation 1.5 barrels of tailings are equivalent to 1.0 barrel of oil (crude). The volume of a barrel of oil is 0.159 m^3 and equivalent to 0.147 t, approximately. The volume capacity of the geotextile tube is 5,521 m^3 which is equivalent to 9,662 t when the treated FFT achieve 85 wt.% solids and dry density of 1.75 t/m^3.

The cost per barrel of oil among the oil sands operators is ranging from 22 CAD $ to 30 CAD $, approximately. Therefore, the total cost (Capex + Opex) in $/dT (dry tonnes of captured tailings) using geotextile tubes, as mentioned above, can also be correlated to the cost of barrel of oil case-by-case among oil sands operators.

Geotextile tube technology is one alternative available in the broader scope of tailings management. The technology operates in the same "fines-dominated" regime as existing operational technologies in the mining industry. To date, operational and capital costs have made most technologies unsustainable from a full-scale fines-management perspective. Development and deployment of any new technology (especially in a time of resource constraints due to the

economic climate) should only occur if clear benefits compared with incumbent technologies can be demonstrated. For simplicity, geotextile tube filtration and dewatering technology performance from 8 wt.% to 50 wt.% solids content in 7 days and 85 wt.% in one year could be competitive with the current fines treatment and filtration technologies deployed commercially at present. Therefore, it is possible that there is a niche application for the geotextile tube technology in the mining industry, since a commercial trial in the oil sands industry, as shown in this research, has already been deployed.

Chapter 8 Recommendations for Further Work

Further work should be generally focused in the following areas:

Hydrogen bonding and steric stabilization at the particle surface – recommend investigate the adsorption of Ca^{2+}, Al^{3+}, and anionic PAM on quartz and kaolinite particles in the range of Ca^{2+} concentrations $\geq$ 31ppm and pH mentioned in this research, focusing on hydrogen bonding and steric stabilization at the particle surface.

Entrapment of bitumen in the open structure of the treated FFT – recommend confirming the entrapment of bitumen in the open structure of the treated FFT (coagulated and flocculated quartz and kaolinite particles).

Chemical stability regarding acid drainage – This research recognizes that geotextile tubes are unsaturated stacks and are susceptible to oxidation. The research findings are limited and should expand more into chemical stability of the tailings. Recommend determining the acid-producing minerals (primary and secondary) and acid-neutralizing minerals that may be present, along with the metal-leaching potential to predict future geochemical behavior. Understanding the mineralogical and geochemical interactions is essential to understand the parameters controlling acid mine drainage formation and to develop effective prevention measures that could be part of the tailings treatment recipe.

To further investigate prevention measures regarding the ARD phenomenon (linked to solid sulfur phases present in some tailings), recommend preparing a preliminary list of test work on the solid phase before and after treating the FFT with the Da Silva's recipe as follows: a) Total sulfur and total carbon by induction furnace; b) Acid-base accounting including determination of neutralization potential by modified Sobek methodology, paste pH, and acid leachable sulfates; and c) Kinetic testing in humidity cells if tailings appear to be acid generating with acid-base accounting.

Investigate potential for carbon capture – As the XRD results of the FFT used in this research have shown moderate to significant differences in carbonates before and after treatment with the Da Silva's recipe, using the QUEMSCAN technique is recommended to further investigate the potential for carbon capture, which is linked to solids phase and carbonates precipitation.

References

Abrams, T. H., Rule, R. W., White, B. E., Cretens, B. J., & McAllister, B. J. (2016). Managing a Sediment Consolidation Area with Geotextile Tubes. In *Proceedings of the 21ˢᵗ First World Dredging Congress, WODCON XXI,* Miami, Florida, USA.

Atesok, G., Somasundaran, P., & Morgan, L. (1988). Adsorption Properties of Ca^{2+} on Na-Kaolinite and its Effect on Flocculation Using Polyacrylamides. *Colloids and Surfaces*, 32, 127–138.

Bernhard D. (2010). Basic Concepts in Environmental Geochemistry of Sulfidic Mine-Waste Management. In E. S. Kumar (Ed.) *Waste Management*. InTech.

Blowes, D. W., & Ptacek, C. J. (1994). Acid-neutralization mechanisms in inactive mine-tailings. In: J. L. Jambor & D. W. Blowes (Eds.), *Short course handbook on environmental geochemistry of sulfide mine-waste*. pp. 271–291. Mineralogical Association of Canada.

Blowes, D. W., Ptacek, C.J., Frind, E. O., Johnson, H. R., Robertson, D. W., & Molson, J. W. (1994). Acid-neutralization reactions in inactive mine-tailings impoundments and their effect on the transport of dissolved metals. In: *International Land Reclamation and Mine Drainage Conference and the Third International Conference on the Abatement of Acid Drainage Conference*, Pittsburgh, Pennsylvania, USA.

Boxill, L.E. (2016). *The Impact of Fabric and Surface Characteristics on the Engineering Behavior of Polymer-Amended Mature Fine Tailings.* [PhD dissertation]. University of British Columbia.

Bratby, J. (2006). *Coagulation and Flocculation in Water and Wastewater Treatment* (2nd ed.). IWA Publishing.

Butt, H. J., Graf, K., & Kappl, M. (2003). *Physics and Chemistry of Interfaces*. Wiley.

Canizares, P., Jimenez, C., Martinez, F., Rodrigo, M. A., & Saez, C. (2009). The pH as a key parameter in the choice between coagulation and electrocoagulation for the treatment of wastewaters, *Journal of Hazardous Materials*, 163, 158–164.

Da Silva, F., Graham, M., Scott, J. D., & Wilson, G. W. (2014). Evaluation of a new treatment technology for improving oil sands tailings management. In *Proceedings of the Canadian Geotechnical Society, GeoRegina 2014*; Regina, Saskatchewan, Canada

Da Silva, F., Graham, M., Wilson, G. W., & Scott, J. D. (2014). Geotextile bags for enhanced dewatering and accelerated consolidation of oil sands mature fine tailings. In *Tailings & Mine Waste 2014*, Keystone, Colorado, USA.

Da Silva, F., Wilson, G. W., Stephens, T., & Castro, N. (2021). Geotextile bags as filtration process to enhance physical stability of oil sands tailings deposits – Concept & lessons learned. In *Tailings and Mine Waste 2021*, Banff, Alberta, Canada.

Da Silva, F. (2022). Geo-composite physicochemical treatment using synthetic fibers for enhanced dewatering, shear strength and consolidation of oil sands fluid fine tailings deposits – concepts and lessons learned. In *26th International Conference on tailings and Mine Waste 2022,* Denver, Colorado, USA.

Da Silva, F. (2023). Stacked deposits of thicken and filtered fluid fine tailings using geotextile tubes – Concept/lessons learned updates. In *25th International Conference on Paste, Thickened and Filtered Tailings 2023,* Banff, Alberta, Canada.

Demirci, S. (1973). *Electrical Charge on Colloidal Gold Particles.* [PhD dissertation]. Middle East Technical University.

Duan, J., & Gregory, J. (1998). The Influence of Silicic Acid on Aluminum Hydroxide Precipitation and Flocculation by Aluminum Salts. *Journal of Inorganic Biochemistry*, 69, 193–201.

Duan, J., & Gregory, J. (2003). Coagulation by Hydrolyzing Metal Salts. *Advances in Colloidal and Interface Science*, 100–102, 475–502.

Fair, A. E., & Beier, N. A. (2012, December 2–5). Collaboration in Canada's oil sands: Fluid fine tailings management, in *Proceedings of the Third International Oil Sands Tailings Conference.* Edmonton, Alberta, Canada.

Ferry, G., & Gill, J. (1962). Transference Studies of Sodium Polyacrylate under Steady State Electrolysis. *Journal of Physical Chemistry,* 66, 999–1003.

Fontana, J., & Thomas, R. (1964). The Configuration of Adsorbed Alkyl-Methacrylate Polymers by Infrared and Sedimentation Studies. *Journal of Physical Chemistry*, 65, 480–482.

Fourie, A., Verdugo, R., Bjelkevik, A., & Torres-Cruz, L. (2022, May 1–5). Geotechnics of mine tailings: a 2022 State of the Art; in *Proceedings of the 20th ICSMGE—State of the Art and Invited Lectures.* Sydney, Australia.

Gan, W., & Liu, Q. (2008). Coagulation of Bitumen with kaolinite in Aqueous Solutions containing Ca, Mg and Fe: Effect of Citric Acid. *Journal of Colloid and Interface Science*, 324, 85–91.

Goldberg, S., Foster, S., & Heick, L. (1991). Flocculation of illite and Kaolinite and illite and Montmorillonite Mixtures as Affected by Sodium Adsorption Ratio and pH. *Clays and Clay Minerals,* 39(4), 375–380.

Gregory, J. (2006). *Particles in Water: Properties and Processes*. CRC Press Taylor & Francis.

Healy. W., & La Mer, K. (1964). Flocculation of Mineral Dispersions by Polymers. In *7th International Mineral Processing Congress*, New York, 1, 359–365.

Heidi, L., Anya, E., Heather, K., & Ania, C. (2021). Geochemical Stability of Oil Sands Tailings. In *Mine Closure Landforms. Journal/Minerals 2021*, 11, 830.

Hunter, J. (1981). *Zeta Potential in Colloid Science: Principles and Applications*. Academic Press p. 283.

Hussain, A., Demirci, S., & Ozbayoglu, G. (1996). Zeta Potential Measurements of Three Clays from Turkey and Effects of Clay on Coal Flotation. *Journal of Colloid and Interface Science*, 184, 535–541.

Jiang, T., Hirasaki, G., & Miller, C. (2009). Characterization of Kaolinite Zeta Potential for Interpretation of Wettability Alteration in Diluted Bitumen Emulsion Separation. *Energy Fuels*, 24(4), 2350–2360.

Jirgensons, B., & Straumanis, M. E. (1962). *A Short Textbook of Colloid Chemistry* (2nd Ed.). Macmillan.

Khachan, M., Bathia, S., & Cetin, D. (2015). The Use of Fibers to Improve Geotextile Tube Dewatering Performance and Stability. In *Geosynthetics 2015*. Portland, Oregon, pp. 1080–1088.

Krystian, W. P. (2007). *Geosynthetics and Geosystems in Hydraulic and Coastal Engineering*. Taylor & Francis.

Kuzkin, F., Nebera, P., & Zolin, N. (1964). Aspects of the Theory of Suspensions Flocculation by Polyacrylamides. In *7th International Mineral Processing Congress*, New York, 1, 347–357.

Lebedeva, E., Fogden, A., Senden, T., Kanackstedt, M. (2010). Kaolinite Wettability – The effect of Salinity, pH and Calcium. In *International Symposium Society Core Analysis*. Halifax, Nova Scotia, Canada.

Masliyah, J., Czarnecki, J., & Xu, Z. (2011). *Handbook on Theory and Practice of Bitumen Recovery from Athabasca Oil Sands*. Kingsley Knowledge Publishing.

Michalowski, L., & Cermak, J. (2003). Triaxial Compression of Sand Reinforced with Fibers. *Journal of Geotechnical and Geo-environmental Engineering*, 129(2), 125–136.

Mitchell, J. K., & Soga, K. (2005). *Fundamentals of Soil Behavior* (3rd ed.). Wiley.

Morgenstern, V. (2017). Dam Safety Risk – From Deviance to Diligence. In *International Geo-Risk 2017*, pp. 19–30.

Pefferkorn, E., Nabzar, L., & Varoqui, R. (1987). Polyacrylamide Na-kaolinite interactions: Effect of electrolyte concentration on polymer adsorption. *Colloid and Polymer Science*, 265, 889.

Peng, F., & Di, P. (1994). Effect of Multivalent Salts – Calcium and Aluminum on the Flocculation of Kaolin Suspension with Anionic Polyacrylamide. *Journal of Colloid and Interface Science*, 164, 229–237.

Scott, J. D., Jeeravipoolvarn, S., & Chalaturnyk, R.J. (2008, September 22–24). Tests for Wide Range of Compressibility and Hydraulic Conductivity of Flocculated Tailings. In *Proceedings of the 61st Canadian Geotechnical Conference*, Edmonton, Alberta, pp. 738–745.

Sergiy, A.L., Bandaru, V., Mahmoud, M., Shobha, K., & George, F. (2015, February 15–18). Mathematical Modeling of the Dewatering of Dredging Sediments in Geotextile Tubes. In *Geosynthetics 2015*, Portland, Oregon, USA.

Vick, S. G. (1996). Tailings dam failure at Omai in Guyana. *Mining Engineering*, 48(11), 34–37.

Sincero A. P., & Sincero G. A. (2003). *Physical-Chemical Treatment of Water and Wastewater*. CRC Press.

Slater, W., Clark, P., & Kitchener, A. (1968). Chemical Factors in the Flocculation of Mineral Slurries with Polymeric Flocculants. In *8th International Mineral Processing Congress*, Leningrad, Russia, 1, 316–324.

Stumm, W., & Morgan, J. J. (1996). *Aquatic Chemistry – Chemical Equilibria and Rates in Natural Waters*. Wiley.

Usoni, L., Rinelli, A., Marabini, M., & Chigi, G. (1968). Selective Properties of Flocculants and Possibilities of their Use in Flotation of Fine Minerals. In *8th International Mineral Processing Congress*, Leningrad, Russia, 1, 514–531.

Van, L. A. (1980). *Behaviour of Quartz Suspensions in the Presence of Calcium Ions and Acrylate Polymers*. Elsevier.

van Olphen, H. (1977). An Introduction to Clay Colloid Chemistry (2nd ed.). Wiley.

Verwey, E., & Overbeek, J. (1948). *Theory of the Stability of Lyophobics Colloids*. Elsevier.

Welch, D. E., Botham, L. C., and Johnson, J.M. (1995, January 17–20). Prediction of tailings effluent flows. In *Tailings and Mine Waste 95 and Summitville Forum Conference*. Fort Collins, Colorado, USA.

Wilson, G.W., Robertson, A.M. (2015). The Value of Failure, Invited Plenary Paper for the Mt. Polley Failure. In *Tailings and Mine Waste 2015*, Vancouver, Canada, pp. 26–28.

Williams, D. J. (2021). Lessons learned from Tailings Dam Failures – Where to Go from Here? *Minerals 2021*, 11, 853.

Zhang, L. L., Fredlund, D. G., Fredlund, M. D., Wilson, G. W. (2014). Modeling the unsaturated soil zone in slope stability analysis. *Canadian Geotechnical Journal*, 51(12), 1384–1398.